
Functional Study of Grapevine (*Vitis
vinifera* L.) Membrane Ion
Transporters Related to Salt
Tolerance

By
Yue Wu

SEPTEMBER 2019
SCHOOL OF AGRICULTURE, FOOD AND WINE
THE UNIVERSITY OF ADELAIDE

Table of Contents

Table of Contents	i
List of included manuscripts	iv
Abstract	v
Declaration	viii
Acknowledgements	ix
Chapter 1: Literature review	1
1.1 Background	1
1.2 Plant salt relations	2
1.3 Grapevine salt tolerance.....	6
1.4 The role of anion transporters in chloride homeostasis	10
1.5 Sodium homeostasis related genes.....	18
1.6 Hypotheses generation and thesis outline	21
References.....	24
Chapter 2: Expression of the grapevine stelar localised anion transporter ALMT2 in Arabidopsis roots reduced shoot Cl⁻ accumulation under salt stress	35
Abstract	38
Introduction.....	39
Materials and methods	41
Results.....	52
Discussion	57
Acknowledgements.....	62
References.....	63
Figures.....	68
Supporting information	78
Chapter 3: Expression of the grapevine <i>NPF2.2</i> in Arabidopsis roots reduces shoot Cl⁻ accumulation under salt stress	98
Abstract.....	101
Introduction.....	102
Materials and methods	105
Results.....	113

Discussion	117
Acknowledgements	122
References	123
Tables and figures	128
Supporting information	137
Chapter 4: Functional differences in transport properties of natural HKT1;1 variants influence shoot Na⁺ exclusion in grapevine rootstocks	149
Chapter 5: The <i>HKT1</i> gene family in grapevine (<i>Vitis vinifera</i> L.) encodes sodium-selective transporters with diverse features	168
Abstract	171
Introduction	172
Materials and methods	175
Results and discussion	179
Acknowledgements	184
References	185
Figures	189
Supporting information	194
Chapter 6: An R-based web app Smart-IV for automated and integrated high throughput electrophysiology data processing	199
Abstract	202
Background	203
TEVC Experiments	206
Smart-IV: overview	208
Smart-IV: automatic IV analysis	211
Smart-IV: one-click data export	213
Results and discussion	214
Conclusion	217
Future perspectives	217
Methods and implementation	219
Acknowledgements	222
References	223
Tables and figures	224
Supporting information	240
Chapter 7: Conclusions and future directions	241

7.1 Background	241
7.2 Characterisation of the putative anion channels/transporters	241
7.3 Characterisation of the <i>HKT</i> s in the QTL for grapevine Na ⁺ exclusion	247
7.4 Development of the R web app “Smart-IV” for automated ABF data IV processing	249
7.5 Summary	250
References	251
Appendix I: The effects of N-terminal YFP tagging on the localisation and function of the grapevine HKT1;1	253
Materials and methods	253
Results and discussion	254
References	256
Appendix II: Structure-function analyses of OsHKT1;3 and VviHKT1;3	257
Materials and methods	257
Results and discussion	259
Summary	261
References	261
Figures and tables	263
Bibliography	269

List of included manuscripts

- Wu, Y., Henderson, S.W., Walker, R.R. and Gilliam, M.** (2019) Expression of the grapevine stelar localised anion transporter ALMT2 in Arabidopsis roots reduced shoot Cl⁻ accumulation under salt stress (*at submission, unpublished*).
- Wu, Y., Henderson, S.W., Walker, R.R. and Gilliam, M.** (2019) Expression of the grapevine NPF2.2 in Arabidopsis roots reduces shoot Cl⁻ accumulation under salt stress (*at submission, unpublished*).
- Henderson, S.W., Dunlevy, J.D., Wu, Y., Blackmore, D.H., Walker, R.R., Edwards, E.J., Gilliam, M. and Walker, A.R.** (2018) Functional differences in transport properties of natural HKT1;1 variants influence shoot Na⁺ exclusion in grapevine rootstocks. *New Phytologist*, **217**, 1113-1127.
- Wu, Y., Henderson, S.W., Wege, S., Zheng, F., Walker, R.R. and Gilliam, M.** (2019) The *HKT1* gene family in grapevine (*Vitis vinifera* L.) encodes sodium-selective transporters with diverse features (*at submission, unpublished*).
- Wu, Y., Li, J. and Gilliam, M.** (2019) An R-based web app Smart-IV for automated and integrated high throughput electrophysiology data processing (*at submission, unpublished*).

Abstract

Grapevines are economically and socially important for the production of wine grapes, table grapes, and dried fruit, and are considered to be sensitive to salt. During salt stress grapevines can suffer from osmotic stress and NaCl toxicity, which can lead to growth reduction, poor fruit set and low yields. Salt tolerant *Vitis* species rootstocks which exclude salts from the grafted *Vitis vinifera* scions can be used to achieve healthier vine growth and low salt wines in the salt affected regions. In this thesis several candidate genes for grapevine salt exclusion are characterised and their potential importance for breeding salt tolerant grapevines is discussed.

Currently the rootstock trait of Cl⁻ exclusion is considered to be the combined effect of multiple genes rather than a single gene. Microarray gene expression analysis has previously compared the gene expression profiles between the roots of the two contrasting grapevine rootstocks – the good Cl⁻ excluder 140 Ruggeri and the poor Cl⁻ excluder K51-40. Four putative Cl⁻ and/or NO₃⁻ transporters which were more highly expressed in 140 Ruggeri were selected for characterisation in this study.

The first two proteins, VviALMT2 and VviALMT8 belong to the Aluminium-activated Malate Transporter family. Here, it was found that both transport multiple substrates including NO₃⁻, Cl⁻ and several organic acids using the *Xenopus laevis* oocyte system. The plasma membrane localised VviALMT2 was more highly expressed in the grapevine root stelar fraction than in the cortical fraction, with gene expression also up-regulated by high [NO₃⁻]. Cell-type specific expression of VviALMT2 in Arabidopsis roots reduced shoot [Cl⁻] under salt stress; therefore, it was proposed that VviALMT2 is beneficial to plants under salt stress by limiting shoot Cl⁻ accumulation.

The other two candidates examined were VviNPF2.1 and VviNPF2.2, which are in the NRT1/PTR family (nitrate/peptide transporter family). Here, it is shown that both VviNPF2.1 and VviNPF2.2 are plasma membrane localised; however, their Cl⁻ and NO₃⁻ conductance could not be determined using *Xenopus laevis* oocytes, and their expression in grapevine roots was down-regulated by high [NO₃⁻]. Salt stress was applied to Arabidopsis plants that exhibited root epidermis and cortex specific VviNPF2.2 expression, and the shoot [Cl⁻] of VviNPF2.2 expressing plants was lower

than that of the non-*VviNPF2.2*-expressing plants. Again the conclusion was made that *VviNPF2.2* may benefit plants by limiting shoot $[Cl^-]$ under salt stress.

For grapevine shoot Na^+ exclusion, a quantitative trait locus named *NaE* was identified, which contains six *HKT* genes. The root expressing plasma membrane localised VisHKT1;1 proteins were found to be strong Na^+ transporters; their allelic variation resulted in different Na^+ conductance and rectification properties, which were linked to the magnitude of shoot $[Na^+]$. Two key amino acid residues of VisHKT1;1 were identified important for determining Na^+ conductance and rectification properties. In this study, by mutating an equivalent residue in bread wheat TaHKT1;5-D, the Na^+ conductance and rectification tested using electrophysiology were successfully altered, which suggested the potential importance of the residue to HKT function.

All other grapevine *HKTs* in the *NaE* QTL were also characterised. The VviHKT1;6 and VviHKT1;7 allelic variants were all plasma membrane localised strong Na^+ transporters, while the VviHKT1;8 allelic variants were endosomal compartment localised weak inwardly rectifying Na^+ transporters. Through RT-qPCR and RNA-seq data analysis, all these *HKTs* were found to be lowly expressed or not expressed in all the tissue types tested. It is suggested that these HKTs could play minor roles in grapevine Na^+ homeostasis compared to the VisHKT1;1.

During this study, the two electrode voltage clamping technique was intensively used to test the substrate and transport activities of the candidate proteins. Conventional IV data analysis using the proprietary software is time consuming and found to be inefficient. Therefore, an R-based web app “Smart-IV” and an R package “abftools” were developed for electrophysiology data reading, automated current, capacitance, conductance and specific current/conductance processing and plotting in R. Two-electrode voltage clamp (TEVC) data analysed using the conventional method were re-analysed using Smart-IV, and the IV output from the Smart-IV was equivalent to the outputs of the proprietary software. The IV analysis process can be reduced to 15 seconds using Smart-IV with the default automatic interval search settings.

To conclude, the findings of this thesis have improved our understanding of: how grapevine ALMT2 and NPF2.2 may be involved in reducing shoot $[Cl^-]$ under salt stress; how some functional and structural functional features of the grapevine and plant

HKT1 result in altered shoot Na⁺ accumulation; and, how an open-sourced tool for electrophysiological data processing can automate and stream data analysis.

Declaration

I certify that this work contains no material which has been accepted for the award of any other degree or diploma in my name, in any university or other tertiary institution and, to the best of my knowledge and belief, contains no material previously published or written by another person, except where due reference has been made in the text. In addition, I certify that no part of this work will, in the future, be used in a submission in my name, for any other degree or diploma in any university or other tertiary institution without the prior approval of the University of Adelaide and where applicable, any partner institution responsible for the joint-award of this degree.

I acknowledge that copyright of published works contained within this thesis resides with the copyright holder(s) of those works.

I also give permission for the digital version of my thesis to be made available on the web, via the University's digital research repository, the Library Search and also through web search engines, unless permission has been granted by the University to restrict access for a period of time.

I acknowledge the support I have received for my research through the provision of an Australian Government Research Training Program Scholarship.

Yue Wu ... 23.09.2019
Date

Acknowledgements

I would like to thank my supervisors for their support during my study. I thank my principal supervisor, Professor Matthew Gilliham for bringing me onto this enjoyable research project, for the guidance during my study and for the critical and enlightening advise on my work. I thank Dr Sam Henderson, especially for his great patience in walking me through nearly all lab techniques, analyses and problems I encountered, and for his continuation in providing valuable ideas after he departed for a new role. I also thank Dr Rob Walker for being my external supervisor; I am grateful that he has never hesitated to provide resources and to offer help, and his feedback has helped me to think from another angle. I have been taken care of by my supervisors and I am lucky to be one of their students.

I thank the University of Adelaide for awarding me the Adelaide Graduate Research Scholarship, which covered my tuition fee as an international student and my living. I thank Wine Australia for funding my research and living, and for the financial support which allowed me to attend and present work at national and international conferences. I thank the Australian government Research Training Program for covering my tuition fee after I became a domestic student. I thank the Australian Research Council Centre of Excellence in Plant Energy Biology and the University of Adelaide, School of Agriculture, Food and Wine for the resources, training, and teaching opportunities.

I am also lucky to have been in an environment full of great people, which have helped me to have come so far. I thank Professor Steve Tyerman for being my independent advisor, and for inspiring me with his questions and comments. Stefanie Wege and Yu Long have devoted a lot of their time to teach me lab techniques, and I benefited from discussing my research with them. Mandy Walker, Jake Dunlevy, Deidre Blackmore and Paul Boss have kindly offered their advise, instruments, techniques and experimental materials. Stephen Pederson accepted our consultation requests and advised on our electrophysiology R project. I thank the above-mentioned people, and all my colleagues for the kind help and for being around. I greatly appreciated it.

Finally, I thank my husband Junda Li, for volunteering to develop the R package so that I can be released from the repetitive TEVC data processing, and for learning the theory of electrophysiology and app development to bring our side project to a higher standard.

Chapter 1: Literature review

1.1 Background

Grapevine is an economically significant crop in many places around the world; it was introduced into Australia in the late 18th century (Krake *et al.* 1999). *Vitis vinifera* L., belonging to the order Rhamnales, is the predominant wine grape species (Iland *et al.* 2011, Robinson 2006). This species has the highest capacity to accumulate sugar compared to all other *Vitis* species (Krake *et al.* 1999), thus making it the major species for winemaking. More than 800 *Vitis vinifera* cultivars, including Cabernet Sauvignon, Chardonnay and Shiraz, are regularly used for winemaking (Iland *et al.* 2011). The grape industry in Australia crushed an average of 1.76 million tonnes per year from 2008 to 2017; in 2018 the crush was 1.79 million tonnes with a total value of AU\$1.11 billion (Wine Australia 2018).

Rootstocks are widely used for enhancing grapevine's tolerance to pests or abiotic stress, and for vigour management. In the late 1800s, the pest phylloxera was inadvertently brought to Europe through the introduction of mildew-resistant *Vitis* species from America, and subsequently contaminated many other viticultural areas in the world (Krake *et al.* 1999). Rootstocks were originally used to protect susceptible *V. vinifera* scions from the devastating effects of phylloxera (Granett *et al.* 2001, Krake *et al.* 1999, Ordish 1972), but it was later found that they can impart other characteristics, such as salt tolerance (Downton 1977a).

Grapevine has been classified as moderately sensitive to salinity, which is defined according to the relative crop yield at different salinity levels (Maas and Hoffman 1977). In the report of Maas and Hoffman (1977), the threshold salinity level for yield decline of the *Vitis* spp. is 1.5 mmho/cm, with the yield reducing by 9.6% for every mmho/cm increase in salinity beyond the threshold. Salinity is naturally high in some Australian soils, due to land clearing and in some cases to relatively high salt concentrations within irrigation water, resulting in salinity problems that are intensified in some regions (ABS 2002). During land clearing, native vegetation was replaced with annual crops and pastures which use less water and have shallower root systems, thus resulting in rising water tables that mobilise the accumulated salts (George *et al.* 1997, McFarlane and Williamson 2002, Walker *et al.* 1999). High priority regions with

dryland salinity issues include some wine regions such as the Riverland, Barossa Valley, Riverina and Goulburn Valley, identified in the National Action Plan for Salinity and Water Quality (NAP, 2001 – 2008) (ABS 2002). Salinity of soil and irrigation water affects both plant growth and grape composition which can negatively impact wine sensory attributes. Salt stress is known to reduce plant water uptake and cause ionic toxicity symptoms in leaves. Salt accumulation in grapes can lead to a salty and soapy taste in juice and wine (de Loryn *et al.* 2014, Iland *et al.* 2011). Legally, Australian wine should contain no more than 607 mg/L of chloride (Cl^-), which is equivalent to 1000 mg/L when expressed as NaCl, although there is no limit for sodium (Na^+) concentration (Commonwealth of Australia 2014). For Australian wine exporters, there are legal limitations for Na^+ in Canada, Lebanon, South Africa and Switzerland (AWRI 2015). It is also recommended by the The International Organisation of Vine and Wine (2011), (2015) to have less than 80 mg/L excess Na^+ (Na^+ content less Cl^- content expressed as Na^+) in wine.

Rootstocks with salt tolerance superior to *Vitis vinifera* have been identified. These rootstocks are good shoot Cl^- and Na^+ excluders (Teakle and Tyerman 2010), and are able to maintain moderate to high vigour scions with good yields under saline irrigation (Walker *et al.* 2002b, Walker *et al.* 2004, Zhang *et al.* 2002). Yield performance is also taken into account for the salt tolerance ability of the rootstock (Maas and Hoffman 1977). The molecular mechanism of rootstock salt exclusion has not been fully characterised. This review will discuss the salinity effects on plants including grapevine, the currently known salt tolerant rootstocks, the potential mechanisms of plant Cl^- and Na^+ homeostasis involved, and the putative Cl^- and Na^+ tolerance mechanisms in grapevine.

1.2 Plant salt relations

1.2.1 Salinity and its effects on plants

Six percent of the world's land is affected by either salinity or sodicity (FAO 2005, Munns 2005). Most of these problems occur naturally (referred to as 'primary salinity') through weathering of parental rocks (Szabolcs 1989) and deposition of oceanic salts by rain and wind (Munns and Tester 2008). However, soil salinity can also arise due to

irrigation and land clearing (referred to as ‘secondary salinity’) (Munns 2011, Munns and Tester 2008). On a world scale, 2 % of the land farmed by dryland agriculture and 20 % of the irrigated land are affected by secondary salinity (FAO 2008). In Australia, 2 million of the 17 million hectares of land farmed by dryland agriculture have various degrees of secondary salinity, and more land has been predicted to be subject to salinisation risk in the near future (Munns and James 2003). Soil and irrigation water contain soluble salts including Na⁺, potassium (K⁺), calcium (Ca²⁺), magnesium (Mg²⁺), Cl⁻, sulphate (SO₄²⁻) and bicarbonate (HCO₃⁻) (Iland *et al.* 2011). In this review the terms salinity and salt will refer to sodium chloride (NaCl).

High concentrations of salts in plant growth media negatively impact plants via osmotic growth limitation and ion toxicity effects (Iland *et al.* 2011). Osmotic stress driven by salt in the soil, which can have a rapid onset, results in a decrease of new shoot growth (Munns 2011, Munns and Tester 2008). When soil water potential is more positive than xylem water potential, water flows from the soil to the plant root xylem (Iland *et al.* 2011, McElrone *et al.* 2013). As the salt concentration in soil water increases, the soil water potential decreases, thus reducing the water potential gradient between soil and xylem, which reduces plant water uptake and causes an osmotic stress. For many crops, the soil solution NaCl concentration threshold is 40 mM, beyond which plant shoot growth reduces significantly (Munns and Sharp 1993, Munns and Tester 2008). The ionic stress due to excessive Na⁺ and Cl⁻ accumulation has a relatively slow onset. The primary visible effects are ‘leaf burn’ and the premature death of older leaves, which were found to be associated with leaf Cl⁻ accumulation in grapevines (Ehlig 1960, Munns 2011, Munns and Tester 2008, Woodham 1956). Ionic stress is known to decrease photosynthesis (Allakhverdiev *et al.* 1999, Allakhverdiev *et al.* 2000a, Allakhverdiev *et al.* 2000b, Downton 1977b, Papageorgiou *et al.* 1998) and it is also considered to have effects on enzyme activities (Bolaños *et al.* 2006) and maintenance of cell turgor and membrane potentials (E_m) (Neumann *et al.* 1988, Suhayda *et al.* 1990).

1.2.2 Salt stress and photosynthesis reduction in grapevine

It was found that partial stomatal closure in response to mild salt treatment (75 mM NaCl) that occurred as laminae chloride concentrations reached 150 – 200 mM, and which reduces the gas exchange and transpiration rates, was the controlling factor of photosynthetic activity reduction in grapevine (Walker *et al.* 1981). When experiencing

salt and drought stress, stomatal closure is the mechanism to protect the plant from desiccation. Stomatal closure is the result of guard cell turgor loss, which is achieved by an abscisic acid (ABA) activated signalling cascade (reviewed in Kollist *et al.* 2014, Kriedemann *et al.* 1975, Loveys and Kriedemann 1974). In a study by Downton and Loveys (1981), mild salt stress treatments (25 mM and 50 mM NaCl) on grapevines were found to trigger 2-3 fold increases in ABA without affecting stomatal resistance; when severe salt treatment (100 mM NaCl) was applied, a 9-fold increase in ABA was observed which induced stomatal closure, thus initiating the osmotic adjustment processes which restores cell turgor and stomatal resistance.

However, it was observed that although stomatal resistance dropped immediately after relief of salt stress, photosynthetic recovery was irreversibly disrupted if the leaf Cl^- concentration exceeded 200 mM before salt stress relief (Walker *et al.* 1981). In the study of Downton *et al.* (1990), photosynthesis reduction in grapevine was mainly due to the decrease of stomatal conductance under mild to moderate salt stress. When lamina Cl^- concentration exceeded 165 mM, non-stomatal inhibition of photosynthesis arose from non-uniform stomatal behaviour. At the same intercellular CO_2 partial pressure, the rate of carbon assimilation decreases as leaf Cl^- concentration increased, which suggested that photorespiration is stimulated by laminae Cl^- accumulation (Downton *et al.* 1990, Ziska *et al.* 1990). It was also reported that high NaCl concentration in leaves reduces photosynthetic activity by reducing ribulose-1,5-bisphosphate carboxylase (an enzyme involved in carbon fixation) activity and leaf chlorophyll content (Greenway and Osmond 1972, Ziska *et al.* 1990).

Ion toxicity is usually associated with excessive accumulation of Na^+ in shoots in many cereal plants, such as wheat (reviewed in Munns *et al.* 2006), barley (Shavrukov *et al.* 2010), rice (Plett *et al.* 2010b) and *Arabidopsis thaliana* (Jha *et al.* 2010, Møller *et al.* 2009). In the case of grapevine and other woody perennials, such as citrus and avocado, effects of ion toxicity are usually considered to be associated with high shoot Cl^- concentrations (Downton 1977b, Iland *et al.* 2011, Storey and Walker 1998, Walker *et al.* 2010, White and Broadley 2001). Photosynthesis reduction in salt-stressed grapevine is widely considered to be highly correlated with laminae Cl^- (Downton *et al.* 1990, Fisarakis *et al.* 2001, Walker *et al.* 1997, Walker *et al.* 1981) as discussed

above, but in a study by Stevens *et al.* (2011), photosynthesis reduction was also associated with scion leaf Na⁺ accumulation on Ramsey rootstocks.

1.2.3 Salt problems – solutions

To manage saline soils, irrigation water containing low levels of dissolved salts should be used, and leaching practices applied to reduce salt contents in the rootzone (Iland *et al.* 2011). Leaching is considered an effective salt management technique which involves application of high quality irrigation water in excess of the plants water requirement to flush salts beyond the rootzone, although this practice is not suitable in areas with high groundwater tables (Lanyon 2011), or when water restrictions are in place, or where water supply is scarce. For soil salinity problems caused by high groundwater tables, using inter row crops with high transpiration rates in the vineyard can lower the water table, thus decreasing salt mobilisation by groundwater (McFarlane and Williamson 2002, Pannell and Ewing 2006).

Drip irrigation by more targeted application of water can increase the efficiency of water use and potentially decrease salt deposition into the soil via irrigation water. It eliminates the concerns of foliar salt accumulation attributed by overhead sprinklers, and the wetted areas are constantly leached which reduces the rootzone salt content. However, salt accumulation still occurs at the periphery of the wetted zone, which is a concern if this periphery is within the rootzone (Hanson and May 2011). Since drip irrigation techniques have been widely adopted in row crops including perennial horticulture and viticulture, water input to land has been significantly reduced in Australia, which also reduced the leaching effects, thus allowing rootzone salt accumulation in the long term (Biswas *et al.* 2008).

Other than soil salinity management, salt tolerance of grapevines can be another solution which is currently achieved by grafting to salt excluding rootstocks (Iland *et al.* 2011). Rootstocks will be discussed in the following section.

1.3 Grapevine salt tolerance

1.3.1 Salt tolerance of rootstocks

Salt exclusion capacity is considered an important indicator of rootstock salt tolerance (Teakle and Tyerman 2010). Black (1956) discovered that the plant *Atriplex hastate*, which is known to tolerate NaCl levels equivalent to sea water, had lower leaf Cl^- content than two other non-tolerant plant species under salt treatments. Furthermore, the mature leaves of *A. hastate* had significantly lower leaf Cl^- concentration than that in roots, despite the observation that Na^+ and K^+ concentrations in leaves and roots were similar. Grapevine rootstocks which can reduce scion Cl^- concentrations were initially observed by Sauer (1968) and Bernstein *et al.* (1969), and coupled to the fact that grapevines are generally relatively good at excluding Na^+ from the shoots, these combined properties of rootstocks are considered to constitute shoot salt exclusion (Greenway and Rogers 1963, Sauer 1968, Tregeagle *et al.* 2010, Walker *et al.* 2010, Walker *et al.* 2018). Downton (1977a) later conducted a study on petiole Cl^- concentrations of some self-rooted grapevines which were known to have nematode or phylloxera tolerance, and ranked the species in the order of ascending petiole Cl^- : *Vitis rupestris* < *V. berlandieri*, *V. riparia* < *V. candicans*, *V. champini*, *V. longii* < *V. cinerea*, *V. cordifolia* < *V. vinifera*. Data also suggested low scion Cl^- accumulation characteristics of the rootstocks Richter 99, Schwarzmann, SO4, Salt Creek (Ramsey) and Harmony (Downton 1977a). Antcliff *et al.* (1983) then investigated Cl^- accumulation patterns of *V. rupestris*, *V. berlandieri*, *V. champini* and *V. cinerea* and some hybrids involving these species, adding 110 Richter, 140 Ruggeri and 1103 Paulsen to the effective Cl^- excluding rootstock category.

Salt exclusion capacity is not the only indicator of salt tolerance. A study which grafted Colombard scions on 25 different rootstocks showed that yield performance under saline conditions correlated with rootstock vigour (Southey and Jooste 1991), thus root vigour and yield performance are also considered indicators of rootstock salt tolerance (Maas and Hoffman 1977, Southey and Jooste 1991, Walker *et al.* 2004, Walker *et al.* 2014, Zhang *et al.* 2002). Walker *et al.* (2014) conducted a 14-year long term trial which investigated the performance of 9 rootstocks (and own roots) grafted to Shiraz and Chardonnay scions under saline irrigation based on the shoot salt exclusion capacity (measured by trunk and juice Na^+ and Cl^- concentrations), yield and root-conferred

vigour (measured by pruning weight), which supported the relatively high salt tolerance of the rootstocks Ramsey, 1103 Paulsen, Schwarzmann and 140 Ruggeri. Salt exclusion capacity is also found to be affected by the scions. For example, scion differences were observed in trunk and juice Na^+ and Cl^- concentrations in a study involving two scions and several rootstocks (Walker *et al.* 2010), although the differences were found to diminish over long term salt exposure (Walker *et al.* 2010, Walker *et al.* 2014).

Although shoot Cl^- accumulation has been considered the major ionic concern for salt-stressed grapevines, it was later found that Na^+ may also be a problem for grapevines subjected to long term salinity. In the final 2 years of a 14-year study by Walker *et al.* (2014) using Chardonnay scions, the juice Na^+ concentration increased when compared to earlier results (Walker *et al.* 2010) on all rootstocks except for 1103 Paulsen. Furthermore, the juice Na^+ concentration was higher than that of Cl^- , which suggests that Na^+ accumulation is a significant concern under long-term saline irrigation. These results compare favourably with findings by Stevens *et al.* (2011), who showed that relative Na^+ accumulation for Colombard on Ramsey was more significant than Cl^- accumulation, and that laminar Na^+ accumulation correlated with yield reduction.

1.3.2 Inheritance of shoot salt exclusion

The inheritance of grapevine Cl^- exclusion was first studied by Newman and Antcliff (1984) on hybrids and backcrosses of *V. berlandieri* and *V. vinifera*. In the backcross progeny there was a distinct segregation which yielded two populations with low and high petiole Cl^- contents respectively, suggesting the trait was determined by a single dominant gene. Another study involving two families derived by backcrossing a different hybrid parent from the crosses between *V. berlandieri* and *V. vinifera* with the same *V. vinifera* variety suggested a single dominant gene derived from *V. berlandieri* in Cl^- exclusion inheritance in one case but not in the other which raised the question of modified phenotypic expression of a major gene (Sykes 1987). In contrast to these findings, Sykes (1985) suggested the possibility of a quantitative inheritance of this trait based on field and glasshouse trials on crosses involving Ramsey (*V. champini*), Villard Blanc (complex hybrid) and Sultana (*V. vinifera*). Gong *et al.* (2011) crossed the Cl^- excluder 140 Ruggeri with the Cl^- includer K51-40 and examined Cl^- exclusion ability of 60 progeny. The continuous variation in shoot Cl^- accumulation suggested that the Cl^- exclusion trait is controlled by multiple genes, which supported the findings of

Sykes (1985). Fort *et al.* (2015) conducted a study on 6 populations derived from 6 crosses of *Vitis* species, which also reported a continuous variation in Cl^- exclusion in the progeny. However, since the variation between replicates of the same genotype were relatively high, the possibility of single dominant gene inheritance pattern could not be eliminated (Fort *et al.* 2015). It is also possible that the genes controlling Cl^- exclusion may be species specific, or under epigenetic control, therefore no definitive statement on the inheritance profile can be made at this stage.

Na^+ exclusion is less studied compared to Cl^- exclusion in grapevine. Inheritance of citrus Na^+ and Cl^- exclusion has been studied which suggested that the inheritance of these traits are independent of each other, and that they are both controlled by multiple genes (Sykes 1992). Two unnamed CSIRO grapevine rootstocks, C5 and C7 are reported to be excellent salt excluders. Shiraz on C7 and Chardonnay on C5 accumulated very low Na^+ and Cl^- (< 50 mg/L) in grape juice, which suggested that the Na^+ and Cl^- exclusion traits can exist together (Walker *et al.* 2014).

However, recently, Henderson *et al.* (2018a) (Chapter 4) have identified a quantitative trait locus (QTL) named *NaE* which was responsible for the variations in grapevine shoot Na^+ accumulation. In a small biparental mapping population of the superior Cl^- excluder 140 Ruggeri and the poor Cl^- excluder rootstock K51-40, 70% of the variation in shoot Na^+ accumulation was associated with the *NaE*. A Na^+ transporter gene in the QTL was able to be functionally characterised, and its allelic variations were successfully linked to the shoot Na^+ accumulation (Henderson *et al.* 2018a).

1.3.3 Shoot salt exclusion mechanisms

The ability to reduce salt loading into the xylem is considered critical in plant salt tolerance. Ions can move across plant tissues through the extracellular space (apoplastic pathway) and via cytoplasmic bridges (through plasmodesmata) between cytoplasm of neighbouring cells (symplastic pathways) (Taiz *et al.* 2015). The way that ions pass through the root epidermis and cortex can be apoplastic, symplastic or a combination of both, but in order to enter the root stele, ions must travel symplastically through the endodermis due to the presence of the lignified or suberized Casparian strip which blocks the apoplastic pathway around endodermis cells (Taiz *et al.* 2015). In plant roots, SLAC and QUAC have been well characterised in barley; both root xylem SLAC (X-

SLAC) and X-QUAC could transport Cl^- and NO_3^- , and their anion transport rates are considered to be significant in reference to the xylem anion loading rate (Gilliham and Tester 2005, Köhler and Raschke 2000). In maize, NO_3^- and Cl^- loading to root xylem was found to be mainly controlled by xylem-parenchyma quickly-activating anion conductance (X-QUAC), which can be inhibited by a water stress and the application of ABA (Gilliham and Tester 2005).

Teakle *et al.* (2007) who studied two lotus species that differed in salt tolerance, found that Cl^- concentration in the xylem and shoots of the less tolerant species was 50 % higher than that in the more tolerant species when treated with 200 mM NaCl. Läubli *et al.* (2008) had similar observations in durum wheat, which showed an at least 3-fold xylem Na^+ and around 2.5- fold xylem Cl^- concentration difference between the tolerant and sensitive lines after 10 days of 50 mM NaCl treatment. These studies both suggest that having lower xylem salt concentrations is highly correlated with plant salt tolerance, but it was not specified if the low xylem salt concentration in tolerant lines was due to different xylem loading ability, or due to other factors such as differences in root salt efflux or ion compartmentation in root tissues.

Another mechanism for plants to reduce xylem loading, which ultimately reduces salt accumulation in shoots, is to reduce net salt uptake of roots which refers to the combination effects of salt influx and efflux. In a study by Abbaspour (2008b), the grapevine rootstock 1103 Paulsen had a higher root $^{36}\text{Cl}^-$ net influx rate than that of K51-40, despite the higher salt exclusion capacity and salt tolerance of 1103 Paulsen. It was later found that in 1103 Paulsen roots, Cl^- efflux from cytoplasm to apoplast was higher than that in K51-40, suggesting a contribution of root salt efflux in reducing shoot Cl^- concentration (Abbaspour *et al.* 2013). In a study of poplar, net Na^+ and Cl^- efflux were observed from the root apex of the salt tolerant *Populus euphratica* after 15 days of 100 mM NaCl treatment, but there was no significant efflux from that of salt sensitive *Populus popularis* (Sun *et al.* 2009). Therefore the salt efflux capacity in roots might be an important factor in plant salt tolerance.

Both intra- and inter-cellular compartmentation are considered to reduce xylem loading of salt. In terms of intracellular regulation, as mentioned above, it was suggested that the salt tolerant *Vitis* spp. rootstock 1103 Paulsen had a higher cytoplasm to vacuole Cl^- flux than that of K51-40 (Abbaspour *et al.* 2013). In an earlier study, the Na^+ and

Cl⁻ concentration in vacuoles of endodermis and pericycle cells of grapevine roots were significantly higher than the cytoplasmic concentrations, and the more tolerant genotype had a 17 % higher vacuolar Cl⁻ concentration in pericycle cells than that of the more sensitive genotype (Storey *et al.* 2003). In relation to intercellular compartmentation, the study by Storey *et al.* (2003) also found that the average Na⁺ and Cl⁻ concentrations in vacuoles of pericycle cells were more than double the concentrations in those of root endodermis in the grapevines under 25 mM NaCl stress, suggesting a role of the pericycle in reducing salt entering the xylem. In another study of durum wheat in 50 mM NaCl stress, it was found that in the more salt tolerant genotype with lower Na⁺ root-to-shoot translocation rate, Na⁺ concentration in roots peaked at the pericycle and decreased significantly at the xylem parenchyma, while in the salt sensitive high transport genotype, Na⁺ concentration peaked at the xylem parenchyma (Läuchli *et al.* 2008).

Another salt tolerance mechanism, other than reducing xylem loading of salt, is phloem recirculation, which transports salts out of the sensitive tissues in plants. It has potential to contribute to plant salt tolerance, however, since the phloem salt fluxes were found to be insignificant compared to the fluxes in xylem, its contribution to salt tolerance is considered limited (reviewed in Teakle and Tyerman 2010).

1.4 The role of anion transporters in chloride homeostasis

1.4.1 Active and passive transport of Cl⁻ across the plasma membrane

The plasma membrane of plant cells has a highly negative membrane potential which would be expected to drive cellular Cl⁻ efflux passively. Previous studies observed that when exposed to a sudden increase in extracellular Cl⁻ concentration, plant plasma membranes experience a rapid depolarisation followed by a slow hyperpolarisation during which the cytosolic Cl⁻ and H⁺ concentrations increased, which suggested a Cl⁻/nH⁺ symport mechanism of Cl⁻ uptake (Felle 1994, Sanders 1980). By calculating the free energy change, more than 1 H⁺ is required in the symport to accumulate Cl⁻ (Felle 1994). This Cl⁻ uptake is against the E_m difference and was strongly stimulated by ATP, which indicates its active transport nature (Sanders 1980). The slow

hyperpolarisation is the result of active H^+ export by plasma membrane H^+ -ATPase, given the evidence that membrane depolarisation was significantly accelerated in acidic medium by H^+ -ATPase inhibitors (Sanders 1980). When the concentration of Cl^- outside the cell is higher than that in the cytoplasm which makes the E_m more positive than the reversal potential of Cl^- , passive Cl^- influx would occur via the outwardly rectifying anion conductance (ORAC) which polarises the E_m (Skerrett and Tyerman 1994, Teakle and Tyerman 2010, Zhang *et al.* 2004). Lorenzen *et al.* (2004) observed an inhibitory effect on the passive Cl^- influx in root cytoplasm under salt stress when Ca^{2+} replaced the Na^+ and became the sole counter ion in the environment; hence it was speculated that the passive Cl^- influx was coupled by Na^+ . However, Teakle and Tyerman (2010) pointed out that in the study of Lorenzen *et al.* (2004), after 1.5 h exposure of plant cells to 100 mM NaCl, the reversal potential of Cl^- was reduced to -15 mV, which did not support passive Cl^- influx since it is unlikely that a viable cell can have an E_m so positive. Therefore, it is likely that passive Cl^- influx occurs only at the early stage of high external Cl^- exposure. When Cl^-_{cyt} concentration is stabilised under high external Cl^- , Cl^- influx becomes active (Teakle and Tyerman 2010).

1.4.2 Chloride channel (CLC)

CLC is a well-studied family of proteins in mammals and plants. In the model plant *A. thaliana*, 7 members of the CLC family have been identified (Hechenberger *et al.* 1996). Later in rice (*Oryza sativa*) and grapevine (*V. vinifera*), 7 CLC genes have also been identified respectively (Diédhiou and Gollmack 2006). CLC-4 and CLC-5 in mammals have been characterised as 2 Cl^-/H^+ antiporters (Henderson *et al.* 2014b, Picollo and Pusch 2005), and the bacterial *Escherichia coli* CLC1 was suggested as a 2 Cl^-/H^+ exchanger (Accardi and Miller 2004).

Several Arabidopsis CLC proteins, such as AtCLCa, AtCLCb and AtCLCc have been found to localise to the tonoplast and function in NO_3^- homeostasis (Geelen *et al.* 2000a, Harada *et al.* 2004, Von der Fecht-Bartenbach *et al.* 2010). The first CLC characterised in Arabidopsis, AtCLCa was found to be a 2 NO_3^-/H^+ antiporter which facilitates NO_3^- accumulation in vacuoles against the monovalent anion concentration gradient (De Angeli *et al.* 2006, Teakle and Tyerman 2010). Later, by promoter- β -glucuronidase enzyme (GUS) staining, AtCLCa was found to be expressed in guard cells in Arabidopsis cotyledons and mature leaves (Wege *et al.* 2014). The role of AtCLCa in

guard cells was also investigated in the same study. Since AtCLCa is known to function in vacuolar anion accumulation, it was expected that it functioned in stomatal opening. Interestingly, although experimental results supported the hypothesis, the results also suggested a role of AtCLCa in vacuolar anion efflux since the *atclca* knockout mutants had impaired stomatal closure under exposure to ABA (Wege *et al.* 2014). Interaction on the tonoplast between AtCLCa and open stomata 1 (OST1), an ABA-activated protein kinase that regulates stomatal aperture, was confirmed; phosphorylation of AtCLCa by OST1 increased AtCLCa dependent anion efflux from vacuoles (Mustilli *et al.* 2002, Wege *et al.* 2014).

There is evidence that some plant CLC proteins are involved in salt tolerance. AtCLCc is highly expressed in guard cells (Jossier *et al.* 2010). The *atclcc* mutants showed impaired stomatal movement in response to white light (which induces stomatal opening). AtCLCc was previously characterised to transport NO_3^- (De Angeli *et al.* 2006, Geelen *et al.* 2000b), but since supplementation with Cl^- rather than NO_3^- impaired stomatal aperture of the *atclcc* knockout mutants, the role of AtCLCc for stomata movement is considered dependent on Cl^- (Jossier *et al.* 2010). Although in that study the substrate of AtCLCc was not determined by electrophysiological methods, the expression level of *AtCLCc* was found up-regulated by salt stress; and the *atclcc* knockout mutant displayed lower biomass under salt stress, while this phenotype could be complemented by the over expression of *AtCLCc* (Jossier *et al.* 2010). This evidence suggests that AtCLCc may be involved in plant salt tolerance. AtCLCg is also tonoplast localised but it is highly expressed in the mesophyll, hydathodes and phloem rather than in the guard cells; the *atclcg* knockout mutant displayed reduced biomass and increased shoot Cl^- accumulation under NaCl stress, which suggested that it could play a role in salt tolerance (Nguyen *et al.* 2016). However, since the substrates of AtCLCg have not been characterised yet, the possible mechanism of its involvement in salt tolerance could only be speculated. Key residues have been found to determine the $\text{NO}_3^-/\text{Cl}^-$ selectivity in CLC proteins. Due to the differences in the amino acids of selectivity filters in the channel proteins, *Escherichia coli* CLC1 selects Cl^- over NO_3^- while AtCLCa selects NO_3^- over Cl^- (Accardi and Miller 2004, De Angeli *et al.* 2009). A serine/proline difference in the peptide sequence G(S/P)GIPE has been consistently found between mammalian CLC-5 isoforms and AtCLCa. When the proline in AtCLCa is mutated to serine, AtCLCa loses its selectivity of NO_3^- over Cl^- ; and when the serine

in CLC-5 is mutated to proline, CLC-5 gains NO_3^-/H^+ exchange efficiency (Bergsdorf *et al.* 2009a, Wege *et al.* 2010). The sequence GSGIPE was found in grapevine (*Vitis Vinifera*) VviCLCc1, VviCLCc2, VviCLCd and VviCLCg which suggests that these CLCs are likely to be Cl^- selective (Henderson *et al.* 2014b). It was also found that when an amino acid mutation E203A was induced at the gating glutamate of AtCLCa, the proton coupling character of this protein was lost, suggesting that AtCLCa is converted from an anion/proton antiporter to an anion channel by this mutation (Bergsdorf *et al.* 2009a). VviCLCg consists of A203 rather than E203, thus it is likely to be a Cl^- selective anion channel (Henderson *et al.* 2014b).

Plant CLCs have different expression patterns. Using reverse transcription polymerase chain reaction (RT-PCR), *AtCLCa-d* were found to have steady transcript abundance throughout the growth stages, while *AtCLCe-g* showed increased expression during plant growth (Lv *et al.* 2009). *AtCLCa, c, d* and *g* are consistently highly expressed in all tissue types tested. *AtCLCb* transcripts are predominantly expressed in roots, whereas *AtCLCe* transcripts are highly abundant only in leaves but not in other organs. *AtCLCf* is more highly expressed in roots, leaves and stems but less expressed in flowers and siliques (Lv *et al.* 2009). Using similar methods, *VviCLCc2* was found to be expressed only in the flowers and pre-veraison berries which suggest a reproductive role. *VviCLCf, g* and *c1* were highly expressed in all tissues including roots, and *VviCLCc1* and *g* transcripts were more abundant in stelar enriched part of roots. These results suggest the possibility of their involvement in grapevine salt exclusion, but the change in transcript abundance was not statistically significant in response to salt treatments (Henderson *et al.* 2014b).

1.4.3 Cation-chloride cotransporter (CCC)

Cation-chloride cotransporters (CCC) are secondary active transporters which transport K^+ and/or Na^+ coupled to Cl^- across membranes (Haas 1994). Depending on the co-transported cations, CCC consists of 3 groups, which are $\text{K}^+:\text{Cl}^-$ cotransporters (KCC), $\text{Na}^+:\text{Cl}^-$ cotransporters (NCC), and $\text{K}^+:\text{Na}^+:2\text{Cl}^-$ cotransporters (NKCC) (Colmenero-Flores *et al.* 2007). Functional characterisation of AtCCC showed that it belongs to the NKCC group and it is preferentially expressed in root and shoot vasculature. By knocking out *AtCCC* with T-DNA insertion, the Arabidopsis plants exhibited shorter organs including roots, inflorescence stem and siliques, and impaired seed development;

and the shoot/root Cl^- accumulation ratio in the mutant was significantly higher compared to the control under salt stress (Colmenero-Flores *et al.* 2007). Thus AtCCC is predicted to be involved in the active xylem retrieval of Cl^- . However, another study of AtCCC and VviCCC showed that both CCCs are localised to Golgi and *trans*-Golgi network (TGN) (Henderson *et al.* 2015), which suggests that these CCC proteins are unlikely to directly function in xylem Cl^- retrieval; and the VviCCC's transcript abundance in grapevine roots was not regulated by the Cl^- treatments. It was discussed that plant salt homeostasis can be regulated by endomembrane and endosome salt trafficking processes (Munns and Gilliham 2015); but the phenotypes of the Arabidopsis and rice *ccc* knockout mutants suggest that salt homeostasis is not the only processes disrupted (Chen *et al.* 2016, Colmenero-Flores *et al.* 2007, Henderson *et al.* 2018b). There are several proposed functions of the plant CCC proteins but not yet confirmed (reviewed in Henderson *et al.* 2018b), therefore it is uncertain whether they have roles in plant salt tolerance.

1.4.4 Aluminium-activated malate transporter (ALMT)

Some plants can increase their Al^{3+} tolerance by malate efflux from roots which forms nontoxic stable complexes with toxic Al^{3+} in soil (Sasaki *et al.* 2004). The wheat aluminium-activated malate transporter (*Triticum aestivum* ALMT1) was the first ALMT characterised; it localises to the root cell plasma membrane, and it was found to be responsible for Al^{3+} induced malate efflux and therefore considered to contribute to the Al^{3+} tolerance of the plants (Sasaki *et al.* 2004). Later more ALMT proteins were characterised; their substrate specificity varied and many have roles other than organic acid efflux for Al^{3+} tolerance (De Angeli *et al.* 2013a, De Angeli *et al.* 2013b, Ligaba *et al.* 2012). When *Zea mays* ALMT1 (ZmALMT1) was expressed in *Xenopus laevis* oocytes with decreasing extracellular Cl^- activities, the outward current was reduced (Piñeros *et al.* 2008). The same study also suggested that the selectivity of ZmALMT1 for malate over Cl^- reduces as external Cl^- concentration rises, which suggests a role of ALMT in Cl^- uptake at high extracellular Cl^- concentrations (Piñeros *et al.* 2008, Teakle and Tyerman 2010). The tonoplast localised AtALMT9 in Arabidopsis was characterised as a Cl^- channel which responds to cytosolic malate levels, and knock out of AtALMT9 impaired stomatal opening (De Angeli *et al.* 2013b). Then another study observed that AtALMT9 is highly expressed in the root stele and the *Atalmt9* knockout

mutant plants have reduced shoot Cl^- and Na^+ accumulation after salt treatments, which suggests that AtALMT9 could contribute to shoot Cl^- loading by vacuolar Cl^- sequestration in vascular cells (Baetz *et al.* 2016). AtALMT12 is another ALMT which does not function in Al^{3+} tolerance; it is highly expressed in the guard cells and was found to transport malate and Cl^- (Meyer *et al.* 2010, Sasaki *et al.* 2010). The mutant line *atalmt12* showed impaired stomata closure when exposed to darkness, CO_2 and ABA (Meyer *et al.* 2010). Given the Cl^- permeability and the root stelar expression of AtALMT12 (Meyer *et al.* 2010, Sasaki *et al.* 2010), it was proposed that AtALMT12 could potentially have a role in xylem loading for root-to-shoot Cl^- translocation (Li *et al.* 2017b).

1.4.5 Slow anion channel-associated channels (SLAC and SLAH)

Rapid (R) and slow (S)-type anion channels can participate in stomatal movement by anion efflux from guard cells. The activation time of R-type channels is in millisecond scale, while seconds are needed to activate S-type channels (reviewed in Kollist *et al.* 2014). In guard cells, anion efflux shifts the E_m more positive than the equilibrium potential of K^+ (E_K) which leads to K^+ efflux from guard cells, resulting in guard cell turgor loss and stomata closure (reviewed in Kollist *et al.* 2014). The stomata expressing slow-anion channel associated 1 (AtSLAC1) was found to affect guard cell anion homeostasis and the S-type anion currents, and was found to be essential for stomata's ability to respond to ozone, CO_2 and decreasing air humidity – so was proposed as the protein underlying this conductance (Negi *et al.* 2008, Vahisalu *et al.* 2008). Later AtSLAC1 was functionally characterised in *Xenopus* oocytes; it was found to be more permeable to NO_3^- than to Cl^- , and its anion transport activity is regulated by kinases and phosphatases (Geiger *et al.* 2009, Lee *et al.* 2009). The SLAC1 homologue AtSLAH3 is expressed in multiple tissue and cell types across the plant (Negi *et al.* 2008); it was found to induce NO_3^- dependent currents, and its anion transport activity is also regulated by kinases and phosphatases like AtSLAC1 (Geiger *et al.* 2011).

The SLAC1 homologue AtSLAH1 was only expressed in root vasculature (Negi *et al.* 2008). Qiu *et al.* (2016) discovered that the expression level of *AtSLAH1* was significantly down-regulated by salt stress, and the overexpression of *AtSLAH1* in the root stele mediated higher shoot Cl^- accumulation under salt stress. However, the

substrate of AtSLAH1 could not be found in the *Xenopus* oocyte system, even when co-expressed with two protein kinases. In the same study, the over-expression of the NO_3^- and Cl^- transporter gene *AtSLAH3* in the root stele did not affect the shoot NO_3^- levels; however, since the Cl^- accumulation was reduced, the over-expression of *AtSLAH3* resulted in a higher $\text{NO}_3^-/\text{Cl}^-$ ratio in shoots. In the same year, the expression patterns of AtSLAH1 and AtSLAH3 in roots were further characterised by Cubero-Font *et al.* (2016); both of them were expressed in the root xylem-pole parenchyma, therefore their interactions were studied. The expression of AtSLAH1 with AtSLAH3 in the *Xenopus* oocyte system was able to induce large Cl^- dependent currents in the absence of protein kinases, and it was proposed that AtSLAH1 and AtSLAH3 form the mechanism of gated NO_3^- and Cl^- loading to the root xylem (Cubero-Font *et al.* 2016), which could contribute to plant salt tolerance.

1.4.6 Nitrate transporter 1/peptide transporter family (NPF)

The Nitrate transporter 1/peptide transporter family (NPF) which has 8 subfamilies (NPF1-8) was defined to conform the nitrate/peptide transporter gene families into a unified nomenclature (Léran *et al.* 2014). Since most studies on nitrate/peptide transporters did not use this new classification system, some transporters will be discussed using the old family classification, but the new name will be included in parentheses.

A large gene family in plants, nitrate transporter (NRT), has two subclasses – the low affinity nitrate transporters NRT1, also known as NRT1/peptide transporter (NRT1/PTR), and the high or dual affinity NRT2. The first nitrate transporter isolated, chlorate resistant mutant 1 (CHL1, later renamed to AtNRT1.1 then renamed to AtNPF6.3), was shown to be a proton coupled nitrate transporter using the *Xenopus* oocyte system (Léran *et al.* 2014, Tsay *et al.* 1993, Tsay *et al.* 2007). Later, oligopeptide transporter encoding genes which share similarities with the sequence of *CHL1* have been found independently in animals, plants, fungi and bacteria, and these genes were grouped as *NRT1* family (Tsay *et al.* 1993, Tsay *et al.* 2007 and the refs. there in). More than 50 *NRT1* have been found in Arabidopsis and 80 have been found in rice, therefore it is not surprising that they have been found to have other functions and substrates other than NO_3^- (Tsay *et al.* 2007). *NRT2* in higher plants needs to be co-expressed with a second protein, nitrate assimilation related protein 2 (NAR2), to function as a

nitrate transporter (Miller *et al.* 2007, Quesada *et al.* 1994, Zhou *et al.* 2000). The *Xenopus* oocyte expression study of a *Aspergillus nidulans* *NRT2* has found that it functioned in Cl^- uptake in addition to NO_3^- uptake (Zhou *et al.* 2000). The Arabidopsis *NRT1.1* (*AtNPF6.3*) can function in auxin uptake in a nitrate regulated manner, which supported the hypothesis that NRTs are not selective for a single substrate (Krouk *et al.* 2010). In another study, an *NRT1* was found stably expressed in a salt excluding citrus rootstock but suppressed in a salt includer in growth medium containing 50 mM Cl^- (Brumos *et al.* 2009).

Although most NRT proteins are proton symporters, the Arabidopsis nitrate excretion transporter 1 (*AtNAXT1*, renamed to *AtNPF2.7*), was functionally characterised to be a passive nitrate uniporter, and is responsible for root NO_3^- efflux in acidic medium and when the cytoplasm is acidified (Segonzac *et al.* 2007, Teakle and Tyerman 2010). *AtNPF2.7* and 6 other genes, *AtNPF2.1* to *AtNPF2.6* are closely related, which form a clade in the *NPF2* subfamily (Henderson *et al.* 2014a, L eran *et al.* 2014). Later, 3 members of the clade, *AtNPF2.3*, *AtNPF2.4* and *AtNPF2.5* have been characterised (Li *et al.* 2016, Li *et al.* 2017a, Taochy *et al.* 2015). *AtNPF2.3* is NO_3^- selective and localised to the plasma membrane; *AtNPF2.3* is highly expressed in root pericycle cells, and when the loss-of-function mutants were exposed to salt stress, root to shoot NO_3^- translocation, shoot NO_3^- content and shoot biomass reduced, which suggests that *NPF2.3* has an important role in long distance NO_3^- transport which contributes to salt tolerance (Taochy *et al.* 2015). *AtNPF2.4* is a plasma membrane localised Cl^- selective transporter which also functions in passive Cl^- efflux from cells. The gene was highly expressed in the root stele, and shoot Cl^- accumulation positively correlated with the expression level of *AtNPF2.4*, which suggests a role of *AtNPF2.4* in long distance Cl^- transport from root to shoot (Li *et al.* 2016). *AtNPF2.5* was also plasma membrane localised but more highly expressed in the root cortex than in the stele; the gene expression level was found to negatively correlate with shoot Cl^- accumulation, therefore it was suggested that *AtNPF2.5* contributes to Cl^- extrusion from root cortical cell cytoplasm to the external medium (Li *et al.* 2017a).

1.5 Sodium homeostasis related genes

1.5.1 Cytoplasmic sodium extrusion and related genes

When root cells are exposed to relatively high extracellular Na^+ concentrations, the electrochemical gradient favours passive Na^+ influx across the plasma membrane (reviewed in Tyerman and Skerrett 1999). It is important for plant cells to maintain a high cytoplasmic K^+/Na^+ ratio for effective enzyme activities. Plants maintain low cytoplasmic Na^+ concentrations generally by actively exporting Na^+ across the plasma membrane and tonoplast, or by having a low membrane permeability to Na^+ (reviewed in Tyerman and Skerrett 1999). Na^+ sequestration into vacuoles is mainly mediated by the Na^+/H^+ antiporter NHX1 which was first identified in Arabidopsis (Apse *et al.* 1999, Gaxiola *et al.* 1999). AtNHX1 was found to localise to the tonoplast, and over expression of *AtNHX1* was found to complement the salt sensitive phenotype of the *nhx1* mutant yeasts and was able to sustain growth of Arabidopsis in up to 200 mM NaCl media (Apse *et al.* 1999, Gaxiola *et al.* 1999, Horie and Schroeder 2004). More recent data suggests that AtNHX1 has a predominant role in K^+ sequestration rather than Na^+ (Barragán *et al.* 2012). Na^+ extrusion via the plasma membrane, an important factor of salt tolerance, is mediated by the salt overly sensitive (SOS) pathway (Horie and Schroeder 2004, Wu *et al.* 1996). Characterisation of the Arabidopsis plasma membrane localised Na^+/H^+ antiporter SOS1 showed that *sos1* mutant plants were sensitive to Na^+ and Li^+ , and growth of these plants was negatively impacted on K^+ deficient media (Shi *et al.* 2000, Wu *et al.* 1996). AtSOS1 was then found to be a Na^+ transporter when expressed in yeast; it is preferentially expressed in the epidermis of the root tips and the xylem parenchyma, and shoot Na^+ within the *sos1* mutant plant accumulated differently in response to mild and high salt stress, hence it was suggested that AtSOS1 functions in root Na^+ efflux or xylem Na^+ loading depending on the environmental Na^+ concentrations (Shi *et al.* 2002). *SOS2* was found to encode a protein kinase, the mutation of which would result in higher sensitivity of plants to high external Na^+ and low K^+ (Liu *et al.* 2000). *SOS3* is a Ca^{2+} binding protein which physically interacts with *SOS2* and functions in Ca^{2+} dependent *SOS2* protein kinase activation (Halfter *et al.* 2000). Later a SOS signalling pathway was proposed that the Ca^{2+} sensor *SOS3* activates the *SOS2* protein kinase which phosphorylates the *SOS1* Na^+ transporter at the plasma membrane (Quintero *et al.* 2002).

However, more recent studies have found evidence to suggest that the signalling pathway that regulates Na⁺ fluxes through SOS1 is more complicated than the earlier findings. There was evidence that tonoplast Na⁺/H⁺ antiport activities are regulated by SOS2 independently of SOS3, which suggested that the SOS signalling pathway may also regulate tonoplast Na⁺ transport using a different mechanism (Qiu *et al.* 2004). A phospholipase D signalling pathway independent of the SOS2-SOS3 complex was also found to regulate SOS1 (Yu *et al.* 2010), which suggests that the effect of SOS1 on Na⁺ homeostasis may be regulated by a more sophisticated system (Ji *et al.* 2013).

1.5.2 High-affinity potassium transporter (HKT)

The high-affinity K⁺ transporter gene *HKT* was first isolated from wheat (*Triticum aestivum*) roots and was found to complement the K⁺ uptake defect of a mutant yeast strain on a low K⁺ medium (Schachtman and Schroeder 1994). It was originally named TaHKT1 which was characterised as a proton-K⁺ symporter (Schachtman and Schroeder 1994), but later it was shown to co-transport Na⁺ and K⁺ in *Xenopus* oocytes and yeast systems, and eventually renamed to TaHKT2;1 (Platten *et al.* 2006, Rubio *et al.* 1995, Waters *et al.* 2013, Yeo 2007). However, the findings in heterologous expression systems may not represent the true function of the HKTs *in planta*. Several heterologous expression studies found K⁺/Na⁺ symport activities of group 1 HKTs when expressed in yeast, but not in *Xenopus* oocytes, e.g. AtHKT1;1, HvHKT1;5 from barley (*Hordeum vulgare*), and OsHKT1;5 from rice. The characterised transport mechanisms may be specific to external ionic environments used in heterologous expression experiments, which may not be physiologically relevant (reviewed in Waters *et al.* 2013). Moreover, an earlier study following the first isolation of *HKT* tested the Na⁺ coupled K⁺ symport hypothesis *in planta*, but all terrestrial plant species tested were able to sustain K⁺ uptake in the absence of Na⁺, which suggested that either the HKT is not a K⁺/Na⁺ symporter or this HKT is not the major K⁺ uptake transporter (Maathuis *et al.* 1996).

HKTs are now classified into two subfamilies (Platten *et al.* 2006); the HKT1 group members are generally Na⁺ uniporters, while the HKT2 members are dual K⁺/Na⁺ transporters (can behave as low affinity Na⁺ uniporters at high Na⁺ concentration) (Waters *et al.* 2013). Class 1 and 2 HKT proteins were shown to have diverse expression patterns and electrophysiological properties (Jabnoue *et al.* 2009). Several HKT1s

were found to have the potential to contribute to plant salinity tolerance. AtHKT1;1 was expressed in the leaf and root vasculature and found to reduce shoot Na⁺ accumulation by retrieving Na⁺ from the transpiration stream (Berthomieu *et al.* 2003, Gong *et al.* 2004, Mäser *et al.* 2002a, Plett *et al.* 2010a, Sunarpi *et al.* 2005). Its orthologues OsHKT1;5, TmHKT1;4-A2, TmHKT1;5-A and TaHKT1;5-D were also found to contribute to shoot Na⁺ accumulation. OsHKT1;5 in rice was expressed in the root and basal node vasculature which was proposed to affect shoot Na⁺ accumulation by enabling Na⁺ retrieval from phloem (Kobayashi *et al.* 2017, Ren *et al.* 2005b). TmHKT1;4-A2 and TmHKT1;5-A in wheat were able to significantly decrease shoot Na⁺ concentrations (James *et al.* 2011, Munns *et al.* 2012); the knock-down of the wheat root stelar expressing *TaHKT1;5-D* was found to increase the shoot Na⁺ contents (Byrt *et al.* 2014).

Whilst the Arabidopsis genome possesses only a single HKT locus, other plant species contain multiple HKTs. The HKT family is likely to have an important role in long distance Na⁺ transport which contributes to plant salt tolerance (Horie and Schroeder 2004). Like rice and wheat, the grapevine genome contains multiple HKT loci, which may have different substrate affinities, tissue localisations and, therefore, diverse functions. Furthermore, the Na⁺ selectivity of class 1 HKTs has been attributed to S-G-G-G residues in the channel pore (Mäser *et al.* 2002b), but other amino acid residues may be crucial for functional properties such as substrate affinity, channel conductance and rectification. Recently, Henderson *et al.* (2018a) (Chapter 4) identified a QTL named *NaE* for grapevine leaf Na⁺ accumulation by examining the leaf Na⁺ contents in a population of 140 Ruggeri × K51-40 hybrids, within which 6 closely located *HKT1* genes were found. The root expressing *HKT1;1* encodes a plasma membrane localised Na⁺ transporter and was more highly expressed in the root stelar fraction than in the cortical fraction. Two key amino acid residues were also found to alter the Na⁺ rectification properties of the VisHKT1;1 allelic variants, and the allelic variation was linked to grapevine leaf Na⁺ accumulation. It was therefore proposed that HKT1;1 plays an important role in retrieving Na⁺ from the root xylem, which contributes to Na⁺ exclusion by reducing root-to-shoot Na⁺ translocation. However, using the *Xenopus* oocyte expression system, another root expressing *HKT* in the QTL, *VviHKT1;3*, was not found to be a Na⁺ and/or K⁺ transporter gene. The other *HKT1*s in the QTL remain uncharacterised, and their roles in grapevine Na⁺ homeostasis are not yet revealed.

1.6 Hypotheses generation and thesis outline

The above review suggests that many plant ion transporters have been found to affect salt accumulation in shoots, or to contribute to plant salt tolerance. The functional characterisation of some putative root expressing Na⁺ or Cl⁻ transporters could increase our knowledge of Na⁺ and Cl⁻ homeostasis in grapevines and could lead to the identification of genes with key roles in grapevine salt exclusion or salt tolerance.

To identify genes which could contribute to grapevine shoot Cl⁻ exclusion at the root level, a microarray gene expression study by Henderson *et al.* (2014a) compared the root gene expression levels between the Cl⁻ excluder rootstock 140 Ruggeri and the Cl⁻ includer K51-40. Several genes from the families with known Cl⁻ transporting or salt tolerance contributing members were found to be significantly more highly expressed in 140 Ruggeri than in K51-40. Two *ALMT* genes *VviALMT2* and *VviALMT8* were more highly expressed in 140 Ruggeri; given that *AtALMT9* was demonstrated to affect shoot Na⁺ and Cl⁻ accumulation under salt stress (Baetz *et al.* 2016), these two grapevine *ALMT*s could potentially have roles in regulating root-to-shoot salt transport. Two *AtNPF2.1* to *2.7* homologues, *VviNPF2.1* and *VviNPF2.2* were also more highly expressed in the roots of 140 Ruggeri, which suggests they could contribute to passive Cl⁻ efflux to the root apoplast and/or long distance Cl⁻ transport (Henderson *et al.* 2014a).

As already mentioned, the grapevine root expressing *HKT1;1* in the *NaE* QTL has recently been identified as a key gene in grapevine shoot Na⁺ accumulation (Henderson *et al.* 2018a). However, functions of the other closely located *HKT1* genes within the QTL have not yet been revealed. These *HKT1* genes can be considered to have potential roles in Na⁺ homeostasis, which could contribute to grapevine Na⁺ exclusion or partitioning.

In summary, the identified key facts and knowledge gaps are:

- a. Ion channels and/or transporters could contribute to shoot salt exclusion by ion extrusion from the roots, by participating in controlling ion movements from the cytosol of xylem parenchyma cells to the root xylem, or by sequestering ions into vacuoles of xylem parenchyma and/or cortical cells. Several plant gene

families including *ALMT*, *NPF* and *HKT* were found to have members which could alter plant shoot Na^+ and Cl^- concentration or could directly contribute to plant performance under salt stress. However, few of their grapevine homologues have been studied; although the grapevine *HKT1;1* has been linked to shoot Na^+ exclusion, the key genes for Cl^- exclusion in grapevine rootstocks remain to be uncovered.

- b. By characterising the substrates, the subcellular localisation, and the expression pattern of a putative ion transporter, its putative role in salt tolerance – as well as a possible mechanism of action – can be predicted with more certainty.
- c. The putative anion transporter genes *VviALMT2*, *VviALMT8*, *VviNPF2.1* and *VviNPF2.2* are significantly more highly expressed in the good Cl^- excluder 140 Ruggeri than in the poor excluder K51-40, and they have been proposed to participate in grapevine Cl^- exclusion. Plant *HKT1* transporters have been demonstrated to be highly relevant to shoot Na^+ accumulation and homeostasis. A better understanding of the grapevine salt exclusion mechanism can be achieved by functionally characterising these candidates.

The following hypotheses have been generated based on the facts and knowledge gaps:

- a. *VviALMT2*, *VviALMT8*, *VviNPF2.1* and *VviNPF2.2* are membrane Cl^- transporters which contribute to reducing grapevine root-to-shoot Cl^- transport.
- b. The grapevine *HKT1* members in the shoot Na^+ exclusion QTL are membrane Na^+ transporters which regulate grapevine Na^+ homeostasis.
- c. The functional characterisation of these putative ion transporters will lead to the discovery of key genes for grapevine salt tolerance, and will contribute to the development of genetic markers for breeding salinity tolerant grapevine rootstocks.

To test these hypotheses, this study aims to:

- a. To determine the sub-cellular localisation and substrates of the 4 putative anion transporters/channels,
- b. To ectopically express candidate genes from grapevine (and their promoters) in a model plant host, and investigate their physiological roles *in planta*,

- c. To functionally characterise the grapevine HKT1s and determine their Na⁺ transport activities in heterologous expression systems.

This thesis contains the work to achieve these goals. Here the outline of the thesis is presented:

- **Chapter 1** is a preliminary literature review to outline the known facts and knowledge gaps related to the genes contributing to plant and grapevine salt exclusion and tolerance (this chapter).
- **Chapter 2** investigates the function of VviALMT2 and VviALMT8 by an *in vitro* electrophysiological approach and by transient gene expression *in planta*.
- **Chapter 3** investigates the function of VviNPF2.1 and VviNPF2.2 using anion tracers, gene expression analyses and transient gene expression *in planta*.
- **Chapter 4** investigates a putative rectification regulating amino acid residue S506 on TaHKT1;5-D equivalent to the R534 in VisHKT1;1 using two electrode voltage clamping (my contribution to Henderson *et al.* (2018a)).
- **Chapter 5** investigates the localisation and function of the *HKT1s* other than HKT1;1 in the shoot Na⁺ exclusion QTL *NaE* by analysing their expression patterns and electrophysiological properties.
- **Chapter 6** develops an R-based app Smart-IV and an R package abftools for automated electrophysiological data analysis, and compares the data outputs with published data.
- **Chapter 7** summarises the major findings on the genes characterised in this study, and discusses the remaining questions and future directions.

Several appendices are also included of work conducted during my study but are incomplete or published works where I did not make the major contribution as follows:

- **Appendix I** investigates the effects of N-terminal YFP tagging on the localisation and function of the grapevine HKT1;1.
- **Appendix II** investigates the structural-functional properties of OsHKT1;3 and VviHKT1;3.

References

- Abbaspour, N.** (2008) A comparative study of Cl transport across the roots of two grapevine rootstocks, K 51-40 and Paulsen, differing in salt tolerance. In *Discipline of Wine and Horticulture*. Adelaide: University of Adelaide.
- Abbaspour, N., Kaiser, B. and Tyerman, S.** (2013) Chloride transport and compartmentation within main and lateral roots of two grapevine rootstocks differing in salt tolerance. *Trees*, **27**, 1317-1325.
- ABS** (2002) Salinity on Australian Farms, 2002: Australian Bureau of Statistics.
- Accardi, A. and Miller, C.** (2004) Secondary active transport mediated by a prokaryotic homologue of ClC Cl⁻ channels. *Nature*, **427**, 803-807.
- Allakhverdiev, S.I., Nishiyama, Y., Suzuki, I., Tasaka, Y. and Murata, N.** (1999) Genetic engineering of the unsaturation of fatty acids in membrane lipids alters the tolerance of *Synechocystis* to salt stress. *Proceedings of the National Academy of Sciences*, **96**, 5862-5867.
- Allakhverdiev, S.I., Sakamoto, A., Nishiyama, Y., Inaba, M. and Murata, N.** (2000a) Ionic and osmotic effects of NaCl-induced inactivation of photosystems I and II in *Synechococcus* sp. *Plant Physiology*, **123**, 1047-1056.
- Allakhverdiev, S.I., Sakamoto, A., Nishiyama, Y. and Murata, N.** (2000b) Inactivation of photosystems I and II in response to osmotic stress in *Synechococcus*. contribution of water channels. *Plant Physiology*, **122**, 1201-1208.
- Antcliff, A.J., Newman, H.P. and Barrett, H.C.** (1983) Variation in chloride accumulation in some American species of grapevine. *Vitis*, **22**, 357-362.
- Apse, M.P., Aharon, G.S., Snedden, W.A. and Blumwald, E.** (1999) Salt tolerance conferred by overexpression of a vacuolar Na⁺/H⁺ antiport in *Arabidopsis*. *Science*, **285**, 1256-1258.
- AWRI** (2015) Analytical requirements for the export of Australian wine: Sodium standards: The Australian Wine Research Institute.
- Baetz, U., Eisenach, C., Tohge, T., Martinoia, E. and De Angeli, A.** (2016) Vacuolar chloride fluxes impact ion content and distribution during early salinity stress. *Plant Physiology*.
- Barragán, V., Leidi, E.O., Andrés, Z., Rubio, L., De Luca, A., Fernández, J.A., Cubero, B. and Pardo, J.M.** (2012) Ion exchangers NHX1 and NHX2 mediate active potassium uptake into vacuoles to regulate cell turgor and stomatal function in *Arabidopsis*. *The Plant Cell*, **24**, 1127-1142.
- Bergsdorf, E.-Y., Zdebik, A.A. and Jentsch, T.J.** (2009) Residues important for nitrate/proton coupling in plant and mammalian CLC transporters. *Journal of Biological Chemistry*, **284**, 11184-11193.
- Bernstein, L., Ehlig, C.F. and Clark, R.A.** (1969) Effect of grape rootstocks on chloride accumulation in leaves. *Journal of the American Society for Horticultural Science*, **94**, 584-590.
- Berthomieu, P., Conéjéro, G., Nublat, A., Brackenbury, W.J., Lambert, C., Savio, C., Uozumi, N., Oiki, S., Yamada, K., Cellier, F., Gosti, F., Simonneau, T., Essah, P.A., Tester, M., Véry, A.-A., Sentenac, H. and Casse, F.** (2003) Functional analysis of AtHKT1 in *Arabidopsis* shows that Na⁺ recirculation by the phloem is crucial for salt tolerance. *The EMBO Journal*, **22**, 2004-2014.
- Biswas, T., Bourne, J., McCarthy, M. and Rengasamy, P.** (2008) Sustainable salinity management in your vineyard: South Australian Research and Development Institute.
- Black, R.** (1956) Effect of NaCl in Water Culture on the Ion Uptake and growth of *Atriplex* *Hastata* L. *Australian Journal of Biological Sciences*, **9**, 67-80.

- Bolaños, L., Martín, M., El-Hamdaoui, A., Rivilla, R. and Bonilla, I.** (2006) Nitrogenase inhibition in nodules from pea plants grown under salt stress occurs at the physiological level and can be alleviated by B and Ca. *Plant and Soil*, **280**, 135-142.
- Brumos, J., Colmenero-Flores, J.M., Conesa, A., Izquierdo, P., Sanchez, G., Iglesias, D.J., Lopez-Climent, M.F., Gomez-Cadenas, A. and Talon, M.** (2009) Membrane transporters and carbon metabolism implicated in chloride homeostasis differentiate salt stress responses in tolerant and sensitive *Citrus* rootstocks. *Functional & Integrative Genomics*, **9**, 293-309.
- Byrt, C., Xu, B., Krishnan, M., Lightfoot, D., Athman, A., Jacobs, A., Watson-Haigh, N., Munns, R., Tester, M. and Gilliam, M.** (2014) The Na⁺ transporter, TaHKT1;5-D, limits shoot Na⁺ accumulation in bread wheat. In *The Plant Journal*.
- Chen, Z.C., Yamaji, N., Fujii-Kashino, M. and Ma, J.F.** (2016) A cation-chloride cotransporter gene is required for cell elongation and osmoregulation in rice. *Plant Physiology*, **171**, 494-507.
- Colmenero-Flores, J.M., Martinez, G., Gamba, G., Vazquez, N., Iglesias, D.J., Brumos, J. and Talon, M.** (2007) Identification and functional characterization of cation-chloride cotransporters in plants. *The Plant Journal*, **50**, 278-292.
- Commonwealth of Australia** (2014) Wine production requirements (Australia only): Commonwealth of Australia.
- Cubero-Font, P., Maierhofer, T., Jaslan, J., Rosales, M.A., Espartero, J., Diaz-Rueda, P., Muller, H.M., Hurter, A.L., Al-Rasheid, K.A., Marten, I., Hedrich, R., Colmenero-Flores, J.M. and Geiger, D.** (2016) Silent S-Type anion channel subunit SLAH1 gates SLAH3 open for chloride root-to-shoot translocation. *Current Biology*, **26**, 2213-2220.
- De Angeli, A., Baetz, U., Francisco, R., Zhang, J., Chaves, M. and Regalado, A.** (2013a) The vacuolar channel VvALMT9 mediates malate and tartrate accumulation in berries of *Vitis vinifera*. *Planta*, **238**, 283-291.
- De Angeli, A., Monachello, D., Ephritikhine, G., Frachisse, J.M., Thomine, S., Gambale, F. and Barbier-Brygoo, H.** (2006) The nitrate/proton antiporter AtCLCa mediates nitrate accumulation in plant vacuoles. *Nature*, **442**, 939-942.
- De Angeli, A., Monachello, D., Ephritikhine, G., Frachisse, J.M., Thomine, S., Gambale, F. and Barbier-Brygoo, H.** (2009) CLC-mediated anion transport in plant cells. *Philosophical Transactions of the Royal Society B-Biological Sciences*, **364**, 195-201.
- De Angeli, A., Zhang, J., Meyer, S. and Martinoia, E.** (2013b) AtALMT9 is a malate-activated vacuolar chloride channel required for stomatal opening in *Arabidopsis*. *Nature Communications*, **4**, 1804.
- de Loryn, L.C., Petrie, P.R., Hasted, A.M., Johnson, T.E., Collins, C. and Bastian, S.E.P.** (2014) Evaluation of sensory thresholds and perception of sodium chloride in grape juice and wine. *American Journal of Enology and Viticulture*, **65**, 124-133.
- Diédhiou, C.J. and Gollack, D.** (2006) Salt-dependent regulation of chloride channel transcripts in rice. *Plant Science*, **170**, 793-800.
- Downton, W.J.S.** (1977a) Chloride accumulation in different species of grapevine. *Scientia Horticulturae*, **7**, 249-253.
- Downton, W.J.S.** (1977b) Photosynthesis in salt-stressed grapevines. *Functional Plant Biology*, **4**, 183-192.
- Downton, W.J.S. and Loveys, B.R.** (1981) Abscisic acid content and osmotic relations of salt-stressed grapevine leaves. *Functional Plant Biology*, **8**, 443-452.
- Downton, W.J.S., Loveys, B.R. and Grant, W.J.R.** (1990) Salinity effects on the stomatal behaviour of grapevine. *New Phytologist*, **116**, 499-503.
- Ehlig, C.F.** (1960) Effects of salinity on four varieties of table grapes grown in sand culture. In *Proceedings of the American Society for Horticultural Science*, pp. 323-331.

- FAO** (2005) Global network on integrated soil management for sustainable use of salt-affected soils: FAO Land and Plant Nutrition Management Services Rome.
- FAO** (2008) FAO Land and Plant Nutrition Management Service.
- Felle, H.H.** (1994) The H⁺/Cl⁻ symporter in root-hair cells of *sinapis alba* (an electrophysiological study using ion-selective microelectrodes). *Plant Physiology*, **106**, 1131-1136.
- Fisarakis, I., Chartzoulakis, K. and Stavrakas, D.** (2001) Response of Sultana vines (*V. vinifera* L.) on six rootstocks to NaCl salinity exposure and recovery. *Agricultural Water Management*, **51**, 13-27.
- Fort, K.P., Heinitz, C.C. and Walker, M.A.** (2015) Chloride exclusion patterns in six grapevine populations. *Australian Journal of Grape and Wine Research*, **21**, 147-155.
- Gaxiola, R.A., Rao, R., Sherman, A., Grisafi, P., Alper, S.L. and Fink, G.R.** (1999) The *Arabidopsis thaliana* proton transporters, AtNhx1 and Avp1, can function in cation detoxification in yeast. *Proceedings of the National Academy of Sciences*, **96**, 1480-1485.
- Geelen, D., Lurin, C., Bouchez, D., Frachisse, J.-M., Lelièvre, F., Courtial, B., Barbier-Brygoo, H. and Maurel, C.** (2000a) Disruption of putative anion channel gene AtCLC-a in *Arabidopsis* suggests a role in the regulation of nitrate content. *The Plant Journal*, **21**, 259-267.
- Geelen, D., Lurin, C., Bouchez, D., Frachisse, J.M., Lelievre, F., Courtial, B., Barbier-Brygoo, H. and Maurel, C.** (2000b) Disruption of putative anion channel gene *AtCLC-a* in *Arabidopsis* suggests a role in the regulation of nitrate content. *The Plant Journal*, **21**, 259-267.
- Geiger, D., Maierhofer, T., Al-Rasheid, K.A.S., Scherzer, S., Mumm, P., Liese, A., Ache, P., Wellmann, C., Marten, I., Grill, E., Romeis, T. and Hedrich, R.** (2011) Stomatal closure by fast abscisic acid signaling is mediated by the guard cell anion channel SLAH3 and the receptor RCAR1. *Science Signaling*, **4**, ra32-ra32.
- Geiger, D., Scherzer, S., Mumm, P., Stange, A., Marten, I., Bauer, H., Ache, P., Matschi, S., Liese, A. and Al-Rasheid, K.A.** (2009) Activity of guard cell anion channel SLAC1 is controlled by drought-stress signaling kinase-phosphatase pair. *Proceedings of the National Academy of Sciences*, **106**, 21425-21430.
- George, R., McFarlane, D. and Nulsen, B.** (1997) Salinity threatens the viability of agriculture and ecosystems in Western Australia. *Hydrogeology Journal*, **5**, 6-21.
- Gilliham, M. and Tester, M.** (2005) The regulation of anion loading to the maize root xylem. *Plant Physiology*, **137**, 819-828.
- Gong, H., Blackmore, D., Clingeleffer, P., Sykes, S., Jha, D., Tester, M. and Walker, R.** (2011) Contrast in chloride exclusion between two grapevine genotypes and its variation in their hybrid progeny. *Journal of Experimental Botany*, **62**, 989-999.
- Gong, J.M., Waner, D.A., Horie, T., Li, S.L., Horie, R., Abid, K.B. and Schroeder, J.I.** (2004) Microarray-based rapid cloning of an ion accumulation deletion mutant in *Arabidopsis thaliana*. *Proceedings of the National Academy of Sciences*, **101**, 15404-15409.
- Granett, J., Walker, M.A., Kocsis, L. and Omer, A.D.** (2001) Biology and management of grape phylloxera. *Annual Review of Entomology*, **46**, 387.
- Greenway, H. and Osmond, C.B.** (1972) Salt responses of enzymes from species differing in salt tolerance. *Plant Physiology*, **49**, 256-259.
- Greenway, H. and Rogers, A.** (1963) Growth and ion uptake of *Agropyron elongatum* on saline substrates, as compared with a salt-tolerant variety of *hordeum vulgare*. *Plant and Soil*, **18**, 21-30.
- Haas, M.** (1994) The Na-K-Cl cotransporters. *American Journal of Physiology-Cell Physiology*, **267**, C869-C885.

- Halfter, U., Ishitani, M. and Zhu, J.-K.** (2000) The Arabidopsis SOS2 protein kinase physically interacts with and is activated by the calcium-binding protein SOS3. *Proceedings of the National Academy of Sciences*, **97**, 3735-3740.
- Hanson, B. and May, D.** (2011) *Drip irrigation salinity management for row crops*: UCANR Publications.
- Harada, H., Kuromori, T., Hirayama, T., Shinozaki, K. and Leigh, R.A.** (2004) Quantitative trait loci analysis of nitrate storage in Arabidopsis leading to an investigation of the contribution of the anion channel gene, AtCLC-c, to variation in nitrate levels. *Journal of Experimental Botany*, **55**, 2005-2014.
- Hechenberger, M., Schwappach, B., Fischer, W.N., Frommer, W.B., Jentsch, T.J. and Steinmeyer, K.** (1996) A family of putative chloride channels from Arabidopsis and functional complementation of a yeast strain with a CLC gene disruption. *Journal of Biological Chemistry*, **271**, 33632-33638.
- Henderson, S.W., Baumann, U., Blackmore, D.H., Walker, A.R., Walker, R.R. and Gilliam, M.** (2014a) Shoot chloride exclusion and salt tolerance in grapevine is associated with differential ion transporter expression in roots. *BMC Plant Biology*, **14**.
- Henderson, S.W., Dunlevy, J.D., Wu, Y., Blackmore, D.H., Walker, R.R., Edwards, E.J., Gilliam, M. and Walker, A.R.** (2018a) Functional differences in transport properties of natural HKT1;1 variants influence shoot Na⁺ exclusion in grapevine rootstocks. *New Phytologist*, **217**, 1113-1127.
- Henderson, S.W., Gilliam, M., Tyerman, S.D. and Walker, R.** (2014b) Investigating genes encoding membrane proteins in grapevine (*Vitis vinifera* L.) and *Vitis spp.* rootstocks to determine their role in chloride exclusion.
- Henderson, S.W., Wege, S. and Gilliam, M.** (2018b) Plant cation-chloride cotransporters (CCC): evolutionary origins and functional insights. *International Journal of Molecular Sciences*, **19**, 492.
- Henderson, S.W., Wege, S., Qiu, J., Blackmore, D.H., Walker, A.R., Tyerman, S., Walker, R.R. and Gilliam, M.** (2015) Grapevine and Arabidopsis cation-chloride cotransporters localise to the Golgi and trans-Golgi network and indirectly influence long-distance ion homeostasis and plant salt tolerance. *Plant Physiology*.
- Horie, T. and Schroeder, J.I.** (2004) Sodium transporters in plants. Diverse genes and physiological functions. *Plant Physiology*, **136**, 2457-2462.
- Iland, P., Dry, P., Proffitt, T. and Tyerman, S.** (2011) *The grapevine: from the science to the practice of growing vines for wine*: Patrick Iland Wine Promotions.
- Jabnourne, M., Espeout, S., Mieulet, D., Fizames, C., Verdeil, J.-L., Conéjéro, G., Rodríguez-Navarro, A., Sentenac, H., Guiderdoni, E., Abdelly, C. and Véry, A.-A.** (2009) Diversity in expression patterns and functional properties in the rice HKT transporter family. *Plant Physiology*, **150**, 1955-1971.
- James, R.A., Blake, C., Byrt, C.S. and Munns, R.** (2011) Major genes for Na⁺ exclusion, *Nax1* and *Nax2* (wheat *HKT1;4* and *HKT1;5*), decrease Na⁺ accumulation in bread wheat leaves under saline and waterlogged conditions. *Journal of Experimental Botany*, **62**, 2939-2947.
- Jha, D., Shirley, N., Tester, M. and Roy, S.J.** (2010) Variation in salinity tolerance and shoot sodium accumulation in Arabidopsis ecotypes linked to differences in the natural expression levels of transporters involved in sodium transport. *Plant, Cell & Environment*, **33**, 793-804.
- Ji, H., Pardo, J.M., Batelli, G., Van Oosten, M.J., Bressan, R.A. and Li, X.** (2013) The Salt Overly Sensitive (SOS) pathway: Established and emerging roles. *Molecular Plant*, **6**, 275-286.
- Jossier, M., Kroniewicz, L., Dalmas, F., Le Thiec, D., Ephritikhine, G., Thomine, S., Barbier-Brygoo, H., Vavasseur, A., Filleur, S. and Leonhardt, N.** (2010) The Arabidopsis

- vacuolar anion transporter, AtCLCc, is involved in the regulation of stomatal movements and contributes to salt tolerance. *The Plant Journal*, **64**, 563-576.
- Kobayashi, N.I., Yamaji, N., Yamamoto, H., Okubo, K., Ueno, H., Costa, A., Tanoi, K., Matsumura, H., Fujii-Kashino, M., Horiuchi, T., Nayef, M.A., Shabala, S., An, G., Ma, J.F. and Horie, T.** (2017) OsHKT1;5 mediates Na⁺ exclusion in the vasculature to protect leaf blades and reproductive tissues from salt toxicity in rice. *The Plant Journal*, **91**, 657-670.
- Köhler, B. and Raschke, K.** (2000) The delivery of salts to the xylem. Three types of anion conductance in the plasmalemma of the xylem parenchyma of roots of barley. *Plant Physiology*, **122**, 243-254.
- Kollist, H., Nuhkat, M. and Roelfsema, M.R.G.** (2014) Closing gaps: linking elements that control stomatal movement. *New Phytologist*, **203**, 44-62.
- Krake, L.R., Scott, N.S., Rezaian, M.A. and Taylor, R.H.** (1999) *Graft-transmitted diseases of grapevines* Collingwood, Australia: CSIRO Publishing.
- Kriedemann, P.E., Loveys, B.R. and Downton, W.J.S.** (1975) Internal control of stomatal physiology and photosynthesis. II. Photosynthetic responses to phaseic acid. *Functional Plant Biology*, **2**, 553-567.
- Krouk, G., Lacombe, B., Bielach, A., Perrine-Walker, F., Malinska, K., Mounier, E., Hoyerova, K., Tillard, P., Leon, S., Ljung, K., Zazimalova, E., Benkova, E., Nacry, P. and Gojon, A.** (2010) Nitrate-regulated auxin transport by NRT1.1 defines a mechanism for nutrient sensing in plants. *Developmental Cell*, **18**, 927-937.
- Lanyon, D.** (2011) *Salinity management interpretation guide* Waite Campus, Adelaide: Arris Pty Ltd.
- Läuchli, A., James, R.A., Huang, C.X., McCully, M. and Munns, R.** (2008) Cell-specific localization of Na⁺ in roots of durum wheat and possible control points for salt exclusion. *Plant, Cell & Environment*, **31**, 1565-1574.
- Lee, S.C., Lan, W., Buchanan, B.B. and Luan, S.** (2009) A protein kinase-phosphatase pair interacts with an ion channel to regulate ABA signaling in plant guard cells. *Proceedings of the National Academy of Sciences*, **106**, 21419-21424.
- Léran, S., Varala, K., Boyer, J.-C., Chiurazzi, M., Crawford, N., Daniel-Vedele, F., David, L., Dickstein, R., Fernandez, E., Forde, B., Gassmann, W., Geiger, D., Gojon, A., Gong, J.-M., Halkier, B.A., Harris, J.M., Hedrich, R., Limami, A.M., Rentsch, D., Seo, M., Tsay, Y.-F., Zhang, M., Coruzzi, G. and Lacombe, B.** (2014) A unified nomenclature of NITRATE TRANSPORTER 1/PEPTIDE TRANSPORTER family members in plants. *Trends in plant science*, **19**, 5-9.
- Li, B., Byrt, C., Qiu, J., Baumann, U., Hrmova, M., Evrard, A., Johnson, A.A., Birnbaum, K.D., Mayo, G.M., Jha, D., Henderson, S.W., Tester, M., Gilliam, M. and Roy, S.J.** (2016) Identification of a stelar-localized transport protein that facilitates root-to-shoot transfer of chloride in Arabidopsis. *Plant Physiology*, **170**, 1014-1029.
- Li, B., Qiu, J., Jayakannan, M., Xu, B., Li, Y., Mayo, G.M., Tester, M., Gilliam, M. and Roy, S.J.** (2017a) AtNPF2.5 modulates chloride (Cl⁻) efflux from roots of *Arabidopsis thaliana*. *Frontiers in Plant Science*, **7**, 2013.
- Li, B., Tester, M. and Gilliam, M.** (2017b) Chloride on the move. *Trends in plant science*, **22**, 236-248.
- Ligaba, A., Maron, L., Shaff, J., Kochian, L. and Pineros, M.** (2012) Maize ZmALMT2 is a root anion transporter that mediates constitutive root malate efflux. *Plant, Cell & Environment*, **35**, 1185-1200.
- Liu, J., Ishitani, M., Halfter, U., Kim, C.-S. and Zhu, J.-K.** (2000) The *Arabidopsis thaliana* SOS2 gene encodes a protein kinase that is required for salt tolerance. *Proceedings of the National Academy of Sciences*, **97**, 3730-3734.

- Lorenzen, I., Aberle, T. and Plieth, C.** (2004) Salt stress-induced chloride flux: a study using transgenic *Arabidopsis* expressing a fluorescent anion probe. *The Plant Journal*, **38**, 539-544.
- Loveys, B.R. and Kriedemann, P.E.** (1974) Internal control of stomatal physiology and photosynthesis. I. Stomatal regulation and associated changes in endogenous levels of abscisic and phaseic acids. *Functional Plant Biology*, **1**, 407-415.
- Lv, Q.-d., Tang, R.-j., Liu, H., Gao, X.-s., Li, Y.-z., Zheng, H.-q. and Zhang, H.-x.** (2009) Cloning and molecular analyses of the *Arabidopsis thaliana* chloride channel gene family. *Plant Science*, **176**, 650-661.
- Maas, E.V. and Hoffman, G.J.** (1977) Crop salt tolerance - current assessment. *Journal of the irrigation and drainage division*, **103**, 115-134.
- Maathuis, F.J., Verlin, D., Smith, F.A., Sanders, D., Fernandez, J.A. and Walker, N.A.** (1996) The physiological relevance of Na⁺-coupled K⁺-transport. *Plant Physiology*, **112**, 1609-1616.
- Mäser, P., Eckelman, B., Vaidyanathan, R., Horie, T., Fairbairn, D.J., Kubo, M., Yamagami, M., Yamaguchi, K., Nishimura, M. and Uozumi, N.** (2002a) Altered shoot/root Na⁺ distribution and bifurcating salt sensitivity in *Arabidopsis* by genetic disruption of the Na⁺ transporter AtHKT1. *FEBS letters*, **531**, 157-161.
- Mäser, P., Hosoo, Y., Goshima, S., Horie, T., Eckelman, B., Yamada, K., Yoshida, K., Bakker, E.P., Shinmyo, A., Oiki, S., Schroeder, J.I. and Uozumi, N.** (2002b) Glycine residues in potassium channel-like selectivity filters determine potassium selectivity in four-loop-per-subunit HKT transporters from plants. *Proceedings of the National Academy of Sciences*, **99**, 6428-6433.
- McElrone, A.J., Choat, B., Gambetta, G.A. and Brodersen, C.R.** (2013) Water uptake and transport in vascular plants. *Nature Education Knowledge*, **4**.
- McFarlane, D.J. and Williamson, D.R.** (2002) An overview of water logging and salinity in southwestern Australia as related to the 'Ucarro' experimental catchment. *Agricultural Water Management*, **53**, 5-29.
- Meyer, S., Mumm, P., Imes, D., Endler, A., Weder, B., Al-Rasheid, K.A.S., Geiger, D., Marten, I., Martinoia, E. and Hedrich, R.** (2010) AtALMT12 represents an R-type anion channel required for stomatal movement in *Arabidopsis* guard cells. *The Plant Journal*, **63**, 1054-1062.
- Miller, A.J., Fan, X., Orsel, M., Smith, S.J. and Wells, D.M.** (2007) Nitrate transport and signalling. *Journal of Experimental Botany*, **58**, 2297-2306.
- Møller, I.S., Gilliam, M., Jha, D., Mayo, G.M., Roy, S.J., Coates, J.C., Haseloff, J. and Tester, M.** (2009) Shoot Na⁺ exclusion and increased salinity tolerance engineered by cell type-specific alteration of Na⁺ transport in *Arabidopsis*. *The Plant Cell*, **21**, 2163-2178.
- Munns, R.** (2005) Genes and salt tolerance: bringing them together. *New Phytologist*, **167**, 645-663.
- Munns, R.** (2011) Plant adaptations to salt and water stress: differences and commonalities. *Advances in Botanical Research*, **57**, 1-32.
- Munns, R. and Gilliam, M.** (2015) Salinity tolerance of crops – what is the cost? *New Phytologist*, **208**, 668-673.
- Munns, R. and James, R.A.** (2003) Screening methods for salinity tolerance: a case study with tetraploid wheat. *Plant and Soil*, **253**, 201-218.
- Munns, R., James, R.A. and Läuchli, A.** (2006) Approaches to increasing the salt tolerance of wheat and other cereals. *Journal of Experimental Botany*, **57**, 1025-1043.
- Munns, R., James, R.A., Xu, B., Athman, A., Conn, S.J., Jordans, C., Byrt, C.S., Hare, R.A., Tyerman, S.D., Tester, M., Plett, D. and Gilliam, M.** (2012) Wheat grain yield on saline soils is improved by an ancestral Na⁺ transporter gene. *Nature Biotechnology*, **30**, 360-364.

- Munns, R. and Sharp, R.E.** (1993) Involvement of abscisic acid in controlling plant growth in soil of low water potential. *Australian Journal of Plant Physiology*, **20**, 425-437.
- Munns, R. and Tester, M.** (2008) Mechanisms of salinity tolerance. In *Annual Review of Plant Biology*, pp. 651-681.
- Mustilli, A.-C., Merlot, S., Vavasseur, A., Fenzi, F. and Giraudat, J.** (2002) Arabidopsis OST1 protein kinase mediates the regulation of stomatal aperture by abscisic acid and acts upstream of reactive oxygen species production. *The Plant Cell*, **14**, 3089-3099.
- Negi, J., Matsuda, O., Nagasawa, T., Oba, Y., Takahashi, H., Kawai-Yamada, M., Uchimiya, H., Hashimoto, M. and Iba, K.** (2008) CO₂ regulator SLAC1 and its homologues are essential for anion homeostasis in plant cells. *Nature*, **452**, 483-U413.
- Neumann, P.M., Volkenburgh, E.V. and Cleland, R.E.** (1988) Salinity stress inhibits bean leaf expansion by reducing turgor, not wall extensibility. *Plant Physiology*, **88**, 233-237.
- Newman, H.P. and Antcliff, A.J.** (1984) Chloride accumulation in some hybrids and backcrosses of *Vitis berlandieri* and *Vitis vinifera*. *Vitis*, **23**, 106-112.
- Nguyen, C.T., Agorio, A., Jossier, M., Depré, S., Thomine, S. and Filleur, S.** (2016) Characterization of the chloride channel-like, AtCLCg, involved in chloride tolerance in *Arabidopsis thaliana*. *Plant and Cell Physiology*, **57**, 764-775.
- Ordish, G.** (1972) *The great wine blight*.
- Pannell, D.J. and Ewing, M.A.** (2006) Managing secondary dryland salinity: Options and challenges. *Agricultural Water Management*, **80**, 41-56.
- Papageorgiou, G.C., Alygizaki-Zorba, A., Ladas, N. and Murata, N.** (1998) A method to probe the cytoplasmic osmolality and osmotic water and solute fluxes across the cell membrane of cyanobacteria with chlorophyll a fluorescence: Experiments with *Synechococcus sp.* PCC7942. *Physiologia Plantarum*, **103**, 215-224.
- Piccolo, A. and Pusch, M.** (2005) Chloride/proton antiporter activity of mammalian CLC proteins CLC-4 and CLC-5. *Nature*, **436**, 420-423.
- Piñeros, M.A., Cañado, G.M.A., Maron, L.G., Lyi, S.M., Menossi, M. and Kochian, L.V.** (2008) Not all ALMT1-type transporters mediate aluminum-activated organic acid responses: the case of ZmALMT1 – an anion-selective transporter. *The Plant Journal*, **53**, 352-367.
- Platten, J.D., Cotsaftis, O., Berthomieu, P., Bohnert, H., Davenport, R.J., Fairbairn, D.J., Horie, T., Leigh, R.A., Lin, H.-X. and Luan, S.** (2006) Nomenclature for HKT transporters, key determinants of plant salinity tolerance. *Trends in plant science*, **11**, 372-374.
- Plett, D., Safwat, G., Gilliam, M., Skrumsager Møller, I., Roy, S., Shirley, N., Jacobs, A., Johnson, A. and Tester, M.** (2010a) Improved salinity tolerance of rice through cell type-specific expression of *AtHKT1;1*. *PLoS ONE*, **5**, e12571.
- Plett, D., Safwat, G., Gilliam, M., Skrumsager Møller, I., Roy, S., Shirley, N., Jacobs, A., Johnson, A. and Tester, M.** (2010b) Improved salinity tolerance of rice through cell type-specific expression of *AtHKT1;1*. *PLoS ONE*, **5**, e12571.
- Qiu, J., Henderson, S.W., Tester, M., Roy, S.J. and Gilliam, M.** (2016) SLAH1, a homologue of the slow type anion channel SLAC1, modulates shoot Cl⁻ accumulation and salt tolerance in *Arabidopsis thaliana*. *Journal of Experimental Botany*, **67**, 4495-4505.
- Qiu, Q.-S., Guo, Y., Quintero, F.J., Pardo, J.M., Schumaker, K.S. and Zhu, J.-K.** (2004) Regulation of vacuolar Na⁺/H⁺ exchange in *Arabidopsis thaliana* by the salt-overly-sensitive (SOS) pathway. *Journal of Biological Chemistry*, **279**, 207-215.
- Quesada, A., Galvan, A. and Fernandez, E.** (1994) Identification of nitrate transporter genes in *Chlamydomonas reinhardtii*. *The Plant Journal*, **5**, 407-419.
- Quintero, F.J., Ohta, M., Shi, H., Zhu, J.-K. and Pardo, J.M.** (2002) Reconstitution in yeast of the *Arabidopsis* SOS signaling pathway for Na⁺ homeostasis. *Proceedings of the National Academy of Sciences*, **99**, 9061-9066.

- Ren, Z.H., Gao, J.P., Li, L.G., Cai, X.L., Huang, W., Chao, D.Y., Zhu, M.Z., Wang, Z.Y., Luan, S. and Lin, H.X.** (2005) A rice quantitative trait locus for salt tolerance encodes a sodium transporter. *Nature Genetics*, **37**.
- Robinson, J.** (2006) *The Oxford companion to wine* 3rd edn. Oxford, New York: Oxford University Press.
- Rubio, F., Gassmann, W. and Schroeder, J.I.** (1995) Sodium-driven potassium uptake by the plant potassium transporter HKT1 and mutations conferring salt tolerance. *Science*, **270**, 1660-1663.
- Sanders, D.** (1980) The mechanism of Cl⁻ transport at the plasma membrane of *Chara corallina* L. Cotransport with H⁺. *The Journal of Membrane Biology*, **53**, 129-141.
- Sasaki, T., Mori, I.C., Furuichi, T., Munemasa, S., Toyooka, K., Matsuoka, K., Murata, Y. and Yamamoto, Y.** (2010) Closing plant stomata requires a homolog of an aluminum-activated malate transporter. *Plant and Cell Physiology*, **51**, 354-365.
- Sasaki, T., Yamamoto, Y., Ezaki, B., Katsuhara, M., Ahn, S.J., Ryan, P.R., Delhaize, E. and Matsumoto, H.** (2004) A wheat gene encoding an aluminum-activated malate transporter. *The Plant Journal*, **37**, 645-653.
- Sauer, M.R.** (1968) Effects of vine rootstocks on chloride concentration in Sultana scions. *Vitis*, **7**, 223-226.
- Schachtman, D.P. and Schroeder, J.I.** (1994) Structure and transport mechanism of a high-affinity potassium uptake transporter from higher plants. *Nature*, **370**, 655-658.
- Segonzac, C., Boyer, J.C., Ipotesi, E., Szponarski, W., Tillard, P., Touraine, B., Sommerer, N., Rossignol, M. and Gibrat, R.** (2007) Nitrate efflux at the root plasma membrane: identification of an *Arabidopsis* excretion transporter. *The Plant Cell*, **19**, 3760-3777.
- Shavrukov, Y., Gupta, N., Miyazaki, J., Baho, M., Chalmers, K., Tester, M., Langridge, P. and Collins, N.** (2010) HvNax3—a locus controlling shoot sodium exclusion derived from wild barley (*Hordeum vulgare* ssp. *spontaneum*). *Functional & Integrative Genomics*, **10**, 277-291.
- Shi, H., Ishitani, M., Kim, C. and Zhu, J.-K.** (2000) The *Arabidopsis thaliana* salt tolerance gene SOS1 encodes a putative Na⁺/H⁺ antiporter. *Proceedings of the National Academy of Sciences*, **97**, 6896-6901.
- Shi, H., Quintero, F.J., Pardo, J.M. and Zhu, J.-K.** (2002) The putative plasma membrane Na⁺/H⁺ antiporter SOS1 controls long-distance Na⁺ transport in plants. *The Plant Cell*, **14**, 465-477.
- Skerrett, M. and Tyerman, S.D.** (1994) A channel that allows inwardly directed fluxes of anions in protoplasts derived from wheat roots. *Planta*, **192**, 295-305.
- Southey, J.M. and Jooste, J.H.** (1991) The effect of grapevine rootstock on the performance of *Vitis vinifera* L.(cv. Colombard) on a relatively saline soil. *South African Society for Enology & Viticulture*, **12**, 32-40.
- Stevens, R.M., Harvey, G. and Partington, D.L.** (2011) Irrigation of grapevines with saline water at different growth stages: effects on leaf, wood and juice composition. *Australian Journal of Grape and Wine Research*, **17**, 239-248.
- Storey, R., Schachtman, D.P. and Thomas, M.R.** (2003) Root structure and cellular chloride, sodium and potassium distribution in salinized grapevines. *Plant Cell and Environment*, **26**, 789-800.
- Storey, R. and Walker, R.R.** (1998) Citrus and salinity. *Scientia Horticulturae*, **78**, 39-81.
- Suhayda, C.G., Giannini, J.L., Briskin, D.P. and Shannon, M.C.** (1990) Electrostatic changes in *Lycopersicon esculentum* root plasma membrane resulting from salt stress. *Plant Physiology*, **93**, 471-478.
- Sun, J., Chen, S., Dai, S., Wang, R., Li, N., Shen, X., Zhou, X., Lu, C., Zheng, X. and Hu, Z.** (2009) NaCl-induced alternations of cellular and tissue ion fluxes in roots of salt-resistant and salt-sensitive poplar species. *Plant Physiology*, **149**, 1141-1153.

- Sunarpi, Horie, T., Motoda, J., Kubo, M., Yang, H., Yoda, K., Horie, R., Chan, W.Y., Leung, H.Y., Hattori, K., Konomi, M., Osumi, M., Yamagami, M., Schroeder, J.I. and Uozumi, N.** (2005) Enhanced salt tolerance mediated by AtHKT1 transporter-induced Na⁺ unloading from xylem vessels to xylem parenchyma cells. *The Plant Journal*, **44**.
- Sykes, S.** (1992) The inheritance of salt exclusion in woody perennial fruit species. *Plant and Soil*, **146**, 123-129.
- Sykes, S.R.** (1985) Variation in chloride accumulation by hybrid vines from crosses involving the cultivars Ramsey, Villard Blanc, and Sultana. *American Journal of Enology and Viticulture*, **36**, 30-37.
- Sykes, S.R.** (1987) Variation in chloride accumulation in hybrids and backcrosses of *Vitis berlandieri* and *Vitis vinifera* under glasshouse conditions. *American Journal of Enology and Viticulture*, **38**, 313-320.
- Szabolcs, I.** (1989) *Salt-affected soils* Boca Raton, Florida: CRC Press, Inc.
- Taiz, L., Zeiger, E., Møller, I.M. and Murphy, A.S.** (2015) *Plant physiology and development* Sixth edn.: Sinauer Associates, Inc.
- Taochy, C., Gaillard, I., Ipotesi, E., Oomen, R., Leonhardt, N., Zimmermann, S., Peltier, J.B., Szponarski, W., Simonneau, T. and Sentenac, H.** (2015) The Arabidopsis root stele transporter NPF2.3 contributes to nitrate translocation to shoots under salt stress. *The Plant Journal*, **83**, 466-479.
- Teakle, N., Flowers, T., Real, D. and Colmer, T.** (2007) *Lotus tenuis* tolerates the interactive effects of salinity and waterlogging by 'excluding' Na⁺ and Cl⁻ from the xylem. *Journal of Experimental Botany*, **58**, 2169-2180.
- Teakle, N.L. and Tyerman, S.D.** (2010) Mechanisms of Cl⁻ transport contributing to salt tolerance. *Plant, Cell & Environment*, **33**, 566-589.
- The International Organisation of Vine and Wine** (2011) Compendium of international methods of analysis-OIV: Maximum acceptable limits of various substances contained in wine: International Organisation of Vine and Wine.
- The International Organisation of Vine and Wine** (2015) International code of oenological practices: maximum acceptable limits International Organisation of Vine and Wine.
- Tregeagle, J.M., Tisdall, J.M., Tester, M. and Walker, R.R.** (2010) Cl⁻ uptake, transport and accumulation in grapevine rootstocks of differing capacity for Cl⁻-exclusion. *Functional Plant Biology*, **37**, 665-673.
- Tsay, Y.-F., Schroeder, J.I., Feldmann, K.A. and Crawford, N.M.** (1993) The herbicide sensitivity gene CHL1 of arabidopsis encodes a nitrate-inducible nitrate transporter. *Cell*, **72**, 705-713.
- Tsay, Y.F., Chiu, C.C., Tsai, C.B., Ho, C.H. and Hsu, P.K.** (2007) Nitrate transporters and peptide transporters. *FEBS letters*, **581**, 2290-2300.
- Tyerman, S.D. and Skerrett, I.M.** (1999) Root ion channels and salinity. *Scientia Horticulturae*, **78**, 175-235.
- Vahisalu, T., Kollist, H., Wang, Y.F., Nishimura, N., Chan, W.Y., Valerio, G., Lamminmaki, A., Brosche, M., Moldau, H., Desikan, R., Schroeder, J.I. and Kangasjarvi, J.** (2008) SLAC1 is required for plant guard cell S-type anion channel function in stomatal signalling. *Nature*, **452**, 487-491.
- Von der Fecht-Bartenbach, J., Bogner, M., Dynowski, M. and Ludewig, U.** (2010) CLC-b-mediated NO₃⁻/H⁺ exchange across the tonoplast of *Arabidopsis* vacuoles. *Plant and Cell Physiology*, **51**, 960-968.
- Walker, G.R., Gilfedder, M. and Williams, J.** (1999) *Effectiveness of current farming systems in the control of dryland salinity*: CSIRO Land and Water.
- Walker, R.R., Blackmore, D.H. and Clingeleffer, P.R.** (2010) Impact of rootstock on yield and ion concentrations in petioles, juice and wine of Shiraz and Chardonnay in different

- viticultural environments with different irrigation water salinity. *Australian Journal of Grape and Wine Research*, **16**, 243-257.
- Walker, R.R., Blackmore, D.H., Clingeleffer, P.R. and Correll, R.L.** (2002) Rootstock effects on salt tolerance of irrigated field-grown grapevines (*Vitis vinifera* L. cv. Sultana): 1. Yield and vigour inter-relationships. *Australian Journal of Grape and Wine Research*, **8**, 3-14.
- Walker, R.R., Blackmore, D.H., Clingeleffer, P.R. and Correll, R.L.** (2004) Rootstock effects on salt tolerance of irrigated field-grown grapevines (*Vitis vinifera* L. cv. Sultana) 2. Ion concentrations in leaves and juice. *Australian Journal of Grape and Wine Research*, **10**, 90-99.
- Walker, R.R., Blackmore, D.H., Clingeleffer, P.R. and Emanuelli, D.** (2014) Rootstock type determines tolerance of Chardonnay and Shiraz to long-term saline irrigation. *Australian Journal of Grape and Wine Research*, **20**, 496-506.
- Walker, R.R., Blackmore, D.H., Clingeleffer, P.R. and Iacono, F.** (1997) Effect of salinity and Ramsey rootstock on ion concentrations and carbon dioxide assimilation in leaves of drip-irrigated, field-grown grapevines (*Vitis vinifera* L. cv. Sultana). *Australian Journal of Grape and Wine Research*, **3**, 66-74.
- Walker, R.R., Blackmore, D.H., Gong, H., Henderson, S.W., Gilliham, M. and Walker, A.R.** (2018) Analysis of the salt exclusion phenotype in rooted leaves of grapevine (*Vitis* spp.). *Australian Journal of Grape and Wine Research*, **24**, 317-326.
- Walker, R.R., Torokfalvy, E., Scott, N.S. and Kriedemann, P.E.** (1981) An analysis of photosynthetic response to salt treatment in *Vitis vinifera*. *Functional Plant Biology*, **8**, 359-374.
- Waters, S., Gilliham, M. and Hrmova, M.** (2013) Plant High-Affinity Potassium (HKT) Transporters involved in salinity tolerance: structural insights to probe differences in ion selectivity. *International Journal of Molecular Sciences*, **14**, 7660-7680.
- Wege, S., De Angeli, A., Droillard, M.-J., Kroniewicz, L., Merlot, S., Cornu, D., Gambale, F., Martinoia, E., Barbier-Brygoo, H., Thomine, S., Leonhardt, N. and Filleur, S.** (2014) Phosphorylation of the vacuolar anion exchanger AtCLCa is required for the stomatal response to abscisic acid.
- Wege, S., Jossier, M., Filleur, S., Thomine, S., Barbier-Brygoo, H., Gambale, F. and De Angeli, A.** (2010) The proline 160 in the selectivity filter of the *Arabidopsis* NO₃⁻/H⁺ exchanger AtCLCa is essential for nitrate accumulation in planta. *The Plant Journal*, **63**, 861-869.
- White, P. and Broadley, M.** (2001) Chloride in soils and its uptake and movement within the plant: a review. *Annals of Botany*, **88**, 967-988.
- Wine Australia** (2018) National Vintage Report 2018: Wine Australia.
- Woodham, R.C.** (1956) The chloride status of the irrigated sultana vine and its relation to vine health. *Australian Journal of Agricultural Economics*, **7**, 414-427.
- Wu, S.-J., Ding, L. and Zhu, J.-K.** (1996) SOS1, a genetic locus essential for salt tolerance and potassium acquisition. *The Plant Cell*, **8**, 617-627.
- Yeo, A.R.** (2007) Salinity. In *Plant Solute Transport*. Oxford: Blackwell publishing, pp. 340-370.
- Yu, L., Nie, J., Cao, C., Jin, Y., Yan, M., Wang, F., Liu, J., Xiao, Y., Liang, Y. and Zhang, W.** (2010) Phosphatidic acid mediates salt stress response by regulation of MPK6 in *Arabidopsis thaliana*. *New Phytologist*, **188**, 762-773.
- Zhang, W.-H., Ryan, P.R. and Tyerman, S.D.** (2004) Citrate-Permeable Channels in the Plasma Membrane of Cluster Roots from White Lupin. *Plant Physiology*, **136**, 3771-3783.
- Zhang, X.K., Walker, R.R., Stevens, R.M. and Prior, L.D.** (2002) Yield-salinity relationships of different grapevine (*Vitis vinifera* L.) scion-rootstock combinations. *Australian Journal of Grape and Wine Research*, **8**, 150-156.

- Zhou, J., Trueman, L.J., Boorer, K.J., Theodoulou, F.L., Forde, B.G. and Miller, A.J.** (2000) A high affinity fungal nitrate carrier with two transport mechanisms. *Journal of Biological Chemistry*, **275**, 39894-39899.
- Ziska, L.H., Seemann, J.R. and DeJong, T.M.** (1990) Salinity induced limitations on photosynthesis in *Prunus salicina*, a deciduous tree species. *Plant Physiology*, **93**, 864-870.

Chapter 2: Expression of the grapevine stelar localised anion transporter ALMT2 in Arabidopsis roots reduced shoot Cl⁻ accumulation under salt stress

Yue Wu¹, Sam W Henderson¹, Rob R Walker², Matthew Gilliam^{1,*}

¹ ARC Centre of Excellence in Plant Energy Biology, School of Agriculture, Food and Wine, University of Adelaide, Glen Osmond, South Australia 5064, Australia

² CSIRO Agriculture and Food, Locked Bag 2, Glen Osmond, South Australia 5064, Australia

* Correspondence should be addressed to:

Professor Matthew Gilliam

Email: matthew.gilliam@adelaide.edu.au

Phone: +61 8 8313 8145

Email addresses:

YW: yue.wu@adelaide.edu.au

SWH: sam.henderson@adelaide.edu.au

RRW: rob.walker@csiro.au

MG: matthew.gilliam@adelaide.edu.au

Running title: VviALMT2 reduced shoot Cl⁻ accumulation under salt stress

Key words: nitrate transporter, chloride exclusion, grapevine, ALMT

Statement of Authorship

Title of Paper	Expression of the grapevine vasculature localised anion transporter ALMT2 in Arabidopsis roots reduced shoot Cl ⁻ accumulation under salt stress
Publication Status	<input type="checkbox"/> Published <input type="checkbox"/> Accepted for Publication <input type="checkbox"/> Submitted for Publication <input checked="" type="checkbox"/> Unpublished and Unsubmitted work written in manuscript style
Publication Details	Wu, Y, Henderson, S.W., Walker, R.R., Gilliam, M (2019) Expression of the grapevine vasculature localised anion transporter ALMT2 in Arabidopsis roots reduced shoot Cl ⁻ accumulation under salt stress.

Principal Author

Name of Principal Author (Candidate)	Yue Wu		
Contribution to the Paper	Designed and performed all experiments, analysed the data and wrote the manuscript.		
Overall percentage (%)	75		
Certification:	This paper reports on original research I conducted during the period of my Higher Degree by Research candidature and is not subject to any obligations or contractual agreements with a third party that would constrain its inclusion in this thesis. I am the primary author of this paper.		
Signature		Date	02.07.2019

Co-Author Contributions

By signing the Statement of Authorship, each author certifies that:

- i. the candidate's stated contribution to the publication is accurate (as detailed above);
- ii. permission is granted for the candidate to include the publication in the thesis; and
- iii. the sum of all co-author contributions is equal to 100% less the candidate's stated contribution.

Name of Co-Author	Sam Henderson		
Contribution to the Paper	Contributed to project conception, contributed to the design of experiments, supervised the research and assisted in editing the manuscript.		
Signature		Date	02/07/2019

Name of Co-Author	Rob Walker		
-------------------	------------	--	--

Contribution to the Paper	Supervised the research and assisted in editing the manuscript.		
Signature		Date	5/7/19

Name of Co-Author	Matthew Gilliam		
Contribution to the Paper	Conceived the project, contributed to the design of experiments, supervised the research and assisted in editing the manuscript.		
Signature		Date	01.07.2019

Abstract

Grapevines (*Vitis vinifera*) are economically important crop plants which, when challenged with salt (sodium chloride, NaCl) in soil or irrigation water, tend to accumulate the constituent ions in shoots and berries, and suffer from yield reduction. Grapevine (*Vitis* spp.) rootstocks are known to vary in their capacity for shoot Cl^- exclusion; the rootstock 140 Ruggeri has a superior ability to exclude shoot Cl^- under salt stress compared to K51-40, which accumulates high shoot $[\text{Cl}^-]$ concentrations. Here, two putative anion transporter genes were characterised – Aluminium-activated Malate Transporter family members *VviALMT2* and *VviALMT8* – that were differentially expressed in roots of 140 Ruggeri and K51-40, to find out if they have a role in shoot Cl^- exclusion. By using the *Xenopus* oocyte expression system and two-electrode voltage clamping, *VviALMT2* and *VviALMT8* were found to be permeable to NO_3^- and Cl^- . Gene expression analyses using RT-qPCR revealed that *VviALMT8* was equally expressed between the root vasculature and the cortex and epidermis, whereas *VviALMT2* was more highly expressed in the root vasculature associated cells. *VviALMT8* was localised to a non-identifiable intracellular body, so was not studied further, whereas *VviALMT2* was localised to the plasma membrane. *VviALMT2* expression was up-regulated by high $[\text{NO}_3^-]$ re-supply post starvation. It was found that expression of *VviALMT2* specifically in the Arabidopsis root stele reduced shoot $[\text{Cl}^-]$ after NaCl treatment, which suggests that *VviALMT2* can be beneficial to plants under salt stress, and it could potentially be developed into a gene-based molecular marker for rootstock breeding in the future.

Introduction

Saline soil and irrigation water can have significant negative impacts on crop plants (Munns and Gilliham 2015). Grapevines are economically and socially important for the production of wine grapes, table grapes, and dried fruit, and are considered to be moderately sensitive to salt (Maas and Hoffman 1977). During salt stress, grapevines can suffer from osmotic stress and NaCl toxicity leading to a growth reduction (Prior *et al.* 1992b), poor fruit set (Baby *et al.* 2016) and low yields (Prior *et al.* 1992a, Stevens *et al.* 2011, Walker *et al.* 2002b). When grape berries accumulate excessive amounts of salt, this can: contribute to undesirable sensory attributes such as salty and soapy flavours in berries and wine; reduce yeast growth and result in incomplete conversion of sugar into alcohol during fermentation; and, result in finished wines that contain Na⁺ and Cl⁻ concentrations above legal thresholds (de Loryn *et al.* 2014, Donkin *et al.* 2010, Leske *et al.* 1997, Li *et al.* 2013, Walker *et al.* 2003). Currently, several practices are used to overcome salinity in vineyards. For example, root-zone salts can be leached with high-quality water (Lanyon 2011), salinity caused by a high groundwater table can be managed by planting inter-row crops (McFarlane and Williamson 2002, Pannell and Ewing 2006), and the total salt input into the root-zone can be reduced by using less irrigation water (Hanson and May 2011). Furthermore, salt tolerant rootstocks that exclude salts from the shoot and berries of *Vitis vinifera* scions grafted onto to the rootstocks can be used to achieve healthier vine growth and low salt wines in salt affected regions. Recent studies have focussed on identifying key genes that enable *Vitis* interspecific (*Vis*) grapevine rootstocks to confer shoot salt exclusion to *V. vinifera* scions. The gene *VisHKT1;1*, which encodes a sodium (Na⁺) transporter, has been identified as being important for conferring a large component of the shoot Na⁺ exclusion trait (Henderson *et al.* 2018a), and has potential for use as a genetic marker for rootstock breeding.

The genetic basis for shoot chloride (Cl⁻) exclusion in grapevine rootstocks and other plants is not as well understood as it is for shoot Na⁺ exclusion; the key genes that control long-distance Cl⁻ transport are only just beginning to emerge (Cubero-Font *et al.* 2016, Li *et al.* 2016, Li *et al.* 2017b, Qiu *et al.* 2016, reviewed in Wege *et al.* 2017). Gong *et al.* (2011) crossed two contrasting grapevine rootstocks – the good Cl⁻ excluder 140 Ruggeri and the poor Cl⁻ excluder K51-40 – and tested the leaf Cl⁻ concentration

[Cl⁻] of the hybrids. In that study, there was no clear segregation of the leaf [Cl⁻] trait, which suggested that grapevine shoot Cl⁻ exclusion in that population was likely to be controlled by multiple genes. The major mechanism conferring shoot Cl⁻ exclusion from the grapevine variety 140 Ruggeri compared to K51-40 is reduced Cl⁻ loading of the root xylem (Gong *et al.* 2011), which is predicted to be controlled through the activity of ion channels moving Cl⁻ down its electrochemical gradient from the stelar symplast to xylem apoplast (Gilliham and Tester 2005, Li *et al.* 2017b). Henderson *et al.* (2014a) compared the gene expression profiles between the roots of 140 Ruggeri and K51-40 using microarray hybridisation. A number of genes, predicted to encode membrane-embedded transport proteins, were found to be more highly expressed in the good excluder 140 Ruggeri compared to K51-40. It was hypothesised that by examining the tissue and subcellular localisation, and substrate specificity of the transport proteins differentially expressed between the roots of the two grapevine varieties, the candidate genes capable of directly mediating anion transport to the shoot or its exclusion could be confirmed. However, this hypothesis was not examined by functional testing until now.

Two putative anion transporters from the Aluminium-activated Malate Transporter family, *Vitis vinifera* (*Vvi*) *VviALMT2* and *VviALMT8*, were considered to be priority candidates (Henderson *et al.* 2014a), and have therefore been selected here for further investigation. The first ALMT characterised was a malate transporter from wheat (*Triticum aestivum*, *Ta*, *TaALMT1*) which excretes malate from the root to chelate the toxic ion Al³⁺ (Sasaki *et al.* 2004). Subsequently, it has emerged that most members of the ALMT family are not activated by Al³⁺, transport a range of substrates including malate, tartrate, NO₃⁻ and Cl⁻, and have a variety of physiological roles including stomatal pore regulation (De Angeli *et al.* 2013b), plant nutrient homeostasis (Ligaba *et al.* 2012) and fruit organic acid accumulation (De Angeli *et al.* 2013a). Recently, ALMTs have been shown to be regulated by GABA (Ramesh *et al.* 2015) and (*Arabidopsis thaliana*, *At*) *AtALMT9* from *Arabidopsis* has been implicated in salt tolerance (Baetz *et al.* 2016); *AtALMT12* has also been proposed to load anions to the root xylem to enable their root to shoot transport (Li *et al.* 2017b). Therefore, it was investigated whether *VviALMT2* and *VviALMT8* are involved in anion transport and shoot Cl⁻ exclusion in grapevine, and whether they could potentially be developed into gene-based molecular markers for breeding superior rootstock germplasm in the future.

Materials and methods

Gene cloning and plasmid construction

The coding sequences of *VviALMT2* (VIT_06s0009g00450) and *VviALMT8* (VIT_08s0105g00250) and their respective promoters were amplified from *Vitis vinifera* (cv. Cabernet Sauvignon) root cDNA with Phusion High-Fidelity DNA Polymerase (New England Biolabs), using the primers in Table S1. The PCR products were A-tailed using Taq DNA Polymerase with ThermoPol Buffer (NEB) and were ligated into the vector *pCR8* using *pCR8/GW/TOPO* TA Cloning Kit (Thermo Fisher Scientific); the promoters were ligated into the vector *pENTR* using the *pENTR/D-TOPO* Cloning Kit (Invitrogen). One Shot TOP10 *Escherichia coli* (Invitrogen) were transformed with the entry vectors as per manufacturer's instructions. Plasmids were harvested using an ISOLATE II Plasmid Mini Kit (Bioline), and successful cloning was confirmed by Sanger sequencing.

Subcellular localisation in tobacco (*Nicotiana benthamiana*) leaf epidermal cells

The *VviALMT2* and *VviALMT8* CDS in *pCR8* vectors were recombined into both *pMDC43* and *pMDC83* using LR Clonase II (Life Technologies) to generate binary vectors encoding *2x35S::VviALMT-GFP* and *2x35S::GFP-VviALMT* respectively. The vectors generated by LR recombination were used to transform *E. coli* DH5 α competent cells. Successfully transformed *E.coli* cells were propagated and the plasmids were harvested using an ISOLATE II Plasmid Mini Kit (Bioline). The harvested vectors were used to transform *Agrobacterium tumefaciens* strain Agl-1 using the freeze thaw method, and successful transformation was confirmed by colony PCR.

The transformed *Agrobacterium* colonies were used to inoculate 1 mL of LB liquid starter cultures containing 50 μ g/mL Kanamycin and 50 μ g/mL Rifampicin. *Agrobacteria* harbouring *pB7RWG2 AtCBL1n (AtCBL1n-RFP*, plasma membrane marker) (Karimi *et al.* 2002), ER-rk (*HDEL-mCherry*, ER marker), G-rk (*Man49-mCherry*, Golgi marker), px-rk (*mCherry-PTS1*, peroxisome marker), mt-rk (*ScCOX4-mCherry*, mitochondria marker) (Nelson *et al.* 2007), and *pB7RWG2 SYP61 (SYP61-RFP*, TGN marker) (Arpat *et al.* 2012) were used for co-localisation. *Agrobacteria* harbouring *pEAQ-HT-DEST*, which contains the p19 suppressor of gene silencing

(Sainsbury *et al.* 2009), was used to maximise expression. Starter cultures of *Agrobacterium* harbouring the markers and pEAQ-HT-DEST were prepared from glycerol stocks with appropriate antibiotics. All starter cultures were incubated at 28 °C at 150 rpm for 2 days, after which 4 mL of LB with antibiotics (4 mL) were inoculated with 150 µL of starter culture and incubated at 28 °C at 150 rpm overnight. Cultures were pelleted at 4000 × g and resuspended in AS medium (10 mM MgCl₂, 150 µM acetosyringone and 10 mM MES, pH 5.6). Final suspensions were prepared by combining different cultures together in AS medium to a final OD_{600nm} value indicated in brackets: *pMDC43* or *pMDC83* expression vectors (OD₆₀₀ = 0.5); pEAQ-HT-DEST (OD₆₀₀ = 0.1); co-localising marker (OD₆₀₀ = 0.2 to 1.0). The combined suspensions were infiltrated into the abaxial side of fully expanded leaves of 5-6 week old tobacco (*N. benthamiana*) with a 1 mL syringe.

Two days after infiltration, leaf sections were imaged using a Nikon A1R confocal laser scanning microscope and NIS-Elements C software (Nikon Corporation). Excitation/emission conditions were GFP (488 nm/500 – 550 nm), mCherry and RFP (561 nm/570 – 620 nm), chlorophyll (640 nm/650 – 720 nm).

Gene expression in *Xenopus laevis* oocytes

The *VviALMT2* and *VviALMT8* CDS in pCR8 vector was recombined into the *X. laevis* oocyte expression vector pGEMHE-DEST (Shelden *et al.* 2009) using LR Clonase II (Life Technologies) to generate vectors encoding *T7:ALMT*. The *pGEMHE* recombinant vectors were linearised with *NheI* (New England Biolabs). The capped RNA (cRNA) for oocyte expression was synthesized with the mMACHINE mMACHINE T7 Transcription Kit (Invitrogen) using the linearised vectors as templates.

Stage IV and V *X. laevis* oocytes were selected and were injected with 10 ng of *VviALMT2* cRNA, or *VviALMT8* cRNA or 42 nL of UltraPure distilled water (DNAse, RNAse free, Invitrogen). The oocytes were incubated in Ca²⁺ Ringer's solution (96 mM NaCl, 2 mM KCl, 5 mM MgCl₂, 5 mM HEPES, 0.6 mM CaCl₂, 5% w/v horse serum, 500 µg mL⁻¹ tetracycline and 1x penicillin-streptomycin (Sigma P4333)) for 2 days post injection.

Electrophysiology

Oocyte whole cell currents were recorded using an Oocyte Clamp OC-725C amplifier (Warner Instruments), digitised using an Axon Digidata 1400A (Molecular Devices) and the software Clampex 10.2 (Molecular Devices). The voltage step protocol was set with a holding potential of 0 mV for 300 ms and 300 ms either side of stepwise pulses from +80 mV to -120 mV in 20 mV decrements for 550 ms.

For anion permeability assays, the basal perfusion solution for oocyte current recording contained 6 mM Mg gluconate, 1.8 mM Ca gluconate and 10 mM MES. Basal buffers were supplemented with 10 mM of anion Na salts. The pH of each solution was adjusted to 5.5 using NaOH, and the osmolality was adjusted to 230 mOsm/kg using D-mannitol. To avoid potential artefacts introduced by testing multiple anions on the same oocyte (i.e. through influx transactivating and/or influencing currents in the presence of subsequent anions), each oocyte was only tested in the basal buffer and one of the 10 mM anion buffers. Five oocytes were used to test each buffer.

For NO_3^- and Cl^- conductance assays, the basal bathing solution for oocyte current recording contained 6 mM Mg gluconate, 1.8 mM Ca gluconate and 10 mM MES. Basal buffers were supplemented with 1 to 100 mM of anion Na salt or anion NM-D-G⁺ salt. The pH of each solution was adjusted to 5.5 using NaOH or NM-D-G; the osmolality was adjusted to 230 mOsm/kg using D-mannitol.

For Al^{3+} activation of malate efflux, oocytes were pre-injected with 10 mM of Na malate and incubated in Ca^{2+} Ringer's solution for 1 h. The oocytes were then clamped using stepwise pulses from +10 mV to -130 mV in the perfusion buffers. The basal ND88 perfusion solution contained 96 mM MES, 1.8 mM CaCl_2 , 2 mM KCl, and 0.1 mM of AlCl_3 was supplemented to make the Al^{3+} activation buffer; pH was adjusted to 4.5 using NM-D-G.

For examining potential γ -aminobutyric acid (GABA) inhibition of malate currents, the basal perfusion solution contained 6 mM Mg gluconate, 1.8 mM Ca gluconate and 10 mM MES. Basal buffers were supplemented with 0.1 mM GABA, or 10 mM Na malate, or a combination of both. The pH of each solution was adjusted to 5.5 using NaOH, and the osmolality was adjusted to 230 mOsm/kg using D-mannitol. For inhibition of the

malate efflux currents, oocytes were pre-injected with 10 mM Na malate and incubated in Ca^{2+} Ringer's solution for 1 h prior to TEVC.

Currents mediated by *VviALMT* were determined by subtracting mean currents of water-injected controls from the same batch of oocytes under the same treatments in the same solutions. For ion outward conductance calculations, the reversal potentials (E_{rev}) were determined by fitting 4th order polynomial regressions to the I-V data, with the slope of tangent connecting E_{rev} and $E_{\text{rev}} + 20$ mV used for calculating outward conductance.

Data were analysed using Clampfit (pClamp 10.2, Molecular Devices) or Smart-IV (Wu *et al.* 2019c), and plotted using GraphPad PRISM v.7.00 for Windows (GraphPad).

Isotope fluxes

cRNA encoding *Torpedo marmorata CLC-0*, a chloride channel with known Cl^- and NO_3^- permeability (Bergsdorf *et al.* 2009b), was used as a positive control.

For Cl^- flux assays 42 nL of H^{36}Cl stock solution (11.3 mg/mL Cl^- , 75 $\mu\text{Ci/mL}$) was injected into each water, *CLC-0*, *VviALMT2* and *VviALMT8* injected oocyte. The control group oocytes were immediately washed 3 times in ice cold ND96 buffer (96 mM NaCl, 2 mM KCl, 1.8 mM CaCl_2 , 1 mM MgCl_2 and 5 mM HEPES, pH 7.4), then each individual oocyte was transferred to a scintillation vial containing 200 μL of 10% (w/v) SDS solution. The efflux group oocytes were quickly transferred to room temperature Cl^- -free ND96 buffer (96 mM Na gluconate, 2 mM K gluconate, 1.8 mM Ca gluconate, 1 mM Mg gluconate and 5 mM HEPES, pH 7.4) to allow Cl^- efflux for 1 h. Oocytes were taken out of the efflux buffer and washed 3 times in ice cold Cl free ND96 buffer, then each individual oocyte was transferred to a scintillation vial containing 200 μL of 10% (w/v) SDS solution. The oocytes were allowed to dissolve in the scintillation vials overnight, then 4 mL of liquid scintillation cocktail was added to each vial. The vials were loaded onto a LS6500 Multi-purpose scintillation counter (Beckman Coulter) and energy emission was counted for 2 min in cpm (counts per minute) with the discriminators set to 200 - 800 KeV.

For NO_3^- flux assays, 42 nL of 300 mM K^{15}NO_3 (99.3% atom) was injected into each water, *CLC-0*, *VviALMT2* and *VviALMT8* injected oocyte. The control group oocytes

were immediately washed 3 times in ice cold ND96 buffer (96 mM NaCl, 2 mM KCl, 1.8 mM CaCl₂, 1 mM MgCl₂ and 5 mM MES, pH 5.5), then oocytes were transferred into tin capsules in a 96-well-plate (3 oocytes per capsule). The efflux group oocytes were quickly transferred to room temperature ND96 buffer (pH 5.5) to allow NO₃⁻ efflux for 100 minutes. Oocytes were removed and washed 3 times in ice cold ND96 buffer (pH 5.5), then 3 oocytes were transferred into a tin capsule. The tin capsules were dried in 50 °C oven for 3 days. Samples were sent for analysis in a stable isotope ratio mass spectrometer (Nu Horizon IRMS) in the University of Adelaide Stable Isotope Facility for δ¹⁵N.

RT-qPCR sample preparation

Cabernet Sauvignon hard wood cuttings with 4-6 nodes (8-10 mm in diameter) were collected from the Alverstoke vineyard (Waite Campus, University of Adelaide) before winter pruning. The cuttings were dipped in 1.5 g/L indole butyric acid (Clonex green, Growth technology) and rooted for 9 weeks in a wetted sand heat bed in a 4°C cold room, and transferred into perlite-vermiculite (1:1) in 2L pots as described by Baby *et al.* (2014). Modified ½ strength Hoagland's solution with nutrient regime 2 (Baby *et al.* 2014) was used to water the grapevines in perlite:vermiculite media once per two days. In order to promote inflorescence growth, standard leaf and shoot tip removal was performed as described previously (Baby *et al.* 2014, Mullins and Rajasekaran 1981). Grapevine young leaves from 5-leaf-shoots (E-L stage 12), young inflorescences (E-L stage 12), and well-developed inflorescences (E-L stage 17) were harvested and immediately frozen in liquid nitrogen. The grapevines were transplanted into the "University of California mix" (UC mix, SARDI Plant Growth Services, Plant Research Centre, Urrbrae, South Australia) in 5L pots after flowering (E-L stage 26), at which time roots were harvested. Each grapevine was supplied with 1 L of R.O. water once per week after being transferred to the UC mix. Mature leaves and petiole samples were collected after transplanting (E-L stage 27), and pea sized green berries (E-L stage 31) and berries post-veraison (E-L stage 36-37) were harvested. Each sample contained tissues pooled from 3 plants. The harvested tissue samples were immediately frozen in liquid nitrogen and preserved at -80 °C.

For nitrate responses, grapevine green cuttings with 2 nodes and mature leaves were obtained from pot grown Cabernet Sauvignon, 140 Ruggeri and K51-40 in November

2017 (South Australia). Cuttings were trimmed at the bottom node including removal of nodal leaf and bud. The mature leaf at the top node was trimmed to around 25 cm². The bottom of each cutting was dipped into Clonex Green (Growth Technology) and inserted 3 cm deep into a tray containing wet sand-perlite-vermiculite (2:1:1). The trays were placed in a misting chamber covered with 90% UV shield shade cloth and transparent plastic film. The cuttings were supplied with 35°C bottom heat, and misted with tap water for 20 sec every 20 min from 7 a.m. to 7 p.m. After 3 weeks the rooted cuttings were removed from the tray and replanted into small pots in perlite-vermiculite (1:1) media. The plants were transferred to a controlled environment room (27 °C day and 22°C night, 60% humidity, 16 h photoperiod) watered with 2 g/L Aquasol (Yates) for 6 weeks before being used for experiment.

The grapevines were watered with modified ½ Hoagland's solution (Baby *et al.* 2014) with 0.8 mM total nitrate for 2 weeks (Cochetel *et al.* 2017) before treatments. After 2 weeks, 18 grapevines of each variety were watered with modified ½ Hoagland's solution with 0.8 mM total nitrate, and the same number of grapevines were watered with modified ½ Hoagland's solution with 12 mM total nitrate. After 3 h, 5 plants of each variety of each nitrate treatment were removed from pots, the roots were harvested into individual 50 mL falcon tubes and immediately frozen in liquid nitrogen. After 24 h the roots from the remaining plants were harvested and immediately frozen in liquid nitrogen. Root samples were preserved at -80 °C.

The grapevine tissue samples harvested from the Cabernet Sauvignon hard wood cuttings and the NO₃ treated root samples harvested from the grapevine green cuttings were ground into fine powder with a mortar and pestle, and liquid nitrogen. Approximately 100 mg of each powdered sample was taken for total RNA extraction using the Spectrum Plant Total RNA Kit (Sigma) as per the manufacturer's manual. The eluted total RNA samples were treated with TURBO DNase (Invitrogen) at 37 °C for 30 min. DNase was removed by phenol chloroform extraction and isopropanol precipitation. Each total RNA pellet after isopropanol precipitation was resuspended with 20 µL of Nuclease free water and used for cDNA synthesis. cDNA were synthesized using oligo(dT)₂₀ and SuperScript III Reverse Transcriptase (Invitrogen) as per the manufacturer's manual. All cDNA samples were diluted 1 in 10 when used as PCR or qPCR templates.

RT-qPCR primers specific to *VviALMT2*, *VviALMT8* and 3 housekeeping genes, α -*Tubulin* (*VviTUA*, LOC100260286), *Ubiquitin-conjugating-enzyme-like* (*VviUBC*, LOC100249853) and *Elongation-factor-1- α* (*VviEF1a*, LOC100246711) were designed to amplify fragments between 80 and 250 bp with an optimal GC content between 40% and 60%, and to flank an intron if possible (Table S1). Primers were checked using NCBI primer-BLAST so that they were designed to amplify only one product from each target. PCR targets were amplified from the cDNA using the qPCR primers and *Taq* DNA Polymerase (New England Biolabs). The fragment sizes of PCR products were checked by agarose gel and the correct size products were purified and sequenced. PCR fragments with correct sequences were diluted to 10^{11} copies/ μ L and then 1 in 8 serially diluted and used as standard curve templates for RT-qPCR. RT-qPCR and standard curve PCR were performed on a QuantStudio 12K Flex Real-Time PCR System. Each 10 μ L reaction consisted 1X KAPA SYBR FAST Universal mix (KAPA Biosystems), 1X ROX Low (KAPA Biosystems), 250 nM forward and reverse primers and 1 μ L of 1 in 10 diluted cDNA. The qPCR is consisted of 40 cycles of a 2-step protocol: 95 °C 3 sec, 56 °C 20 sec (followed by data acquisition). The melt curve was performed by heating from 56 °C to 95 °C by 0.05 °C per second with continuous data acquisition. Standard curves were generated by the QuantStudio 12K Flex Real Time PCR System v1.2.2 (Life Technologies), which also calculated the reaction efficiencies of the primer pairs.

cDNA made from stelar enriched and cortex enriched Cl^- -treated grapevine roots was obtained from the material used by Henderson *et al.* (2014a) for RT-qPCR analysis. The RNA samples of grapevine whole roots treated with control or 25 mM Cl^- solutions were also obtained from Henderson *et al.* (2014a) and used to make cDNA for RT-qPCR analysis.

Each qPCR reaction was performed in triplicate. Expression levels (E) of *VviALMT2* and *VviALMT8* were calculated relative to sample 1 of each experiment (as described in the figure legends) using the equation $E = (2 * \text{efficiency})^{(CT_{\text{sample}} - CT_{\text{sample 1}})}$. Expression levels were normalised to the geometric mean of the expression levels of the 3 housekeeping genes (Vandesompele *et al.* 2002).

Corvina microarray gene expression data presentation

RMA-normalized signal intensities were extracted from the Corvina microarray gene expression study by Fasoli *et al.* (2012). Data is presented in a heat map as log₂ mean linearised signal intensities of the 4 probes and 3 biological replicates.

VviALMT promoter driven gene expression in Arabidopsis

The *VviALMT2* and *VviALMT8* promoter in pENTR vectors were recombined into pMDC162 and pMDC204 expression vectors using LR Clonase II (Life Technologies) to generate binary vectors encoding *proVviALMT:GUS* and *proVviALMT:GFP6-HDEL*. The vectors generated by LR recombination were used to transform *E. coli* DH5 α competent cells. Successfully transformed *E. coli* cells were propagated and the plasmids were harvested using the ISOLATE II Plasmid Mini Kit (Bioline), which were then used to transform *A. tumefaciens* strain Agl-1 using the freeze thaw method, and successful transformation was confirmed by colony PCR. *Arabidopsis thaliana* Col-0 plants were transformed using the Agrobacterium-mediated floral dip method (Clough and Bent 1998). Transgenic lines of Arabidopsis were selected by the application of Hygromycin B (Bayer Crop Science) and the presence of T-DNA was confirmed by PCR.

For tissue specific expression analysis via fluorescence, selected two-week-old roots from T3 *proVviALMT2:GFP6-HDEL* and *proVviALMT8:GFP6-HDEL* Arabidopsis were directly imaged or incubated in 15 μ M (10 μ g/mL) propidium iodide (PI) solution in the dark for 15 min then rinsed 3 times with water before imaging. Roots were imaged using a Nikon A1R confocal laser scanning microscope; excitation/emission conditions were GFP (488 nm/ 500 – 550 nm), PI (561 nm/ 570 – 620 nm).

For tissue specific expression analysis via GUS staining, selected two-week-old T2 seedlings of *proVviALMT2:GUS* and *proVviALMT8:GUS* grown on plates, and mature leaves, flowers and siliques from 6-week-old pot-grown plants were taken. Seedlings were directly incubated in GUS staining solution (50 mM NaPO₄, 10 mM EDTA, 0.1% Triton X-100, 0.5 mM potassium ferrocyanide, 0.5 mM potassium ferricyanide, 1 mg/mL X-Gluc) at 37°C for 2 h. Tissues harvested from mature plants were put into GUS staining solution and vacuum infiltrated for 30 minutes, then incubated at 37°C for 5 h. The stained tissues were washed and put into a phosphate-buffered saline (PBS)

fixing solution containing 8 g/L NaCl, 0.2 g/L KCl, 1.44 g/L Na₂HPO₄, 0.24 g/L KH₂PO₄, 4% formaldehyde, 1.25% glutaraldehyde and 4% sucrose, and incubated at 4°C overnight. The fixed tissues were either directly cleared with ethanol or dissected for Technovit 7100 (Kulzer) embedding. For ethanol clearing, fixed tissues were washed with PBS then incubated in each concentration of ethanol (50%, 70%, 90%, 100%, dry ethanol) for 15 min, and left in dry ethanol over night at room temperature. Before imaging, the cleared tissues were rehydrated by incubation in each concentration of ethanol (90%, 70%, 50%, 30%, water) for 15 min and put onto a 0.3% phytigel plate. Images were taken using Nikon SMZ25 stereo microscope. For Technovit embedding of GUS stained tissues, fixed seedlings were washed with PBS then, root and leaf material was embedded in 1% low melting point agarose. Agarose blocks containing tissue samples were trimmed to fit 200 µL thin wall PCR tubes. Trimmed blocks were put into 2 mL tubes and ethanol cleared. The cleared blocks were embedded into 200 µL thin wall PCR tubes using Technovit 7100 (Kulzer) as per manufacturer's protocol. Transverse sections of embedded root and leaf samples were taken using Leica RM2265 Rotary Microtome and mounted on glass slides with DPX. Images were taken using Nikon DS-Ri1 upright research microscope.

Cell type specific ectopic expression of *VviALMT2* in an Arabidopsis enhancer trap line

The Arabidopsis enhancer trap line E2586 for root stele specific transgene expression was obtained from Møller et al. (2009). The *VviALMT2* CDS in the entry vector was recombined into the pTOOL5-*UAS_{GAL4}* (obtained from Plett 2008) destination vector using LR Clonase II (Life Technologies) to generate the binary vector encoding *UAS_{GAL4}:VviALMT2*. The binary vector was used to transform *A. tumefaciens* strain Agl-1 using the freeze thaw method. The Arabidopsis enhancer trap E2586 plants were transformed using the Agrobacterium-mediated floral dip method (Clough and Bent 1998). Transgenic lines of Arabidopsis were selected by the application of foliar spray of 120 mg/L Basta (Bayer Crop Science) mixed with 500 µL/L Silwet L-77 (plantMedia.com). The presence of T-DNA was confirmed by PCR.

Two homozygous T3 lines of E2586 *UAS_{GAL4}:VviALMT2*, line 2B and 3B were selected by Basta foliar spray and genotyping using root cDNA. Root stele specific gene

expression was confirmed by imaging root mGFP5-ER using a Nikon A1R confocal laser scanning microscope (excitation/emission is 488 nm/ 500 – 550 nm).

Phenotyping Arabidopsis root stele specific *VviALMT2* over-expression lines

Homozygous Arabidopsis T3 E2586 *UAS_{GALA}:VviALMT2* line 2B, 3B and non-transformed E2586 seeds were germinated and grown in the hydroponic system in the germination solution (GM) for 3 weeks, and transferred into the standard basal nutrient solution (BNS) as described in Conn *et al.* (2013). For the salt stress experiment, the plants were grown in the BNS for 2 weeks, then the BNS was replaced with high Na⁺ nutrient solution containing 75 mM NaCl activity (Conn *et al.* 2013). Five days post NaCl treatment, the shoots were harvested and the fresh weights were recorded. For the NO₃⁻ starvation and re-supply experiment, the plants were grown in the BNS for 2 weeks, then the BNS was replaced with low NO₃⁻ containing nutrient solution with 0.8 mM total NO₃⁻ (modified from the standard BNS in Conn *et al.* 2013). Seven days post NO₃⁻ starvation treatment, the nutrient solution was replaced with a high NO₃⁻ BNS (12 mM total NO₃⁻, made by addition of 11.2 mM NaNO₃ into the low NO₃⁻ BNS). The shoots (whole rosettes) were harvested 24 h post high NO₃⁻ re-supply and the fresh weights were recorded. Each shoot was put into a 50 mL tube and for every 20 mg of the fresh weight, 1 mL of water was added into the tube. The shoots and the liquid in the tubes were frozen at -20 °C, thawed at room temperature and the tubes were vortexed; this process was repeated 3 times to fully release the cellular contents, and the resulting liquid samples were used for measurement of shoot ion concentrations.

The Cl⁻ concentrations of the liquid samples were measured using a Sherwood 926s Chloride Analyzer (Sherwood Scientific). The NO₃⁻ concentrations were measured using the reaction of NO₃⁻ with salicylic acid under alkaline condition as described in Cataldo *et al.* (1975). In a well of a flat bottom 96-well-plate, 3 μL of each sample was combined with 12 μL of H₂SO₄ containing 5% (w/v) salicylic acid, and incubated at room temperature for 20 min. Then 285 μL of 2N NaOH was mixed into each well and the absorbance at OD_{410nm} was measured. A series of KNO₃ solutions from 0 to 10 mM were used for a standard curve and the [NO₃⁻] of the samples were calculated using the standard curve.

To study the correlation between the Arabidopsis shoot ion concentrations and the root *VviALMT2* expression levels, both roots and shoots of E2586 *UAS_{GAL4}:VviALMT2* lines were harvested post treatments. The shoots were used for [Cl⁻] and/or [NO₃⁻] analyses as described above. The roots were used for RNA extraction, cDNA synthesis and RT-qPCR. Each qPCR reaction was performed in duplicate. Expression levels (E) of *VviALMT2* were calculated relative to the housekeeping gene *AtActin2* (At3G18780, qPCR primers as listed in Jha *et al.* (2010)) and normalised to sample 1 using the equation $E = 2^{-\Delta\Delta CT}$. The relationships between shoot ion contents and gene expression levels were analysed using linear regression.

***In silico* analyses**

The gene sequences of *AtALMT*, *TaALMT*, *ZmALMT*, *BnALMT* and *VviALMT* family members were obtained from their respective reference genomes and the *V. Vinifera* PN40024 genome database using the gene IDs listed in Sharma *et al.* (2016). Protein alignments were generated using Clustal W (Larkin *et al.* 2007), and the phylogenetic tree was generated using Geneious version 8.1.7 with default settings.

Statistical analysis

Statistical analyses were performed using GraphPad PRISM v.7.00 for Windows (GraphPad). All data are presented as mean \pm SE. Means were compared using the Student's t-test.

Results

VviALMT2 and VviALMT8 are both pH sensitive low affinity NO₃⁻ transporters

To investigate potential substrates of VviALMT2 and VviALMT8, two-electrode voltage clamp (TEVC) of *Xenopus* oocytes that were injected with VviALMT2 and VviALMT8 cRNA was performed (Figure 1, Figure S1 and S2). In this study several common ALMT clade I protein substrates were tested, including two monovalent anions of interest, Cl⁻ and NO₃⁻, one divalent anion (SO₄²⁻), three dicarboxylates (malate, tartrate and the malate analogue isophthalate), and one tricarboxylate (citrate). Outward ion conductance was calculated as slopes of I-V linear regressions between the reversal potential and +20 mV. When perfused with 10 mM external anion, both VviALMT2 (Figure 1A, Figure S1A – B) and VviALMT8 (Figure S2A – B) injected oocytes showed a large NO₃⁻ outward conductance at positive membrane potentials (i.e. movement of anion into the oocyte). Both VviALMT2 (Figure 1A) and VviALMT8 (Figure S2A) were also permeable to Cl⁻, malate, tartrate, isophthalate and citrate, but not to SO₄²⁻. The relative affinities for NO₃⁻ and Cl⁻ transport were examined using external concentrations ranging from 0 mM to 100 mM (Figure 1B). The results show that the outward conductance of NO₃⁻ was higher than that of Cl⁻ for VviALMT2 at all concentrations tested (Figure 1B), and the same pattern was observed for VviALMT8 (Figure S2C). The half-saturation constant (K_M) for NO₃⁻ and Cl⁻, calculated using the Michaelis–Menten equation, showed that both VviALMT2 and VviALMT8 transport the two anions in the low-affinity range. These data suggest that VviALMT2 and VviALMT8 have multiple anions as substrates, and are most permeable to NO₃⁻ when moving anions into the cell. Considering that both VviALMT2 and VviALMT8 are found to transport NO₃⁻ and Cl⁻, further characterisation of the proteins for their potential to regulate rootstock shoot Cl⁻ exclusion was conducted.

Plant root cell membrane potentials are ordinarily more negative than -100 mV, which promotes inward anion currents (cellular anion efflux) rather than outward (anion influx). While both VviALMT2- and VviALMT8-expressing oocytes displayed large inward currents at negative E_m , the ionic species carrying these currents could not be resolved by TEVC (Figure S1A, S2B). Therefore, to test whether VviALMT2 and VviALMT8 also mediated NO₃⁻ efflux, VviALMT2- and VviALMT8-expressing *Xenopus* oocytes were injected with the ¹⁵NO₃ tracer and allowed to rest in an efflux

buffer for 100 min. Following this treatment both *VviALMT2*- (Figure 1C) and *VviALMT8*-injected oocytes (Figure S2D), exhibited significant reductions in $\delta^{15}\text{N}$ while water-injected negative control oocytes retained the original level of $\delta^{15}\text{N}$ after 100 min. A similar assay for Cl^- was performed by injecting the radiotracer ^{36}Cl into each oocyte and allowing efflux for 100 min; and both *VviALMT2*- (Figure 1D) and *VviALMT8*-expressing (Figure S2E) oocytes showed slight reductions in tracer activity after 100 min. As a control in both experiments *Torpedo* CLC-0 was used, which according to I-V data of Bergsdorf *et al.* (2009b) should have similar Cl^- and NO_3^- efflux ability. Both *VviALMT2*- and *VviALMT8*-expressing oocytes had comparable $^{15}\text{NO}_3$ efflux activity compared to that of the CLC-0, but their ^{36}Cl efflux was significantly lower than that of CLC-0 during the time period tested.

VviALMT2- and *VviALMT8*-expressing oocytes were tested for pH responses in buffers that contained their most permeable inorganic (NO_3^-) and organic (malate) substrates. The I-V curves show that, for *VviALMT2*- (Figure S1C) and *VviALMT8*-expressing (Figure S2F) oocytes, the magnitudes of inward currents at pH 5.5 were approximately twice as high as the current magnitudes at pH 7.5. Neither ALMT was activated by Al^{3+} (Figure S1D and S2G) or inhibited by GABA (Figure S1E and S2H).

***VviALMT2* is highly expressed in root stele, endodermal passage cells and cortex, but not in epidermis**

To investigate the expression pattern of *VviALMT* in grapevine roots, RT-qPCR was performed using cDNA of root epidermal/cortical and stelar enriched fractions of 3 grapevine cultivars, 140 Ruggeri, Cabernet Sauvignon and K51-40, obtained from Henderson *et al.* (2014a). *VviALMT2* transcripts were more abundant in the stelar enriched fractions of all 3 cultivars than in the cortex enriched fraction (Figure 2A), but *VviALMT8* transcripts levels were similar between stelar and cortical fractions (Figure S3).

Activities of GUS and GFP driven by the *VviALMT* promoters in Arabidopsis were also studied. Whole roots of transgenic Arabidopsis showed a high *proVviALMT2* driven GFP activity in the root stele and cortex, but there was no GFP signal in root epidermis, and it is highly likely that there was no activity in the endodermis (Figure 2B). GUS-stained transgenic Arabidopsis root transverse sections and whole roots showed GUS

activity in the root stele, and passage cells in the endodermis (Figure 2C – D). Therefore, *proVviALMT2* drives protein activity in root stele, cortex and endodermal passage cells in *Arabidopsis*. For *proVviALMT8*, it drove GUS and GFP activities highly in the root stele, endodermal passage cells, and also in the cortical and epidermal regions (Figure S4A – B).

Expression level of *VviALMT2* in grapevine roots is up-regulated by high [NO₃⁻] treatment in some cultivars

Since *VviALMT2* was more highly expressed in roots of 140 Ruggeri than in K51-40 (Figure 2A) (Henderson *et al.* 2014a), and encodes a protein which is permeable to NO₃⁻ and Cl⁻ in *Xenopus* oocytes (Figure 1), its expression level in grapevine roots under different [Cl⁻] and [NO₃⁻] treatments was examined by RT-qPCR. Hydroponically grown, rooted leaves of 140 Ruggeri, Cabernet Sauvignon and K51-40 were treated by Henderson *et al.* (2014a) with either control or 25 mM Cl⁻ nutrient solutions. *VviALMT2* transcript abundance was not regulated by 25 mM [Cl⁻] (Figure 3A). For NO₃⁻ treatments, 140 Ruggeri, Cabernet Sauvignon and K51-40 were propagated from grapevine green cuttings, and NO₃⁻ starved for 2 weeks before re-supplying with modified ½ Hoagland's solution with either low or high [NO₃⁻]. The transcript abundance of *VviALMT2* was higher when roots were re-supplied with high [NO₃⁻] than with low [NO₃⁻] in both Cabernet Sauvignon and K51-40, but not 140 Ruggeri (Figure 3B).

The transcript abundance of *VviALMT8* in the same plant material was also analysed by RT-qPCR, however it was not found to be regulated by either the Cl⁻ or NO₃⁻ treatments, except that the abundance was up-regulated by NO₃⁻ re-supply in K51-40 (Figure S5). For both *VviALMT2* and *VviALMT8*, some expression differences appear to be large in the figures mentioned above but were shown statistically insignificant. Due to the high variability among the replicates in some treatment groups, care should be taken when making conclusions with the expression data.

***VviALMT2* is highly expressed in grapevine fruit related tissue types**

To further explore the expression pattern of *VviALMT* in other grapevine tissue types, RMA-normalized signal intensities were extracted from a previous grapevine (*Vitis vinifera* cv. Corvina) microarray gene expression study (Fasoli *et al.* 2012). Data was

log₂ transformed and used to generate a heat map. The heat map suggested that *VviALMT2* was most highly expressed in reproductive tissue types such as the seed, berry, flower and rachis (Figure S6A), while its expression level in roots was at a median level.

To confirm these findings, Cabernet Sauvignon hardwood cuttings were propagated in pots and RT-qPCR analyses were performed on various tissue types harvested during the growing season. The results showed that *VviALMT2* was most highly expressed in the berry samples pre- and post-veraison, and in well separated flowers, while its expression level was at lower level in roots, but lowest in the petiole, inflorescence and mature leaf (Figure S6B). Consistent with this, GUS staining of *proVviALMT2:GUS* transformed Arabidopsis also showed intense staining of the shoots of seedlings and flowers (Figure S7).

VviALMT8 was found most abundant in bud, root, leaf, flower, and rachis tissues in the Corvina microarray study (Figure S6A). This pattern was confirmed by RT-qPCR analysis of Cabernet Sauvignon tissues (Figure S6C); however, interestingly, the GUS activities driven by *proVviALMT8* in Arabidopsis was highly specific to trichomes on the mature leaves and carpel of the flowers (Figure S4C).

VviALMT2 is a plasma membrane localised protein

Expression of *VviALMT2* with either N- or C-terminal GFP tags in tobacco epidermal cells produced GFP signals that co-localised with the plasma membrane (PM) marker AtCBL1n-RFP (Figure 4A, 4C, Figure S8A). GFP-*VviALMT2* was also co-expressed with the endoplasmic reticulum (ER) marker HDEL-mCherry but co-localisation was poor (Figure 4B, 4D). Punctate GFP dots were regularly observed but they did not co-localise with any organelles. These findings suggest that *VviALMT2* is predominantly a PM localised protein. Conversely, the subcellular localisation of *VviALMT8* was unclear. A C-terminal *ALMT8*-GFP translational fusion was co-expressed with a PM marker (AtCBL1-RFP), an ER marker (HDEL-mCherry), a Golgi marker (Man49-mCherry), a *trans*-Golgi network (TGN) marker (SYP61-RFP), a peroxisome marker (mCherry-PTS1) and a mitochondria marker (ScCOX4-mCherry), and an N-terminal GFP-*ALMT8* fusion was co-expressed with the ER marker. Co-expression of GFP tagged *VviALMT8* with these six different subcellular markers did not show any

overlap between the red and green signals (Figure S8B – H), hence the definitive location of the GFP tagged VviALMT8 signals to a specific membrane was not ascertained.

The increase in VviALMT2 expression in Arabidopsis root vasculature reduced the shoot [Cl⁻]

To study the function of VviALMT2 *in planta*, an Arabidopsis enhancer trap line E2586 was transformed with VviALMT2 for gene over-expression. This line allows root vasculature specific gene expression, which matches the expression pattern of VviALMT2 in grapevine and in Arabidopsis roots (Figure 2). To confirm the root vasculature specific gene expression, the roots were imaged for mGFP5-ER distribution and the GFP signals are within the expected tissue type (Figure 5A). The E2586 VviALMT2 over-expression (OEX) lines (line 2B and 3B) were treated with 75 mM NaCl in hydroponics for 5 days and the shoots were harvested for [Cl⁻] and [NO₃⁻] analyses. The results showed that the VviALMT2 OEX lines had lower shoot [Cl⁻] compared to the non-transformed E2586 line after the NaCl treatment (Figure 5B). Only one of the OEX lines showed a slightly significantly higher shoot [NO₃⁻] than E2586 (Figure 5C), and the shoot [Cl⁻]/[NO₃⁻] ratios of both OEX lines were lower than that of E2586 (Figure 5D). When root VviALMT2 expression levels were correlated with shoot fresh weight, [Cl⁻] and [NO₃⁻] respectively, there was no significant linear relationship between the gene expression levels and the shoot weights (Figure 5E), no significant positive correlation between the gene expression and the shoot [NO₃⁻] (Figure 5F), but there was a significant negative linear correlation between the gene expression and the shoot [Cl⁻] (Figure 5G). And the shoot [Cl⁻]/[NO₃⁻] ratios were negatively correlated with the gene expression levels as well (Figure 5H).

To test the effects of VviALMT2 on shoot [NO₃⁻] without the influence of salt stress, the E2586 VviALMT2 OEX lines were starved with 0.8 mM NO₃⁻ for 7 days and re-supplied with 12 mM NO₃⁻ for 24 h before harvesting. The VviALMT2 OEX lines had similar shoot [NO₃⁻] levels to those of the E2586 shoots (Figure 6A), and the expression levels of VviALMT2 did not have a linear correlation with the shoot [NO₃⁻] (Figure 6B).

Discussion

Higher plant ALMTs were separated into 5 clades based on the evolutionary relationships between grapevine, wheat, Arabidopsis, and rice (Sharma *et al.* 2016). Here, we also observed 5 clades when comparing the phylogenetic relationships of ALMTs from grapevine, Arabidopsis, barley, wheat, maize, and *Brassica napus* (Figure S9), and found that VviALMT2 and 8 belong to clade 1. Many clade 1 proteins, including TaALMT1, AtALMT1, BnALMT1 and BnALMT2 were found to function in Al³⁺ activated malate efflux, which chelates the toxic Al³⁺ and helps confer Al³⁺ tolerance in acid soils (Hoekenga *et al.* 2006, Ligaba *et al.* 2006, Sasaki *et al.* 2004). However, other group 1 proteins; ZmALMT1, ZmALMT2 and HvALMT1 were found to be capable of transporting inorganic anions including Cl⁻ and/or NO₃⁻ and were not activated by Al³⁺ (Gruber *et al.* 2010, Ligaba *et al.* 2012, Piñeros *et al.* 2008), suggesting functions of clade 1 ALMTs outside of Al³⁺ tolerance, and being involved in other aspects of plant anion homeostasis. Sequence analysis shows that VviALMT2 is closely related to both BnALMT2 and ZmALMT2 (Figure S9), but functional data suggests that VviALMT2 is more ZmALMT2-like (Ligaba *et al.* 2012) rather than BnALMT2-like (Ligaba *et al.* 2006). For instance, in the *Xenopus* oocyte system, both VviALMT2 and 8 had a NO₃⁻ outward conductance far higher than that of Cl⁻ and malate (Figure 1A, Figure S2A). Oocytes expressing VviALMT2 and VviALMT8 were loaded with malate and tested using TEVC to find out whether they function in Al³⁺ activated malate efflux, but no significant Al³⁺ induced inward current changes were observed (Figure S1D, Figure S2G), which strongly suggests that they are unlikely to be involved in Al³⁺ tolerance. Furthermore, we tested whether these transporters were regulated by GABA and so potentially involved in metabolic signalling (Gilliham and Tyerman 2016). VviALMT8 possesses the 12 amino acid GABA recognition site (Ramesh *et al.* 2015), whereas VviALMT2 does not. We tested if their inorganic (NO₃⁻) and organic (malate) anion transport activities could be affected by the presence of 1 mM GABA, but neither transporter showed GABA dependant current changes (Figure S1E, Figure S2H, Figure S10). This is significant as these are the first ALMTs examined that are not GABA sensitive so divorcing at least some ALMT from a GABA signalling role. Furthermore, VviALMT8 is GABA insensitive even though it possesses the GABA recognition motif, indicating other regions of the protein are essential for GABA sensitivity in combination with the motif giving weight to this hypothesis

proposed by Ramesh *et al.* (2017). As both ALMT are neither Al^{3+} or GABA sensitive, we propose that VviALMT2 and 8 are more likely to have other functions associated with anion homeostasis in plants.

The VviALMT2 is a plasma membrane localised protein (Figure 4), suggesting that it could have a direct role in plant ion transport across the plasma membrane. VviALMT2 was also found to be more highly expressed in the grapevine root stelar enriched fraction than in the cortical enriched fraction (Figure 2A), which suggests its potential involvement in root to shoot translocation. As we could not locate VviALMT8 to any of the subcellular membranes in tobacco leaf epidermal cells (Figure S8B – H) and in *Arabidopsis* mesophyll protoplasts, and its gene expression levels in root stelar and cortical fractions were similar in grapevines (Figure S3), this protein was not considered a high priority candidate for root-to-shoot anion translocation so is not discussed further in this study.

To study VviALMT2's function in rootstock anion homeostasis, we focused on NO_3^- and Cl^- . VviALMT2's outward conductance to NO_3^- was significantly higher than that of Cl^- in all concentrations tested (Figure 1B), and the efflux activity of the NO_3^- tracer through VviALMT2 was considered higher than of Cl^- within the time period tested (Figure 1C – D). This evidence points to VviALMT2 being more permeable to NO_3^- over Cl^- .

Although VviALMT2 gene is more highly expressed in the good Cl^- excluder 140 Ruggeri (Henderson *et al.* 2014a), the RT-qPCR gene expression analysis on the grapevine roots showed that the expression of VviALMT2 was up-regulated by NO_3^- re-supply after starvation (Figure 3B), but not by Cl^- treatment (Figure 3A, Figure S11A). However, this does not remove the possibility that VviALMT2 contributes to grapevine salt tolerance. NO_3^- and Cl^- are both monovalent inorganic anions and are similar in size; many plant anion transporters were found to transport both NO_3^- and Cl^- , and select NO_3^- over Cl^- (Roberts 2006). Numerous studies on a wide range of plants have observed that abundant NO_3^- in the growth media could reduce Cl^- uptake, and *vice versa*. Multiple studies have discovered that the supplementation of NO_3^- can improve the performance of the plants under salt stress (Lunin and Gallatin 1965), and adequate NO_3^- in growth media was found to reduce the accumulation of Cl^- in plants (Abdolzadeh *et al.* 2008, Gimeno *et al.* 2009, Glass and Siddiqi 1985, Guo *et al.* 2017).

It was observed that the citrus nitrogen accumulation pattern was inversely correlated with the pattern of Cl^- (Bañuls *et al.* 1990). In grapevines, high external $[\text{Cl}^-]$ reduces the $[\text{NO}_3^-]$ in leaves (Abbaspour *et al.* 2014, Fisarakis *et al.* 2005). As VviALMT2 prefers NO_3^- than Cl^- , it has the potential to improve plant Cl^- tolerance by reducing the shoot $[\text{Cl}^-]/[\text{NO}_3^-]$ ratio, rather than functioning in active Cl^- exclusion.

The fact that VviALMT2 was highly expressed in grapevine root stele (Figure 2A) and had high NO_3^- efflux capacity could lead to a theory that it functions in xylem NO_3^- loading. Several stelar expressed anion transporters were previously found to function in anion loading into the root xylem and participate in anion translocation from root to shoot. *AtNPF2.3* is expressed in root pericycle, and the NO_3^- content in xylem sap was reduced in the knockout mutant (Taochy *et al.* 2015); *AtNPF2.4* is highly expressed in the root stele and the *Arabidopsis npf2.4* knockdown mutant had lower shoot Cl^- accumulation (Li *et al.* 2016); *AtSLAH1* and *AtSLAH3* co-expressed in root xylem-pole pericycle and function in gated Cl^- loading into the xylem (Cubero-Font *et al.* 2016). From the *proVviALMT2* driven GFP and GUS activities in *Arabidopsis* roots we can see that the protein activities were also driven in the endodermal passage cells, and weakly driven in the cortex (Figure 2B – D). Although the *proVviALMT2* driven protein activities were not limited to the root stele or xylem parenchyma as the anion transporters mentioned above, a continuous anion transport pathway from cortex, through the endodermal passage cells, to the xylem parenchyma and the xylem vessels could be maintained by VviALMT2. The xylem-parenchyma expression and the NO_3^- transport kinetics of VviALMT2 (Figure S1A – B) suggest that it is likely a xylem-parenchyma quickly-activating anion conductance (X-QUAC) (Köhler and Raschke 2000). X-QUAC was proposed to be the main pathway for NO_3^- and anion loading into the xylem sap (Köhler *et al.* 2002). It is possible that the up-regulation of VviALMT2 expression in roots by post-starvation high $[\text{NO}_3^-]$ re-supply (Figure 3B) is due to the increased demand of xylem NO_3^- in response to the NO_3^- availability. Therefore, we propose that the role of VviALMT2 in grapevine roots is to mediate rapid and high net loading of NO_3^- inside the roots to the xylem, which promotes a better nitrogen status in the shoots.

As discussed above, we developed the hypothesis that the expression of VviALMT2 in roots could benefit the plants under salt stress by promoting NO_3^- loading into the

xylem, hence reducing the shoot $[Cl^-]/[NO_3^-]$ ratio. To test this hypothesis, Arabidopsis root vasculature specific *VviALMT2* constitutive over-expression lines were constructed, and they were treated with 75 mM NaCl in a hydroponics system before being harvested for shoot ion concentration analyses. The $[Cl^-]/[NO_3^-]$ ratios of both *VviALMT2* OEX lines were significantly lower than those of the non-transformed line (Figure 5D), which partially supported our hypothesis; however, the differences were contributed more by the differences in the shoot $[Cl^-]$ than by the shoot $[NO_3^-]$ (Figure 5B – C). To confirm that the ion concentration differences were related to the expression of *VviALMT2*, the shoot $[Cl^-]$ and $[NO_3^-]$ were plotted against the root *VviALMT2* expression levels for linear regression analyses, and we found that the negative correlation between the shoot $[Cl^-]$ and the gene expression levels was statistically significant (Figure 5G), but the positive correlation between the shoot $[NO_3^-]$ and the expression levels was not (Figure 5F). We can conclude with these results that the expression of *VviALMT2* in root vasculature is beneficial to the plants as it could reduce the shoot $[Cl^-]$ under salt stress. As one of the Arabidopsis *VviALMT2* OEX lines showed a slightly significantly higher shoot $[NO_3^-]$ than the non-transformed line (Figure 5C), we suspect that *VviALMT2* still facilitated the accumulation of $[NO_3^-]$ in shoots, but the $[NO_3^-]$ in the nutrient solution and the 75 mM NaCl treatment was not optimal for demonstrating *VviALMT2*'s effect on shoot $[NO_3^-]$. To address this question, we applied the NO_3^- starvation (0.8 mM NO_3^- , 7 days) and re-supply (12 mM NO_3^- , 24 h) treatments on the *VviALMT2* over-expressing Arabidopsis before harvesting. The results show that there was no correlation between root *VviALMT2* expression and shoot $[NO_3^-]$ (Figure 6). These data suggest that *VviALMT2* may well have a physiological role in reducing shoot $[Cl^-]$ accumulation.

It is intriguing, but not unprecedented, that expression of a functional NO_3^- transporter in Arabidopsis roots did not alter shoot $[NO_3^-]$. Compared to the members in the major plant nitrate transporter families (reviewed in Nogueru and Lacombe 2016), *VviALMT2*'s effect on root to shoot NO_3^- translocation may not be clearly discernible. To further test if *VviALMT2* participates directly in NO_3^- homeostasis in plants, a nitrate-transport deficient Arabidopsis line could be used to test if the expression of *VviALMT2* could complement the phenotype. To suggest whether *VviALMT2* reduced shoot $[Cl^-]$ by its preferential loading of NO_3^- over Cl^- into the root xylem, we propose that a more direct or a more sensitive measurement, such as xylem exudate anion flux

or root to shoot anion tracer translocation, could be used in the future to compare the root to shoot anion translocation between the wild type and *VviALMT2* root expression lines.

The Cabernet Sauvignon *VviALMT2* gene expression (Figure S6) and the grapevine microarray analyses (Fasoli *et al.* 2012), and the *proVviALMT2* driven GUS activities in *Arabidopsis* shoots (Figure S7) demonstrated that *VviALMT2* was also highly active in other tissues, especially fruit related tissues including flowers, berries and rachis, which suggested that *VviALMT2* could have other physiological roles. The vacuolar malate and tartrate transporter *VviALMT9* was previously found to be expressed in berry mesocarp, and therefore proposed to function in mediating organic acid accumulation in grape berries (De Angeli *et al.* 2013a). Since *VviALMT2* was also found to transport several organic acids including malate and tartrate (Figure 1A), it is possible that *VviALMT2* could function in shoot organic acid translocation or fruit organic acid homeostasis as well.

Acknowledgements

We thank Yu Long (University of Adelaide) for advice on TEVC; Deidre Blackmore (CSIRO) for assistance with preparing the grapevine green cuttings; Phillip Earl (University of Adelaide) for supplying the grapevine hardwood cuttings; Wendy Sullivan (University of Adelaide) for harvesting oocytes and assistance with the grapevine hardwood cuttings; Jiaen Qiu (University of Adelaide) for help to harvest the grapevine NO₃ treated roots; Stefanie Wege (University of Adelaide) for advice on subcellular localisation in tobacco and supplying the TGN marker; Gwenda Mayo (Adelaide Microscopy) for assistance with the microscopy work; Mandy Walker (CSIRO) for supplying 60 mM NaCl treated Cabernet Sauvignon root samples.. Steve Tyerman (University of Adelaide) was the independent advisor. Y.W. was supported by the University of Adelaide (Adelaide Graduate Research Scholarship) and Wine Australia (AGWA Research Supplementary Scholarship (AGW Ph1502)). This research was funded by Australian grape growers and winemakers through their investment body Wine Australia with matching funds from the Australian government (AGW Ph1502).

References

- Abbaspour, N., Kaiser, B. and Tyerman, S.** (2014) Root apoplastic transport and water relations cannot account for differences in Cl^- transport and $\text{Cl}^-/\text{NO}_3^-$ interactions of two grapevine rootstocks differing in salt tolerance. *Acta Physiologiae Plantarum*, **36**, 687-698.
- Abdolzadeh, A., Shima, K., Lambers, H. and Chiba, K.** (2008) Change in uptake, transport and accumulation of ions in *Nerium oleander* (Rosebay) as affected by different nitrogen sources and salinity. *Annals of Botany*, **102**, 735-746.
- Arpat, A.B., Magliano, P., Wege, S., Rouached, H., Stefanovic, A. and Poirier, Y.** (2012) Functional expression of PHO1 to the Golgi and trans-Golgi network and its role in export of inorganic phosphate. *The Plant Journal*, **71**, 479-491.
- Baby, T., Collins, C., Tyerman, S.D. and Gilliham, M.** (2016) Salinity negatively affects pollen tube growth and fruit set in grapevines and is not mitigated by silicon. *American Journal of Enology and Viticulture*, **67**, 218-228.
- Baby, T., Hocking, B., Tyerman, S.D., Gilliham, M. and Collins, C.** (2014) Modified method for producing grapevine plants in controlled environments. *American Journal of Enology and Viticulture*.
- Baetz, U., Eisenach, C., Tohge, T., Martinoia, E. and De Angeli, A.** (2016) Vacuolar chloride fluxes impact ion content and distribution during early salinity stress. *Plant Physiology*.
- Bañuls, J., Legaz, F. and Primo-Millo, E.** (1990) Effect of salinity on uptake and distribution of chloride and sodium in some citrus scion-rootstock combinations. *Journal of Horticultural Science*, **65**, 715-724.
- Bergsdorf, E.-Y., Zdebik, A.A. and Jentsch, T.J.** (2009) Residues important for nitrate/proton coupling in plant and mammalian CLC transporters. *The Journal of Biological Chemistry*, **284**, 11184-11193.
- Cataldo, D.A., Maroon, M., Schrader, L.E. and Youngs, V.L.** (1975) Rapid colorimetric determination of nitrate in plant tissue by nitration of salicylic acid. *Communications in Soil Science and Plant Analysis*, **6**, 71-80.
- Clough, S.J. and Bent, A.F.** (1998) Floral dip: a simplified method for *Agrobacterium*-mediated transformation of *Arabidopsis thaliana*. *The Plant Journal*, **16**, 735-743.
- Cochetel, N., Escudie, F., Cookson, S.J., Dai, Z., Vivin, P., Bert, P.F., Munoz, M.S., Delrot, S., Klopp, C., Ollat, N. and Lauvergeat, V.** (2017) Root transcriptomic responses of grafted grapevines to heterogeneous nitrogen availability depend on rootstock genotype. *Journal of Experimental Botany*, **68**, 4339-4355.
- Conn, S., Hocking, B., Dayod, M., Xu, B., Athman, A., Henderson, S., Aukett, L., Conn, V., Shearer, M., Fuentes, S., Tyerman, S. and Gilliham, M.** (2013) Protocol: optimising hydroponic growth systems for nutritional and physiological analysis of *Arabidopsis thaliana* and other plants. *Plant Methods*, **9**, 4.
- Cubero-Font, P., Maierhofer, T., Jaslan, J., Rosales, M.A., Espartero, J., Diaz-Rueda, P., Muller, H.M., Hurter, A.L., Al-Rasheid, K.A., Marten, I., Hedrich, R., Colmenero-Flores, J.M. and Geiger, D.** (2016) Silent S-Type anion channel subunit SLAH1 gates SLAH3 open for chloride root-to-shoot translocation. *Current Biology*, **26**, 2213-2220.
- De Angeli, A., Baetz, U., Francisco, R., Zhang, J., Chaves, M. and Regalado, A.** (2013a) The vacuolar channel VvALMT9 mediates malate and tartrate accumulation in berries of *Vitis vinifera*. *Planta*, **238**, 283-291.
- De Angeli, A., Zhang, J., Meyer, S. and Martinoia, E.** (2013b) AtALMT9 is a malate-activated vacuolar chloride channel required for stomatal opening in *Arabidopsis*. *Nature Communications*, **4**, 1804.

- de Loryn, L.C., Petrie, P.R., Hasted, A.M., Johnson, T.E., Collins, C. and Bastian, S.E.P.** (2014) Evaluation of sensory thresholds and perception of sodium chloride in grape juice and wine. *American Journal of Enology and Viticulture*, **65**, 124-133.
- Donkin, R., Robinson, S., Sumbly, K., Harris, V., McBryde, C. and Jiranek, V.** (2010) Sodium chloride in Australian grape juice and its effect on alcoholic and malolactic fermentation. *American Journal of Enology and Viticulture*, **61**, 392-400.
- Fasoli, M., Dal Santo, S., Zenoni, S., Torrielli, G.B., Farina, L., Zamboni, A., Porceddu, A., Venturini, L., Bicego, M., Murino, V., Ferrarini, A., Delledonne, M. and Pezzotti, M.** (2012) The grapevine expression atlas reveals a deep transcriptome shift driving the entire plant into a maturation program. *The Plant Cell*, **24**, 3489-3505.
- Fisarakis, I., Nikolaou, N., Tsikalas, P., Therios, I. and Stavrakas, D.** (2005) Effect of salinity and rootstock on concentration of potassium, calcium, magnesium, phosphorus, and nitrate–nitrogen in Thompson Seedless grapevine. *Journal of Plant Nutrition*, **27**, 2117-2134.
- Gilliham, M. and Tester, M.** (2005) The regulation of anion loading to the maize root xylem. *Plant Physiology*, **137**, 819-828.
- Gilliham, M. and Tyerman, S.D.** (2016) Linking metabolism to membrane signaling: the GABA–malate connection. *Trends in Plant Science*, **21**, 295-301.
- Gimeno, V., Syvertsen, J.P., Nieves, M., Simón, I., Martínez, V. and García-Sánchez, F.** (2009) Additional nitrogen fertilization affects salt tolerance of lemon trees on different rootstocks. *Scientia Horticulturae*, **121**, 298-305.
- Glass, A.D.M. and Siddiqi, M.Y.** (1985) Nitrate inhibition of chloride influx in barley: Implications for a proposed chloride homeostat. *Journal of Experimental Botany*, **36**, 556-566.
- Gong, H., Blackmore, D., Clingeleffer, P., Sykes, S., Jha, D., Tester, M. and Walker, R.** (2011) Contrast in chloride exclusion between two grapevine genotypes and its variation in their hybrid progeny. *Journal of Experimental Botany*, **62**, 989-999.
- Gruber, B.D., Ryan, P.R., Richardson, A.E., Tyerman, S.D., Ramesh, S., Hebb, D.M., Howitt, S.M. and Delhaize, E.** (2010) HvALMT1 from barley is involved in the transport of organic anions. *Journal of Experimental Botany*, **61**, 1455-1467.
- Guo, J., Zhou, Q., Li, X., Yu, B. and Luo, Q.** (2017) Enhancing NO₃⁻ supply confers NaCl tolerance by adjusting Cl⁻ uptake and transport in *G. max* & *G. soja*. *Journal of soil science and plant nutrition*, **17**, 194-202.
- Hanson, B. and May, D.** (2011) *Drip irrigation salinity management for row crops*: UCANR Publications.
- Henderson, S.W., Baumann, U., Blackmore, D.H., Walker, A.R., Walker, R.R. and Gilliham, M.** (2014) Shoot chloride exclusion and salt tolerance in grapevine is associated with differential ion transporter expression in roots. *BMC Plant Biology*, **14**.
- Henderson, S.W., Dunlevy, J.D., Wu, Y., Blackmore, D.H., Walker, R.R., Edwards, E.J., Gilliham, M. and Walker, A.R.** (2018) Functional differences in transport properties of natural HKT1;1 variants influence shoot Na⁺ exclusion in grapevine rootstocks. *New Phytologist*, **217**, 1113-1127.
- Hoekenga, O.A., Maron, L.G., Pineros, M.A., Cancado, G.M., Shaff, J., Kobayashi, Y., Ryan, P.R., Dong, B., Delhaize, E., Sasaki, T., Matsumoto, H., Yamamoto, Y., Koyama, H. and Kochian, L.V.** (2006) AtALMT1, which encodes a malate transporter, is identified as one of several genes critical for aluminum tolerance in Arabidopsis. *Proceedings of the National Academy of Sciences*, **103**, 9738-9743.
- Jha, D., Shirley, N., Tester, M. and Roy, S.J.** (2010) Variation in salinity tolerance and shoot sodium accumulation in Arabidopsis ecotypes linked to differences in the natural expression levels of transporters involved in sodium transport. *Plant, Cell & Environment*, **33**, 793-804.

- Karimi, M., Inze, D. and Depicker, A.** (2002) GATEWAY vectors for Agrobacterium-mediated plant transformation. *Trends in Plant Science*, **7**, 193-195.
- Köhler, B. and Raschke, K.** (2000) The delivery of salts to the xylem. Three types of anion conductance in the plasmalemma of the xylem parenchyma of roots of barley. *Plant Physiology*, **122**, 243-254.
- Köhler, B., Wegner, L.H., Osipov, V. and Raschke, K.** (2002) Loading of nitrate into the xylem: apoplastic nitrate controls the voltage dependence of X-QUAC, the main anion conductance in xylem-parenchyma cells of barley roots. *The Plant Journal*, **30**, 133-142.
- Lanyon, D.** (2011) *Salinity management interpretation guide* Waite Campus, Adelaide: Arris Pty Ltd.
- Larkin, M.A., Blackshields, G., Brown, N.P., Chenna, R., McGettigan, P.A., McWilliam, H., Valentin, F., Wallace, I.M., Wilm, A., Lopez, R., Thompson, J.D., Gibson, T.J. and Higgins, D.G.** (2007) Clustal W and Clustal X version 2.0. *Bioinformatics*, **23**, 2947-2948.
- Leske, P.A., Sas, A.N., Coulter, A.D., Stockley, C.S. and Lee, T.H.** (1997) The composition of Australian grape juice: chloride, sodium and sulfate ions. *Australian Journal of Grape and Wine Research*, **3**, 26-30.
- Li, B., Byrt, C., Qiu, J., Baumann, U., Hrmova, M., Evrard, A., Johnson, A.A., Birnbaum, K.D., Mayo, G.M., Jha, D., Henderson, S.W., Tester, M., Gilliham, M. and Roy, S.J.** (2016) Identification of a stelar-localized transport protein that facilitates root-to-shoot transfer of chloride in Arabidopsis. *Plant Physiology*, **170**, 1014-1029.
- Li, B., Tester, M. and Gilliham, M.** (2017) Chloride on the move. *Trends in Plant Science*, **22**, 236-248.
- Li, X.L., Wang, C.R., Li, X.Y., Yao, Y.X. and Hao, Y.J.** (2013) Modifications of Kyoho grape berry quality under long-term NaCl treatment. *Food chemistry*, **139**, 931-937.
- Ligaba, A., Katsuhara, M., Ryan, P.R., Shibasaka, M. and Matsumoto, H.** (2006) The *BnALMT1* and *BnALMT2* genes from rape encode aluminum-activated malate transporters that enhance the aluminum resistance of plant cells. *Plant Physiology*, **142**, 1294-1303.
- Ligaba, A., Maron, L., Shaff, J., Kochian, L. and Pineros, M.** (2012) Maize *ZmALMT2* is a root anion transporter that mediates constitutive root malate efflux. *Plant, Cell & Environment*, **35**, 1185-1200.
- Lunin, J. and Gallatin, M.H.** (1965) Salinity-fertility interactions in relation to the growth and composition of beans. I. Effect of N, P, and K. *Agronomy Journal*, **57**, 339-342.
- Maas, E.V. and Hoffman, G.J.** (1977) Crop salt tolerance - current assessment. *Journal of the Irrigation and Drainage Division*, **103**, 115-134.
- McFarlane, D.J. and Williamson, D.R.** (2002) An overview of water logging and salinity in southwestern Australia as related to the 'Ucarro' experimental catchment. *Agricultural Water Management*, **53**, 5-29.
- Møller, I.S., Gilliham, M., Jha, D., Mayo, G.M., Roy, S.J., Coates, J.C., Haseloff, J. and Tester, M.** (2009) Shoot Na⁺ exclusion and increased salinity tolerance engineered by cell type-specific alteration of Na⁺ transport in Arabidopsis. *The Plant Cell*, **21**, 2163-2178.
- Mullins, M.G. and Rajasekaran, K.** (1981) Fruiting cuttings: Revised method for producing test plants of grapevine cultivars. *American Journal of Enology and Viticulture*, **32**, 35-40.
- Munns, R. and Gilliham, M.** (2015) Salinity tolerance of crops – what is the cost? *New Phytologist*, **208**, 668-673.
- Nelson, B.K., Cai, X. and Nebenführ, A.** (2007) A multicolored set of *in vivo* organelle markers for co-localization studies in Arabidopsis and other plants. *The Plant Journal*, **51**, 1126-1136.
- Noguero, M. and Lacombe, B.** (2016) Transporters involved in root nitrate uptake and sensing by Arabidopsis. *Frontiers in plant science*, **7**, 1391-1391.

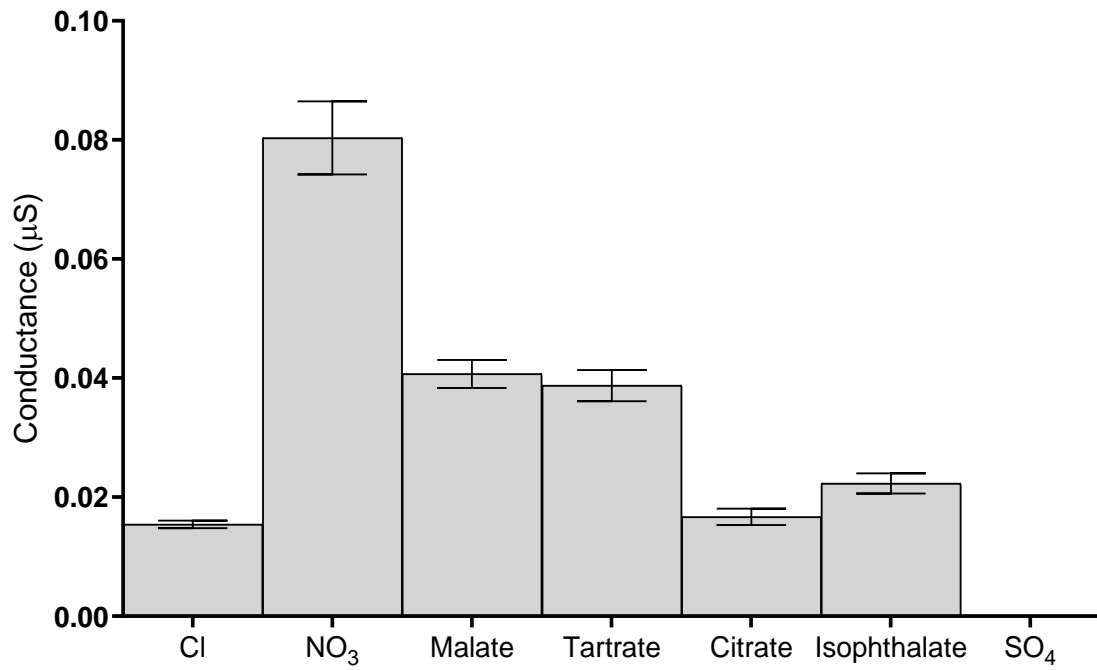
- Pannell, D.J. and Ewing, M.A.** (2006) Managing secondary dryland salinity: Options and challenges. *Agricultural Water Management*, **80**, 41-56.
- Piñeros, M.A., Cançado, G.M.A., Maron, L.G., Lyi, S.M., Menossi, M. and Kochian, L.V.** (2008) Not all ALMT1-type transporters mediate aluminum-activated organic acid responses: the case of ZmALMT1 – an anion-selective transporter. *The Plant Journal*, **53**, 352-367.
- Plett, D.C.** (2008) Spatial and temporal alterations of gene expression in rice.
- Prior, L.D., Grieve, A.M. and Cullis, B.R.** (1992a) Sodium chloride and soil texture interactions in irrigated field grown sultana grapevines. I. Yield and fruit quality. *Australian Journal of Agricultural Research*, **43**, 1051-1066.
- Prior, L.D., Grieve, A.M. and Cullis, B.R.** (1992b) Sodium chloride and soil texture interactions in irrigated field grown sultana grapevines. II. Plant mineral content, growth and physiology. *Australian Journal of Agricultural Research*, **43**, 1067-1083.
- Qiu, J., Henderson, S.W., Tester, M., Roy, S.J. and Gilliham, M.** (2016) SLAH1, a homologue of the slow type anion channel SLAC1, modulates shoot Cl⁻ accumulation and salt tolerance in *Arabidopsis thaliana*. *Journal of Experimental Botany*, **67**, 4495-4505.
- Ramesh, S.A., Tyerman, S.D., Gilliham, M. and Xu, B.** (2017) γ -Aminobutyric acid (GABA) signalling in plants. *Cellular and Molecular Life Sciences*, **74**, 1577-1603.
- Ramesh, S.A., Tyerman, S.D., Xu, B., Bose, J., Kaur, S., Conn, V., Domingos, P., Ullah, S., Wege, S., Shabala, S., Feijo, J.A., Ryan, P.R. and Gilliham, M.** (2015) GABA signalling modulates plant growth by directly regulating the activity of plant-specific anion transporters. *Nature Communications*, **6**.
- Roberts, S.K.** (2006) Plasma membrane anion channels in higher plants and their putative functions in roots. *New Phytologist*, **169**, 647-666.
- Sainsbury, F., Thuenemann, E.C. and Lomonosoff, G.P.** (2009) pEAQ: versatile expression vectors for easy and quick transient expression of heterologous proteins in plants. *Plant Biotechnology Journal*, **7**, 682-693.
- Sasaki, T., Yamamoto, Y., Ezaki, B., Katsuhara, M., Ahn, S.J., Ryan, P.R., Delhaize, E. and Matsumoto, H.** (2004) A wheat gene encoding an aluminum-activated malate transporter. *The Plant Journal*, **37**, 645-653.
- Sharma, T., Dreyer, I., Kochian, L. and Piñeros, M.A.** (2016) The ALMT Family of organic acid transporters in plants and their involvement in detoxification and nutrient security. *Frontiers in Plant Science*, **7**, 1488.
- Shelden, M.C., Howitt, S.M., Kaiser, B.N. and Tyerman, S.D.** (2009) Identification and functional characterisation of aquaporins in the grapevine, *Vitis vinifera*. *Functional Plant Biology*, **36**, 1065-1078.
- Stevens, R.M., Harvey, G. and Partington, D.L.** (2011) Irrigation of grapevines with saline water at different growth stages: effects on leaf, wood and juice composition. *Australian Journal of Grape and Wine Research*, **17**, 239-248.
- Taochy, C., Gaillard, I., Ipotesi, E., Oomen, R., Leonhardt, N., Zimmermann, S., Peltier, J.B., Szponarski, W., Simonneau, T. and Sentenac, H.** (2015) The Arabidopsis root stele transporter NPF2.3 contributes to nitrate translocation to shoots under salt stress. *The Plant Journal*, **83**, 466-479.
- Vandesompele, J., De Preter, K., Pattyn, F., Poppe, B., Van Roy, N., De Paepe, A. and Speleman, F.** (2002) Accurate normalization of real-time quantitative RT-PCR data by geometric averaging of multiple internal control genes. *Genome Biology*, **3**, research0034.0031-research0034.0011.
- Walker, R.R., Blackmore, D.H., Clingeffer, P.R. and Correll, R.L.** (2002) Rootstock effects on salt tolerance of irrigated field-grown grapevines (*Vitis vinifera* L. cv. Sultana): 1. Yield and vigour inter-relationships. *Australian Journal of Grape and Wine Research*, **8**, 3-14.

- Walker, R.R., Blackmore, D.H., Clingeleffer, P.R., Godden, P., Francis, L., Valente, P. and Robinson, E.** (2003) Salinity effects on vines and wines. *Bulletin de l'Office International de la Vigne et du Vin*, **76**, 200-227.
- Wege, S., Gilliam, M. and Henderson, S.W.** (2017) Chloride: not simply a 'cheap osmoticum', but a beneficial plant macronutrient. *Journal of Experimental Botany*, **68**, 3057-3069.
- Wu, Y., Li, J. and Gilliam, M.** (2019) An R-based web app Smart-IV for automated and integrated high throughput electrophysiology data processing.

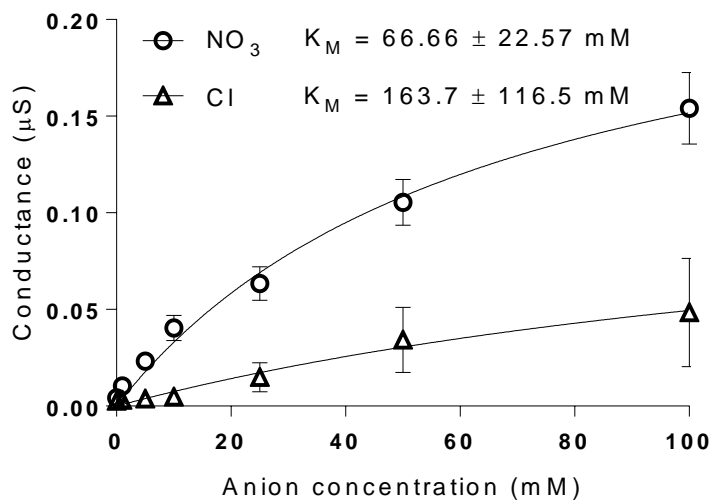
Figures

Figure 1

A



B



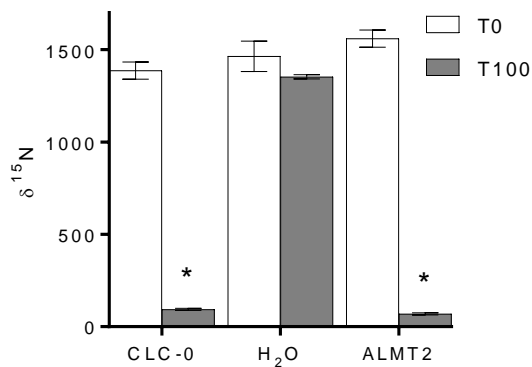
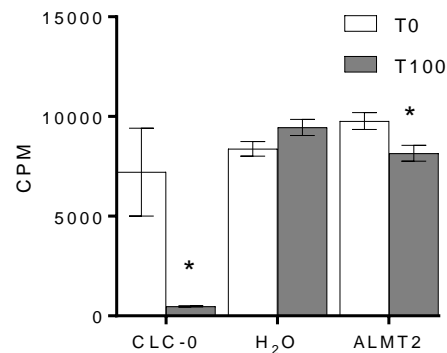
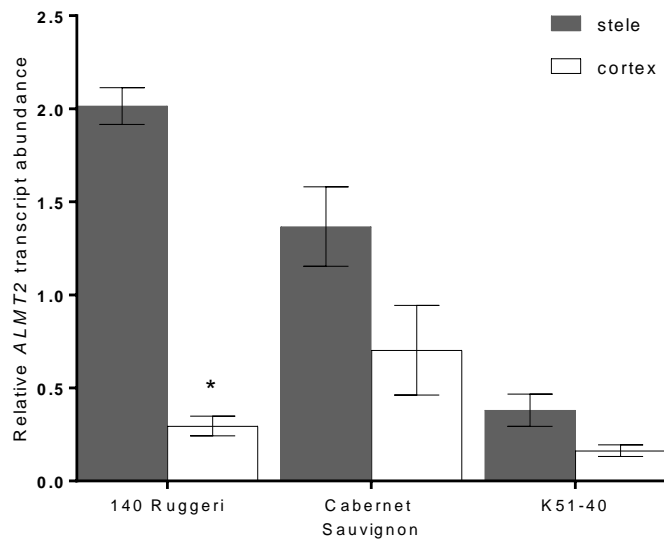
C**D**

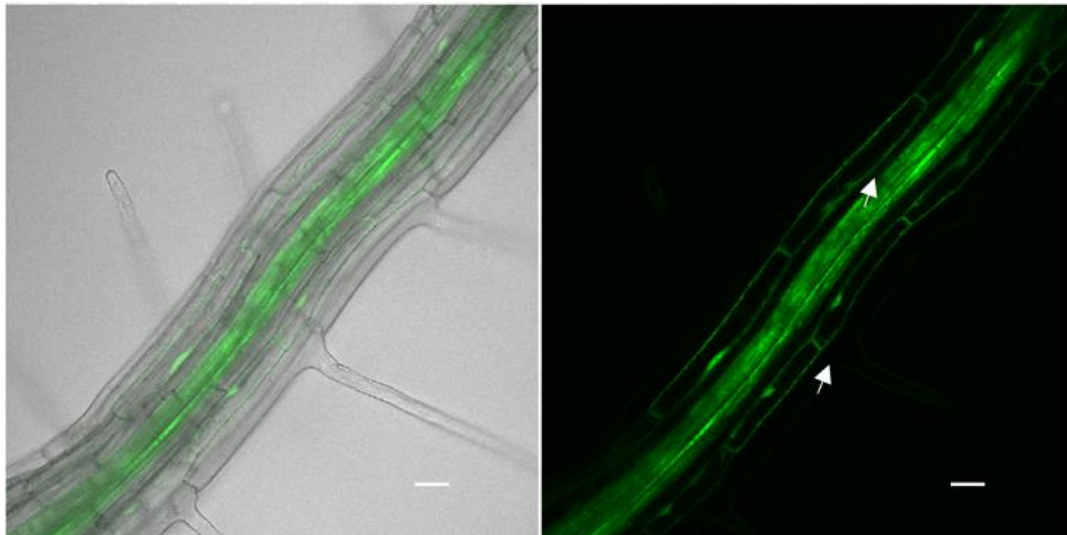
Figure 1: VviALMT2 is permeable to multiple organic and inorganic anions, and is most permeable to NO_3^- . (A) Anion outward conductance of VviALMT2 was calculated from whole cell TEVC data of VviALMT2 expressing *Xenopus* oocytes in the presence of 10 mM of different anions. Data are means \pm SE ($n \geq 5$ oocytes). (B) Michealis-Menten kinetics of NO_3^- and Cl^- uptake through VviALMT2 expressing oocytes show that VviALMT2 is a low affinity anion transporter. Currents through oocytes were recorded using TEVC when perfused with buffers with anion concentrations from 0 to 100 mM. Outward conductance at reversal potential is plotted against anion concentrations. The substrate concentration at which the half-maximal uptake rate is reached (K_M) was calculated from the Michealis-Menten regression of the conductance of each anion. Data are mean \pm SE ($n \geq 9$ oocytes). (C) VviALMT2 functions in NO_3^- efflux. Gene expressing or control oocytes were injected with K^{15}NO_3 and tested for $\delta^{15}\text{N}$ before (T0) and after being incubated in the efflux buffers for 100 min (T100). *Torpedo* CLC-0 was used as a positive control. Asterisk indicates significant differences between $\delta^{15}\text{N}$ measurements at T0 and T100 (mean \pm SE, $n \geq 5$ replicates, $P < 0.01$, Student's t-test). (D) VviALMT2 might function in Cl^- efflux. Gene expressing or control oocytes were injected with H^{36}Cl and tested for tracer activity (CPM) before (T0) and after being incubated in the efflux buffers for 100 min (T100). Asterisk indicates significant differences between CPM measurements at T0 and T100 (mean \pm SE, $n = 3-6$ oocytes, $P < 0.05$, Student's t-test).

Figure 2

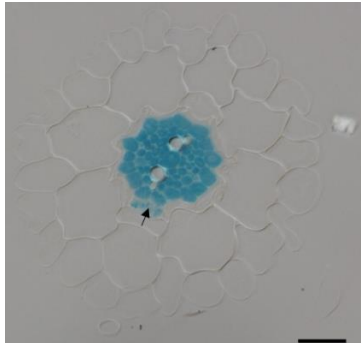
A



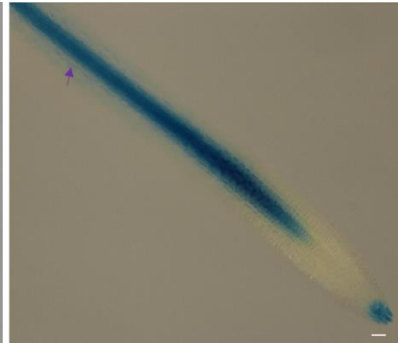
B



C



D



E

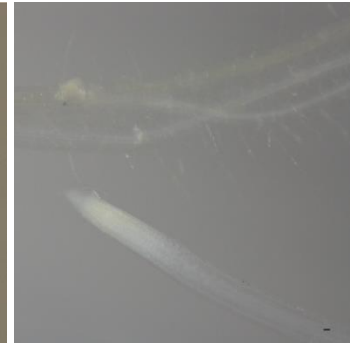
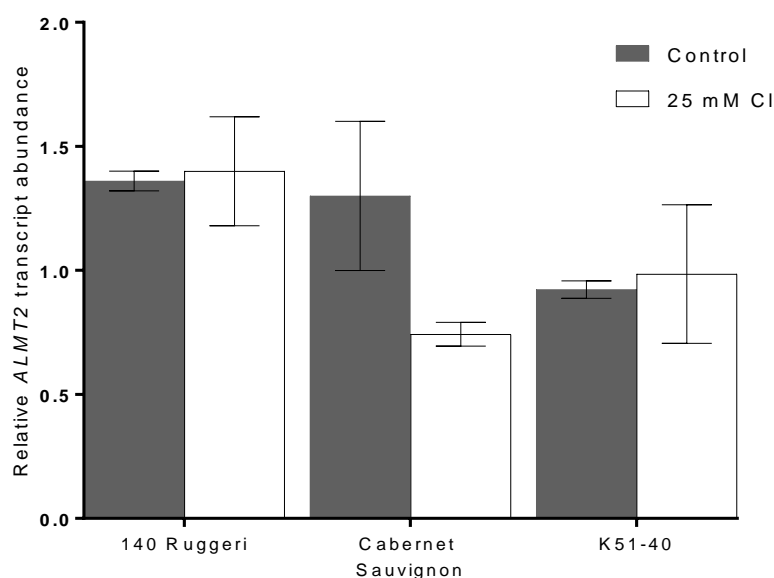


Figure 2: *VviALMT2* is highly expressed in root stele, endodermal passage cells and cortex. (A) *VviALMT2* is more abundant in the root stelar enriched fractions than the

cortex enriched fractions of 140 Ruggeri. RT-qPCR was performed on cDNA derived from cortical or stelar enriched fractions of hydroponically grown roots harvested from the rooted leaves of 3 different grapevine cultivars. Relative gene expression levels were calculated in reference to the 3 housekeeping genes. Data is mean expression level relative to the Cabernet Sauvignon cortical replicate $1 \pm SE$ (n = 3 replicates). Asterisk indicates significant differences between expression levels in stele and cortex ($P < 0.01$, Student's t-test). (B) Arabidopsis root images show the *proVviALMT2* driven GFP activity in stele and cortex, but not in epidermis and endodermis. *proVviALMT2:GFP6-HDEL* transformed Arabidopsis roots were imaged using a confocal microscope. White arrows point out that GFP signals are not observed in endodermis and epidermis. Scale bars = 20 μm . (C – D) Arabidopsis root images show the *proVviALMT2* driven GUS activity in stele, endodermal passage cells (black arrow) and cortex (purple arrow). *proVviALMT2:GUS* transformed Arabidopsis roots were GUS stained for (C) transverse section or (D) whole root imaging. (E) Wild-type Arabidopsis roots were used as negative control for the GUS staining experiment which show no stains. Scale bars = 20 μm .

Figure 3

A



B

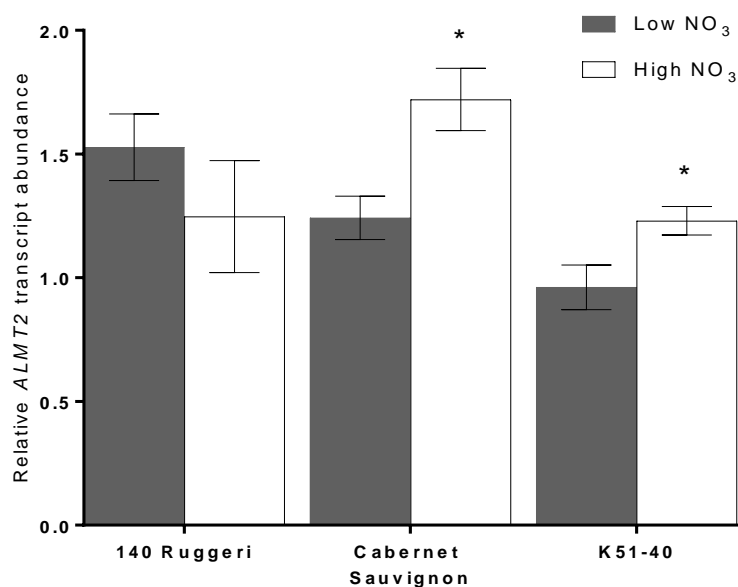


Figure 3: Expression level of *VviALMT2* in grapevine roots is up-regulated by post-starvation high $[\text{NO}_3^-]$ re-supply, but not by mild Cl^- stress. Relative grapevine root gene expression levels were analysed using RT-qPCR and calculated in reference to the 3 housekeeping genes. Expression levels were normalised to Cabernet Sauvignon control sample 1. (A) Relative *VviALMT2* gene expression levels in grapevine roots does not respond to 25 mM Cl^- stress. Grapevine rooted leaves grown in hydroponics were treated with either control or 25 mM Cl^- solution before harvesting. Data are

means \pm SE (n = 2-3 replicates). (B) Relative *VviALMT2* gene expression levels in grapevine roots were up-regulated by NO₃⁻ re-supply post starvation. Grapevine green cuttings were grown in perlite: vermiculite media and NO₃⁻ starved for 2 weeks before treating with either low [NO₃⁻] (0.8 mM) or high [NO₃⁻] (12 mM) solutions. Roots were harvested 24 h post treatments. Data are means \pm SE (n = 3 replicates). Asterisk indicates significant differences between expression levels in low and high [NO₃⁻] treated roots (P < 0.05, Student's t-test).

Figure 4

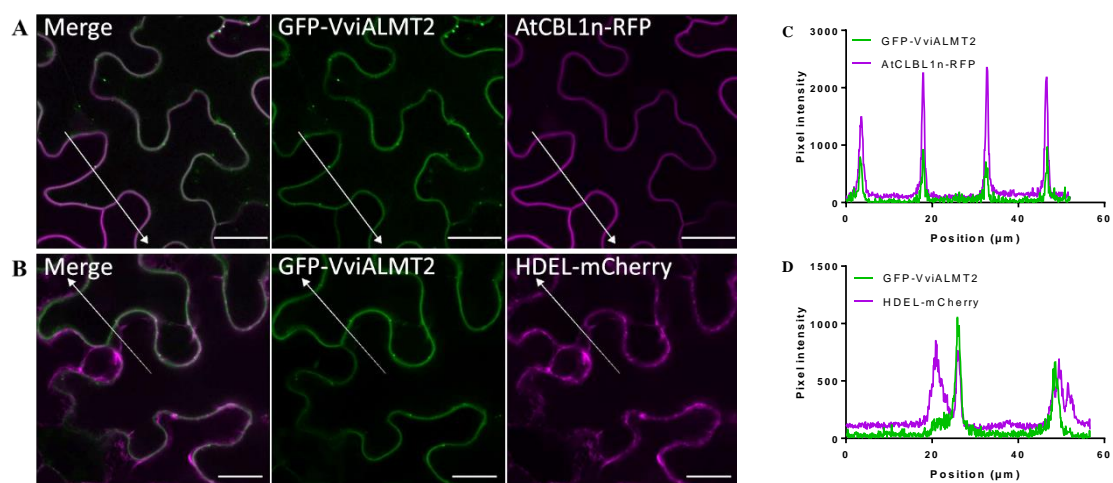
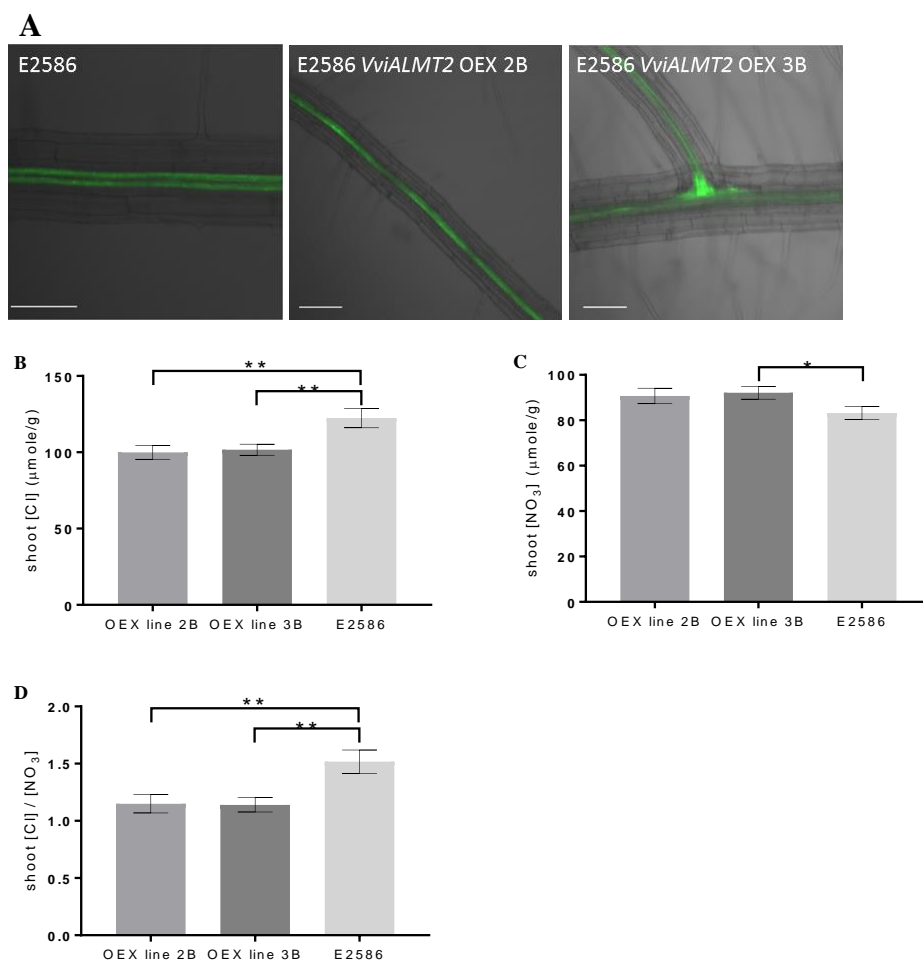


Figure 4: VviALMT2 is localised to the plasma membrane. Confocal laser scanning micrographs show (A – B) GFP-VviALMT2 co-localisation with (A) the plasma membrane (PM) marker AtCBL1n-RFP (representative of $n = 10$), and poor co-localisation with (B) the endoplasmic reticulum (ER) marker HDEL-mCherry (representative of $n = 5$) in tobacco cells. The abaxial side of tobacco (*N. benthamina*) leaves were imaged 2 days after agrobacterium infiltration. Scale bars = 20 μm. (C – D) Signal profiles of GFP (green) and RFP or mCherry (magenta) corresponding to the white arrow in the microscopic images in (A – B). Overlapping peaks indicate co-localisation between the two signals.

Figure 5



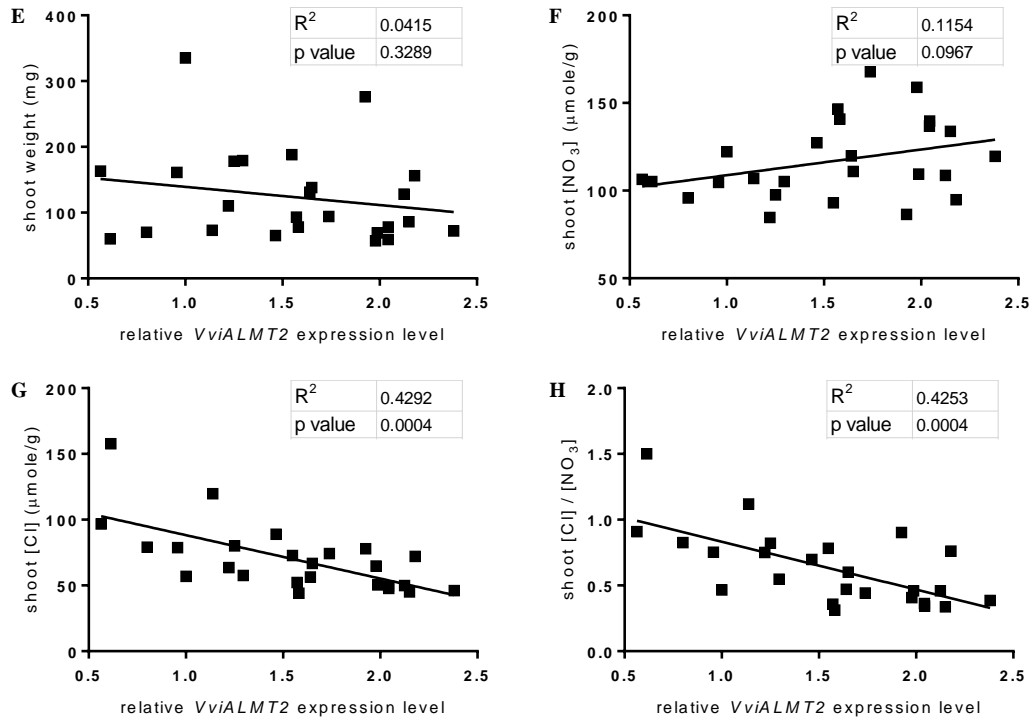


Figure 5: The increase in *VviALMT2* expression in Arabidopsis root vasculature reduces the shoot $[Cl^-]$ post 75 mM NaCl treatment. (A) The enhancer trap line E2586 mGFP5-ER expression pattern showed root vasculature specific transgene over-expression. Scale bars = 100 μm . (B–D) The Arabidopsis E2586 *VviALMT2* over-expression (OEX) line 2B and 3B have (B) lower shoot $[Cl^-]$ than the non-transformed E2586 line after the 75 mM NaCl treatment; (C) the OEX line 3B had slightly significantly higher shoot $[NO_3^-]$ than the E2586 line, (D) and the $[Cl^-]/[NO_3^-]$ ratios of both OEX lines were lower than those of the E2586 line. Data are means \pm SEM ($n = 22-24$ samples). Asterisk indicates statistically significant differences ($P < 0.05$, Student's t-test). (E – H) The relative *VviALMT2* expression levels in Arabidopsis roots did not have significant correlations with (E) the shoot fresh weights or (F) the shoot $[NO_3^-]$; but the expression levels had negative linear correlations with (G) the shoot $[Cl^-]$ as well as (H) the shoot $[Cl^-]/[NO_3^-]$ ratios. The R^2 values show the goodness of the linear regression fit and the p values show the statistically significant difference of the slope from zero.

Figure 6

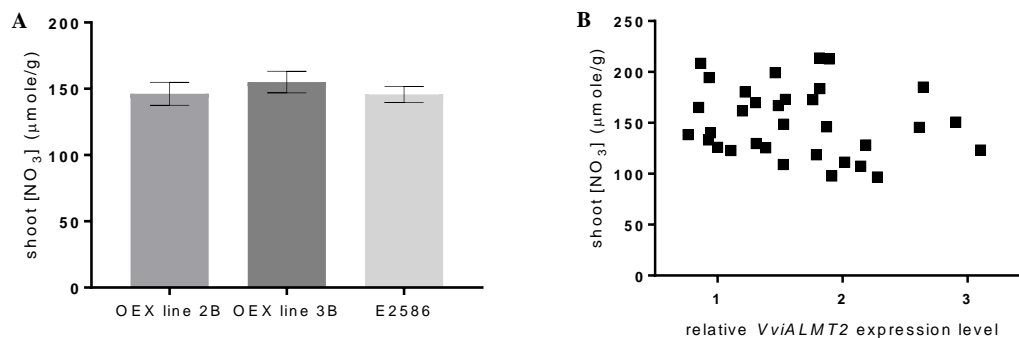
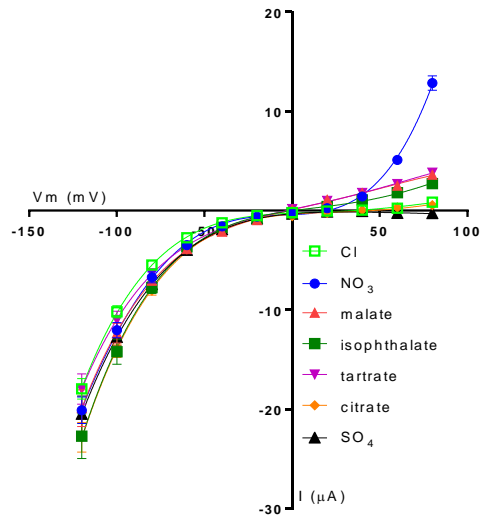


Figure 6: The *VviALMT2* expression in Arabidopsis root vasculature is not correlated with shoot [NO₃⁻] post the NO₃⁻ starvation and re-supply treatment. (A) The Arabidopsis E2586 *VviALMT2* over-expression (OEX) line 2B and 3B have similar shoot [NO₃⁻] compared to the non-transformed E2586 line after the NO₃⁻ starvation and re-supply treatment. Data are means \pm SEM (n = 11-18 samples). (B) The relative *VviALMT2* expression levels in Arabidopsis roots did not have a linear correlation with the shoot [NO₃⁻].

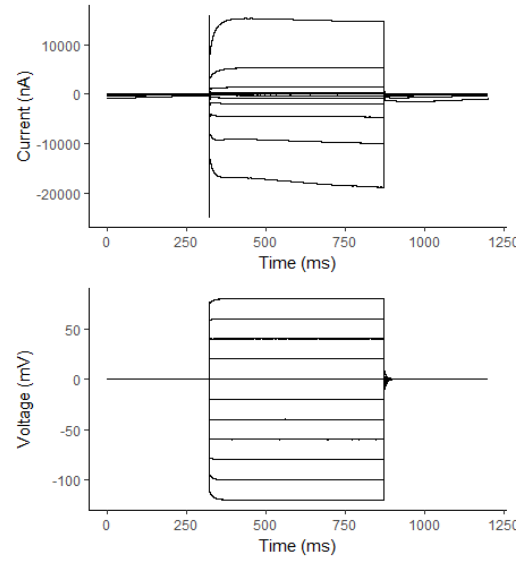
Supporting information

Figure S1

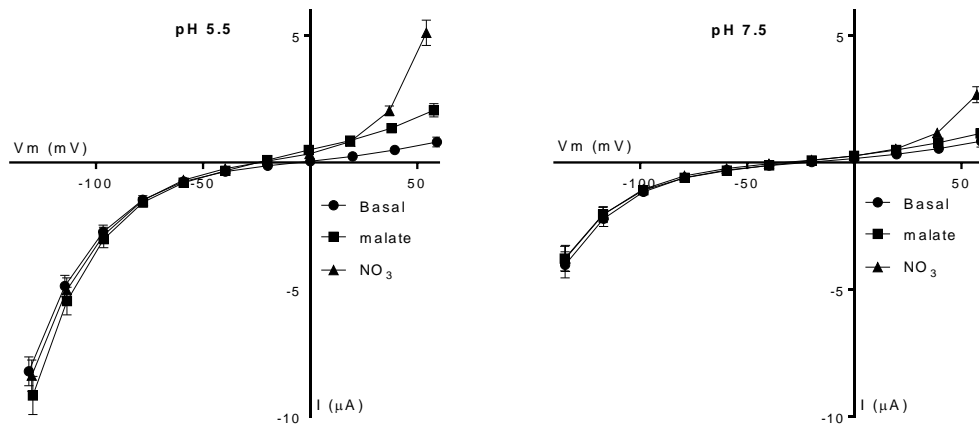
A



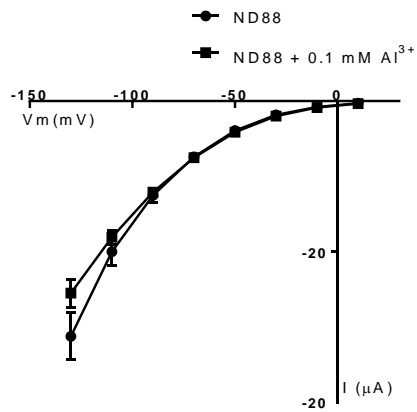
B



C



D



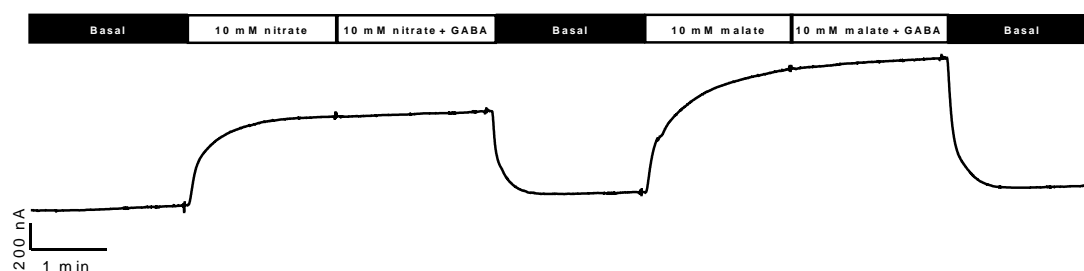
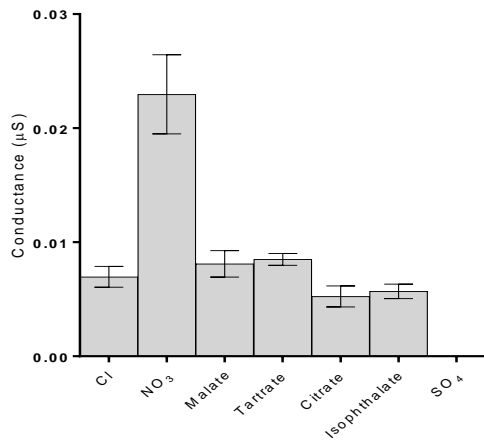
E

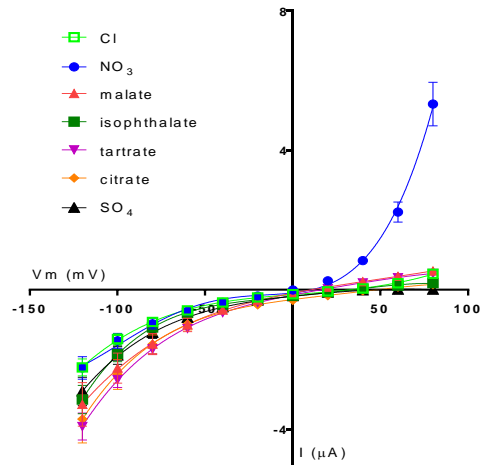
Figure S1: Electrophysiological characteristics of *Xenopus* oocytes expressing *VviALMT2*. (A) I-V data of the anion conductance experiment in Figure 1A. Anions are shown inset. Data are mean \pm SE (n = 5 oocytes). (B) Current traces from a typical *VviALMT2* expressing oocyte. The oocyte was TEVC tested using stepwise pulses from +80 mV to -120 mV (illustrated in the bottom figure) in the basal buffer containing 10 mM of NaNO₃. (C) *VviALMT2* expressing oocytes conferred larger currents at pH 5.5 (left) than at pH 7.5 (right). *VviALMT2* expressing oocytes were TEVC tested in basal buffers at either pH 5.5 or pH 7.5. Data are current means of *VviALMT2* expressing oocytes following subtraction of means of corresponding water injected oocytes \pm SE (n = 7). (D) *VviALMT2* expressing oocytes did not mediate Al³⁺ activated malate efflux. Oocytes were loaded with 10 mM of Na malate and voltage clamped in the ND88 perfusion buffer with or without 0.1 mM AlCl₃. Data are mean \pm SE (n = 8 oocytes). (E) The currents through the *VviALMT2* expressing oocyte were not affected by 1 mM of GABA. The oocyte was TEVC tested using the gap-free protocol in the perfusion buffers labelled in the current trace graph at 50 mV.

Figure S2

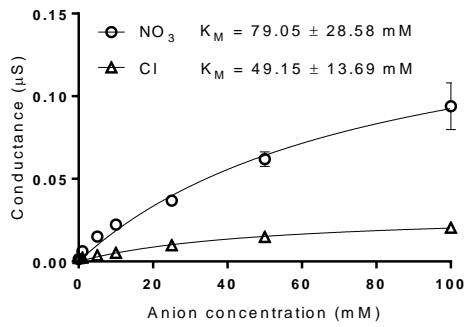
A



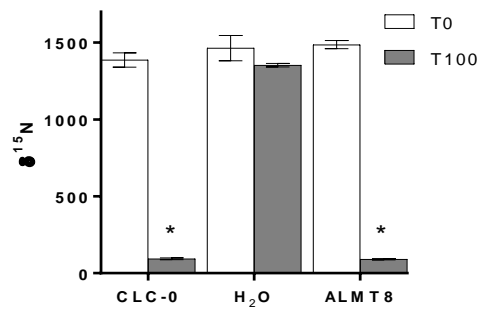
B



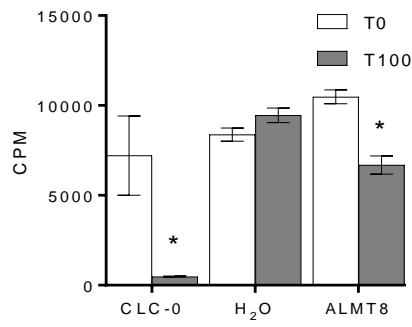
C



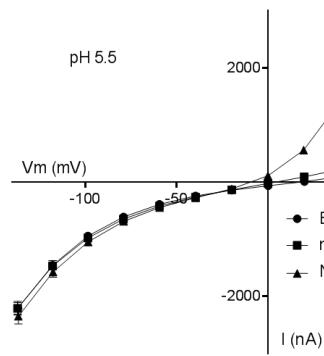
D



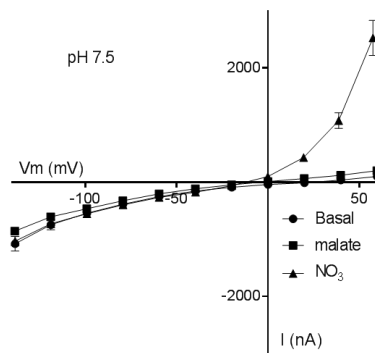
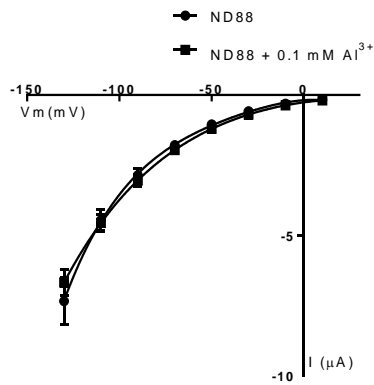
E



F



G



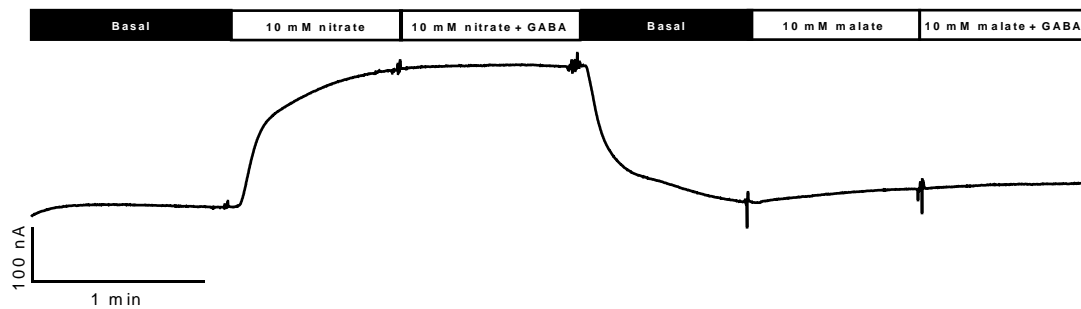
H

Figure S2: *VviALMT8* is a low affinity NO_3^- , Cl^- and organic acid transporter which is more active at lower pH than at neutral pH. (A) Anion outward conductance of *VviALMT8* calculated from whole cell TEVC data of *VviALMT8* expressing *Xenopus* oocytes shows that *VviALMT8* is permeable to multiple anions, especially NO_3^- . Oocytes were tested with perfusion buffers containing 10 mM of different anions. Data are mean \pm SE ($n \geq 5$ oocytes). (B) The current-voltage relationship plot of the data from the same experiment. (C) Michealis-Menten kinetics of NO_3^- and Cl^- uptake through *VviALMT8* expressing oocytes show that *VviALMT8* is a low affinity anion transporter. Currents through oocytes were recorded using TEVC when perfused with buffers with anion concentrations from 0 to 100 mM. Outward conductance between E_{rev} and +20 mV was plotted against anion concentration. The substrate concentration at which the half-maximal uptake rate is reached (K_m) was calculated from the Michealis-Menten regression of the conductance of each anion. Data are mean \pm SE ($n \geq 4$ oocytes). (D) *VviALMT8* also functions in NO_3^- efflux. Gene expressing or control oocytes were injected with K^{15}NO_3 and tested for $\delta^{15}\text{N}$ before (T0) and after being incubated in the efflux buffers for 100 min (T100). *Torpedo* CLC-0 was used as a positive control. Asterisk indicates significant differences between $\delta^{15}\text{N}$ measurements at T0 and T100 (mean \pm SE, $n \geq 5$ replicates, $P < 0.01$, Student's t-test). (E) *VviALMT8* functions in Cl^- efflux. *VviALMT8* expressing or control oocytes were injected with ^{36}Cl and tested for CPM before (T0) and after being incubated in the efflux buffers for 100 min (T100). Asterisk indicates significant differences between CPM measurements at T0 and T100 (mean \pm SE, $n = 3-6$ oocytes, $P < 0.01$, Student's t-test). (F) *VviALMT8* expressing oocytes conferred larger currents at pH 5.5 (top) than at pH 7.5 (bottom). Gene expressing oocytes were TEVC tested at either pH 5.5 or pH 7.5, and data are presented as I-V curves. Data are current means of *VviALMT8* expressing oocytes subtract means of corresponding water injected oocytes \pm SE ($n \geq 5$). (G) *VviALMT8*

expressing oocytes were not mediating Al^{3+} activated malate efflux. Oocytes were loaded with 10 mM of Na malate and TEVC tested in the ND88 perfusion buffer with or without 0.1 mM AlCl_3 . Data are mean \pm SE (n = 5 oocytes). (H) The currents through the VviALMT8 expressing oocyte were not affected by 1 mM of GABA. The oocyte was TEVC tested using the gap-free protocol in the perfusion buffers labelled in the current trace graph at 50 mV.

Figure S3

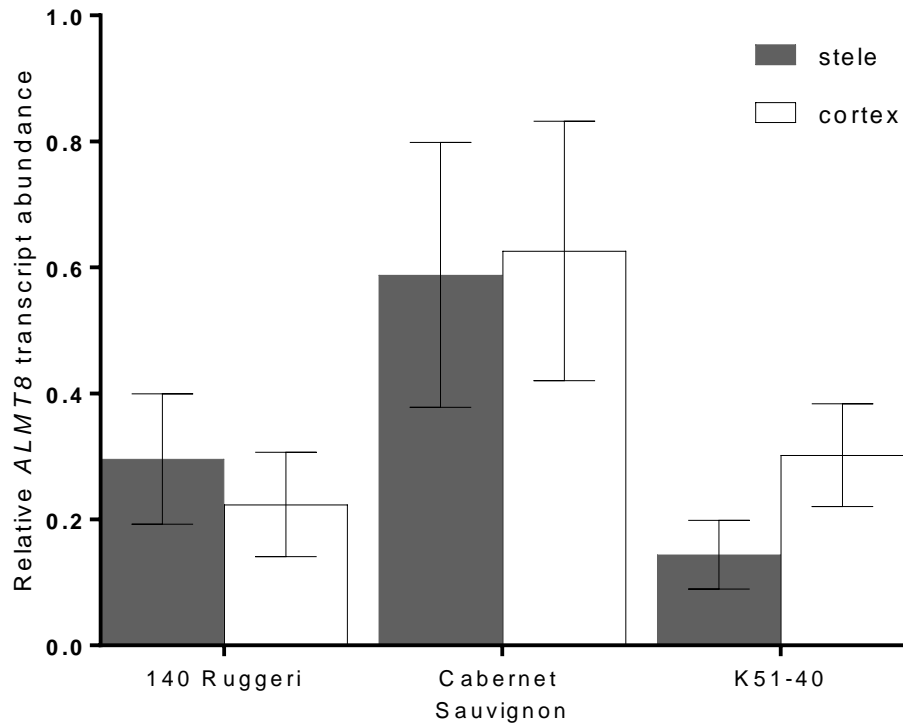
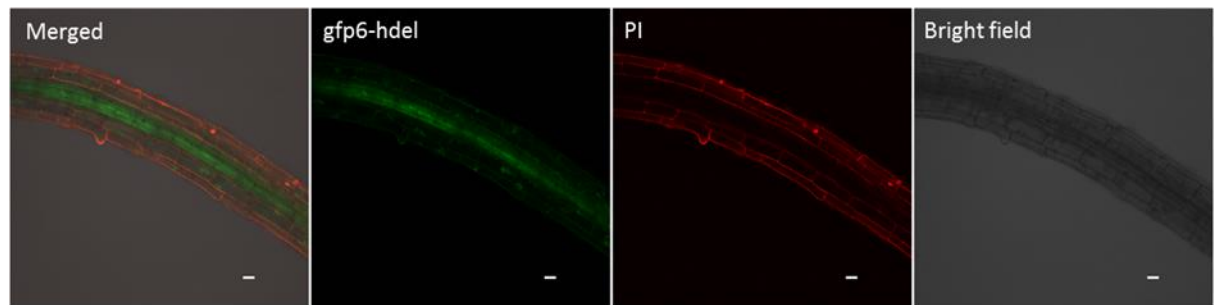


Figure S3: *VviALMT8* is not differentially expressed between grapevine root stelar and cortex enriched fractions. RT-qPCR was performed on cDNA derived from cortical or stelar enriched fractions of hydroponically grown roots harvested from the rooted leaves of 3 different grapevine cultivars, 140 Ruggeri, Cabernet Sauvignon and K51-40. Relative gene expression levels were calculated in reference to 3 housekeeping genes. Data is mean expression level relative to the Cabernet Sauvignon cortical replicate $1 \pm SE$ ($n = 3$ replicates).

Figure S4

A



B



C

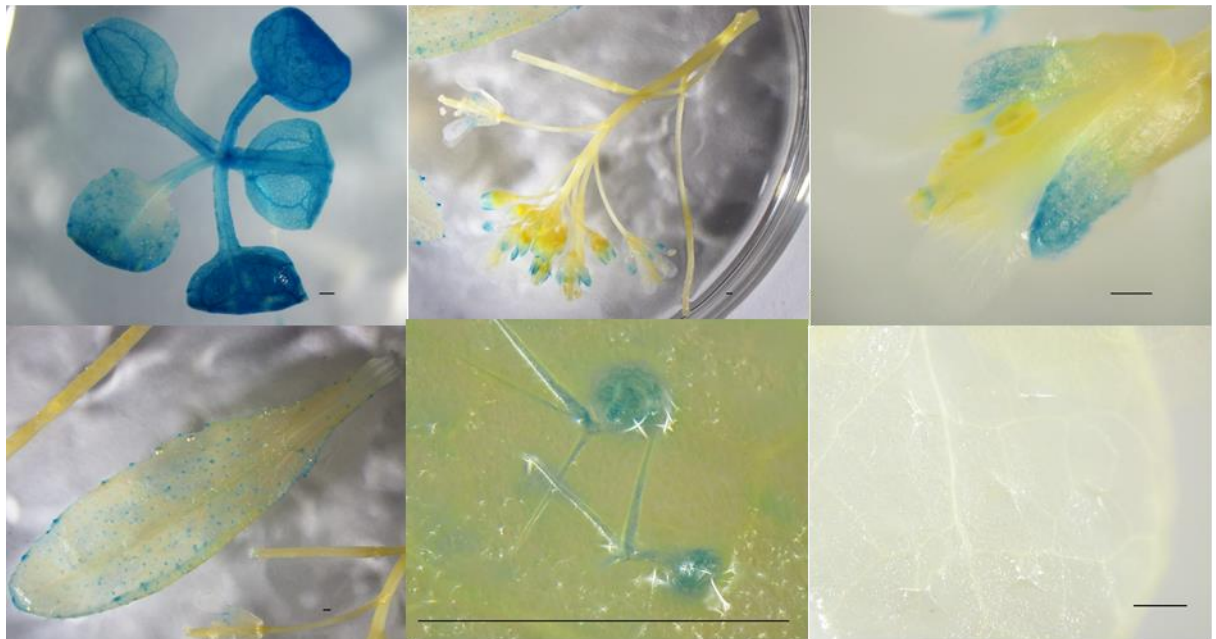


Figure S4: *proVviALMT8* driven GFP and GUS activities in Arabidopsis tissues. (A) Arabidopsis root images showing the *proVviALMT8* driven GFP activity in stele, cortex, and epidermis. *proVviALMT8*:GFP6-HDEL transformed Arabidopsis roots were stained with PI before imaging using a confocal microscope. Scale bars = 20 μ m. (B)

Arabidopsis root images showing the *proVviALMT8* driven GUS activity in stele, endodermal passage cells and cortex (left and middle). Arrow points to a stained passage cell in endodermis. Wild-type Col-0 Arabidopsis roots were GUS stained and used as negative controls (right). Scale bars = 20 μm . (C) A *proVviALMT8:GUS* transformed Arabidopsis seedling (top left), stems, flowers and siliques (top middle and right), a mature leaf (bottom left) and trichomes (bottom middle) were GUS stained and imaged using a stereo microscope. Wild-type Col-0 Arabidopsis plants were GUS stained and used as negative controls (bottom right). Scale bars = 500 μm .

Figure S5

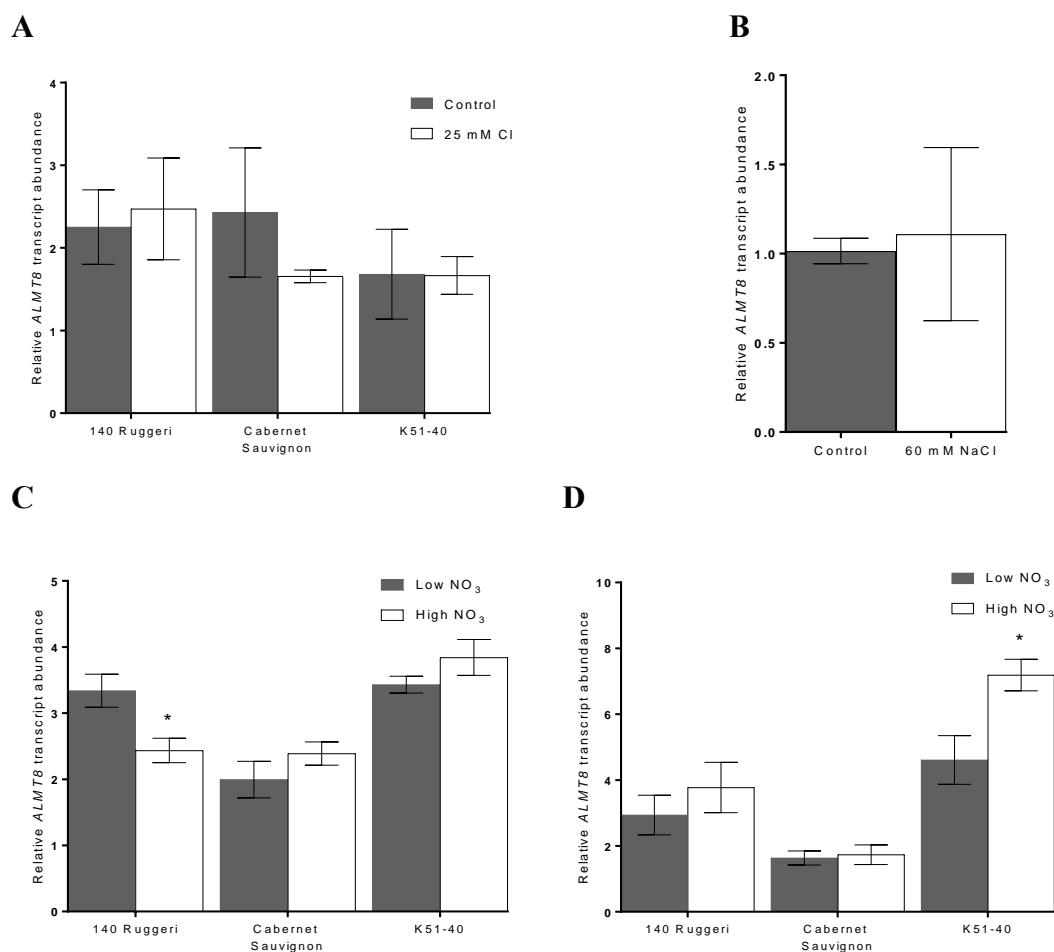
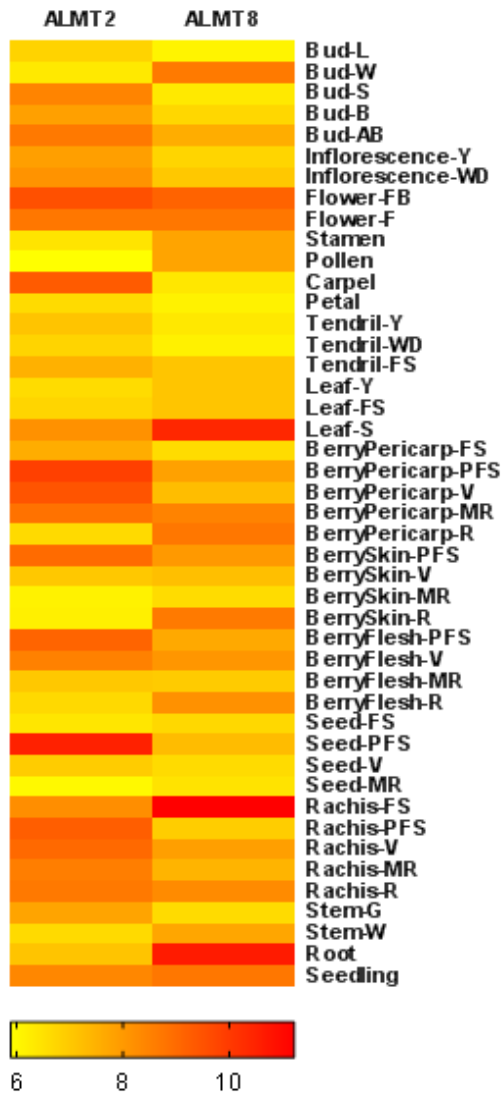


Figure S5: Expression levels of *VviALMT8* in grapevine roots does not respond to Cl^- stress or post-starvation high $[\text{NO}_3^-]$ re-supply. Grapevine plantlets were treated with different nutrient solutions and the roots were harvested for RT-qPCR. Relative gene expression levels were calculated in reference to 3 housekeeping genes. (A) Relative *VviALMT8* gene expression levels in grapevine roots did not respond to 25 mM Cl^- stress. Grapevine rooted leaves grown in hydroponics were treated with either control or 25 mM Cl^- solution before harvesting. Expression levels were normalised to Cabernet Sauvignon control sample 1. Data are means \pm SE (n = 3 replicates). (B) Relative *VviALMT8* expression levels in Cabernet Sauvignon roots does not respond to 60 mM NaCl stress. Expression levels of each gene were normalised to control sample 1. Data are means \pm SE (n = 2-3 replicates). (C – D) Relative *VviALMT8* expression levels in roots were not regulated by NO_3^- re-supply post starvation. Grapevine green cuttings were grown in perlite: vermiculite media and NO_3^- starved for 2 weeks before

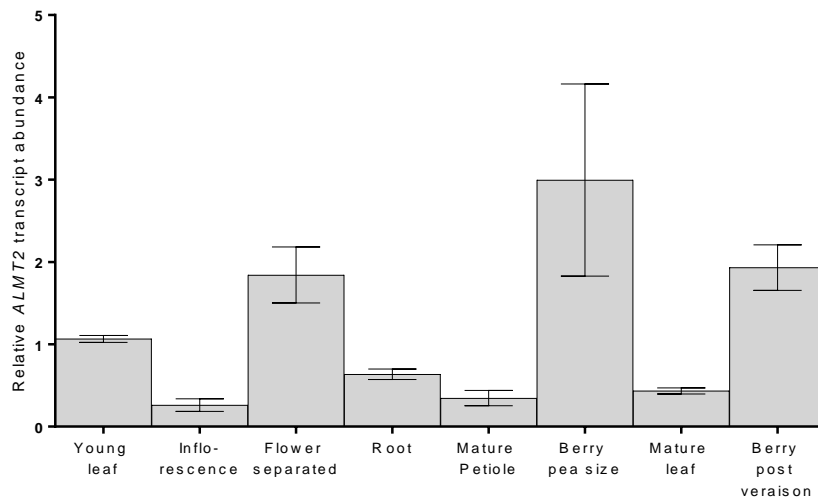
treatments. Plants were then watered with either low $[\text{NO}_3^-]$ (0.8 mM) or high $[\text{NO}_3^-]$ (12 mM) solutions. Root tissues were harvested (C) 3 h or (D) 24 h post treatments. Expression levels were normalised to Cabernet Sauvignon low NO_3^- sample 1 in the respective dataset. Data are means \pm SE (n = 3-4 replicates). Asterisk indicates significant differences between expression levels in low and high $[\text{NO}_3^-]$ treated roots ($P < 0.05$, Student's t-test).

Figure S6

A



B



C

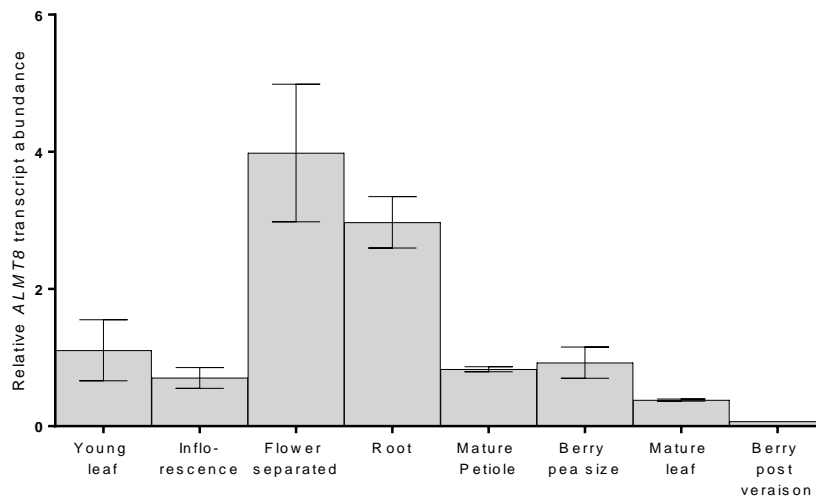


Figure S6: *VviALMT2* is most highly expressed in flower and berry related tissues, while *VviALMT8* is most highly expressed in roots, flowers and seedlings. (A) RMA-normalized signal intensities were obtained from the microarray gene expression study by Fasoli *et al.* (2012). Data presented in the heat map is the log₂ mean transformed signal intensities of the 4 probes and 3 biological predicates. (B – C) Relative expression levels of (B) *VviALMT2* and (C) *VviALMT8* in different tissue types of Cabernet Sauvignon. Cabernet Sauvignon plants were propagated from hard wood cuttings in pots and tissue samples were collected during the growing season. Each sample contains tissues harvested from 3 individual plants. RT-qPCR analysis was performed and the expression levels were normalised to the geometric mean of the expression levels of 3 housekeeping genes. Transcript abundance of each gene was relative to the abundance in young leaf sample 1. Data are mean ± SE (n = 3 samples).

Figure S7

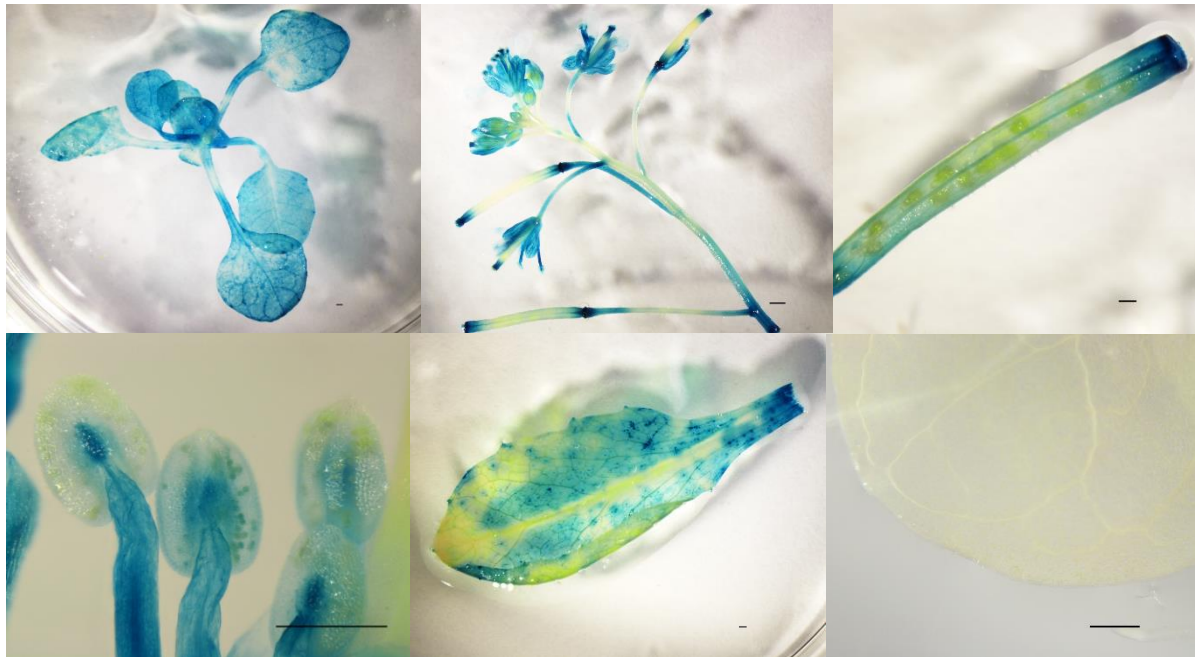


Figure S7: *proVviALMT2* driven GUS activity in other Arabidopsis tissues. A *proVviALMT2:GUS* transformed Arabidopsis seedling shoot (top left), stems, flowers and siliques (top middle and right), anthers (bottom left) and a mature leaf (bottom middle) were GUS stained and imaged using a stereo microscope. Wild-type Col-0 Arabidopsis plants were GUS stained and used as negative controls (bottom right). Scale bars = 500 μm .

Figure S8

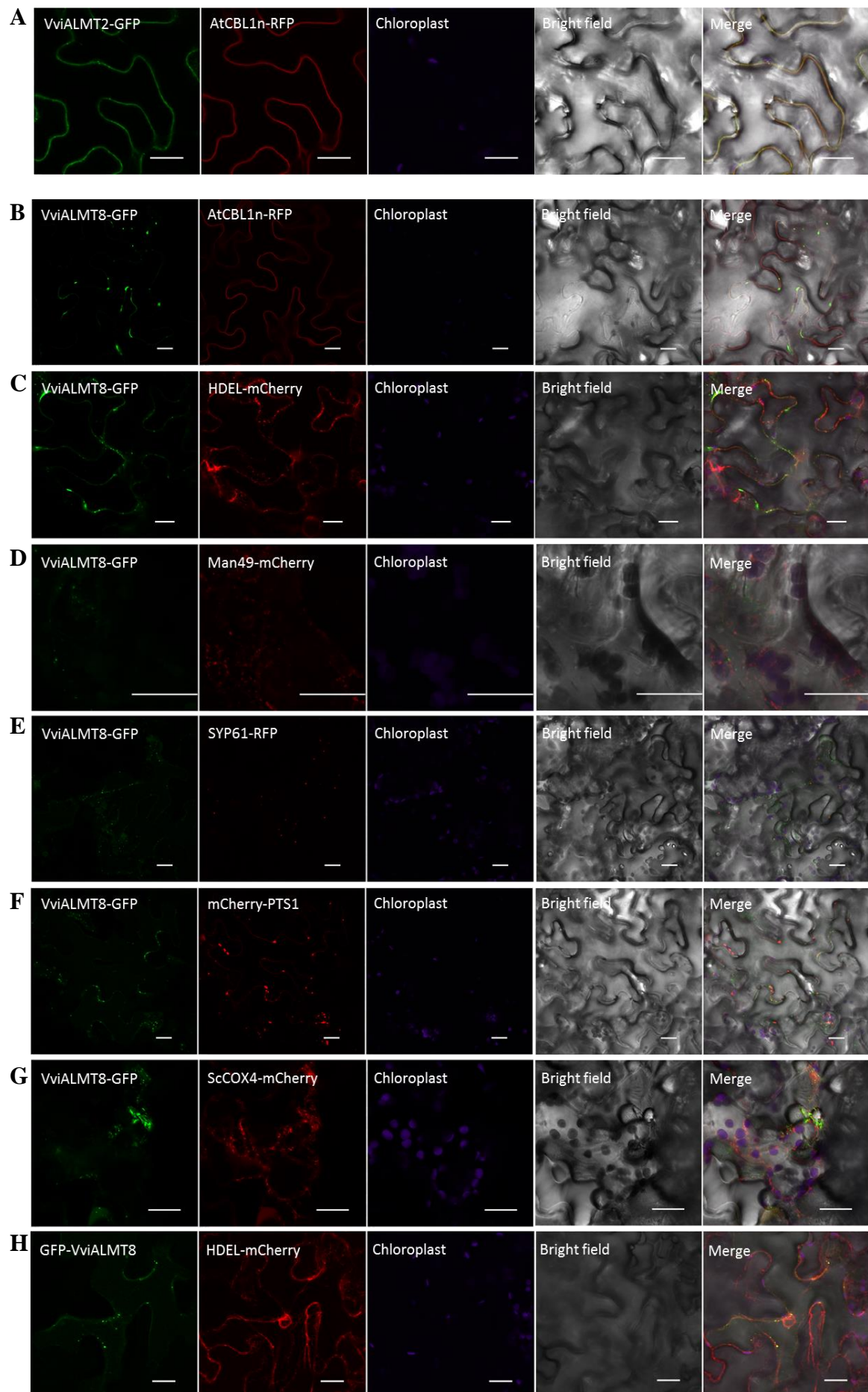


Figure S8: Subcellular localisation of N or C-terminal GFP tagged VviALMT2 and VviALMT8. (A) Tobacco cells transiently expressing *VviALMT2-GFP* with the PM marker. (B – G) Tobacco cells expressing *VviALMT8-GFP* with the mCherry or RFP tagged subcellular markers. (B) PM marker, (C) ER marker, (D) Golgi marker, (E) TGN marker, (F) peroxisome marker and (G) mitochondria marker. (H) Tobacco cells expressing *GFP-VviALMT8* with the ER marker. Cells were imaged 2 days post agro-infiltration using a confocal laser scanning microscope. Scale bars = 20 μm .

Figure S9

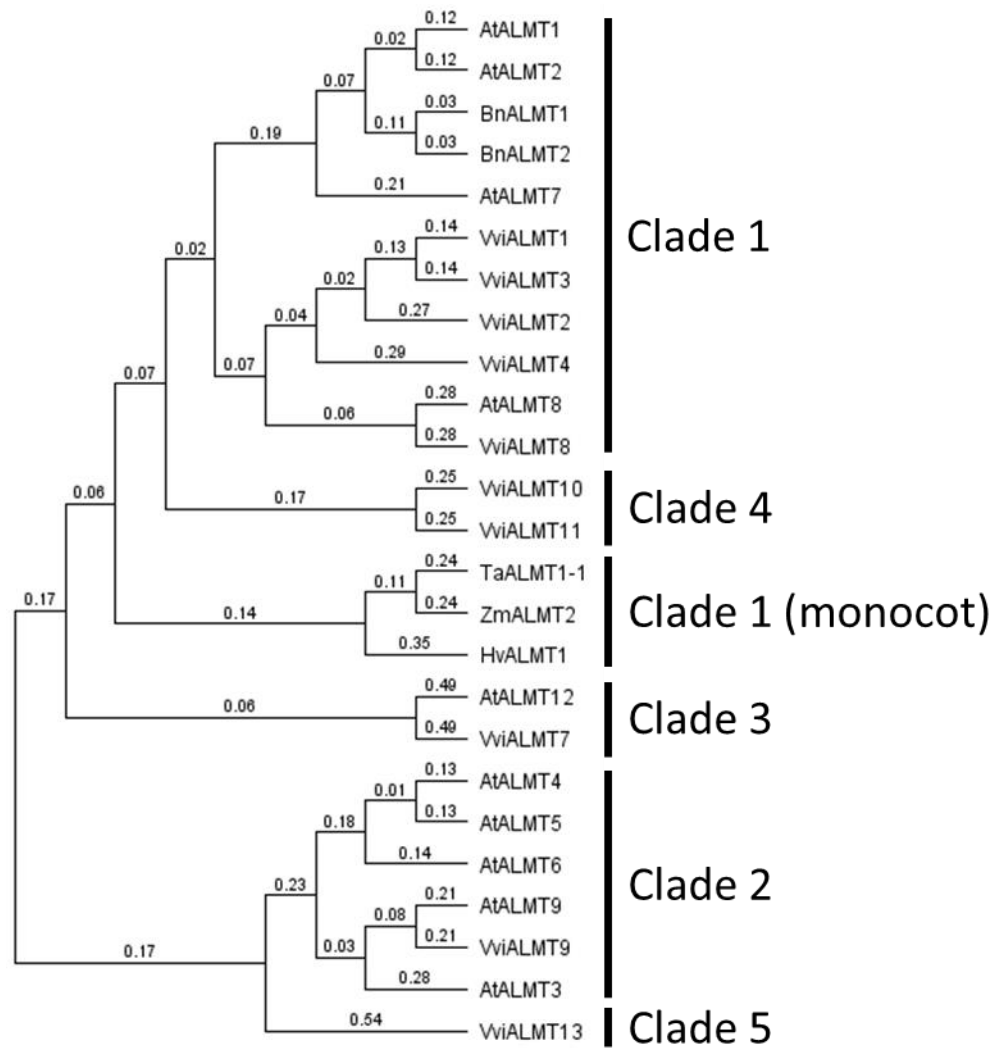
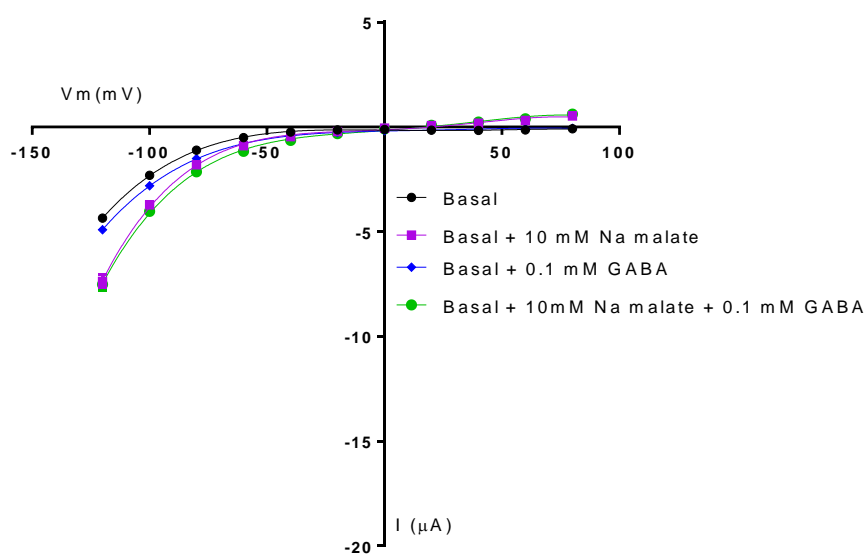


Figure S9: The phylogenetic relationship of ALMTs from grapevine, Arabidopsis, barley, wheat, maize and *Brassica napus*. Protein alignments were generated using Clustal W (Larkin *et al.* 2007), and the phylogenetic tree was generated using Geneious version 8.1.7 with default settings.

Figure S10

A



B

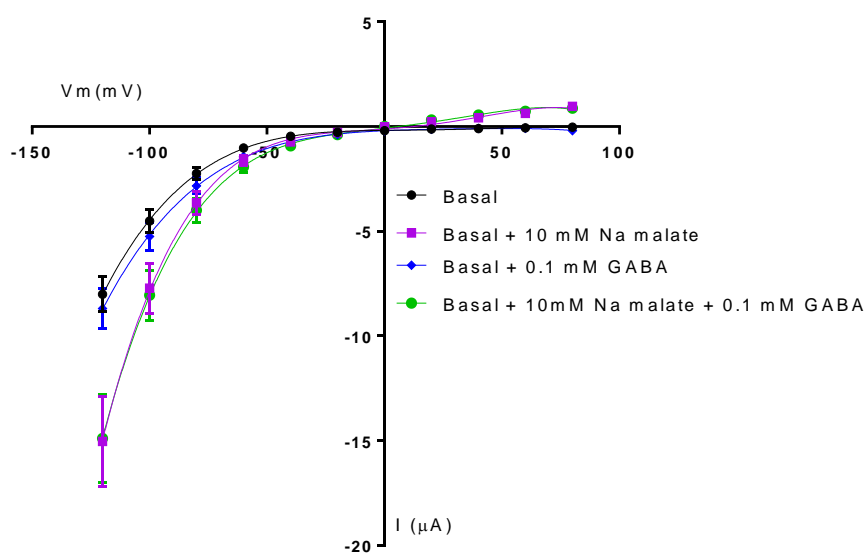


Figure S10: The currents through the VviALMT2 in *Xenopus* oocytes are not affected by GABA, but the anion efflux currents are enhanced by malate. (A) The inward currents of VviALMT2 expressing oocytes were enhanced by the addition of 10 mM Na malate in the perfusion buffer but not affected by the addition of 0.1 mM GABA. Data are mean \pm SE ($n = 7$ oocytes). (B) The inward currents of 10 mM Na malate injected VviALMT2 expressing oocytes were enhanced by the addition of malate in the perfusion buffer, but not affected by the addition of GABA. Oocytes were clamped in the perfusion buffers indicated. Currents mediated by VviALMT2 were determined by

subtracting the mean currents of water-injected controls from the same batch of oocytes under the same treatments in the same solutions. Data are mean \pm SE (n = 5 oocytes).

Figure S11

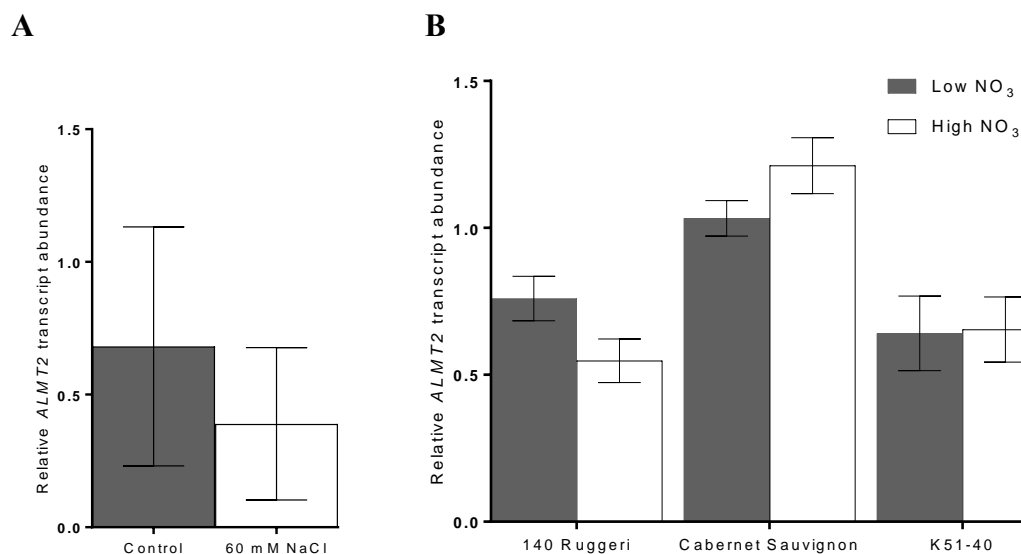


Figure S11: Expression of *VviALMT2* in grapevine roots is not regulated by 60 mM NaCl stress; the expression levels did not change at 3 h after post-starvation high $[\text{NO}_3^-]$ re-supply. Grapevine plantlets were treated with different nutrient solutions and the roots were harvested for RT-qPCR. Relative gene expression levels were calculated in reference to 3 housekeeping genes. (A) Relative *VviALMT2* expression levels in Cabernet Sauvignon roots did not respond to 60 mM NaCl stress. Expression levels of each gene were normalised to control sample 1. Data are means \pm SE ($n = 2$ replicates). (B) Relative *VviALMT2* expression levels in roots were not regulated by NO_3^- re-supply post starvation. Grapevine green cuttings were grown in perlite: vermiculite media and NO_3^- starved for 2 weeks before treatments. Plants were then watered with either low $[\text{NO}_3^-]$ (0.8 mM) or high $[\text{NO}_3^-]$ (12 mM) solutions. Root tissues were harvested 3 hours post treatments for RT-qPCR, and were normalised to Cabernet Sauvignon low NO_3^- sample 1. Data are means \pm SE ($n = 3-4$ replicates).

Table S1: Primers used in this study for molecular cloning and qPCR analyses.

Gene name	Direction	Sequence (5'-3')	Technique	
<i>VviALMT2</i>	Forward	ATGGAGATGGAATCTGCAAGCC	Molecular cloning	
	Reverse	TTACAACACCACACGTGGAACG		
<i>VviALMT2</i> without stop codon	Forward	ATGGAGATGGAATCTGCAAGCC		
	Reverse	CAACACCACACGTGGAACGG		
<i>proVviALMT2</i>	Forward	CACCACCCTTGCCCCTGGTTAG		
	Reverse	AGCTAAATTGTTGATGGAAGGC		
<i>VviALMT8</i>	Forward	ATGGAAATTGCAGCAGAA		
	Reverse	TCAACACATATTTACATGACTTTCA		
<i>VviALMT8</i> without stop codon	Forward	ATGGAAATTGCAGCAGAA		
	Reverse	ACACATATTTACATGACTTTCATC		
<i>proVviALMT8</i>	Forward	CACCATCAAGGCCATGAACCCATA		
	Reverse	GGTTAATGAGTGTTGGGGTTCG		
<i>VviALMT2</i> qPCR fragment	Forward	CCAAGTGTATCGCCAGAAAAA		RT-qPCR analysis
	Reverse	GTTATACTAACTTGGGGGCAGTCTA		
<i>VviALMT8</i> qPCR fragment	Forward	CCGTTTCAGGTTCCGTCAT		
	Reverse	GGTCTGTCATTGTTTTGATTGC		
<i>VviEF1-α</i> qPCR fragment	Forward	GAACTGGGTGCTTGATAGGC		
	Reverse	AACCAAAATATCCGGAGTAAAAGA		
<i>VviTUA</i> qPCR fragment	Forward	CAAAACCAAACGGACTGTTCAAT		
	Reverse	GCACCTTAGCAAGATCACCC		
<i>VviUBC</i> qPCR fragment	Forward	GTGGAGCCCTGCACTTACC		
	Reverse	GAGGGTCGTCAGGATTTGGA		
<i>AtACT2</i> qPCR fragment	Forward	TGAGCAAAGAAATCACAGCACT		
	Reverse	CCTGGACCTGCCTCATCATAC		

Chapter 3: Expression of the grapevine *NPF2.2* in *Arabidopsis* roots reduces shoot Cl^- accumulation under salt stress

Yue Wu¹, Sam W Henderson¹, Rob R Walker², Matthew Gilliam^{1,*}

¹ ARC Centre of Excellence in Plant Energy Biology, School of Agriculture, Food and Wine, University of Adelaide, Glen Osmond, South Australia 5064, Australia

² CSIRO Agriculture and Food, Locked Bag 2, Glen Osmond, South Australia 5064, Australia

* Correspondence should be addressed to:

Professor Matthew Gilliam

Email: matthew.gilliam@adelaide.edu.au

Phone: +61 8 8313 8145

Email addresses:

YW: yue.wu@adelaide.edu.au

SWH: sam.henderson@adelaide.edu.au

RRW: rob.walker@csiro.au

MG: matthew.gilliam@adelaide.edu.au

Running title: VviNPF2.2 reduces shoot Cl^- accumulation under salt stress

Key words: chloride exclusion, grapevine, NPF

Statement of Authorship

Title of Paper	Expression of the grapevine <i>NPF2.2</i> in Arabidopsis roots reduces shoot Cl ⁻ accumulation under salt stress
Publication Status	<input type="checkbox"/> Published <input type="checkbox"/> Accepted for Publication <input type="checkbox"/> Submitted for Publication <input checked="" type="checkbox"/> Unpublished and Unsubmitted work written in manuscript style
Publication Details	Wu, Y., Henderson, S.W., Walker, R.R., Gilliam, M (2019) Expression of the grapevine <i>NPF2.2</i> in Arabidopsis roots reduces shoot Cl ⁻ accumulation under salt stress.

Principal Author

Name of Principal Author (Candidate)	Yue Wu		
Contribution to the Paper	Designed and performed all experiments, analysed the data and wrote the manuscript.		
Overall percentage (%)	75		
Certification:	This paper reports on original research I conducted during the period of my Higher Degree by Research candidature and is not subject to any obligations or contractual agreements with a third party that would constrain its inclusion in this thesis. I am the primary author of this paper.		
Signature		Date	02.07.2019

Co-Author Contributions

By signing the Statement of Authorship, each author certifies that:

- i. the candidate's stated contribution to the publication is accurate (as detailed above);
- ii. permission is granted for the candidate to include the publication in the thesis; and
- iii. the sum of all co-author contributions is equal to 100% less the candidate's stated contribution.

Name of Co-Author	Sam Henderson		
Contribution to the Paper	Contributed to project conception, contributed to design of experiments, supervised the research and assisted in editing the manuscript.		
Signature		Date	03/07/2019

Name of Co-Author	Rob Walker		
-------------------	------------	--	--

Contribution to the Paper	Supervised the research and assisted in editing the manuscript.		
Signature		Date	5/7/19

Name of Co-Author	Matthew Gilliam		
Contribution to the Paper	Conceived the project, supervised the research and assisted in editing the manuscript.		
Signature		Date	01.07.2019

Abstract

Chloride and nitrate are known to compete with each other for transport sites in plants as they are both monovalent and are similar in size. While NO_3^- is consumed by the plants as an important nitrogen source, Cl^- is not metabolised and can accumulate in plants, which leads to ion toxicity. Elevated Cl^- in the soil solution can compromise plant NO_3^- uptake, which is detrimental for plant growth and yield. Grapevines are economically important, moderately salt sensitive crop plants; commercially important grapevine scion varieties are generally sensitive to moderately salt sensitive when grown on their own roots and their grafting to tolerant rootstocks with high capacity for salt exclusion is a common practise to reduce salt impacts on the plant. Two grapevine rootstocks – 140 Ruggeri and K51-40 – are known for their contrasting capacity for shoot Cl^- exclusion; 140 Ruggeri is a good Cl^- excluder and K51-40 a poor excluder. Here, we examine two nitrate/peptide transporter family members, *VviNPF2.1* and *VviNPF2.2*, which were previously found to be more highly expressed in 140 Ruggeri roots. We aimed to use RT-qPCR gene-expression analyses to study the expression responses of these genes to environmental Cl^- and NO_3^- , and to use heterologous systems to study the functional properties of these proteins. RT-qPCR revealed that the expression of both *VviNPFs* were down-regulated by high $[\text{NO}_3^-]$ re-supply post starvation, while their expression was not affected by 25 mM Cl^- ; they were also both not differentially expressed between the root stelar and the root cortical fractions. Anion permeability tests using the *Xenopus laevis* oocyte expression system were conducted, but found to be inconclusive. Constitutive expression of *VviNPF2.2* in Arabidopsis root epidermis and cortex reduced shoot $[\text{Cl}^-]$ after NaCl treatment; we concluded that *VviNPF2.2* can be beneficial to plants when expressed in roots, by reducing shoot Cl^- accumulation under salt stress.

Introduction

Nitrate (NO_3^-) is an anion and a preferred form of the plant macronutrient nitrogen required for protein synthesis. Chloride (Cl^-) is an inorganic anion that is actively absorbed by plant roots at macronutrient levels, and has roles in photosynthesis and cell expansion (Wege *et al.* 2017). A well-known antagonism exists between both anions, whereby high Cl^- supply in the root-zone reduces NO_3^- uptake, and *vice versa* (Glass and Siddiqi 1985). Mechanisms that govern this anionic antagonism are not fully understood, but are thought to often involve transport competition through the same membrane proteins.

As the number of characterised plant transporters is expanding, notable examples of NO_3^- and Cl^- permeable families, or single proteins, have emerged. For example, Slow Anion Channel Homolog 3 (SLAH3) functions as a NO_3^- efflux carrier in stomatal guard cells (Geiger *et al.* 2011), but interacts with SLAH1 in roots for loading Cl^- towards the xylem (Cubero-Font *et al.* 2016). Similarly, the Nitrate Transporter 1/Peptide Transporter Family (NPF) was first identified through AtNPF6.3, which transports NO_3^- (Tsay *et al.* 1993). However AtNPF6.3 was later shown to transport auxin (Krouk *et al.* 2010), while some of the Arabidopsis NPF2 members were found to contribute to Cl^- homeostasis (Li *et al.* 2016, Li *et al.* 2017a), as were NPFs from Maize (Wen *et al.* 2017).

The possibility that putative uncharacterised plant NO_3^- transporters and channels may also be selective for Cl^- , and therefore have a role in salt-tolerance, is compelling. AtNPF2.4, which was a root stelar localised protein, was more permeable to Cl^- than to NO_3^- in *Xenopus laevis* oocytes, and AtNPF2.4 expression was positively correlated with shoot Cl^- accumulation (Li *et al.* 2016). AtNPF2.5 was a root cortex-localised Cl^- transporter, and reduced AtNPF2.5 expression resulted in increased shoot Cl^- accumulation under salt stress (Li *et al.* 2017a). On the other hand, the root pericycle localised NO_3^- transporter AtNPF2.3 was found to positively affect shoot [NO_3^-] and biomass production under salt stress, which linked this NO_3^- transporter to plant salt tolerance (Taochy *et al.* 2015).

Salt accumulation within arable land, and salts brought to the root zone by rain and irrigation water, are big challenges to salt sensitive crop plants (Munns and Gilliam

2015, Walker *et al.* 2002a). Grapevine (*Vitis vinifera*) is an important crop species that is cultivated for table grape, dried grape and wine production, and is moderately sensitive to salt, especially to chloride (Cl^-) (Maas and Hoffman 1977). Salinity can affect both grape and wine production; grape growers may experience declining yield and crop quality due to salt stress (Baby *et al.* 2016, Prior *et al.* 1992a, Prior *et al.* 1992b, Stevens *et al.* 2011, Walker *et al.* 2002b), while winemakers may face difficulties with fermentation (Donkin *et al.* 2010, Li *et al.* 2013, Walker *et al.* 2003) and encounter unfavourable wine sensory properties (de Loryn *et al.* 2014) from salt affected fruit. Plants can be osmotically stressed when the salt concentration in the root zone is high, and high amounts of sodium (Na^+) and Cl^- uptake into the shoot can cause ionic toxicity, which results in leaf burn and affects berry development (Walker and Clingeleffer 2009). Over-accumulation of NaCl in berries can cause salty and soapy tastes which are carried over to the juice and wine (de Loryn *et al.* 2014). The salts in the grapes are also likely to contribute to unfavourably higher must or juice pH (Berg and Keefer 1958, Walker *et al.* 2007), and lead to yeast salt stress in the ferment (Donkin *et al.* 2010). The wines produced from salt-affected grapes also need to comply with legal Na^+ and Cl^- requirements (de Loryn *et al.* 2014, Leske *et al.* 1997), which can incur extra costs during winemaking in order to comply with legal limits for salt concentration in wine.

Grafting to salt-excluding rootstocks is one important approach to manage the salinity problem in vineyards by reducing the amount of salt transported from root to scion. Salt exclusion by grapevine rootstocks can be achieved by several pathways, including salt efflux from the root (Abbaspour 2008a, Abbaspour *et al.* 2013), salt compartmentalisation in the vacuoles (Teakle and Tyerman 2010, Walker *et al.* 2018), reduction of root to shoot salt loading at the root xylem (Gong *et al.* 2011, Tregeagle *et al.* 2006), and xylem retrieval of salts (Teakle and Tyerman 2010). Underlying genes which contribute to these processes have been discovered and studied recently (reviewed in Li *et al.* 2017b). Gong *et al.* (2011) screened the progeny from a cross between the Cl^- excluding rootstock 140 Ruggeri and the poor Cl^- excluder K51-40; the shoot Cl^- concentration [Cl^-] trait of the hybrids showed no clear segregation, which suggested that in that population the grapevine shoot Cl^- exclusion was not likely to be controlled by a single gene. In order to discover more genes related to the grapevine rootstock salt exclusion, Henderson *et al.* (2014a) conducted a microarray grapevine root gene expression study which compared the expression profiles between 140

Ruggeri and K51-40. It was predicted that 140 Ruggeri rootstocks reduce root to shoot Cl^- translocation through regulation of Cl^- movement down its electrochemical gradient from the stelar symplast to xylem apoplast (Gilliham and Tester 2005, Li *et al.* 2017b). Therefore we hypothesise that by examining the localisation and the substrate specificity of the putative membrane-embedded anion transporters which have been shown to be more highly expressed in 140 Ruggeri than in K51-40, we can identify candidate genes which may mediate the transport of anions and contribute to Cl^- exclusion.

In the microarray gene expression study conducted by Henderson *et al.* (2014a), two putative anion transporters from the NPF Family, *VviNPF2.1* and *VviNPF2.2*, were both significantly more highly expressed in the roots of 140 Ruggeri than in K51-40 under control conditions (Table 1), therefore they were identified as priority candidates for Cl^- exclusion in grapevine. When comparing their expression levels between the 50 mM Cl^- and control treatments of the same germplasm, the differences were considered not significant according to the fold change, p and B value thresholds in Henderson *et al.* (2014a) (Table 1). The NPF family is a relatively recent nomenclature which was created to incorporate genes (mainly members in the NRT, PTR, AIT and GTR families) based on their sequence homology; members in the NPF family are grouped into 8 subfamilies according to their phylogenetic relationships (Léran *et al.* 2014). According to the phylogenetic relationships, *VviNPF2.1* and *VviNPF2.2* are most closely related to the *AtNPF2.1* to *AtNPF2.7* subgroup (Henderson *et al.* 2014a). Functional studies in the recent decade have suggested Cl^- and NO_3^- as the two major inorganic substrates of several *AtNPF2* subgroup members (Krouk *et al.* 2010, Li *et al.* 2016, Li *et al.* 2017a, Taochy *et al.* 2015). Therefore, we propose that the expression differences of the putative Cl^- and/or NO_3^- transporter gene *VviNPF2.1* and *VviNPF2.2* may contribute to the Cl^- exclusion capacity differences between 140 Ruggeri and K51-40. In this study we aimed to investigate whether *VviNPF2.1* and *VviNPF2.2* are involved in Cl^- or NO_3^- transport and are related to grapevine Cl^- exclusion or salt tolerance, and whether the findings can facilitate the development of gene-based molecular markers for rootstock breeding in the future.

Materials and methods

Gene cloning and plasmid construction

The coding sequences (CDS) of *VviNPF2.1* (VIT_06s0004g03520) and *VviNPF2.2* (VIT_06s0004g03530) and their respective promoters (1.2 – 1.6 kb upstream of the start codon of CDS) were amplified from *V. vinifera* (cv. Cabernet Sauvignon) root cDNA with Phusion High-Fidelity DNA Polymerase (New England Biolabs), using the primers in Table S1. The PCR products were ligated into the pCR8 or pENTR vectors as described in Wu *et al.* (2019b). The cloned promoter region of *VviNPF2.1* is named *proVviNPF2.1* (-1206 to -1 bp), and the promoter of *VviNPF2.2* is named *proVviNPF2.2* (-1551 to -1 bp) in this study.

Microarray gene expression data presentation

Robust Multi-array Average (RMA) normalized signal intensities were extracted from the Corvina microarray gene expression study by Fasoli *et al.* (2012). Data is presented in a heat map as log₂ mean transformed signal intensities of the 4 probes and 3 biological replicates.

RT-qPCR

Grapevine green cuttings with 2 nodes and mature leaves were obtained from glasshouse-grown, potted vines of Cabernet Sauvignon, 140 Ruggeri and K51-40 in November 2017 (Waite Campus, University of Adelaide) for the NO₃⁻ responses experiment. Cuttings were propagated and treated with 0.8 mM or 12 mM NO₃ as described in Wu *et al.* (2019b). Root samples were taken after 3 and 24 h after treatments were applied and were immediately frozen in liquid nitrogen; total RNA and cDNA of these samples was made as described in Wu *et al.* (2019b).

Cabernet Sauvignon hard wood cuttings with 4-6 nodes (8-10 mm in diameter) were collected from the Alverstoke vineyard (Waite Campus, University of Adelaide) before winter pruning and propagated as described in Wu *et al.* (2019b). A cDNA series consisting of grapevine young leaves from 5-leaf-shoots (E-L stage 12), young inflorescences (E-L stage 12), well developed inflorescences (E-L stage 17), roots at E-L stage 26, mature leaves and petiole samples (E-L stage 27), pea sized green berries

(E-L stage 31) and berries post-veraison (E-L stage 36-37) were made as described in Wu *et al.* (2019b).

Two sets of grapevine hydroponically grown rooted leaf cDNA or RNA samples were also obtained from Henderson *et al.* (2014a). The cDNA samples of stelar enriched and cortex enriched 25 mM Cl⁻ treated grapevine roots was obtained for RT-qPCR gene expression analysis. The RNA samples of grapevine whole roots treated with control or 25 mM Cl⁻ stress solutions were used to make cDNA.

RT-qPCR primers specific to *VviNPF2.1* and *VviNPF2.2* were designed to amplify fragments between 80 and 250 bp with an optimal GC content between 40% and 60%, and to flank an intron if possible (Table S1). The qPCR primers of the 3 housekeeping genes, *α-Tubulin* (*VviTUA*), *Ubiquitin-conjugating-enzyme-like* (*VviUBC*) and *Elongation-factor-1-α* (*VviEF1a*), were obtained from Wu *et al.* (2019b). The qPCR primers were checked for specificity and RT-qPCR was performed as described in Wu *et al.* (2019b). Expression levels (E) of *VviNPF2.1* and *VviNPF2.2* were calculated relative to sample 1 of each experiment (as described in the figure legends) using the equation $E = (2 * \text{efficiency})^{(CT_{\text{sample}} - CT_{\text{sample 1}})}$. Expression levels were normalised to the geometric mean of the expression levels of the 3 housekeeping genes (Vandesompele *et al.* 2002).

Subcellular localisation in Arabidopsis (*Arabidopsis thaliana*) mesophyll protoplasts

The *VviNPF2.1* and *VviNPF2.2* CDS in pCR8 vectors were recombined into both pYFP-attR and pattR-YFP using LR Clonase II (Life Technologies) to generate vectors encoding 35S:*EYFP-VviNPF* and 35S:*VviNPF-EYFP* respectively. The vectors generated by LR recombination were used to transform *E. coli* DH5α competent cells. Successfully transformed *E. coli* cells were propagated and the plasmids were harvested.

Arabidopsis mesophyll protoplasts were harvested by the Tape-*Arabidopsis* Sandwich method (Wu *et al.* 2009). Protoplasts were transfected using a modified TEAMP method (Yoo *et al.* 2007). Approximately 15 µg of each of the recombinant plasmids were added to 0.2 mL of MMg solution (4 mM MES, 0.4 M d-mannitol, 15 mM MgCl₂) containing approximately 5 × 10⁴ protoplasts at room temperature. An equal volume of 30% (w/v) PEG (MW 4000) solution in 0.1 M CaCl₂ and 0.2 M D-mannitol was added

to the mixture and incubated at room temperature for 5 min. W2 wash solution (1 M MES, 0.4 M D-mannitol, 15 mM KCl, 10 mM CaCl₂ and 5 mM MgCl₂) was slowly added to the mixture to a total volume of 2 mL after incubation. The mixture was gently mixed and the protoplasts were pelleted by centrifugation at 100 × g for 1 min. The supernatant was discarded and the wash step was repeated twice using W2 solution. The protoplasts were resuspended with 1 mL of W2 solution and transferred to a 12-well plate pre-coated with 1% BSA for incubation. The protoplasts were incubated under normal day light regime for 16 h at room temperature.

Transfected protoplasts were imaged after incubation using a Nikon A1R confocal laser scanning microscope and NIS-Elements C software (Nikon Corporation). FM4-64 was added to the protoplast mixture in a 1 in 1000 ratio as a plasma membrane (PM) marker, and the protoplasts were imaged after a 10-15 minute incubation at room temperature. Excitation/ emission conditions were YFP (488 nm/500 – 550 nm), FM4-64 (561 nm/570 – 620 nm), chlorophyll (640 nm/650 – 720).

***VviNPF* promoter driven gene expression in Arabidopsis**

The *VviNPF2.1* and *VviNPF2.2* promoters in pCR8 and pENTR vectors were recombined into pMDC162 and pMDC204 expression vectors using LR Clonase II (Life Technologies) to generate binary vectors encoding *proVviNPF:GUS*, and *proVviNPF:GFP6-HDEL*. The vectors were used for transformation of *Arabidopsis thaliana* Col-0 plants as described in Wu *et al.* (2019b). Transgenic lines of Arabidopsis were selected by the application of Hygromycin B (Bayer Crop Science) and the presence of T-DNA was confirmed by PCR.

Selected *proVviNPF2.1:GFP6-HDEL* and *proVviNPF2.2:GFP6-HDEL* transformed Arabidopsis T3 two-week-old roots were incubated in 15 μM (10 μg/mL) propidium iodide (PI) solution in the dark for 15 min then rinsed 3 times with water. Roots were imaged using a Nikon A1R confocal laser scanning microscope; excitation/ emission conditions were GFP (488 nm/ 500 – 550 nm), PI (561 nm/ 570 – 620 nm).

Selected *proVviNPF2.1:GUS* and *proVviNPF2.2:GUS* transformed Arabidopsis T2 two-week-old seedlings grown on plates were GUS stained, fixed, Technovit embedded and sectioned as described in Wu *et al.* (2019b). The whole root images were taken

using Nikon SMZ25 stereo microscope, and the transverse section images were obtained using Nikon DS-Ri1 upright research microscope.

***In silico* analyses**

The *AtNPF* and *VviNPF* gene sequences were obtained from the *A. thaliana* Col-0 reference genome and the *V. vinifera* PN40024 genome database using the gene IDs listed in Léran *et al.* (2014). Protein alignments were generated using Clustal W (Larkin *et al.* 2007), and the phylogenetic tree was generated using Geneious version 8.1.7 with default settings.

Gene expression in *Xenopus laevis* oocytes

The *VviNPF2.1* and *VviNPF2.2* CDS in pCR8 vector was recombined into the *Xenopus* oocyte expression vector pGEMHE-DEST (Shelden *et al.* 2009) using LR Clonase II (Life Technologies) to generate vectors encoding T7:*VviNPF*. The *pGEMHE* recombinant vectors were linearised with SbfI or NheI (New England Biolabs). The capped RNA (cRNA) for oocyte expression was synthesized with the mMACHINE mMACHINE T7 Transcription Kit (Invitrogen) using the linearised vectors as templates.

Stage IV and V *X. laevis* oocytes were selected and were injected with 25 ng of *VviNPF2.1* or *VviNPF2.2* cRNA, or 42nL of water. The oocytes were incubated in a Ca²⁺ Ringer's solution (96 mM NaCl, 2 mM KCl, 5 mM MgCl₂, 5 mM HEPES, 0.6 mM CaCl₂, 5% w/v horse serum, 500 µg mL⁻¹ tetracycline and 1x penicillin-streptomycin (Sigma P4333)) for 2 days post injection.

Electrophysiology with *Xenopus laevis* oocytes

For anion permeability assays, the basal perfusion solution for oocyte current recording contained 6 mM Mg gluconate, 1.8 mM Ca gluconate and 10 mM MES. Basal buffers were supplemented with 50 mM of NM-D-G Cl or NM-D-G NO₃. The pH of each solution was adjusted to 5.5 using MES, and osmolality was adjusted to 230 mOsm/kg using D-mannitol. Oocyte whole cell currents were recorded using an Oocyte Clamp OC-725C amplifier (Warner Instruments), digitised using an Axon Digidata 1400A (Molecular Devices) and the software Clampex 10.2 (Molecular Devices). The voltage

step protocol was set with a holding potential of -40 mV for 300 ms and 300 ms either side of stepwise pulses from +80 mV to -120 mV in 20 mV decrements for 550 ms. Data were analysed using Smart-IV (Wu *et al.* 2019c), and plotted using GraphPad PRISM v.7.00 for Windows (GraphPad).

Anion tracer fluxes and [Cl⁻] measurements in *Xenopus* oocytes

Torpedo marmorata CLC-0, a chloride channel with known Cl⁻ and NO₃⁻ permeability (Bergsdorf *et al.* 2009b), was used as a positive control. For the Cl⁻ tracer influx assays, the influx buffer was made by adding 13.3 μL of H³⁶Cl stock solution (11.3 mg/mL Cl⁻, 75 μCi/mL) into 1 mL of ND96 buffer (96 mM NaCl, 2 mM KCl, 1.8 mM CaCl₂, 1 mM MgCl₂ and 5 mM HEPES, pH 7.4). Water injected and gene expressing oocytes were incubated in the influx buffer for 1 h. Oocytes were taken out of the efflux buffer and washed 3 times in ice cold ND96 buffer, then each individual oocyte was transferred to a scintillation vial containing 200 μL of 10% (w/v) SDS solution. For Cl⁻ efflux assays, 42 nL of H³⁶Cl stock solution (11.3 mg/mL Cl⁻, 75 μCi/mL) was injected into each of the water injected and gene expressing oocytes. The control group oocytes were immediately washed 3 times in ice cold ND96 buffer, then each individual oocyte was transferred to a scintillation vial containing 200 μL of 10% (w/v) SDS solution. The efflux group oocytes were quickly transferred to room temperature Cl⁻-free ND96 buffer (96 mM Na gluconate, 2 mM K gluconate, 1.8 mM Ca gluconate, 1 mM Mg gluconate and 5 mM HEPES, pH 7.4) to allow Cl⁻ efflux for 1 h. Oocytes were taken out of the efflux buffer and washed 3 times in ice cold Cl⁻-free ND96 buffer, then each individual oocyte was transferred to a scintillation vial containing SDS solution. All oocytes were allowed to dissolve in the SDS overnight, then 4 mL of liquid scintillation cocktail was added to each vial. The vials were loaded onto a LS6500 Multi-purpose scintillation counter (Beckman Coulter) and energy emission was counted for 2 min in cpm (counts per minute) with the discriminators set to 200 - 800 KeV.

For the NO₃⁻ tracer influx experiment, the influx buffer was made by adding 30 mM of Na¹⁵NO₃ (99.3% atom) into the ND96 buffer (pH 7.4). Water injected and gene expressing oocytes were incubated in the influx buffer for 2 h. Oocytes were taken out of the efflux buffer and washed 3 times in ice cold ND96 containing 30 mM NaNO₃, then they were transferred into tin capsules in a 96-well-plate (2 oocytes per capsule). For NO₃⁻ efflux experiment, 42 nL of 300 mM K¹⁵NO₃ (99.3% atom) was injected into

each of the water injected and gene expressing oocytes. The oocytes were immediately transferred into an ND96 buffer (96 mM NaCl, 2 mM KCl, 1.8 mM CaCl₂, 1 mM MgCl₂ and 5 mM MES, pH 5.5) to allow efflux for 1 h. Oocytes were then washed 3 times in ice cold ND96 buffer (pH 5.5), and they were transferred into tin capsules (3 oocytes per capsule). The tin capsules were oven-dried at 50 °C oven for 3 days. Samples were sent for analysis in a stable isotope ratio mass spectrometer (Nu Horizon IRMS) in the University of Adelaide Stable Isotope Facility for $\delta^{15}\text{N}$.

For the oocyte nominal [Cl⁻] tests, cRNA or water injected oocytes were incubated in the Ca²⁺ Ringer's solution for 2 days. The oocytes were washed in ice cold HMg solution (6 mM Mg gluconate, 1.8 mM Ca gluconate, 10 mM MES, pH 6.5) and digested in 550 μL of 1% HNO₃ in 1.5 mL tubes (7 to 10 oocytes per tube). The [Cl⁻] in the supernatant was tested using a Sherwood Model 926 Chloride Analyzer (Sherwood Scientific) as per manufacturer's protocol, and the [Cl⁻] concentration in the solution was converted to [Cl⁻] per oocyte assuming an average oocyte is 400 nL in volume.

Cell type specific expression of *VviNPF2.2* in Arabidopsis enhancer trap line

The Arabidopsis enhancer trap line J1551 for root epidermis and cortex specific transgene expression was obtained from (Plett *et al.* 2010a). The *VviNPF2.1* and *VviNPF2.2* CDS in the entry vectors were recombined into the pTOOL5-*UAS_{GAL4}* destination vector (obtained from Plett 2008) respectively using LR Clonase II (Life Technologies) to generate the binary vectors encoding *UAS_{GAL4}:VviNPF2.1* and *UAS_{GAL4}:VviNPF2.2*. The binary vector was used to transform *A. tumefaciens* strain Agl-1 using the freeze thaw method. The Arabidopsis enhancer trap J1551 plants were transformed using the Agrobacterium-mediated floral dip method (Clough and Bent 1998). Transgenic lines of Arabidopsis were selected by the application of foliar spray of 120 mg/L Basta (Bayer Crop Science) mixed with 500 $\mu\text{L/L}$ Silwet L-77 (plantMedia.com). The presence of T-DNA was confirmed by PCR.

Two heterozygous T2 lines of J1551 *UAS_{GAL4}:VviNPF2.2*, line 3 and 4 were selected by Basta foliar spray and genotyping using the root cDNA. The root epidermis and cortex specific gene expression was confirmed by imaging the root mGFP5-ER using

a Nikon A1R confocal laser scanning microscope (excitation/emission is 488 nm/ 500 – 550 nm).

Phenotyping Arabidopsis root epidermis and cortex specific *VviNPF2.2* expression lines

The T2 heterozygous Arabidopsis T2 J1551 *UAS_{GAL4}:VviNPF2.2* line 3 and 4 were germinated and grown in the hydroponic system in the germination solution (GM) for 3 weeks, and transferred into the standard basal nutrient solution (BNS) as described in Conn *et al.* (2013). The plants were grown in the BNS for 2 weeks, then the BNS was replaced with the high Na⁺ nutrient solution containing 75 mM NaCl (Conn *et al.* 2013). Five days post 75 mM NaCl treatment the rosettes were harvested and the fresh weights were recorded. Each rosette was put into a 50 mL tube and for every 20 mg of the fresh weight, 1 mL of water was added into the tube. The rosettes and the liquid in the tubes were frozen at -20 °C, thawed at room temperature and the tubes were vortexed; this process was repeated 3 times to fully release the cellular contents, and the resulting liquid samples were used for ion concentration measurements. The plant roots were harvested for RNA extraction and cDNA synthesis. RT-qPCR was performed using the cDNA to differentiate the null segregants and *VviNPF2.2* expressing individuals. Each qPCR reaction was performed in duplicate. Expression levels (E) of *VviNPF2.2* were calculated relative to the housekeeping gene *AtActin2* (At3G18780, qPCR primers as listed in Jha *et al.* (2010)) and normalised to sample 1 using the equation $E = 2^{-\Delta\Delta CT}$. Semi qPCR was also performed using several root cDNA samples of each line to visualise the relative expression levels on gel. Sample 1 – 3 of each line and a non-transformed J1551 root cDNA sample was used as templates in 2-step PCR reactions for 32 cycles. The PCR products were run on an electrophoresis gel and the gel image was taken using a ChemiDoc Touch Imaging System (BIO-RAD).

The Cl⁻ concentrations of the liquid samples were measured using the Sherwood Model 926s Chloride Analyzer (Sherwood Scientific). The NO₃⁻ concentrations were measured using the reaction of NO₃⁻ with salicylic acid under alkaline condition as described in Cataldo *et al.* (1975), and the modifications were as described in Wu *et al.* (2019b). To study the correlation between the Arabidopsis shoot Cl⁻ concentrations and the root *VviNPF2.2* expression levels, the relationships between shoot ion contents and gene expression levels were analysed using linear regression.

Statistical analysis

Statistical analyses were performed using GraphPad PRISM v.7.00 for Windows (GraphPad). All data are presented as mean \pm SE. Means were compared using the Student's t-test.

Results

Expression levels of both *VviNPF2.1* and *VviNPF2.2* in grapevine roots were down-regulated by post-starvation high [NO₃⁻] re-supply in some cultivars

The expression levels of *VviNPF2.1* and *VviNPF2.2* in grapevine roots in response to different [NO₃⁻] and [Cl⁻] treatments were investigated. For NO₃⁻ treatments, 3 grapevine cultivars – 140 Ruggeri, Cabernet Sauvignon and K51-40 – were propagated from green cuttings and NO₃⁻ starved with 0.8 mM total NO₃⁻. The plants were then supplied with either low NO₃⁻ (0.8 mM, same as the NO₃⁻ starvation condition) or high NO₃⁻ (12 mM) solutions (Cochetel *et al.* 2017). The transcript abundance of *VviNPF2.1* and *VviNPF2.2* 24 h post NO₃⁻ treatment were both higher in the roots supplied with low [NO₃⁻] than in the roots resupplied with high [NO₃⁻] in 140 Ruggeri and K51-40 (Figure 1A – B).

For Cl⁻ treatments, rooted leaves of 140 Ruggeri, Cabernet Sauvignon and K51-40 were grown in hydroponics and treated with either control or 25 mM Cl⁻ nutrient solutions (Henderson *et al.* 2014a). RT-qPCR results showed that the transcript abundance in roots was not regulated by 25 mM [Cl⁻] stress (Figure 1C – D). For both *VviNPF2.1* and *VviNPF2.2*, some expression differences appear to be large in Figure 1 but were shown statistically insignificant. Due to the high variability among the replicates in some treatment groups, care should be taken when making conclusions with the expression data.

***VviNPF2.1* and *VviNPF2.2* encode plasma membrane localised proteins and are highly expressed in grapevine roots and leaves**

Expression of *VviNPF2.1* and *VviNPF2.1* with YFP tags in *Arabidopsis* mesophyll protoplasts produced YFP signals that co-localised with the dye FM4-64, which after short time periods predominantly stains the plasma membrane (Figure 2, Figure S1). This subcellular localisation is consistent with most characterised plant NPF proteins to date (Corratge-Faillie and Lacombe 2017).

To investigate the expression pattern of *VviNPF2.1* and *VviNPF2.2*, RT-qPCR was performed using cDNA of root epidermal/cortical enriched and stelar enriched fractions of 3 grapevine cultivars, 140 Ruggeri, Cabernet Sauvignon and K51-40. Neither

VviNPF2.1 nor *VviNPF2.2* were differentially expressed between the enriched fractions of all 3 cultivars (Figure 3A – B). Activity of GUS and GFP driven by the *VviNPF2.1* and *VviNPF2.2* promoters in roots of Arabidopsis were also studied. Under both promoters, GFP activity was observed in root stelar and cortical tissues, although more activity was seen in the stele (Figure 3C – D). Similarly, GUS activity in Arabidopsis root transverse sections was detectable in the root stele and endodermis, including passage cells (Figure 3E – F), while *proVviNPF2.2* also drove GUS activity in the cortex in several whole root sections (Figure 3G).

Cabernet Sauvignon hard wood cuttings were propagated in pots and RT-qPCR gene expression analyses were performed on various tissue types harvested during the growing season. Both *VviNPF2.1* and *VviNPF2.2* were most highly expressed in the root, young leaf and mature leaf samples, and their expression levels in post-veraison berries were very low (Figure 4). Similar patterns were also observed in the microarray gene expression data extracted from Fasoli *et al.* (2012) (Figure S2).

***VviNPF2.1* and *VviNPF2.2* display high sequence homology**

VviNPF2.1 and *VviNPF2.2* have a very close phylogenetic relationship and they are closely related to Arabidopsis NPF2.1 to 2.7 (Figure S3A). These two genes are located next to each other in chromosome 6 in the grapevine reference genome (*V. vinifera* cultivar PN40024) with no other genes in between (Figure S3B). Protein alignment revealed that *VviNPF2.1* and *VviNPF2.2* have a high degree of homology (Figure S3C) as their amino acid sequences are 96.71% identical and 97.7% similar, and their promoter regions (approximately 1.2 kb upstream the start codon) are 92.16% identical (alignment not shown). An Arabidopsis homologue, AtNPF2.3, was also included in the protein alignment, but both the *VviNPF2*s and the AtNPF2.3 have relatively low similarity to AtNPF6.3 (Figure S3C), which has a known crystal structure.

***VviNPF2.1* and *VviNPF2.2* appear not functioning in NO₃⁻ or Cl⁻ transport in *Xenopus* oocytes**

To determine the substrates of *VviNPF2.1* and *VviNPF2.2*, we performed TEVC using *Xenopus* oocytes expressing the two *VviNPF* genes. Basal buffers containing either 50 mM NO₃⁻ or Cl⁻ were used in the external perfusion solution to test the anion permeability of *VviNPF2.1* and *VviNPF2.2*. There were statistically significant 50 mM

NO_3^- and Cl^- induced anion influx currents (outward currents at 80 mV) for both VviNPF2.1 and VviNPF2.2 expressing oocytes, and there were no NO_3^- and Cl^- induced anion efflux currents for all genotypes; however, similar significant NO_3^- and Cl^- induced outward currents were observed for the water injected negative control oocytes (Figure S4A – F). Inward currents were also observed for VviNPF2.2, whereas these were not present from VviNPF2.1 or water injected controls (Figure S4G – H)

Since isotope flux assays can detect both electrogenic and electroneutral transport, ^{36}Cl and $^{15}\text{NO}_3$ were used to test the anion flux through VviNPF2.1 and VviNPF2.2 in *Xenopus* oocytes. To determine if the proteins mediated Cl^- influx, cRNA or water injected oocytes were incubated in a buffer containing ^{36}Cl , and tracer uptake was measured. The positive control (*Torpedo* CLC-0) is a strong bi-directional Cl^- and NO_3^- channel, which should mediate Cl^- and NO_3^- tracer influx and efflux across the oocytes (Bergsdorf *et al.* 2009b). As expected, CLC-0 control oocytes had a significant tracer uptake, however the VviNPF2.1 and VviNPF2.2 expressing oocytes mediated slightly less ^{36}Cl influx than the water injected negative control oocytes (Figure S5A). To determine whether VviNPF2.1 and VviNPF2.2 function in Cl^- efflux, the oocytes were injected with ^{36}Cl and incubated in a Cl^- efflux buffer and then tested for tracer activities. The CLC-0 control oocytes were found to have significant tracer efflux during the time period, however VviNPF2.1 and VviNPF2.2 expressing oocytes did not show ^{36}Cl efflux (Figure S5C). Similar experiments were also performed using $^{15}\text{NO}_3$. The oocytes were incubated in a buffer containing $^{15}\text{NO}_3$, and the $\delta^{15}\text{N}$ value were analysed in a stable isotope ratio mass spectrometer. The results show that *Torpedo* CLC-0 mediated significant tracer uptake while the VviNPF2.1 expressing oocytes had a slightly lower $\delta^{15}\text{N}$ value than the negative control oocytes (Figure S5B), which suggests that less $^{15}\text{NO}_3$ influx occurred in the *VviNPF2.1* expressing oocytes than in the negative controls. To test if VviNPF2.1 mediates NO_3^- efflux, the oocytes were injected with $^{15}\text{NO}_3$ and allowed to rest in an efflux buffer for 1 h. The positive control oocytes had a significant decrease in $\delta^{15}\text{N}$, but the oocytes expressing VviNPF2.1 showed no reduction in $\delta^{15}\text{N}$ compared to the negative control (Figure S5D), which suggests that VviNPF2.1 did not mediate NO_3^- efflux from the oocytes.

Nominal Cl^- concentrations were also tested using control or *VviNPF* expressing oocytes which were incubated in Ringer's solution for 2 days. The concentrations of

nominal Cl^- in both VviNPF2.1 and VviNPF2.2 expressing oocytes were not different from the concentration in water injected control oocytes, while the positive control oocytes had lower $[\text{Cl}^-]$ (Figure S5E).

Expression of VviNPF2.2 in Arabidopsis root epidermis and cortex reduced shoot $[\text{Cl}^-]$ post salt treatment

To study the function of VviNPF2.1 and VviNPF2.2 *in planta*, the Arabidopsis enhancer trap line J1551 (Plett *et al.* 2010a) was transformed with VviNPF2.1 or VviNPF2.2 for gene expression in root epidermis and cortex. To confirm the cell type specific gene expression, the roots were imaged for mGFP5-ER distribution and the GFP signals are found in epidermis, cortex and endodermis (Figure 5A). The J1551 VviNPF2.2 over-expression (OEX) lines (T2 line 3 and 4) were treated with 75 mM NaCl in hydroponics for 5 days and the shoots were harvested for $[\text{Cl}^-]$ and $[\text{NO}_3^-]$ analyses. The results show that the VviNPF2.2 OEX lines have lower shoot $[\text{Cl}^-]$ compared to the T2 null segregants after the NaCl treatment (Figure 5B), while the shoot $[\text{NO}_3^-]$ concentration of each genotype were similar (Figure 5C). The expression levels of VviNPF2.2 in the OEX line 3 and line 4 were highly different. VviNPF2.2 and AtACT2 PCR fragments were amplified by semi-quantitative RT-PCR from three independent transformants. This showed that VviNPF2.2 was significantly more highly expressed in the OEX line 3 than in line 4 (Figure 5D). The expression levels of all samples were analysed by RT-qPCR and the shoot $[\text{Cl}^-]$ were plotted against the relative expression levels, and the linear regression analyses show that the shoot $[\text{Cl}^-]$ did not have linear relationships with the VviNPF2.2 expression levels for both OEX lines (Figure 5E – F).

Discussion

The localisation, expression patterns and functional characteristics of some shoot Cl^- exclusion related proteins previously characterised could be used to predict whether *VviNPF2.1* and *VviNPF2.2* have potential roles in grapevine shoot Cl^- exclusion. *AtNPF2.4*, and the *AtSLAH1/AtSLAH3* complex, were found to be plasma membrane localised stelar-expressed Cl^- transporters which regulate root-to-shoot Cl^- translocation (Cubero-Font *et al.* 2016, Li *et al.* 2016). *AtNPF2.5* was also a PM localised root cortex expressed Cl^- transporter which could reduce shoot Cl^- accumulation, possibly by Cl^- efflux from the cortex (Li *et al.* 2017a). *AtALMT9*, was identified as a tonoplast localised Cl^- transporter in guard cells and vasculature, and was observed to participate in plant early salinity response (Baetz *et al.* 2016, De Angeli *et al.* 2013a).

In our study, both *VviNPF2.1* and *VviNPF2.2* were localised to the plasma membrane (Figure 2, Figure S1), therefore if functional in transport they may catalyse movement into or out of cells. According to the grapevine root stelar and cortex RT-qPCR results, *VviNPF2.1* and *VviNPF2.2* were not differentially expressed between the two fractions (Figure 3A – B). However, the promoter driven GUS and GFP expression in *Arabidopsis* roots displayed more intense stain or fluorescence in the stele than in the cortex (Figure 3C – H). Our promoter-reporter findings are consistent with a previous study where the GUS reporter was driven by the *VvNPF3.1* and *VvNPF3.2* promoters in *Arabidopsis* vasculature (Pike *et al.* 2013). The discrepancy between RT-qPCR and protein reporter results might have arisen because the promoter driven GUS and GFP expression assays in *Arabidopsis* were not quantitative, and the grapevine promoters were exogenous to *Arabidopsis* and did not contain all the elements necessary for controlling expression. When the gene expression levels in other grapevine tissues were analysed by RT-qPCR and microarray hybridisation, *VviNPF2.1* and *VviNPF2.2* were also highly expressed in leaves, flowers, rachis and pre-veraison berries (Figure 4, Figure S2). Therefore, according to the expression patterns, it is likely that *VviNPF2.1* and *VviNPF2.2* participate in ion transport not only in roots, but also in shoots and reproductive tissues.

We were unable to confirm the substrates of *VviNPF2.1* and *VviNPF2.2* using the *Xenopus* oocyte expression system. The *VviNPF2.1*- and *VviNPF2.2*- expressing

oocytes were tested for anion conductance by electrophysiology in buffers containing Cl^- or NO_3^- . Statistically significant Cl^- and NO_3^- induced outward currents (positive currents) could be detected in the *VviNPF2.1*- and *VviNPF2.2*- expressing oocytes (Figure S4), in the range of those detected for maize NPF6.4 and NPF6.6 (Wen *et al.* 2017). Given that the water injected control oocytes also had statistically significant NO_3^- induced outward currents (Figure S4F), we were unable with electrophysiology to determine whether these were indeed currents carried by VviNPF or through endogenous channels, as it has been found that endogenous channels can increase in their activity upon expression of heterologous proteins (Roy *et al.* 2008, Tzounopoulos *et al.* 1995). We therefore decided to use anion isotopes, which would detect both electrogenic and non-electrogenic Cl^- and NO_3^- movements across the plasma membrane of the VviNPF expressing oocytes. Interestingly, in these experiments, the *VviNPF2.1*- and *VviNPF2.2*-expressing oocytes both contained statistically significantly less $^{36}\text{Cl}^-$ tracer than the negative controls, while the average $\delta^{15}\text{N}$ of the *VviNPF2.1*-expressing oocytes was lower than that of the negative controls (Figure S5A – B). These results are counterintuitive as they suggest that VviNPF expression in oocytes inhibits the anion tracer uptake and are in fact opposite to that indicated by electrophysiology for VviNPF2.1. To determine whether these results were due to anion efflux activities through the VviNPF, tracers were injected into the VviNPF expressing oocytes, but no significant efflux was detected (Figure S5C – D). It has been previously found that the NO_3^- transport activities of AtNPF2.3 could not be observed in the *Xenopus* oocyte system using either TEVC or $^{15}\text{NO}_3^-$ tracer, and the possibility of *Xenopus* oocytes not being a suitable system for the functional characterisation of some NPF proteins was discussed (Taochy *et al.* 2015). Regarding the observation that the *VviNPF2.1* expressing oocytes had lower $\delta^{15}\text{N}$ levels in the $^{15}\text{NO}_3^-$ tracer uptake experiment (Figure S5B), similar data were found in a previous $^{15}\text{NO}_3^-$ tracer uptake experiment performed by Leran *et al.* (2015); in their study, some of the NPF expressing oocytes displayed lower relative ^{15}N accumulation than that of the negative control oocytes, but the possible reasons were not discussed. Therefore we would draw the same conclusion as Taochy *et al.* (2015), that the *Xenopus* expression system might not be suitable for the functional characterisation of some NPFs, including VviNPF2.1 and VviNPF2.2. Instead, future studies into grapevine NPF proteins could use the *Lactococcus lactis* expression system that was used to successfully characterise AtNPF2.3 (Taochy *et al.* 2015).

We also attempted to predict whether *VviNPF2.1* and *VviNPF2.2* are NO_3^- transporters by comparing their sequences to *AtNPF6.3*, whose crystal structure has been revealed (Parker and Newstead 2014, Sun *et al.* 2014). In *AtNPF6.3*, the charged residue His-356 functions in binding the NO_3^- which has entered the NO_3^- harbouring pocket, and the mutation H356A abolished the NO_3^- transport feature of the protein. It was also predicted that the NO_3^- conductance of the *AtNPF6.3*-like proteins are conferred by the combination of a polar and a hydrophobic residues at positions equivalent to His-356 and Phe-511 (Sun *et al.* 2014). However, the equivalent residues within *VviNPF2.1*, *VviNPF2.2* and the NO_3^- transporter *VviNPF2.3* are all hydrophobic (Figure S3C). Given the phylogenetic distance (Léran *et al.* 2014) and the protein sequence homology (approximately 30% identity, Figure S3C) between *AtNPF6.3* and the NPF2s, we suggest that the *AtNPF6.3* model is not suitable for predicting the NO_3^- transporting feature of these NPF2 proteins.

Although both *VviNPF2.1* and *VviNPF2.2* were more highly expressed in 140 Ruggeri than in K51-40 (Henderson *et al.* 2014a), their expression levels in grapevines were regulated by NO_3^- treatments rather than Cl^- stress (Figure 1). Neither the microarray gene expression analysis on 50 mM Cl^- treated grapevine roots (Henderson *et al.* 2014a) (Table 1) nor the RT-qPCR analyses on the 25 mM Cl^- treated grapevine roots (Figure 1C – D) and the 60 mM NaCl treated Cabernet Sauvignon roots (Figure S6) showed any differential expression of these two genes between the control and salt treated roots. The expression levels of *VviNPF2.1* and *VviNPF2.2* were down-regulated by post-starvation high [NO_3^-] re-supply in whole roots of 140 Ruggeri and K51-40 (Figure 1A – B), which points to the likeliness that both *VviNPF2.1* and *VviNPF2.2* function in NO_3^- transport.

Given the Cl^- and the NO_3^- responses of *VviNPF2.1* and *VviNPF2.2* expression, it is more likely that the functions of the proteins that they encode are NO_3^- transport related. However, plant salt tolerance is not only contributed by shoot Cl^- exclusion. The shoot NO_3^- to Cl^- ratio could be important in plant salt tolerance as well. Both NO_3^- and Cl^- are monovalent anions with similar sizes; it is common for a plant anion transporter to be permeable to both NO_3^- and Cl^- , and generally the NO_3^- selectivity is higher than that of Cl^- (Roberts 2006). This is not surprising, given that Cl^- , despite its smaller ionic radius, has a more tightly bound hydration shell than NO_3^- (Wege *et al.* 2017).

Adequate or abundant NO_3^- supply to plants were known to improve salt stress tolerance of the plants and to reduce shoot Cl^- accumulation (Abdolzadeh *et al.* 2008, Gimeno *et al.* 2009, Glass and Siddiqi 1985, Guo *et al.* 2017, Lunin and Gallatin 1965). In grapevines, the $[\text{NO}_3^-]$ in leaves could be reduced by high environmental $[\text{Cl}^-]$ (Abbaspour *et al.* 2014, Fisarakis *et al.* 2005), which suggests that NO_3^- and Cl^- could compete in the uptake and transport processes when the plants are challenged with excessive Cl^- . Two Arabidopsis NO_3^- transporters in the NPF family, AtNPF2.3 and AtNPF7.3, were found to affect plant growth under salt stress, however in opposite ways. The disruption of the root xylem parenchyma expressing gene *AtNPF2.3* decreased root to shoot NO_3^- translocation and the shoot biomass under salt stress (Taochy *et al.* 2015). In the case of *AtNPF7.3*, its expression was down regulated by salt stress, and the disruption of this gene improved the seed germination rate when treated with a range of salt concentrations (Chen *et al.* 2012). These findings suggest that the maintenance of plant NO_3^- status by the NO_3^- transporters are important to plant health during salt stress.

As a plant system is likely to be more suitable for the functional characterisation of these VviNPFs, *VviNPF2.1* and *VviNPF2.2* were expressed in Arabidopsis root epidermis and cortex by transforming an enhancer trap line J1551. Originally, we intended to use the Microelectrode Ion Flux Estimations (MIFE) technique (Shabala *et al.* 2006) to monitor the Cl^- and NO_3^- concentration changes near the root surface of control plants and the Arabidopsis *VviNPF* over-expression lines, so that we could determine whether these VviNPFs could facilitate Cl^- and/or NO_3^- movements in plant roots. However, when we were testing the shoot ion content phenotypes of the *VviNPF2.2* OEX lines before conducting MIFE, we found that the expression of *VviNPF2.2* in root epidermis and cortex reduced shoot $[\text{Cl}^-]$ after being treated with 75 mM NaCl (Figure 5B). This suggests that the expression of *VviNPF2.2* in root epidermis and cortex was beneficial to the plants as it could reduce the shoot $[\text{Cl}^-]$ under salt stress. We suspect this shoot $[\text{Cl}^-]$ reducing phenotype could have been achieved by the *VviNPF2.2* mediated Cl^- efflux from root cells to the external media, which is similar to the proposed function of AtNPF2.5 (Li *et al.* 2017a).

In this study, the expression patterns of *VviNPF2.1* and *VviNPF2.2* in all experiments were highly similar. *VviNPF2.1* and *VviNPF2.2* are adjacent to one another on

chromosome 6. According to the sequence analysis, *VviNPF2.1* and *VviNPF2.2* are highly similar (96.71% identity) (Figure S3C), and so are the promoter regions cloned in this study (92.16% identity, alignment not shown). This is likely to be a result of a gene duplication during evolution. Gene duplications are considered important evolutionary events which create chances for the emergence of new genes with new functions or more specific functions (reviewed in Taylor and Raes 2004). Considering the similarities between the sequences, the tissue expression patterns, and the expression responses to NO_3^- and Cl^- of *VviNPF2.1* and *VviNPF2.2*, it is possible that they have not yet evolved to the stage which expressional differences emerge.

Acknowledgements

We thank Yu Long (University of Adelaide) for advice on TEVC; Deidre Blackmore (CSIRO) for assistance with preparing the grapevine green cuttings; Phillip Earl (University of Adelaide) for supplying the grapevine hardwood cuttings; Wendy Sullivan (University of Adelaide) for harvesting oocytes and assistance with the grapevine hardwood cuttings; Jiaen Qiu (University of Adelaide) for help to harvest the grapevine NO₃ treated roots; Gwenda Mayo (Adelaide Microscopy) for assistance with the microscopy work. Mandy Walker (CSIRO) for supplying 60 mM NaCl treated Cabernet Sauvignon root samples. Steve Tyerman (University of Adelaide) was the independent advisor. Y.W. was supported by the University of Adelaide (Adelaide Graduate Research Scholarship) and Wine Australia (AGWA Research Supplementary Scholarship (AGW Ph1502)). This research was funded by Australian grape growers and winemakers through their investment body Wine Australia with matching funds from the Australian government (AGW Ph1502).

References

- Abbaspour, N.** (2008) A comparative study of Cl⁻ transport across the roots of two grapevine rootstocks, K 51-40 and Paulsen, differing in salt tolerance. In *Discipline of Wine and Horticulture*. Adelaide: University of Adelaide.
- Abbaspour, N., Kaiser, B. and Tyerman, S.** (2013) Chloride transport and compartmentation within main and lateral roots of two grapevine rootstocks differing in salt tolerance. *Trees*, **27**, 1317-1325.
- Abbaspour, N., Kaiser, B. and Tyerman, S.** (2014) Root apoplastic transport and water relations cannot account for differences in Cl⁻ transport and Cl⁻/NO₃⁻ interactions of two grapevine rootstocks differing in salt tolerance. *Acta Physiologiae Plantarum*, **36**, 687-698.
- Abdolzadeh, A., Shima, K., Lambers, H. and Chiba, K.** (2008) Change in uptake, transport and accumulation of ions in *Nerium oleander* (Rosebay) as affected by different nitrogen sources and salinity. *Annals of Botany*, **102**, 735-746.
- Baby, T., Collins, C., Tyerman, S.D. and Gilliham, M.** (2016) Salinity negatively affects pollen tube growth and fruit set in grapevines and is not mitigated by silicon. *American Journal of Enology and Viticulture*, **67**, 218-228.
- Baby, T., Hocking, B., Tyerman, S.D., Gilliham, M. and Collins, C.** (2014) Modified method for producing grapevine plants in controlled environments. *American Journal of Enology and Viticulture*.
- Baetz, U., Eisenach, C., Tohge, T., Martinoia, E. and De Angeli, A.** (2016) Vacuolar chloride fluxes impact ion content and distribution during early salinity stress. *Plant Physiology*.
- Berg, H.W. and Keefer, R.M.** (1958) Analytical determination of tartrate stability in wine. I. Potassium bitartrate. *American Journal of Enology and Viticulture*, **9**, 180-193.
- Bergsdorf, E.-Y., Zdebik, A.A. and Jentsch, T.J.** (2009) Residues important for nitrate/proton coupling in plant and mammalian CLC transporters. *The Journal of Biological Chemistry*, **284**, 11184-11193.
- Cataldo, D.A., Maroon, M., Schrader, L.E. and Youngs, V.L.** (1975) Rapid colorimetric determination of nitrate in plant tissue by nitration of salicylic acid. *Communications in Soil Science and Plant Analysis*, **6**, 71-80.
- Chen, C.-Z., Lv, X.-F., Li, J.-Y., Yi, H.-Y. and Gong, J.-M.** (2012) Arabidopsis NRT1.5 is another essential component in the regulation of nitrate reallocation and stress tolerance. *Plant Physiology*, **159**, 1582-1590.
- Clough, S.J. and Bent, A.F.** (1998) Floral dip: a simplified method for Agrobacterium-mediated transformation of *Arabidopsis thaliana*. *The Plant Journal*, **16**, 735-743.
- Cochetel, N., Escudie, F., Cookson, S.J., Dai, Z., Vivin, P., Bert, P.F., Munoz, M.S., Delrot, S., Klopp, C., Ollat, N. and Lauvergeat, V.** (2017) Root transcriptomic responses of grafted grapevines to heterogeneous nitrogen availability depend on rootstock genotype. *Journal of Experimental Botany*, **68**, 4339-4355.
- Conn, S., Hocking, B., Dayod, M., Xu, B., Athman, A., Henderson, S., Aukett, L., Conn, V., Shearer, M., Fuentes, S., Tyerman, S. and Gilliham, M.** (2013) Protocol: optimising hydroponic growth systems for nutritional and physiological analysis of *Arabidopsis thaliana* and other plants. *Plant Methods*, **9**, 4.
- Corratge-Faillie, C. and Lacombe, B.** (2017) Substrate (un)specificity of Arabidopsis NRT1/PTR FAMILY (NPF) proteins. *Journal of Experimental Botany*.
- Cubero-Font, P., Maierhofer, T., Jaslan, J., Rosales, M.A., Espartero, J., Diaz-Rueda, P., Muller, H.M., Hurter, A.L., Al-Rasheid, K.A., Marten, I., Hedrich, R., Colmenero-Flores, J.M. and Geiger, D.** (2016) Silent S-Type anion channel subunit SLAH1 gates SLAH3 open for chloride root-to-shoot translocation. *Current Biology*, **26**, 2213-2220.

- De Angeli, A., Baetz, U., Francisco, R., Zhang, J., Chaves, M. and Regalado, A.** (2013) The vacuolar channel VvALMT9 mediates malate and tartrate accumulation in berries of *Vitis vinifera*. *Planta*, **238**, 283-291.
- de Loryn, L.C., Petrie, P.R., Hasted, A.M., Johnson, T.E., Collins, C. and Bastian, S.E.P.** (2014) Evaluation of sensory thresholds and perception of sodium chloride in grape juice and wine. *American Journal of Enology and Viticulture*, **65**, 124-133.
- Donkin, R., Robinson, S., Sumby, K., Harris, V., McBryde, C. and Jiranek, V.** (2010) Sodium chloride in Australian grape juice and its effect on alcoholic and malolactic fermentation. *American Journal of Enology and Viticulture*, **61**, 392-400.
- Fasoli, M., Dal Santo, S., Zenoni, S., Tornielli, G.B., Farina, L., Zamboni, A., Porceddu, A., Venturini, L., Bicego, M., Murino, V., Ferrarini, A., Delledonne, M. and Pezzotti, M.** (2012) The grapevine expression atlas reveals a deep transcriptome shift driving the entire plant into a maturation program. *The Plant Cell*, **24**, 3489-3505.
- Fisarakis, I., Nikolaou, N., Tsikalas, P., Therios, I. and Stavrakas, D.** (2005) Effect of salinity and rootstock on concentration of potassium, calcium, magnesium, phosphorus, and nitrate–nitrogen in Thompson Seedless grapevine. *Journal of Plant Nutrition*, **27**, 2117-2134.
- Geiger, D., Maierhofer, T., AL-Rasheid, K.A.S., Scherzer, S., Mumm, P., Liese, A., Ache, P., Wellmann, C., Marten, I., Grill, E., Romeis, T. and Hedrich, R.** (2011) Stomatal closure by fast abscisic acid signaling is mediated by the guard cell anion channel SLAH3 and the receptor RCAR1. *Science Signaling*, **4**, ra32-ra32.
- Gilliham, M. and Tester, M.** (2005) The regulation of anion loading to the maize root xylem. *Plant Physiology*, **137**, 819-828.
- Gimeno, V., Syvertsen, J.P., Nieves, M., Simón, I., Martínez, V. and García-Sánchez, F.** (2009) Additional nitrogen fertilization affects salt tolerance of lemon trees on different rootstocks. *Scientia Horticulturae*, **121**, 298-305.
- Glass, A.D.M. and Siddiqi, M.Y.** (1985) Nitrate inhibition of chloride influx in barley: Implications for a proposed chloride homeostat. *Journal of Experimental Botany*, **36**, 556-566.
- Gong, H., Blackmore, D., Clingeleffer, P., Sykes, S., Jha, D., Tester, M. and Walker, R.** (2011) Contrast in chloride exclusion between two grapevine genotypes and its variation in their hybrid progeny. *Journal of Experimental Botany*, **62**, 989-999.
- Guo, J., Zhou, Q., Li, X., Yu, B. and Luo, Q.** (2017) Enhancing NO₃⁻ supply confers NaCl tolerance by adjusting Cl⁻ uptake and transport in *G. max* & *G. soja*. *Journal of soil science and plant nutrition*, **17**, 194-202.
- Henderson, S.W., Baumann, U., Blackmore, D.H., Walker, A.R., Walker, R.R. and Gilliham, M.** (2014) Shoot chloride exclusion and salt tolerance in grapevine is associated with differential ion transporter expression in roots. *BMC Plant Biology*, **14**.
- Jha, D., Shirley, N., Tester, M. and Roy, S.J.** (2010) Variation in salinity tolerance and shoot sodium accumulation in Arabidopsis ecotypes linked to differences in the natural expression levels of transporters involved in sodium transport. *Plant, Cell & Environment*, **33**, 793-804.
- Krouk, G., Lacombe, B., Bielach, A., Perrine-Walker, F., Malinska, K., Mounier, E., Hoyerova, K., Tillard, P., Leon, S., Ljung, K., Zazimalova, E., Benkova, E., Nacry, P. and Gojon, A.** (2010) Nitrate-regulated auxin transport by NRT1.1 defines a mechanism for nutrient sensing in plants. *Developmental Cell*, **18**, 927-937.
- Larkin, M.A., Blackshields, G., Brown, N.P., Chenna, R., McGettigan, P.A., McWilliam, H., Valentin, F., Wallace, I.M., Wilm, A., Lopez, R., Thompson, J.D., Gibson, T.J. and Higgins, D.G.** (2007) Clustal W and Clustal X version 2.0. *Bioinformatics*, **23**, 2947-2948.

- Leran, S., Garg, B., Boursiac, Y., Corratge-Faillie, C., Brachet, C., Tillard, P., Gojon, A. and Lacombe, B. (2015) AtNPF5.5, a nitrate transporter affecting nitrogen accumulation in Arabidopsis embryo. *Scientific Reports*, **5**, 7962.
- Léran, S., Varala, K., Boyer, J.-C., Chiurazzi, M., Crawford, N., Daniel-Vedele, F., David, L., Dickstein, R., Fernandez, E., Forde, B., Gassmann, W., Geiger, D., Gojon, A., Gong, J.-M., Halkier, B.A., Harris, J.M., Hedrich, R., Limami, A.M., Rentsch, D., Seo, M., Tsay, Y.-F., Zhang, M., Coruzzi, G. and Lacombe, B. (2014) A unified nomenclature of NITRATE TRANSPORTER 1/PEPTIDE TRANSPORTER family members in plants. *Trends in Plant Science*, **19**, 5-9.
- Leske, P.A., Sas, A.N., Coulter, A.D., Stockley, C.S. and Lee, T.H. (1997) The composition of Australian grape juice: chloride, sodium and sulfate ions. *Australian Journal of Grape and Wine Research*, **3**, 26-30.
- Li, B., Byrt, C., Qiu, J., Baumann, U., Hrmova, M., Evrard, A., Johnson, A.A., Birnbaum, K.D., Mayo, G.M., Jha, D., Henderson, S.W., Tester, M., Gilliham, M. and Roy, S.J. (2016) Identification of a stelar-localized transport protein that facilitates root-to-shoot transfer of chloride in Arabidopsis. *Plant Physiology*, **170**, 1014-1029.
- Li, B., Qiu, J., Jayakannan, M., Xu, B., Li, Y., Mayo, G.M., Tester, M., Gilliham, M. and Roy, S.J. (2017a) AtNPF2.5 modulates chloride (Cl⁻) efflux from roots of *Arabidopsis thaliana*. *Frontiers in Plant Science*, **7**, 2013.
- Li, B., Tester, M. and Gilliham, M. (2017b) Chloride on the move. *Trends in Plant Science*, **22**, 236-248.
- Li, X.L., Wang, C.R., Li, X.Y., Yao, Y.X. and Hao, Y.J. (2013) Modifications of Kyoho grape berry quality under long-term NaCl treatment. *Food chemistry*, **139**, 931-937.
- Lunin, J. and Gallatin, M.H. (1965) Salinity-fertility interactions in relation to the growth and composition of beans. I. Effect of N, P, and K. *Agronomy Journal*, **57**, 339-342.
- Maas, E.V. and Hoffman, G.J. (1977) Crop salt tolerance - current assessment. *Journal of the Irrigation and Drainage Division*, **103**, 115-134.
- Munns, R. and Gilliham, M. (2015) Salinity tolerance of crops – what is the cost? *New Phytologist*, **208**, 668-673.
- Parker, J.L. and Newstead, S. (2014) Molecular basis of nitrate uptake by the plant nitrate transporter NRT1.1. *Nature*, **507**, 68.
- Pike, S., Gao, F., Kim, M.J., Kim, S.H., Schachtman, D.P. and Gassmann, W. (2013) Members of the NPF3 transporter subfamily encode pathogen-inducible nitrate/nitrite transporters in grapevine and arabidopsis. *Plant and Cell Physiology*, **55**, 162-170.
- Plett, D., Safwat, G., Gilliham, M., Skrumsager Moller, I., Roy, S., Shirley, N., Jacobs, A., Johnson, A. and Tester, M. (2010) Improved salinity tolerance of rice through cell type-specific expression of *AtHKT1;1*. *PLoS One*, **5**, e12571.
- Plett, D.C. (2008) Spatial and temporal alterations of gene expression in rice.
- Prior, L.D., Grieve, A.M. and Cullis, B.R. (1992a) Sodium chloride and soil texture interactions in irrigated field grown sultana grapevines. I. Yield and fruit quality. *Australian Journal of Agricultural Research*, **43**, 1051-1066.
- Prior, L.D., Grieve, A.M. and Cullis, B.R. (1992b) Sodium chloride and soil texture interactions in irrigated field grown sultana grapevines. II. Plant mineral content, growth and physiology. *Australian Journal of Agricultural Research*, **43**, 1067-1083.
- Qiu, J., Henderson, S.W., Tester, M., Roy, S.J. and Gilliham, M. (2016) SLAH1, a homologue of the slow type anion channel SLAC1, modulates shoot Cl⁻ accumulation and salt tolerance in *Arabidopsis thaliana*. *Journal of Experimental Botany*, **67**, 4495-4505.
- Roberts, S.K. (2006) Plasma membrane anion channels in higher plants and their putative functions in roots. *New Phytologist*, **169**, 647-666.
- Roy, S.J., Gilliham, M., Berger, B., Essah, P.A., Cheffings, C., Miller, A.J., Davenport, R.J., Liu, L.-H., Skynner, M.J., Davies, J.M., Richardson, P., Leigh, R.A. and Tester, M. (2008)

- Investigating glutamate receptor-like gene co-expression in *Arabidopsis thaliana*. *Plant, Cell & Environment*, **31**, 861-871.
- Shabala, L., Ross, T., McMeekin, T. and Shabala, S.** (2006) Non-invasive microelectrode ion flux measurements to study adaptive responses of microorganisms to the environment. *FEMS Microbiology Reviews*, **30**, 472-486.
- Shelden, M.C., Howitt, S.M., Kaiser, B.N. and Tyerman, S.D.** (2009) Identification and functional characterisation of aquaporins in the grapevine, *Vitis vinifera*. *Functional Plant Biology*, **36**, 1065-1078.
- Stevens, R.M., Harvey, G. and Partington, D.L.** (2011) Irrigation of grapevines with saline water at different growth stages: effects on leaf, wood and juice composition. *Australian Journal of Grape and Wine Research*, **17**, 239-248.
- Sun, J., Bankston, J.R., Payandeh, J., Hinds, T.R., Zagotta, W.N. and Zheng, N.** (2014) Crystal structure of the plant dual-affinity nitrate transporter NRT1.1. *Nature*, **507**, 73.
- Taochy, C., Gaillard, I., Ipotesi, E., Oomen, R., Leonhardt, N., Zimmermann, S., Peltier, J.B., Szponarski, W., Simonneau, T. and Sentenac, H.** (2015) The Arabidopsis root stele transporter NPF2.3 contributes to nitrate translocation to shoots under salt stress. *The Plant Journal*, **83**, 466-479.
- Taylor, J.S. and Raes, J.** (2004) Duplication and divergence: The evolution of new genes and old ideas. *Annual Review of Genetics*, **38**, 615-643.
- Teakle, N.L. and Tyerman, S.D.** (2010) Mechanisms of Cl⁻ transport contributing to salt tolerance. *Plant, Cell & Environment*, **33**, 566-589.
- Tregeagle, J.M., Tisdall, J.M., Blackmore, D.H. and Walker, R.R.** (2006) A diminished capacity for chloride exclusion by grapevine rootstocks following long-term saline irrigation in an inland versus a coastal region of Australia. *Australian Journal of Grape and Wine Research*, **12**, 178-191.
- Tsay, Y.-F., Schroeder, J.I., Feldmann, K.A. and Crawford, N.M.** (1993) The herbicide sensitivity gene CHL1 of Arabidopsis encodes a nitrate-inducible nitrate transporter. *Cell*, **72**, 705-713.
- Tzounopoulos, T., Maylie, J. and Adelman, J.P.** (1995) Induction of endogenous channels by high levels of heterologous membrane proteins in *Xenopus* oocytes. *Biophysical Journal*, **69**, 904-908.
- Vandesompele, J., De Preter, K., Pattyn, F., Poppe, B., Van Roy, N., De Paepe, A. and Speleman, F.** (2002) Accurate normalization of real-time quantitative RT-PCR data by geometric averaging of multiple internal control genes. *Genome Biology*, **3**, research0034.0031-research0034.0011.
- Walker, R. and Clingeleffer, P.** (2009) Rootstock attributes and selection for Australian conditions. *Australian Viticulture*, **13**, 70-76.
- Walker, R.R., Blackmore, D., Clingeleffer, P. and Gibberd, M.** (2002a) How vines deal with salt. In *Managing Water: Australian Society of Viticulture and Oenology*.
- Walker, R.R., Blackmore, D.H., Clingeleffer, P.R. and Correll, R.L.** (2002b) Rootstock effects on salt tolerance of irrigated field-grown grapevines (*Vitis vinifera* L. cv. Sultana): 1. Yield and vigour inter-relationships. *Australian Journal of Grape and Wine Research*, **8**, 3-14.
- Walker, R.R., Blackmore, D.H., Clingeleffer, P.R., Godden, P., Francis, L., Valente, P. and Robinson, E.** (2003) Salinity effects on vines and wines. *Bulletin de l'Office. International de la Vigne et du Vin*, **76**, 200-227.
- Walker, R.R., Blackmore, D.H., Clingeleffer, P.R. and Tarr, C.R.** (2007) Rootstock effects on salt tolerance of irrigated field-grown grapevines (*Vitis vinifera* L. cv. Sultana). 3. Fresh fruit composition and dried grape quality. *Australian Journal of Grape and Wine Research*, **13**, 130-141.

- Walker, R.R., Blackmore, D.H., Gong, H., Henderson, S.W., Gilliam, M. and Walker, A.R.** (2018) Analysis of the salt exclusion phenotype in rooted leaves of grapevine (*Vitis* spp.). *Australian Journal of Grape and Wine Research*, **24**, 317-326.
- Wege, S., Gilliam, M. and Henderson, S.W.** (2017) Chloride: not simply a 'cheap osmoticum', but a beneficial plant macronutrient. *Journal of Experimental Botany*, **68**, 3057-3069.
- Wen, Z., Tyerman, S.D., Dechorgnat, J., Ovchinnikova, E., Dhugga, K.S. and Kaiser, B.N.** (2017) Maize NPF6 proteins are homologs of Arabidopsis CHL1 that are selective for both nitrate and chloride. *The Plant Cell*, **29**, 2581-2596.
- Wu, F.H., Shen, S.C., Lee, L.Y., Lee, S.H., Chan, M.T. and Lin, C.S.** (2009) Tape-Arabidopsis sandwich - a simpler Arabidopsis protoplast isolation method. *Plant Methods*, **5**, 16.
- Wu, Y., Henderson, S.W., Walker, R.R. and Gilliam, M.** (2019a) Expression of the grapevine stelar localised anion transporter ALMT2 in Arabidopsis roots reduced shoot Cl⁻ accumulation under salt stress.
- Wu, Y., Li, J. and Gilliam, M.** (2019b) An R-based web app Smart-IV for automated and integrated high throughput electrophysiology data processing.
- Yoo, S.D., Cho, Y.H. and Sheen, J.** (2007) Arabidopsis mesophyll protoplasts: a versatile cell system for transient gene expression analysis. *Nat. Protoc.*, **2**, 1565-1572.

Tables and figures

Table 1: A microarray gene expression study (Henderson *et al.* 2014a) show that *VviNPF2.1* and *VviNPF2.2* are both more highly expressed in the roots of 140 Ruggeri (140R) than in K51-40, however their expression levels were not significantly affected by the 50 mM Cl⁻ treatment in 140 Ruggeri, Cabernet Sauvignon (CS) and K51-40 roots. The data (obtained with permission of Henderson *et al.* (2014a)) is presented as log(2) gene expression fold change (FC) with adjusted p values and B values.

	Control vs. Control			50 mM Cl vs. Control								
	140R - K51-40			140R 50Cl - 140R Ctrl			CS 50Cl - CS Ctrl			K51-40 50Cl - K51-40 Ctrl		
	log(2) FC	adj.P.Val	B	log(2) FC	adj.P.Val	B	log(2) FC	adj.P.Val	B	log(2) FC	adj.P.Val	B
<i>VviNPF2.1</i>	1.27	0.00	34.49	0.16	0.53	-5.62	-0.22	0.19	-5.09	0.05	0.94	-6.41
<i>VviNPF2.2</i>	1.61	0.00	66.55	-0.01	0.99	-6.24	-0.21	0.11	-4.52	-0.40	0.00	-0.44

Figure 1

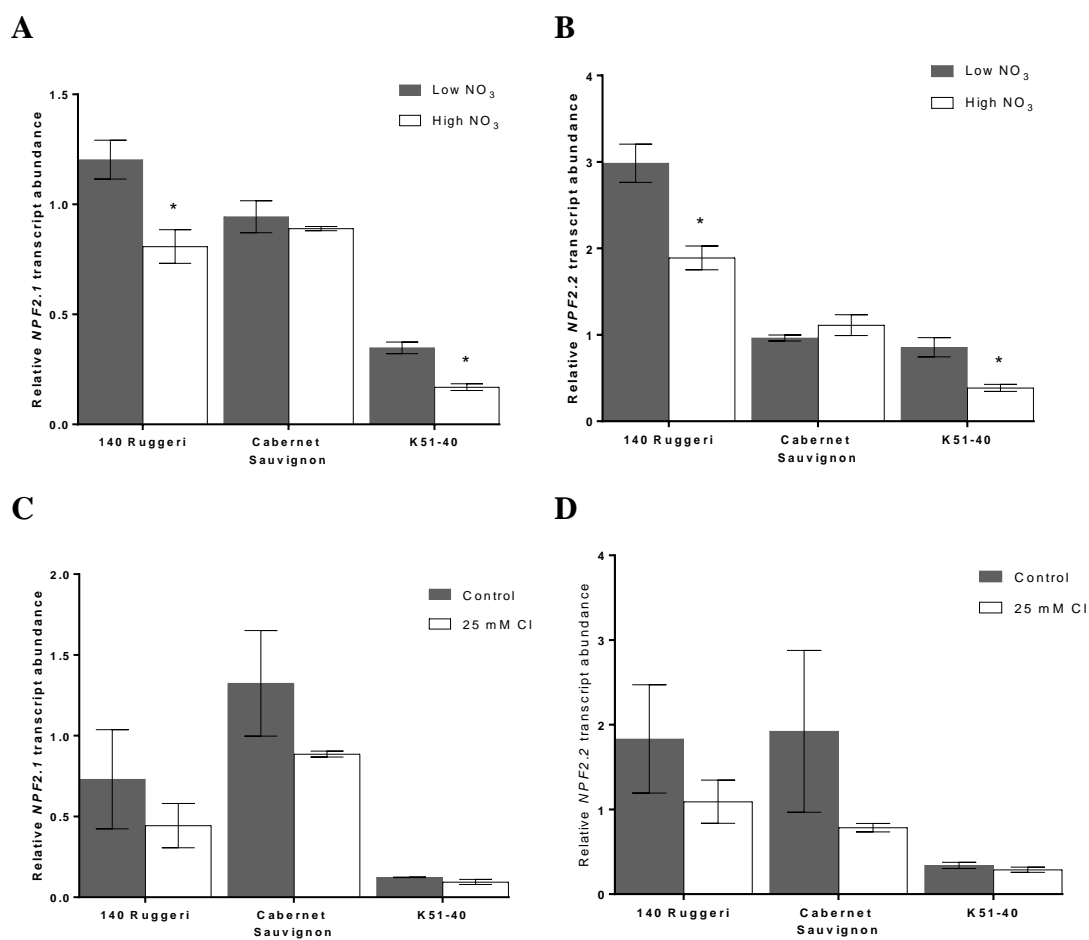


Figure 1: Expression levels of *VviNPF2.1* and *VviNPF2.2* in roots of grapevine rootstock cuttings are down-regulated by post-starvation high [NO₃⁻] re-supply, but not affected by Cl⁻ treatment. (A – B) Relative (A) *VviNPF2.1* and (B) *VviNPF2.2* transcript abundance in grapevine roots in response to the low NO₃⁻ control condition (0.8 mM, grey bars) or high NO₃⁻ re-supply post starvation (12 mM, white bars) post starvation. (C – D) Relative (C) *VviNPF2.1* and (D) *VviNPF2.2* gene expression levels in grapevine roots in response to control (grey bars) or 25 mM Cl⁻ stress (white bars). Asterisk indicates significant difference between treatments (p < 0.05, Student's t-test). Data are mean ± SE (n = 3 replicates), and presented relative to Cabernet Sauvignon control sample 1.

Figure 2

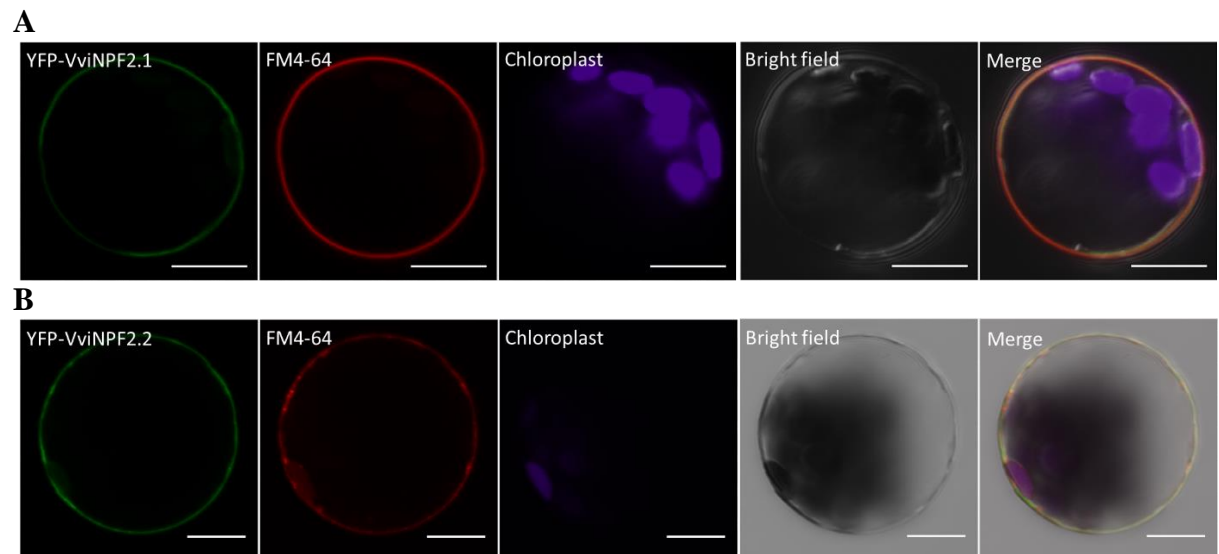


Figure 2: VviNPF2.1 and VviNPF2.2 localise to the plasma membrane (PM) in *Arabidopsis* mesophyll protoplasts. Confocal microscopic images show (A) co-localisation of YFP-VviNPF2.1 with the dye FM4-64, and (B) co-localisation of YFP-VviNPF2.2 with the dye FM4-64. Whole protoplasts were imaged 16 hours post transfection with vectors coding *35S:YFP-VviNPF*. FM4-64 was applied to the protoplasts 15 min before imaging. Scale bars = 10 μ m.

Figure 3

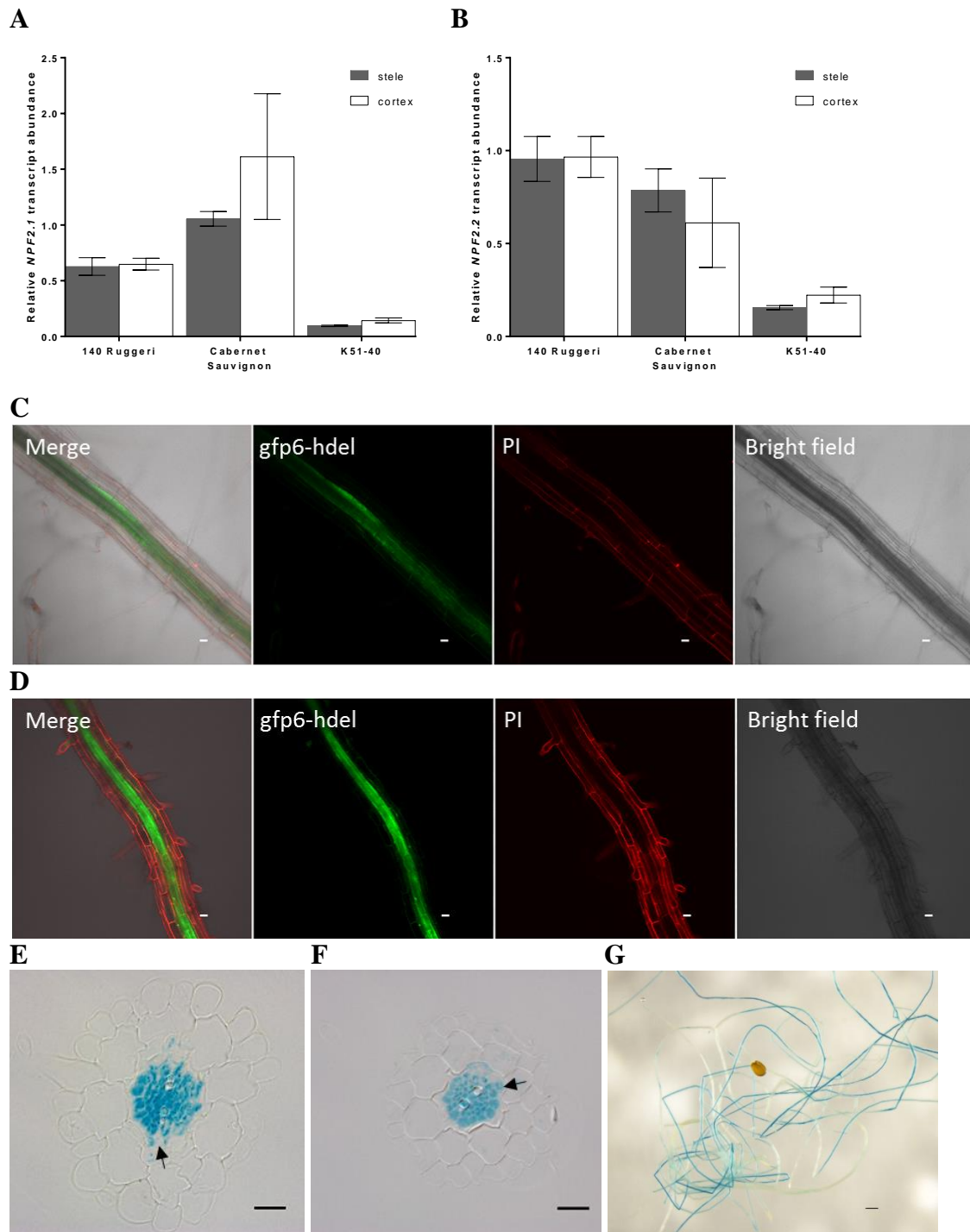
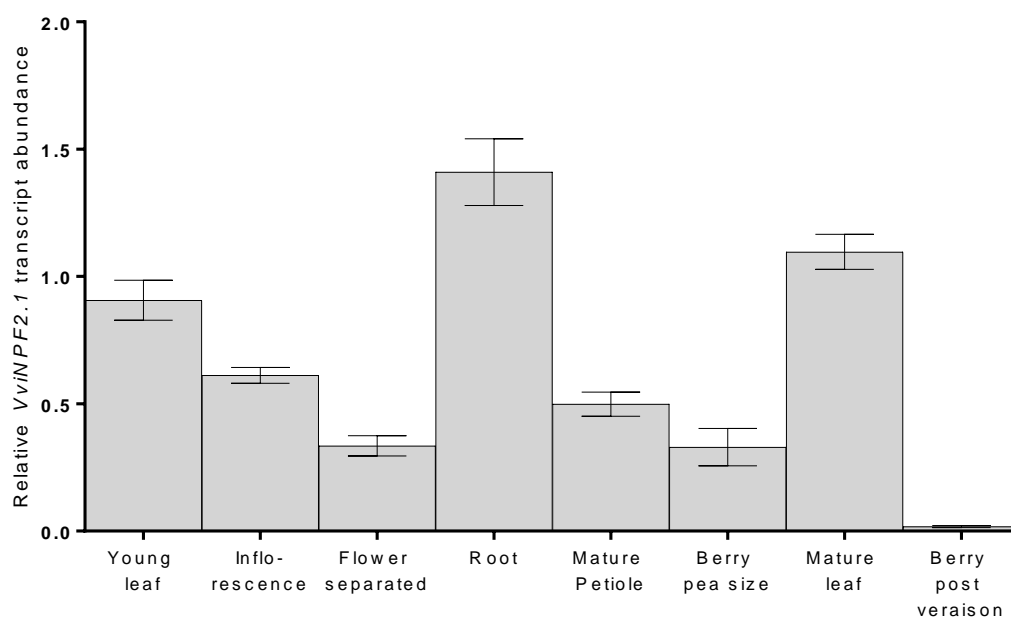


Figure 3: Expression patterns of *VviNPF2.1* and *VviNPF2.2* in roots. (A – B) Transcript abundance of (A) *VviNPF2.1* and (B) *VviNPF2.2* in root stelar-enriched (grey bars) or root cortex/epidermis-enriched (white bars) fractions of hydroponically grown roots harvested from rooted-leaves of 140 Ruggeri, Cabernet Sauvignon and K51-40. Data are the mean normalised expression level relative to the Cabernet Sauvignon cortical

replicate $1 \pm \text{SE}$ ($n = 3$). (C – D) The (C) *proVviNPF2.1*, and (D) *proVviNPF2.2* driven GFP activities in Arabidopsis roots. Roots were stained with propidium iodide and imaged using a confocal microscope. Scale bars = 20 μm . (E – F) The (E) *proVviNPF2.1* and (F) *proVviNPF2.2* driven GUS activities in Arabidopsis root transverse sections. The black arrows point to endodermal passage cells. Scale bars = 20 μm . (G) The *proVviNPF2.2* driven GUS activities in Arabidopsis whole root show that the GUS expression pattern was not uniform across the whole root system. Scale bar = 500 μm .

Figure 4

A



B

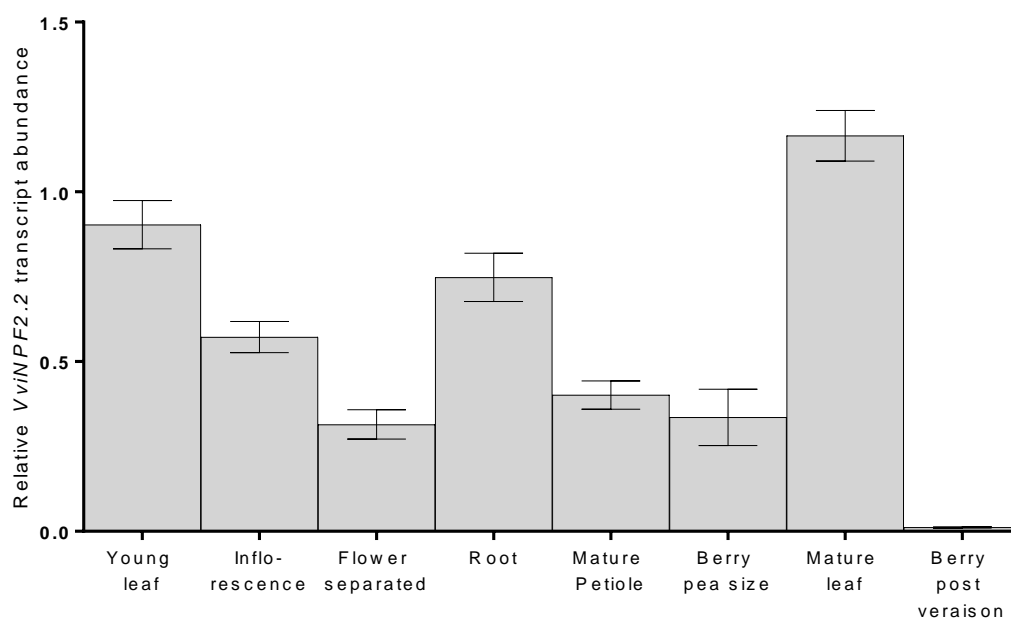


Figure 4: Both *VviNPF2.1* and *VviNPF2.2* are most abundant in grapevine roots and leaves. (A – B) Relative transcript abundance of (A) *VviNPF2.1* and (B) *VviNPF2.2* in different tissue types of Cabernet Sauvignon. Cabernet Sauvignon plants were propagated from hard wood cuttings in pots and tissue samples were collected during

the growing season. Each sample contains tissues harvested from 3 individual plants. Transcript abundance of each gene is relative to the abundance in young leaf sample 1. Data are mean \pm SE ($n = 3$).

Figure 5

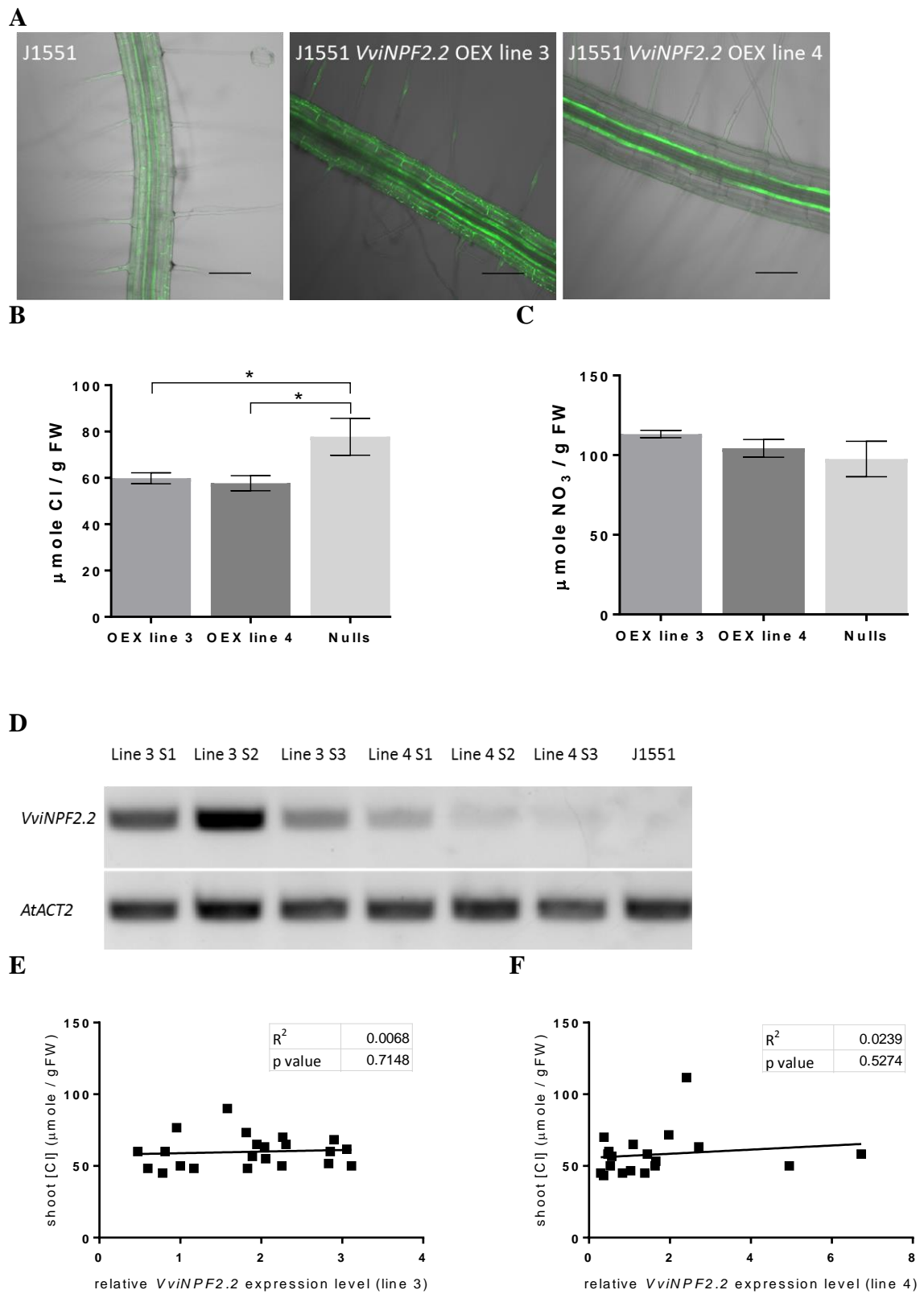


Figure 5: Over-expressing of *VviNPF2.2* in *Arabidopsis* root epidermis, cortex and endodermis reduced the shoot [Cl⁻] post 75 mM NaCl treatment. (A) The enhancer trap

line J1551 mGFP5-ER expression pattern showed root vasculature specific transgene over-expression. Scale bars = 100 μm . (B – C) The Arabidopsis J1551 *VviNPF2.2* over-expression (OEX) line 3 and 4 have (B) lower shoot $[\text{Cl}^-]$ than the null segregants (nulls) after the 75 mM NaCl treatment and (C) similar shoot $[\text{NO}_3^-]$ compare to the nulls. Data are means \pm SE (OEX lines, n = 21-22 samples; nulls, n = 12 samples). Asterisks indicate statistically significant differences ($p < 0.05$, student's t-test). (D) The Arabidopsis *VviNPF2.2* OEX line 4 roots had lower transgene expression levels than those of the OEX line 3 roots. The electrophoresis gel image shows *VviNPF2.2* and *AtACT2* (housekeeping gene) PCR fragments amplified from root cDNA of the OEX line 3 sample 1–3 (S1–S3), the OEX line 1–3 (S1–S3) and a non-transformed J1551. (E – F) The relative expression levels of *VviNPF2.2* in Arabidopsis (E) OEX line 3 and (F) OEX line 4 roots did not have linear correlations with the shoot $[\text{Cl}^-]$. The expression levels were normalised to sample 1 of each line respectively. The R^2 values show the goodness of the linear regression fit and the p values show the statistical significant difference of the slope from zero.

Supporting information

Figure S1

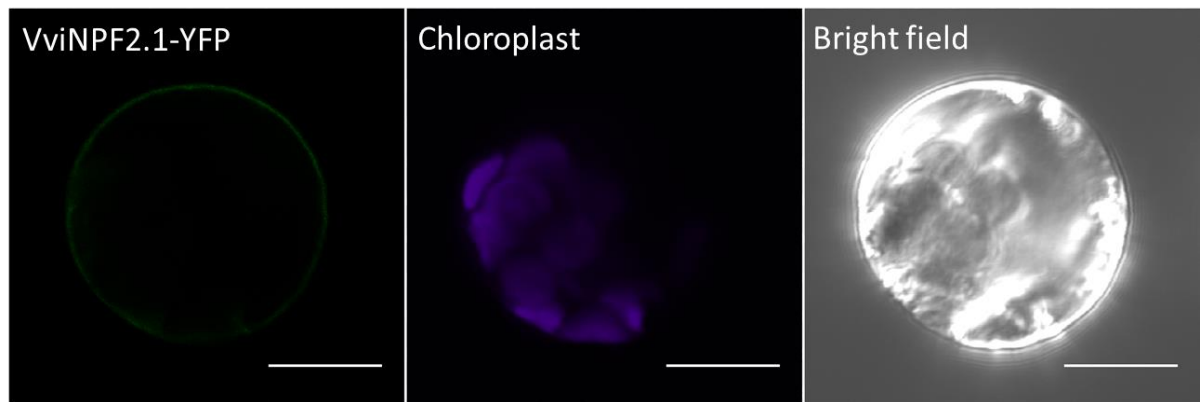


Figure S1: VviNPF2.1-YFP localised to the plasma membrane in *Arabidopsis* mesophyll protoplasts. Whole protoplasts were imaged 16 hours post transfection with vectors coding *35S:VviNPF2.1-EYFP*. Scale bars = 10 μm .

Figure S2

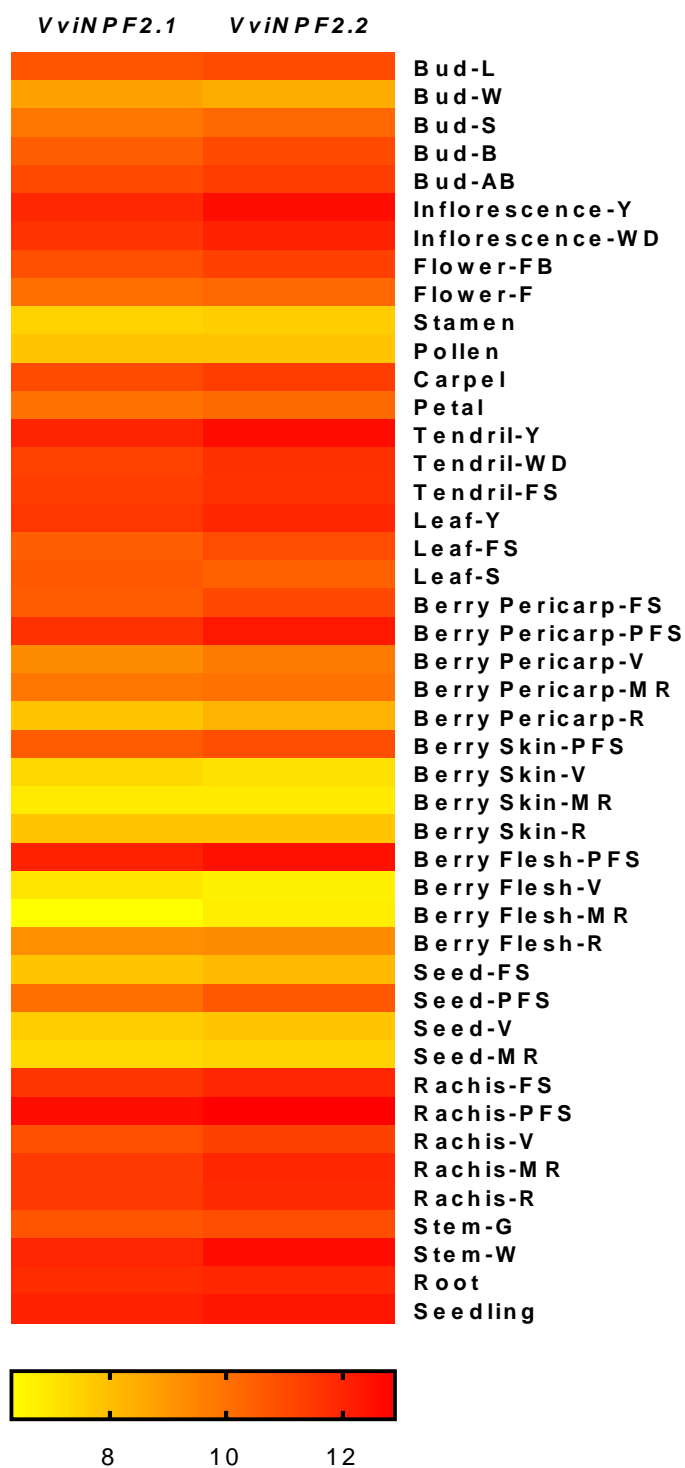
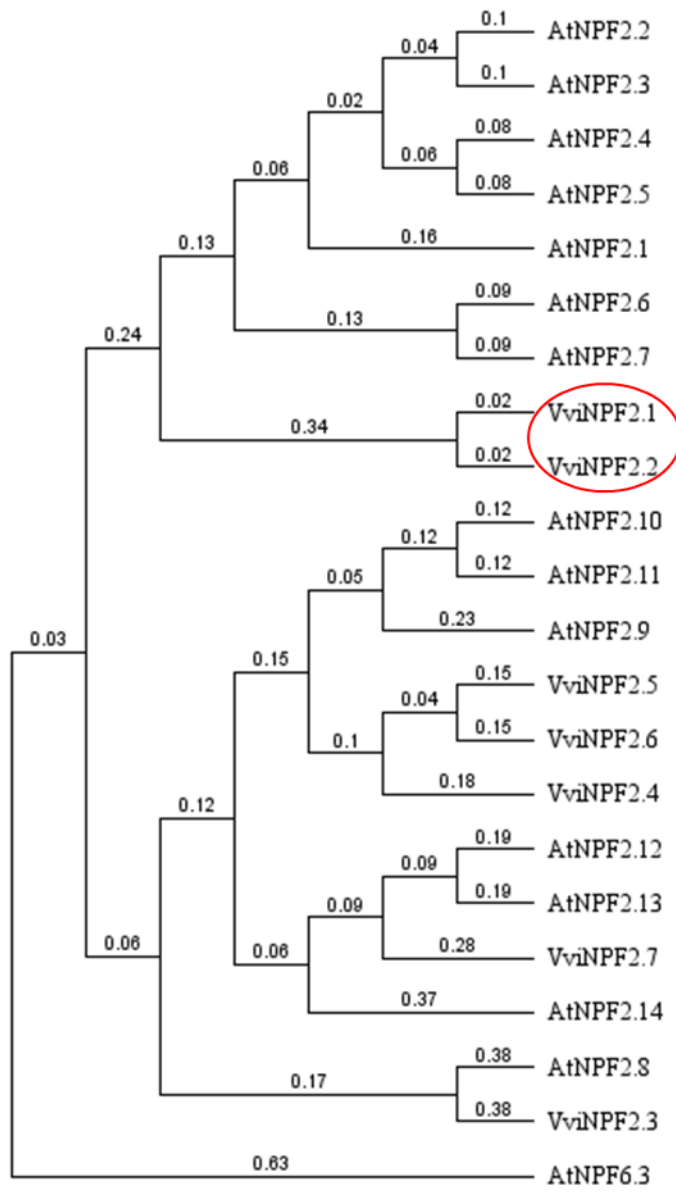


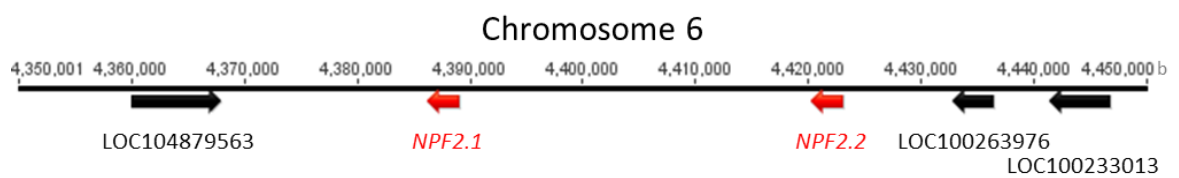
Figure S2: *VviNPF2.1* and *VviNPF2.2* have similar expression patterns in the grapevine (*V. vinifera*, cv. Corvina). RMA-normalized signal intensities from the microarray gene expression study by Fasoli *et al.* (2012). Data presented in the heat map are the log₂ mean transformed signal intensities of the 4 probes and 3 biological predicates.

Figure S3

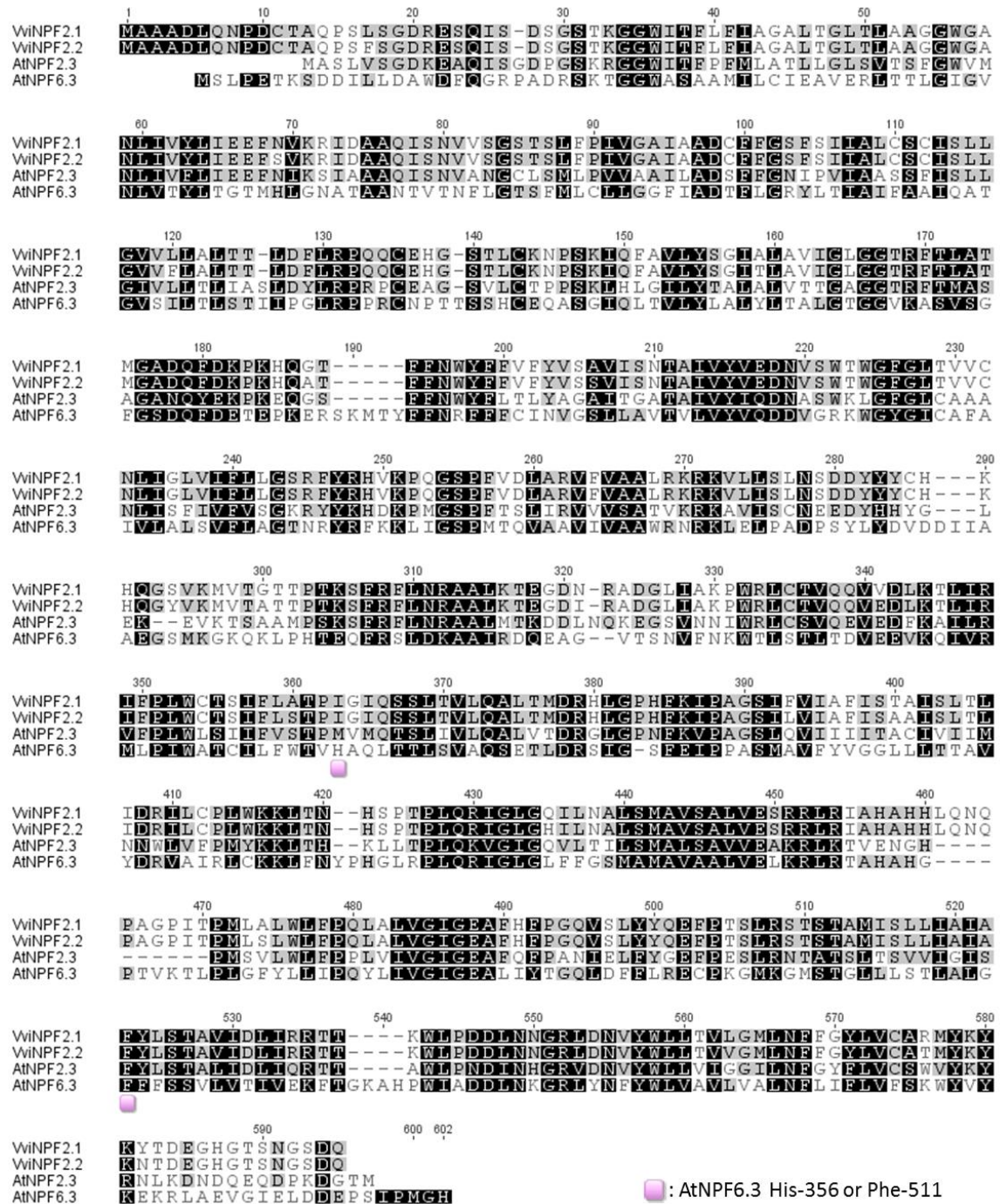
A



B



C



		% similarity			
		VviNPF2.1	VviNPF2.2	AtNPF2.3	AtNPF6.3
% identity	VviNPF2.1	X	97.7	70.2	50.8
	VviNPF2.2	96.71	X	69.9	50.4
	AtNPF2.3	51.58	51.58	X	49.2
	AtNPF6.3	32.77	32.43	27.71	X

Figure S3: VviNPF2.1 and VviNPF2.2 proteins share a high sequence homology. (A) The phylogenetic relationship of grapevine and Arabidopsis NPF2 family members,

with AtNPF6.3 shown as the outgroup. (B) The location of VviNPF2.1 and VviNPF2.2 on grapevine chromosome 6. (C) The protein sequence alignment of VviNPF2.1, VviNPF2.2, AtNPF2.3 (At3g45680) and AtNPF6.3 (At1g12110). The key residues for the NO₃⁻ transporting feature of AtNPF6.3 are labelled.

Figure S4

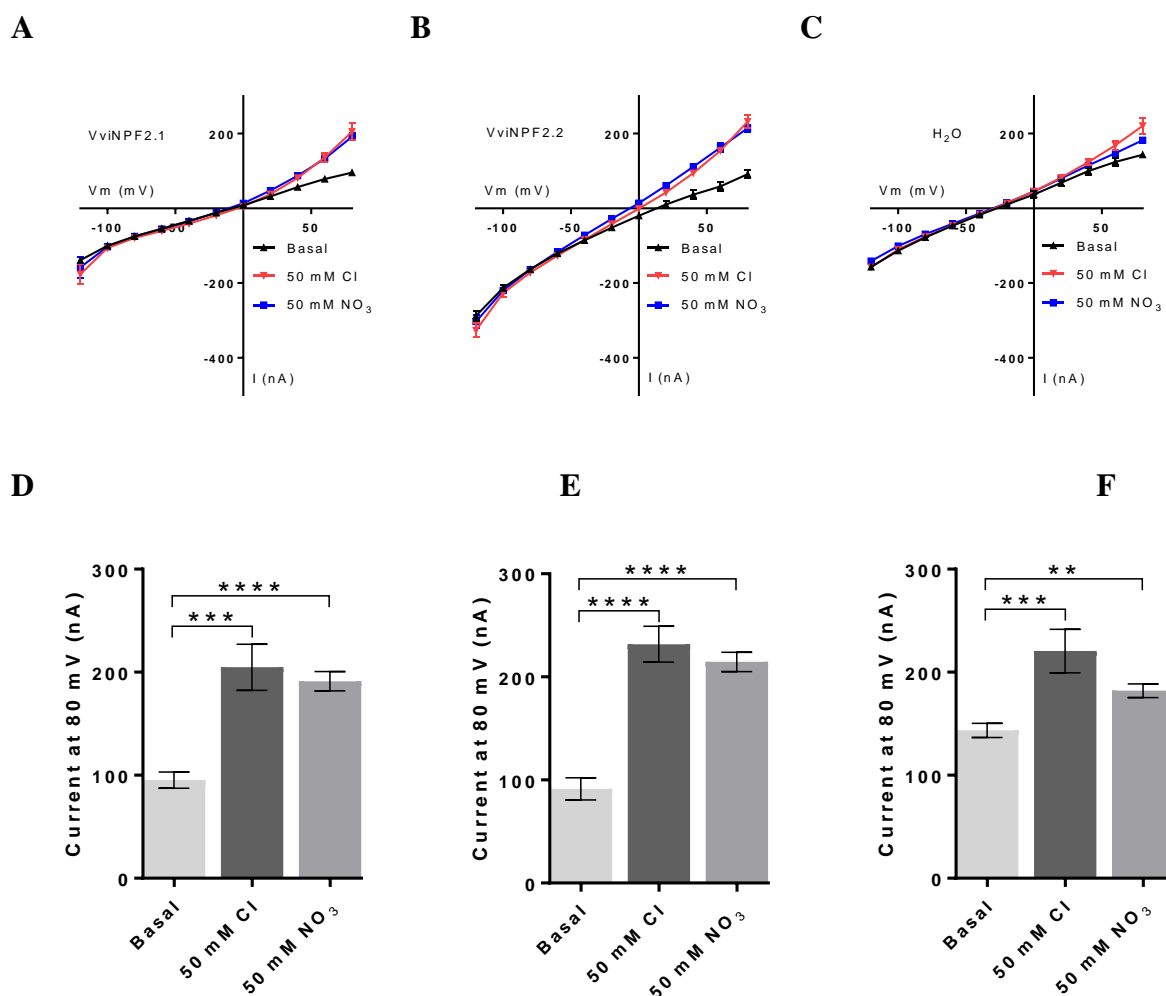


Figure S4: The electrophysiological properties of VviNPF2.1 and VviNPF2.2 expressing *Xenopus* oocytes. (A – C) I-V relationship of the (A) VviNPF2.1, (B) VviNPF2.2 expressing oocytes and (C) water injected controls tested in NM-D-G Cl or NM-D-G NO₃ perfusion buffers using TEVC (mean \pm SE, $n = 10$ oocytes). (D – F) Mean outward currents of (D) VviNPF2.1, (E) VviNPF2.2 expressing oocytes and (F) controls at 80 mV. Asterisks indicate statistically significant difference between the basal buffer currents and the anion buffer currents (2 asterisks: $P < 0.01$; 3 asterisks: $P < 0.001$; 4 asterisks: $P < 0.0001$, Student's t -test).

Figure S5

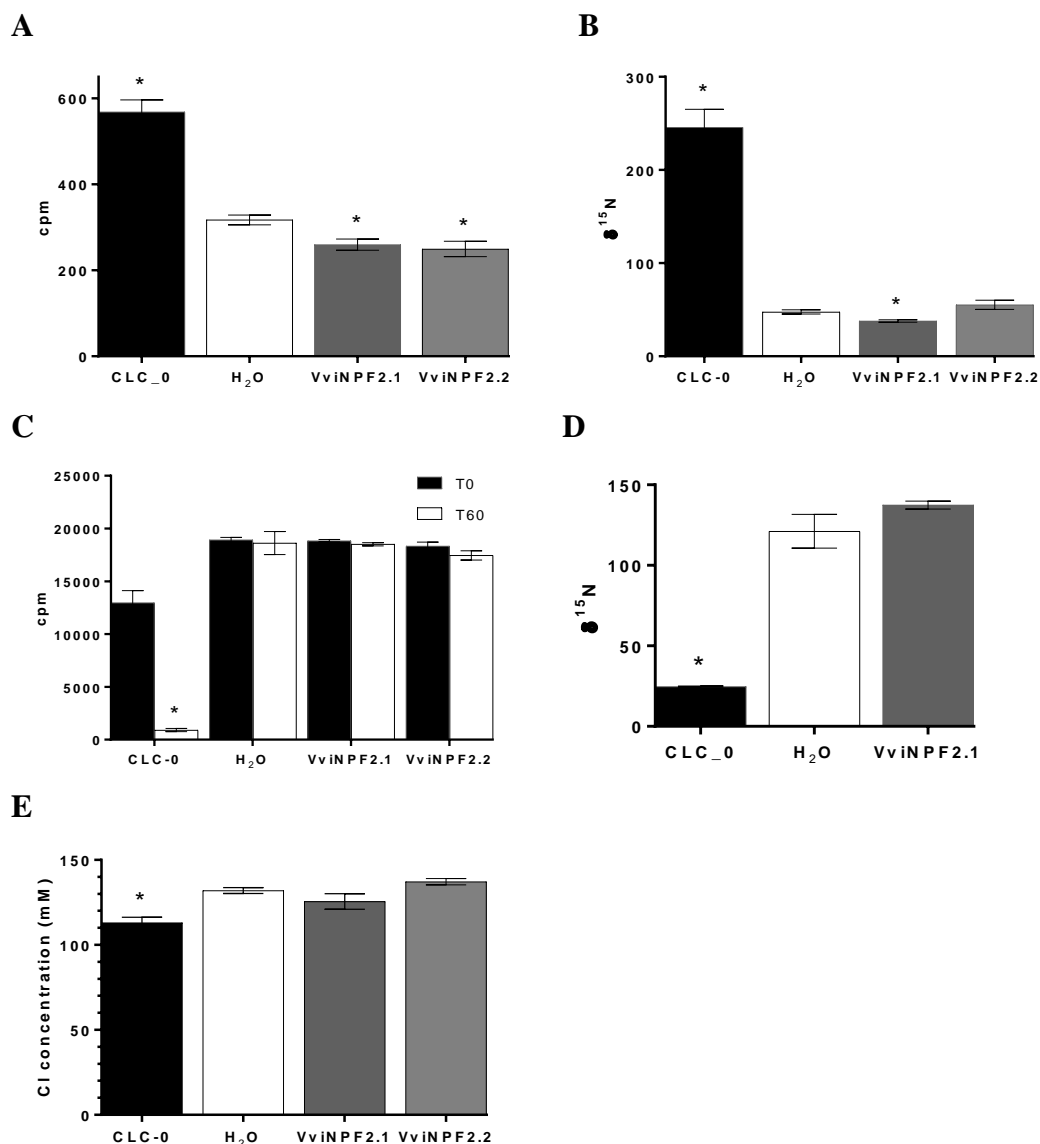


Figure S5: The anion transport activities of VviNPF2.1 and VviNPF2.2 expressing *Xenopus* oocytes. (A) Oocyte isotope levels after incubation in influx solutions containing ^{36}Cl . Asterisks indicate statistically significant differences between cRNA-injected oocytes and in the water-injected controls (mean \pm SE, $n = 10-11$ oocytes, $P < 0.01$, Student's t-test). (B) Oocyte isotope levels after incubation in influx solutions containing $^{15}\text{NO}_3$. Asterisks indicate statistically significant difference between cRNA-injected oocytes and in the water-injected controls (mean \pm SE, $n = 4-5$ samples, $P < 0.05$, Student's t-test). (C) ^{36}Cl injected oocyte isotope levels before (T0) and after (T60) incubation in efflux buffer. Asterisk indicates statistically significant differences between T0 and T60 (mean \pm SE, $n = 4-5$ oocytes, $P < 0.01$, Student's t-test). (D) $^{15}\text{NO}_3$ injected oocyte isotope levels after incubation in the efflux buffer for 60 min. Asterisk

indicates statistically significant differences between the $\delta^{15}\text{N}$ in the cRNA injected oocytes and in the water injected controls (mean \pm SE, $n = 5-6$ samples, $P < 0.01$, Student's t-test). (E) The $[\text{Cl}^-]$ in oocytes 2 days post incubation in Ca^{2+} Ringer's solution. Asterisk indicates statistically significant differences between the $[\text{Cl}^-]$ in the cRNA injected oocytes and in the water injected controls (mean \pm SE, $n = 5$ samples, $P < 0.05$, Student's t-test).

Figure S6

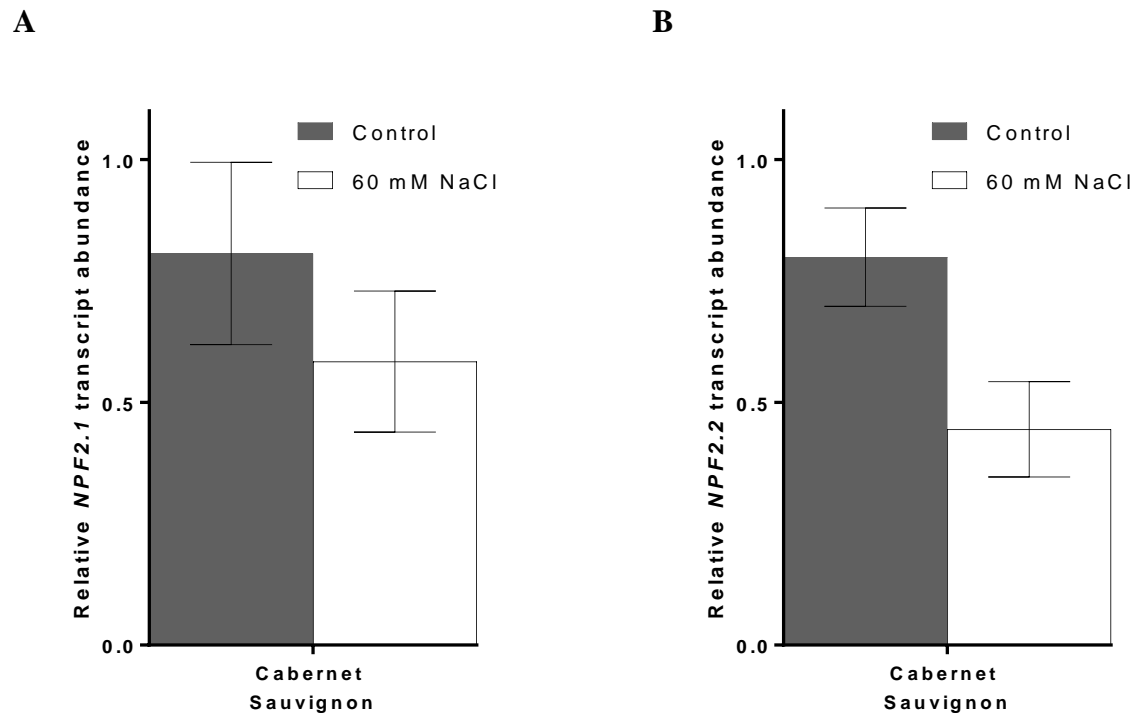


Figure S6: Expression levels of *VviNPF2.1* and *VviNPF2.2* in roots of Cabernet Sauvignon are not affected by the application of 60 mM NaCl. (A – B) Relative (A) *VviNPF2.1* and (B) *VviNPF2.2* transcript abundance in Cabernet Sauvignon roots in response to control (grey bars) or 60 mM NaCl stress (white bars). No statistically significant differences between the control and treatment groups are found ($p < 0.05$, Student's t-test). Data are mean \pm SE ($n = 3$ replicates), and presented relative to Cabernet Sauvignon control sample 1.

Figure S7

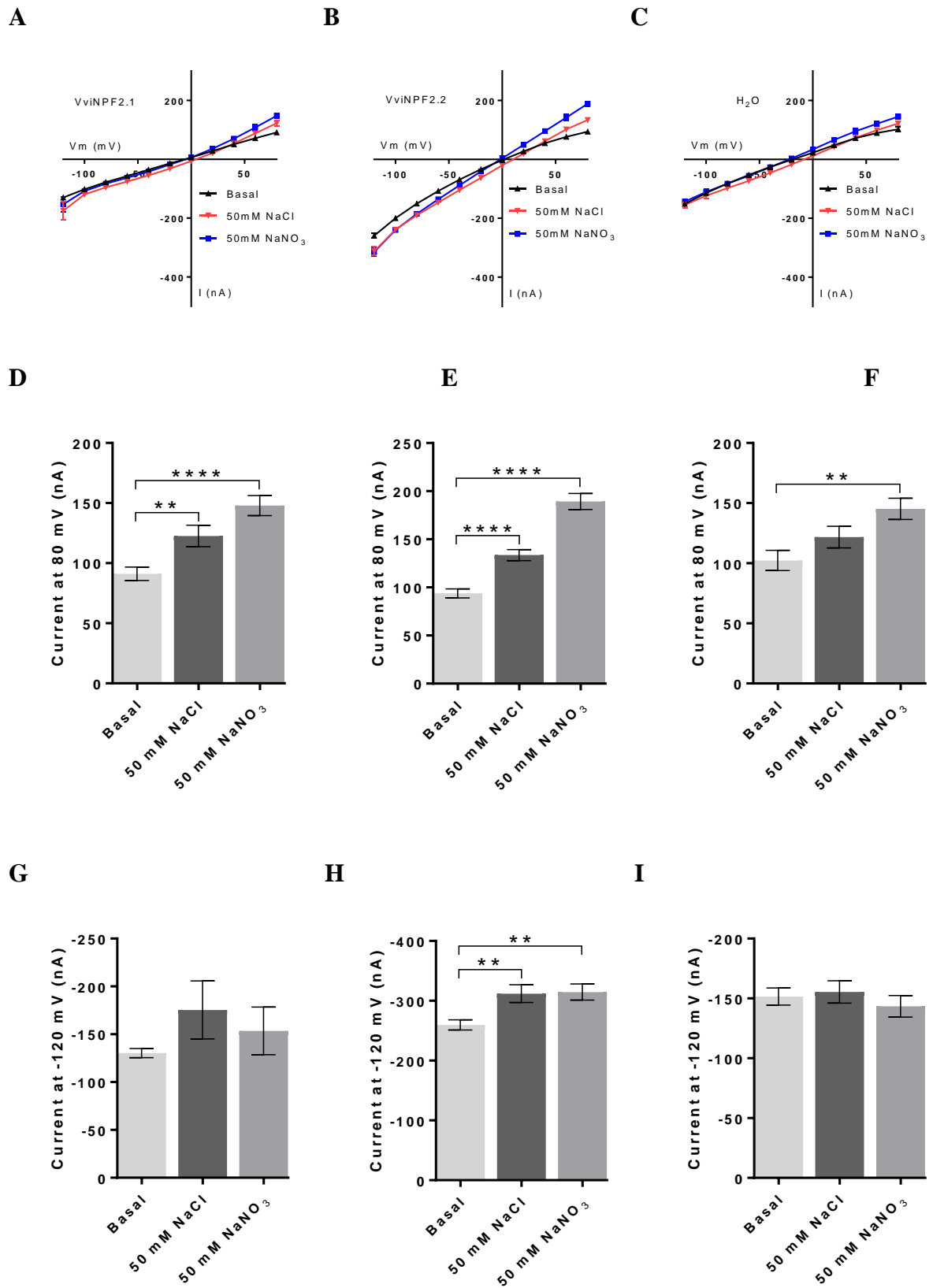


Figure S7: The electrophysiological properties of VviNPF2.1 and VviNPF2.2 expressing *Xenopus* oocytes in Na anion buffers. (A – C) I-V relationship of the (A) VviNPF2.1, (B) VviNPF2.2 expressing oocytes and (C) water injected controls tested in NaCl or NaNO₃ perfusion buffers using TEVC (mean ± SE, *n* = 10 oocytes). (D – F) Mean outward currents of (D) VviNPF2.1, (E) VviNPF2.2 expressing oocytes and (F) controls at 80 mV. (G – I) Mean inward currents of (G) VviNPF2.1, (H) VviNPF2.2 expressing oocytes and (I) controls at -120 mV. Asterisks indicate statistically significant difference between the basal buffer currents and the anion buffer currents (2 asterisks: *P* < 0.01; 4 asterisks: *P* < 0.0001, Student's t-test).

Table S1: Primers used in this study for molecular cloning and RT-qPCR analyses.

Gene	Direction	Sequence (5'-3')	Technique
<i>VviNPF2.1/VviNPF2.2</i>	Forward	ATGGCAGCCGCAGACCTGCAAA	Molecular cloning
	Reverse	TCACTGATCGGACCCATTACTTG	
<i>VviNPF2.1/VviNPF2.2</i> without stop codon	Forward	ATGGCAGCCGCAGACCTGCAAA	
	Reverse	CTGATCGGACCCATTACTTGTC	
<i>proVviNPF2.1</i>	Forward	GTTAGATCCACTTGGTTCATTTG	
	Reverse	TTGGTCTATGTTATTTGGTATATGAG	
<i>proVviNPF2.2</i>	Forward	<u>CACCCCTACCCATGACATTCCCA</u>	
	Reverse	TTGGTCTATGTTATTTGGTATATGAG	
<i>VviNPF2.1</i> qPCR fragment	Forward	GCCAAATTCTCAATGCCCTT	RT-qPCR analysis
	Reverse	CAGGCTGGTTCTGGAGGTG	
<i>VviNPF2.2</i> qPCR fragment	Forward	ATCGCATCCTATGTCCATTATG	
	Reverse	CAGGCTGGTTCTGGAGGTG	
<i>VviEF1-α</i> qPCR fragment	Forward	GAAGTGGGTGCTTGATAGGC	
	Reverse	AACCAAATATCCGGAGTAAAAGA	
<i>VviTUA</i> qPCR fragment	Forward	CAAAACCAAACGGACTGTTCAAT	
	Reverse	GCACCTTAGCAAGATCACCC	
<i>VviUBC</i> qPCR fragment	Forward	GTGGAGCCCTGCACTTACC	
	Reverse	GAGGGTCGTCAGGATTTGGA	

Chapter 4: Functional differences in transport properties of natural HKT1;1 variants influence shoot Na⁺ exclusion in grapevine rootstocks

Sam W. Henderson^{1, *}, Jake D. Dunlevy^{2, *}, Yue Wu¹, Deidre H. Blackmore², Rob R. Walker², Everard J. Edwards², Matthew Gilliam^{1, †} and Amanda R. Walker^{2, †}

¹ ARC Centre of Excellence in Plant Energy Biology, School of Agriculture, Food and Wine, University of Adelaide, Glen Osmond, South Australia 5064, Australia

² CSIRO Agriculture and Food, Locked Bag 2, Glen Osmond, South Australia 5064, Australia

* These authors contributed equally

† Correspondence should be addressed to:

Professor Matthew Gilliam

Email: matthew.gilliam@adelaide.edu.au

Phone: +61 8 8313 8145

Dr Amanda R. Walker

Email: mandy.walker@csiro.au

Phone: +61 8 8303 8629

Email addresses:

SWH: sam.henderson@adelaide.edu.au

JDD: jake.dunlevy@csiro.au

YW: yue.wu@adelaide.edu.au

DHB: deidre.blackmore@csiro.au

RRW: rob.walker@csiro.au

EJE: everard.edwards@csiro.au

MG: matthew.gilliam@adelaide.edu.au

ARW: mandy.walker@csiro.au

Key words: 140 Ruggeri, hybrids, K51-40, North American rootstocks, salinity, site-directed mutagenesis, *Xenopus laevis* oocytes, yeast

Statement of Authorship

Title of Paper	Functional differences in transport properties of natural HKT1;1 variants influence shoot Na ⁺ exclusion in grapevine rootstocks
Publication Status	<input checked="" type="checkbox"/> Published <input type="checkbox"/> Accepted for Publication <input type="checkbox"/> Submitted for Publication <input type="checkbox"/> Unpublished and Unsubmitted work written in manuscript style
Publication Details	Henderson, S.W., Dunlevy, J.D., Wu, Y., Blackmore, D.H., Walker, R.R., Edwards, E.J., Gilliam, M. and Walker, A.R. (2018) Functional differences in transport properties of natural HKT1;1 variants influence shoot Na ⁺ exclusion in grapevine rootstocks. <i>New Phytologist</i> , 217, 1113-1127.

Principal Authors

By signing the Statement of Authorship, each author certifies that:

- i. the candidate's stated contribution to the publication is accurate;
- ii. permission is granted for the candidate to include the publication in the thesis; and
- iii. the sum of all co-author contributions is equal to 100% less the candidate's stated contribution.

Name of Principal Author	Sam Henderson		
Contribution to the Paper	Performed yeast assays, qRT-PCR, cloning, confocal microscopy, site-directed mutagenesis and electrophysiology of grapevine HKT variants, analysed the data and wrote the manuscript.		
Signature		Date	03/07/2019

Name of Principal Author	Jake Dunlevy		
Contribution to the Paper	Performed linkage mapping, QTL analysis, primer design, cloning of <i>HKT1;1</i> allelic variants, and sequencing of <i>HKT1;1</i> from <i>Vitis</i> species, devised and performed grapevine Na ⁺ screens, analysed the data and wrote the manuscript.		
Signature		Date	5/7/2019

Co-Author Contributions

Name of Co-Author (Candidate)	Yue Wu
Contribution to the Paper	Performed mutagenesis and electrophysiology of TaHKT1;5-D.
Overall percentage (%)	10
Certification:	This paper reports on original research I conducted during the period of my Higher Degree by Research candidature and is not subject to any obligations or contractual agreements with a third party that would constrain its inclusion in this

	thesis.		
Signature		Date	02.07.2019

Name of Co-Author	Deidre Blackmore		
Contribution to the Paper	Devised and performed grapevine Na ⁺ screens and measured the leaf Na ⁺ content.		
Signature		Date	5/7/19



Name of Co-Author	Rob Walker		
Contribution to the Paper	Devised and performed grapevine Na ⁺ screens, supervised the research and revised the manuscript.		
Signature		Date	5/7/19

Name of Co-Author	Everard Edwards		
Contribution to the Paper	Devised and performed grapevine Na ⁺ screens.		
Signature		Date	4/7/19

Name of Co-Author	Matthew Gilliam		
Contribution to the Paper	Supervised the research and revised the manuscript.		
Signature		Date	01.07.2019

Name of Co-Author	Mandy Walker		
Contribution to the Paper	Devised and performed grapevine Na ⁺ screens, supervised the research and revised the manuscript. Grant holder for this work		
Signature		Date	5/7/19

Functional differences in transport properties of natural HKT1;1 variants influence shoot Na⁺ exclusion in grapevine rootstocks

Sam W. Henderson^{1*} , Jake D. Dunlevy^{2*}, Yue Wu¹, Deidre H. Blackmore², Rob R. Walker², Everard J. Edwards², Matthew Gilliham^{1†}  and Amanda R. Walker^{2†}

¹ARC Centre of Excellence in Plant Energy Biology, School of Agriculture, Food and Wine, University of Adelaide, PMB1, Glen Osmond, South Australia 5064, Australia; ²CSIRO Agriculture & Food, Locked Bag 2, Glen Osmond, South Australia 5064, Australia

Summary

Authors for correspondence:

Matthew Gilliham

Tel: +61 8 8313 8145

Email: matthew.gilliham@adelaide.edu.au

Amanda R. Walker

Tel: +61 8 83038629

Email: mandy.walker@csiro.au

Received: 9 August 2017

Accepted: 9 October 2017

New Phytologist (2018) **217**: 1113–1127

doi: 10.1111/nph.14888

Key words: 140 Ruggeri, hybrids, K51-40, North American rootstocks, salinity, site-directed mutagenesis, *Xenopus laevis* oocytes, yeast.

- Under salinity, *Vitis* spp. rootstocks can mediate salt (NaCl) exclusion from grafted *V. vinifera* scions enabling higher grapevine yields and production of superior wines with lower salt content. Until now, the genetic and mechanistic elements controlling sodium (Na⁺) exclusion in grapevine were unknown.
- Using a cross between two *Vitis* interspecific hybrid rootstocks, we mapped a dominant quantitative trait locus (QTL) associated with leaf Na⁺ exclusion (*NaE*) under salinity stress. The *NaE* locus encodes six high-affinity potassium transporters (HKT). Transcript profiling and functional characterization in heterologous systems identified *VisHKT1;1* as the best candidate gene for controlling leaf Na⁺ exclusion.
- We characterized four proteins encoded by unique *VisHKT1;1* alleles from the parents, and revealed that the dominant HKT variants exhibit greater Na⁺ conductance with less rectification than the recessive variants. Mutagenesis of *VisHKT1;1* and *TaHKT1.5-D* from bread wheat, demonstrated that charged amino acid residues in the eighth predicted transmembrane domain of HKT proteins reduces inward Na⁺ conductance, and causes inward rectification of Na⁺ transport.
- The origin of the recessive *VisHKT1;1* alleles was traced to *V. champinii* and *V. rupestris*. We propose that the genetic and functional data presented here will assist with breeding Na⁺-tolerant grapevine rootstocks.

Introduction

Saline soils and irrigation water reduce growth and productivity of crop species worldwide, which has negative economic, environmental and social impacts (Pannell, 2001; Munns & Gilliham, 2015). Grapevine (*Vitis vinifera* L.) is moderately sensitive to irrigation water and soil salinity (Maas & Hoffman, 1977), suffering decreased growth and yield (Prior *et al.*, 1992; Walker *et al.*, 2002; Stevens *et al.*, 2011). In addition, fruit and wine quality can be reduced due to the accumulation of sodium (Na⁺) and chloride (Cl⁻) ions in berries (Li *et al.*, 2013). Unfavourable salty and soapy attributes in wine are associated with excessive wine Na⁺ and Cl⁻ concentrations (Walker *et al.*, 2003; de Loryn *et al.*, 2014), whereas high salt concentrations in grape juice reduce fermentation efficiency by decreasing the viability of wine yeasts, and result in undesirable increases in acetic acid content of wine (Donkin *et al.*, 2010). Some countries impose legal limits for Na⁺ and Cl⁻ concentrations permissible in wines (Leske *et al.*, 1997; de Loryn *et al.*, 2014). The

Organisation Internationale de la Vigne et du Vin (OIV) recommends a maximum free Na⁺ concentration of 60 mg l⁻¹ in wine (Stockley & Lloyd-Davies, 2001). Wineries often reject fruit with Na⁺ concentrations above this level. Growers may attempt to negate salinity in vineyards by flushing salts from soils with large volumes of irrigation water. However, this practice is not economically viable or practical in regions with limited quality water – a problem expected to worsen with climate change (Elliott *et al.*, 2014). A more cost-effective and efficient approach to limit the effects of salinity on grapevines is by grafting onto rootstocks that can restrict root-to-shoot transport of Na⁺ and Cl⁻, a trait referred to as shoot ion exclusion. Because wineries use Na⁺ concentrations in berries and grape juice as a basis for rejection, finding a genetic solution for shoot Na⁺ accumulation in grapevine would be advantageous to the wine industry so it can maintain quality wine production in salt-affected regions.

Grapevine rootstocks derived from wild North American *Vitis* species were first used in viticulture in the late 19th Century to provide resistance to the soil-born parasite phylloxera, which destroyed vineyards throughout Europe – an episode called the Great French Wine Blight (Stevenson, 1980). An estimated 80% of vines in vineyards worldwide are now grafted onto interspecific

*These authors contributed equally to this work.

†Senior authors.

rootstocks (Ollat *et al.*, 2016). Rootstocks are selected for beneficial traits including phylloxera resistance (Benheim *et al.*, 2012), nematode resistance (Ferris *et al.*, 2012), controlled vigour and yield (Walker *et al.*, 2002), drought resistance (Serra *et al.*, 2014) and ion exclusion (Tregagle *et al.*, 2010). Rootstock breeding programmes can utilize marker-assisted selection to hasten the pyramiding of key rootstock traits into new elite genotypes (Ollat *et al.*, 2016), yet little is currently known about the genetic mechanisms controlling ion exclusion in grapevines.

Most grapevine studies have concentrated on Cl^- toxicity (Ehlig, 1960; Downton, 1977a; Walker *et al.*, 2004) and the mechanistic basis of Cl^- exclusion from shoots (Gong *et al.*, 2011; Henderson *et al.*, 2014, 2015; Fort *et al.*, 2015). In other crops, shoot Na^+ exclusion is more widely studied and it is acknowledged that the major component of both Na^+ and Cl^- exclusion from plant shoots occurs via root-based mechanisms (Munns & Gilliam, 2015; Li *et al.*, 2017). As a result, Na^+ exclusion from leaves correlates well with exclusion from berries (Supporting Information Fig. S1; Walker *et al.*, 2004), and can be used as a proxy measure of whole shoot Na^+ exclusion *per se*.

Quantitative trait loci (QTLs) for shoot Na^+ exclusion in bread wheat (*Kna1*), durum wheat (*Nax1* and *Nax2*), rice (*SKC1*) and tomato are underpinned by genes encoding high-affinity potassium (K^+) transporter (HKT) proteins (Ren *et al.*, 2005; Byrt *et al.*, 2007; James *et al.*, 2011; Asins *et al.*, 2013). HKT proteins belong to the Ktr/TrK/HKT family of monovalent cation transporters present in plants, bacteria and fungi, but not in animals (Corratgé-Faillie *et al.*, 2010). Proteins from the HKT1 subgroup selectively transport Na^+ over other cations (Mäser *et al.*, 2002; Horie *et al.*, 2009; Waters *et al.*, 2013), and confer Na^+ exclusion from shoots through retrieval of Na^+ from root xylem vessels into surrounding xylem parenchyma cells (Sunarpi *et al.*, 2005; Davenport *et al.*, 2007; Möller *et al.*, 2009; Byrt *et al.*, 2014). Emerging evidence indicates that molecular mechanisms of HKT1-mediated salinity tolerance between plants may depend upon not only expression differences, but also, in some cases, subtle differences in functional properties that may be attributed to single amino acid substitutions and possible allelic variations (Ren *et al.*, 2005; Rus *et al.*, 2006; Baxter *et al.*, 2010; Cotsaftis *et al.*, 2012; Ali *et al.*, 2016; Tounsi *et al.*, 2016). The benefits of identifying natural variants of HKT has been demonstrated with HKT1.5 from salt-tolerant wheat *Triticum monococcum* which, when introgressed into salt-sensitive *T. durum*, increased grain yield on saline soil by 25% in the field (Munns *et al.*, 2012).

Here, we examine the genetic basis of Na^+ exclusion in grapevine. We take advantage of a family of heterozygous hybrid vines derived from a cross between two interspecific rootstock hybrids K51-40 (*V. champinii* × *V. riparia*) and 140 Ruggeri (*V. berlandieri* syn. *V. cinerea* var. *Helleri* × *V. rupestris*) that was previously shown to exhibit variation in leaf Na^+ by 30-fold (Gong *et al.*, 2014). We identified a QTL, named *NaE* for Na^+ exclusion, containing six closely located *HKT1* genes, of which one was expressed in roots and encoded a functional Na^+ transporter. Differences in *HKT1;1* alleles from the parent rootstocks were identified and used to investigate the importance of key amino acid residues contributing to differences in Na^+ transport

properties and variation in shoot Na^+ exclusion in the hybrid progeny. The identified single nucleotide polymorphisms are being utilized by breeding programmes for generating Na^+ -excluding rootstock germplasm via marker-assisted selection.

Materials and Methods

Grapevine material and Na^+ screens

A family of 40 hybrid rootstocks from a cross between K51-40 (*Vitis champinii* × *V. riparia*) and 140 Ruggeri (*V. berlandieri* × *V. rupestris*) (Gong *et al.*, 2011), together with both parents, were screened for leaf sodium (Na^+) exclusion ability in The Plant Accelerator Phenomics Facility, Adelaide, Australia in December 2013. Dormant cuttings were callused for 2 wk at 28°C (Yalumba Nursery, Nuriootpa, SA, Australia) and transferred to a 50:50 sand:perlite mix under regular misting for 4 wk to initiate root development. Rooted cuttings were transplanted into 1.8 kg of potting mix (6 mm Premium Mix Van Schaik's; Biogro, Mt Gambier, SA, Australia) in 2.5-l pots, established for 4 wk, then loaded onto The Plant Accelerator's conveyor belt. Before loading, vines were trimmed to a single shoot and axillary growth was continually removed. Each genotype consisted of three replicate vines, in three randomized blocks. Salt applications, consisting of 10:6:1:1 ratio of Cl^- : Na^+ : Mg^{2+} : Ca^{2+} , were applied to pots in containers (to avoid run through) on days 1, 3 and 7, equating to soil Na^+ concentrations ramping from 21 to 42 to a final concentration of 60 mM. On all other days, the pots were automatically weighed and watered to a target weight to replace water lost through evapotranspiration, ensuring all pots maintained equivalent salt concentrations at full water capacity. On Day 13, laminae of fully matured leaves of each vine were harvested and dried at 65°C for 2 d. For determining Na^+ content, powdered sample (100 mg) was digested in 2 ml concentrated HNO_3 at 95°C, diluted to 12 ml with deionized water, and analysed by CSIRO Analytical Services Unit (Adelaide) using inductively coupled plasma optical emission spectrophotometry (ThermoFisher, Cambridge, UK).

In a subsequent experiment in 2014, five selected hybrid progeny, the parents, accessions of the grandparent species, *V. champinii* 'Dogridge', *V. riparia* 'Gloire', *V. berlandieri* 'R1xMazade' and *V. rupestris* 'du Lot', and 10 common *V. vinifera* cultivars, were screened to compare Na^+ exclusion abilities. Establishment of cutting material and experimental conditions were similar to the first hybrid Na^+ screen, except final salt application occurred on Day 8, and leaves were harvested on Day 19.

Linkage mapping and QTL analysis

Genome-wide single nucleotide polymorphism (SNP) data were generated by Diversity Arrays Technology Pty Ltd (Canberra, Australia) using DArTSeq™ genotype by sequencing (GBS). This uses *PstI/TaqI* restriction digestion of genomic DNA followed by *PstI*-specific adapter targeted short-read sequencing using HiSeq2500 (Illumina, San Diego, CA, USA). The DArTSeq

methods were performed as described in Courtois *et al.* (2013), except that the sequence reads were aligned to the grapevine reference genome (Jaillon *et al.*, 2007). SNP markers aligned to the genome and those with call rates of 1 were used to construct a consensus linkage map, in JOINMAP[®] v.4.1 software using maximum-likelihood mapping (Van Ooijen, 2006). A consensus framework of linkage groups was obtained using a logarithm of odds (LOD) likelihood score between 3.0 and 5.0, and the Haldane mapping function to calculate the genetic distance between markers. Chromosome assignment of linkage groups was determined from the alignment of DArTSeq SNP reads to the grapevine reference genome (Jaillon *et al.*, 2007). Quantitative trait loci (QTLs) for Na⁺ exclusion were investigated using interval mapping analysis performed in MAPQTL[®] v.6 (Van Ooijen & Kyazma, 2009). The permutation test was used to estimate the genome wide empirical threshold for QTL detection based on LOD values of $P < 0.01$. Interval mapping resulted in a single significant QTL. To identify potential small modifying QTLs, multiple QTL mapping (MQM) analysis was undertaken with the strongest marker from this QTL used as a cofactor. No other significant QTLs were detected.

Sequencing and cloning

VviHKT1;1 and *VviHKT1;3* coding sequences (HKT, high-affinity potassium transporters) were PCR-amplified from *V. vinifera* (cv Cabernet Sauvignon) root cDNA using Phusion Polymerase (ThermoFisher Scientific) and primers designed to these gene sequences (Table S1). Purified fragments were ligated to pCR8/GW/TOPO. To identify polymorphisms in each genotype, the *VisHKT1;1* gene was PCR-amplified from K51-40 and 140 Ruggeri genomic DNA, and sequenced (accession numbers in Table S2). Using polymorphisms as a reference, coding sequences of *VisHKT1;1* allelic variants were PCR-amplified from root cDNA of parent rootstocks using PfuUltra II Fusion HS DNA Polymerase (Agilent, Santa Clara, CA, USA), and ligated to pENTR/D-TOPO. *VisHKT1;1-E^K* and *VisHKT1;1-e^R* were isolated from K51-40, and *VisHKT1;1-E^R* and *VisHKT1;1-e^R* from 140 Ruggeri. Cleavage-amplified polymorphic sequence (CAPS) markers designed to score the inheritance of each allele are given in Table S3.

VviHKT1;1 sequences from *V. champinii*, *V. riparia*, *V. berlandieri*, *V. rupestris*, and *V. vinifera* cultivars Grenache, Merlot, Pinot noir, Shiraz, Chardonnay, Pinot gris, Riesling, Sauvignon blanc and Semillon, were obtained by sequencing PCR products amplified from genomic DNA.

Subcellular localization

Vitis vinifera (cv Cabernet Sauvignon) *VviHKT1;1* without a stop codon was recombined with pMDC83 (Curtis & Grossniklaus, 2003) using LR Clonase II (Life Technologies, Carlsbad, CA, USA) to generate *2x35S::VviHKT1;1-GFP*. Plasmid ER-rk containing HDEL-mCherry (Nelson *et al.*, 2007) was used for co-localization. Plasmid pUBN-GFP-DEST (Grefen *et al.*, 2010) was used to express cytosolic green fluorescent protein (GFP).

Plasmid pEAQ-HT-DEST harbouring p19 gene-silencing suppressor was used to maximize expression (Sainsbury *et al.*, 2009). Vectors were incorporated into *Agrobacterium tumefaciens* (Agl-1) via freeze-thawing. Overnight cultures of *A. tumefaciens* harbouring pMDC83-*VviHKT1;1*, ER-rk, pUBN-GFP-DEST or pEAQ-HT-DEST were resuspended in 10 mM MgCl₂, 150 μM acetosyringone and 10 mM MES pH 5.6. Cultures were combined as follows with final OD₆₀₀ shown in brackets: pMDC83-*VviHKT1;1* (0.5) and pEAQ-HT-DEST (0.2); pMDC83-*VviHKT1;1* (0.5), ER-rk (0.2) and pEAQ-HT-DEST (0.2); pUBN-GFP-DEST (0.5) and pEAQ-HT-DEST (0.2). Bacterial suspensions were infiltrated into the abaxial side of fully expanded leaves of 5-wk-old *Nicotiana benthamiana* with a 1-ml syringe. Leaf sections were imaged after 2 d using a Nikon A1R confocal laser scanning microscope with ×63 water objective lens and NIS-ELEMENTS C software (Nikon Corp., Tokyo, Japan). FM4-64 (Sigma, St Louis, MO, USA) was used to infiltrate tobacco leaves and imaged after 10 min at room temperature. Under these conditions, the plasma membrane (not endomembrane) is predominantly stained. Excitation/emission conditions were GFP (488 nm/500–550 nm), FM4-64 and mCherry (561 nm/570–620 nm).

Site-directed mutagenesis

Site-directed mutants of *VisHKT1;1* allelic variants were generated in yeast and *Xenopus laevis* expression vectors. Mutagenesis was performed by inverse PCR of expression vectors using primers (see Table S1) with 15-bp overlaps at their 5' ends, and mutations incorporated within. Reactions contained 0.2 ng plasmid, 500 nM forward and reverse primers and 0.25 units Phusion Polymerase (ThermoFisher Scientific) in 25 μl. Reactions were treated with Cloning Enhancer (Clontech Laboratories Inc., Mountain View, CA, USA), and re-circularized using In-Fusion HD (Clontech).

Oocyte expression assays

cDNAs encoding *VisHKT1;1* variants were recombined into the *X. laevis* expression vector pGEMHE-DEST, using LR Clonase II (Life Technologies). Plasmids were linearized with *NheI* or *SbfI* (New England Biolabs, Ipswich, MA, USA). Capped RNA (cRNA) was synthesized *in vitro* with mMessage mMachine T7 kit (Ambion, Carlsbad, CA, USA) using linear plasmids as templates. cRNA was purified by phenol/chloroform extraction followed by ethanol precipitation and elution in water. Stage V and VI oocytes were injected with 42 nl cRNA (21 ng), or sterile water. Injected oocytes were incubated in calcium Ringers solution (96 mM NaCl, 2 mM KCl, 5 mM MgCl, 0.6 mM CaCl₂, 5 mM Hepes, 5% (v/v) horse serum, 500 μg ml⁻¹ tetracycline and 1× penicillin-streptomycin (Sigma P4333)). Electrophysiology was performed 1 d after injection.

Electrophysiology

Whole-cell currents were recorded using two-electrode voltage clamping (TEVC) on a Roboocyte with integrated ClampAmp

amplifier (Multichannel Systems, Reutlingen, BW, Germany). Electrodes were filled with 3 M KCl. Oocytes were perfused with solutions containing 1.8 mM CaCl₂, 6 mM MgCl₂, 10 mM MES, variable Na⁺-gluconate, pH 5.5 (adjusted with Tris) and osmolality of 230 mOsm kg⁻¹ (adjusted with D-mannitol). From a holding potential of -40 mV, oocytes were clamped stepwise from +60 mV to -140 mV in 20 mV decrements for 550 ms. Currents mediated by grapevine or wheat HKT1;1 were determined by subtracting mean currents of water-injected controls from the same batch of oocytes in the same solutions.

Yeast assays

VisHKT1;1 variants and VviHKT1;3 (Cabernet Sauvignon) were recombined into pYES-DEST52 using LR Clonase II (Life Technologies). *Saccharomyces cerevisiae* strain INVSc2 (MATa, *his3A-1*, *ura3-52*) was transformed with plasmids using the lithium acetate procedure. Transformants were selected on yeast nitrogen base (YNB) (Difco) without uracil, with 2% (w/v) D-glucose. For Na⁺ toxicity assays, yeast was grown overnight in YNB without phosphates or NaCl (MP Biomedicals, Santa Ana, CA, USA), supplemented with 1 g l⁻¹ KH₂PO₄, 95 mg l⁻¹ L-histidine-HCl, and 2% (w/v) D-glucose. Yeast was diluted to an OD₆₀₀ of 1.0 in sterile water. Ten-fold serial dilutions were prepared in sterile water, and 5 µl spotted onto plates containing YNB without phosphates and without NaCl (MP Biomedicals), supplemented with 1 g l⁻¹ KH₂PO₄, 95 mg l⁻¹ L-histidine-HCl, 1.5% (w/v) D-raffinose, 0.001–0.005% (w/v) D-galactose for induction and 0.25% phytagel (Sigma). The basal Na⁺ concentration was c. 500 µM from phytagel. For Na⁺ toxicity screening, growth was monitored on media containing 50 mM NaCl. Control plates to demonstrate equal dilutions contained 2% (w/v) D-glucose. Plates were incubated at 28°C for 3 d.

Quantitative real time PCR (qPCR)

RNA from root stele and root epidermis/cortex enriched tissue was prepared from grapevine rooted leaves as described previously (Henderson *et al.*, 2014). cDNA was synthesized from 0.5 µg total RNA using Superscript III (Life Technologies) following the manufacturers' procedures. qPCR was performed on a QuantStudio 12K Flex Real-Time PCR machine (Thermo Fisher Scientific). Ten microlitre qPCR reactions contained 250 nM forward and reverse primer, 1× KAPA SYBR FAST qPCR Master Mix (KAPA Biosystems, Charlestown, MA, USA) and 1 µl cDNA (diluted 1 : 4). Triplicate reactions were performed using 40 cycles of the following: 95°C 1 s, 55°C 15 s, 72°C 5 s. Melt curve analysis was performed to ensure a single band was amplified. Relative expression levels were calculated using primer pair efficiencies (*E*) and normalized to *VvElongation-factor-1-α* using the formula ($E_{HKT1;1}^{\Delta ct} / E_{EF1-\alpha}^{\Delta ct}$).

VisHKT1;1 allele-specific qPCR reactions were performed using forward and reverse primers (Table S1) containing allele-specific SNPs in their 3' terminal base. Specificity was achieved by performing reactions as described above, except annealing at 63°C. Allele copy numbers were estimated by interpolation from

standard curves made from serial dilutions of linearized pGEM-HE plasmids quantified by UV-spectrophotometry. Data were normalized to cDNA volume. The sum of two allele copy numbers was compared to total copies of *VisHKT1;1* transcript using nonspecific primers in the same samples.

Statistical analysis

Data were analysed using GraphPad PRISM v.7.00 for Windows (GraphPad, La Jolla, CA, USA). All data are presented as mean ± SE. Means were compared using the different statistical tests described in the figure legends.

Results

Mapping a major QTL for Na⁺ exclusion in a hybrid grapevine population

We aimed to detect QTL for leaf Na⁺ exclusion in a population of hybrid rootstocks derived from a cross between K51-40 and 140 Ruggeri (Gong *et al.*, 2014). Forty hybrids were exposed to a mixed cation treatment for 13 d, and the lower leaves (lamina only) were harvested for analysis of Na⁺ accumulation. A >40-fold difference in Na⁺ accumulation was seen within the hybrid progeny with the lowest, 0.005% DW, and the highest, 0.213% DW, whereas two parents K51-40 and 140 Ruggeri had similar leaf Na⁺ concentrations of 0.016 and 0.015% DW, respectively (Fig. 1a). The transgressive variation seen in this near-Mendelian trait indicated that it was probably heterozygous in each parent. A broad sense heritability score of 0.91 was estimated for Na⁺ exclusion in this population, suggesting a high degree of genetic control.

GBS was performed on the 40 hybrids and parents. The resulting SNP data were used to construct a consensus linkage map consisting of 514 SNP markers distributed over 19 linkage groups, at a mean interval of 5.3 cM (Fig. S2). A single major QTL explaining up to 72% of the genetic variation in Na⁺ exclusion was identified on chromosome 11, spanning a 42-cM region of c. 14 Mb (Fig. 1b). We named this locus *NaE*, for Na⁺ exclusion. SNP markers underlying the peak of the *NaE* QTL were used to group the 40 hybrids based on their inheritance of this locus, and confirmed that the associated alleles were likely to be heterozygous in both parents (Fig. 1a). This analysis revealed that the Na⁺ exclusion trait is dominant over Na⁺ accumulation, because hybrids with low Na⁺ accumulation generally were associated with the inheritance of one or more dominant loci, designated as *NaE^K* and *NaE^R* for excluder locus derived from K51-40 and 140 Ruggeri. By contrast, high Na⁺ accumulation generally was associated with the inheritance of two recessive loci, designated *Nae^K* and *Nae^R* (Fig. 1a).

Based on the grapevine reference genome (Jaillon *et al.*, 2007), the *NaE* locus contains 583 genes (Table S4). Six *HKT1* genes were clustered within a 320-Kb region located close to the peak LOD score of the *NaE* locus (Fig. 1b,c) and knowledge of Na⁺ exclusion from other plant species suggested that members of the *HKT1* family were strong candidate genes. Phylogenetic analysis

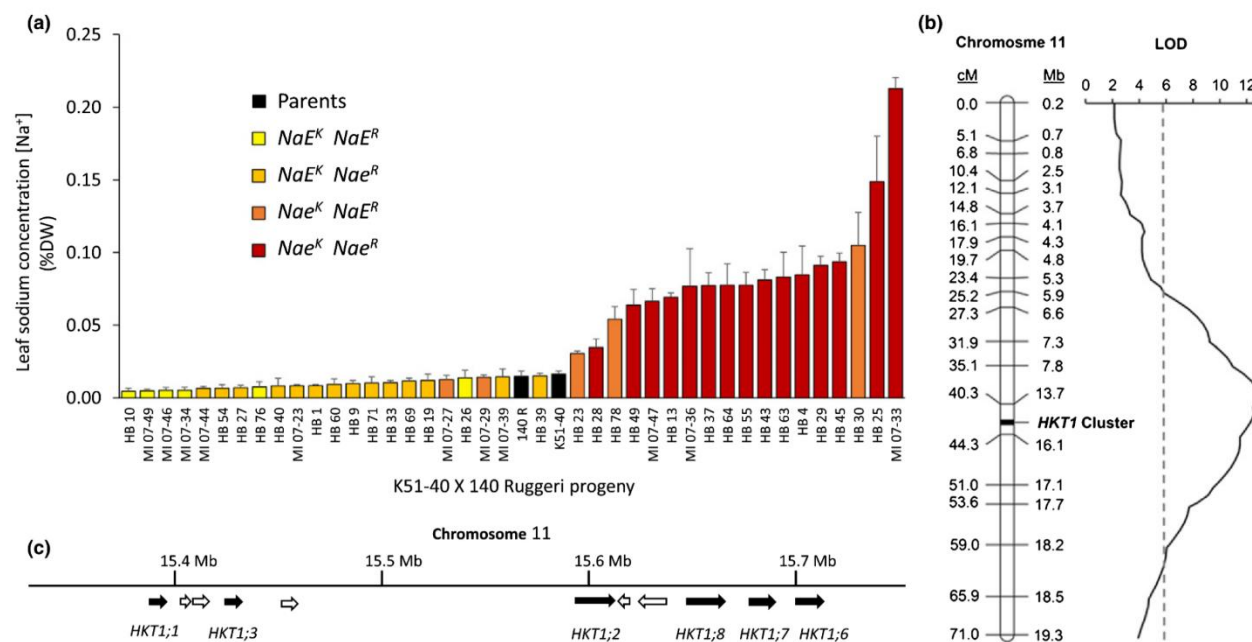


Fig. 1 Sodium (Na^+) exclusion is associated with a major quantitative trait locus (QTL), *NaE*, on chromosome 11 which contains a cluster of six *HKT1* genes. (a) Leaf Na^+ concentration in a population of *Vitis* interspecific rootstock hybrids. The parents K51-40 and 140 Ruggeri are indicated in black. Hybrid progeny are coloured according to their inheritance of single nucleotide polymorphism (SNP) markers at 13.7 Mb within the Na^+ exclusion (*NaE*) locus. Hybrids homozygous for the dominant *NaE* locus are indicated in yellow and progeny homozygous for recessive *nae* locus are indicated in red. Progeny heterozygous for a dominant *NaE^K* locus from K51-40 and a recessive *nae^R* locus from 140 Ruggeri are indicated in mustard, whereas progeny heterozygous for a recessive *nae^K* locus from K51-40 and dominant *NaE^R* locus from 140 Ruggeri are indicated in orange. Bars are mean + SE of three biological replicates. (b) Schematic of chromosome 11 Na^+ exclusion QTL mapping interval, shows logarithm of odds (LOD) score against map units (in cM) (left) and the physical position of SNPs (in Mb) corresponding to the grapevine reference sequence (right). Vertical dashed line represents the genome-wide significance threshold P -value of 0.01. (c) Relative positions of *HKT1* genes (black arrows) on part of chromosome 11 based on the grapevine reference genome. *VviHKT1;1* (VIT_211s0103g00010), *VviHKT1;3* (VIT_211s0103g00050), *VviHKT1;2* (VIT_211s0103g00090), *VviHKT1;8* (VIT_211s0103g00130), *VviHKT1;7* (VIT_211s0103g00140), *VviHKT1;6* (VIT_211s0103g00150). White arrows signify unrelated genes. Not to scale.

of these grapevine *HKT1*s against *HKT*s from other plant species has been reported previously (Ali *et al.*, 2012). This showed that, of the well-characterized *HKT*s, all grapevine *HKT1*s are most similar to rice *OsHKT1;1*. The grapevine *HKT1*s fall into two subclades, whereby *VviHKT1;1*, *VviHKT1;2* and *VviHKT1;3* share a degree of homology (53–63% identity), and *VviHKT1;6*, *VviHKT1;7* and *VviHKT1;8* share higher sequence similarity (85–97% identity) (Fig. S3).

HKT1;1 is expressed in the root stele and encodes a Na^+ selective plasma membrane transporter

In wheat and Arabidopsis, *HKT* proteins in roots regulate Na^+ accumulation in shoots by controlling Na^+ retrieval from root xylem vessels (Davenport *et al.*, 2007; Munns *et al.*, 2012; Byrt *et al.*, 2014). We therefore mined genome-wide expression data to determine which grapevine *HKT1* transcripts were expressed in roots. Only two *HKT1* transcripts, *VviHKT1;1* and *VviHKT1;3* were highly abundant in whole roots of *V. vinifera*, and both transcripts were present at similar levels (Fig. 2a). To identify whether *VviHKT1;1* and *VviHKT1;3* encoded Na^+ transport proteins, full-length cDNAs corresponding to each

protein were isolated and expressed in *X. laevis* oocytes. When oocytes were clamped at negative membrane potentials, *VviHKT1;1* mediated large inward currents (2 μA at -140 mV) in the presence of 30 mM Na^+ (Fig. 2b), whereas *VviHKT1;3* did not increase currents above the level of the water control (Fig. 2b). Furthermore, functional characterization in yeast indicated that *VviHKT1.3* did not function as a Na^+ transporter because its expression did not lead to inhibition of yeast growth on plates containing 50 mM Na^+ unlike *AtHKT1* (Fig. S4). These findings implicate *HKT1;1* as a gene important for Na^+ exclusion in grapevine, whereas the function of *HKT1;3* remains unknown.

Quantitative PCR of root epidermal/cortical and stelar fractions of K51-40 and 140 Ruggeri showed that *HKT1;1* transcripts were more abundant in the root stele of both genotypes (Fig. 2c). Expression of *VviHKT1;1* with a C-terminal GFP tag in tobacco epidermis showed a strong signal that co-localized with the lipophilic dye FM4-64 at the plasma membrane, but did not co-localize with free cytoplasmic GFP, or the endoplasmic reticulum (ER) marker HDEL-mCherry (Fig. 2d,e). These findings confirm that *VviHKT1;1* protein is likely to be localized on the plasma membrane of grapevine root stelar cells.

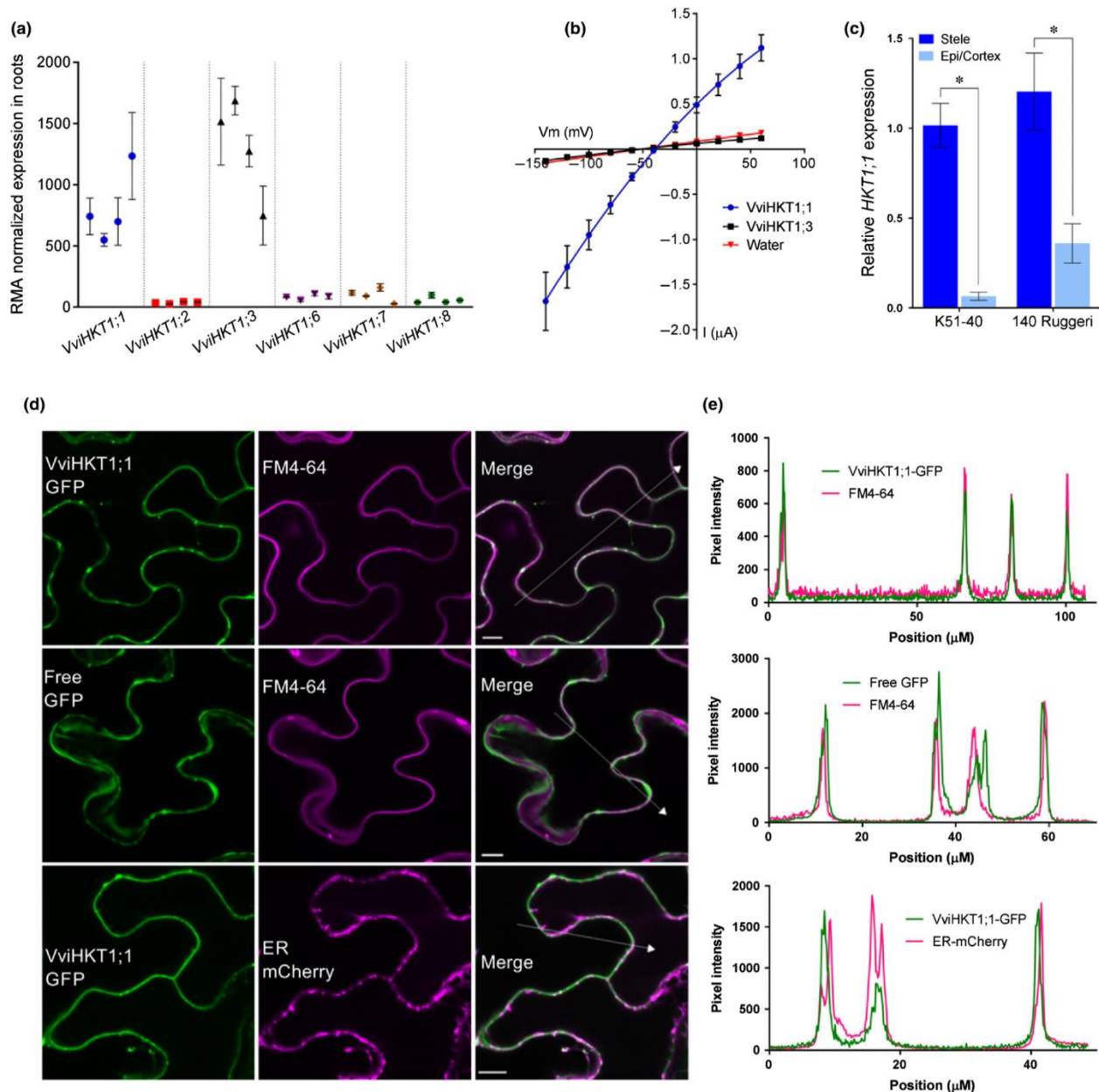


Fig. 2 HKT1;1 is a functional sodium (Na^+) transporter on the plasma membrane of grapevine root stele cells. (a) Expression level of high-affinity potassium (K^+) transporter (*HKT*) transcripts in *Vitis vinifera* roots determined by microarray hybridization. Each point represents a unique probe from the microarray. Data are mean \pm SE of three biological replicates. Data are from Fasoli *et al.* (2012). (b) Current–voltage relationship of *Xenopus laevis* oocytes injected with water (red diamonds) *VviHKT1;3* (black squares) or *VviHKT1;1* (blue circles). Oocytes were clamped from +60 to –140 mV in a solution containing 10 mM Na^+ -gluconate, pH 5.5. Data are mean \pm SE ($n = 3$ oocytes). (c) Relative *HKT1;1* transcript abundance in root tissue enriched in stele (dark blue bars) or epidermal/cortical cells (light blue bars) from grapevine rootstocks K51-40 and 140 Ruggeri. Data are means \pm SE of three biological replicates of pooled tissue from multiple plants. Data are relative to the K51-40 stele replicate with the greatest transcript abundance. Asterisk denotes significant difference between tissue types ($P < 0.05$; Student's *t*-test). (d) Tobacco (*Nicotiana benthamina*) leaf epidermal cells expressing *VviHKT1;1*-GFP (upper panels), free GFP (middle panels), or *VviHKT1;1*-GFP plus the endoplasmic reticulum (ER) marker HDEL-mCherry (lower panels). Leaves in the upper and middle panels were imaged 10 min after infiltration with FM4-64, which predominantly stained the plasma membrane. Leaves were imaged by confocal microscopy 2 d after agroinfiltration. Bars, 10 μm . (e) Signal profiles of GFP (green) and FM4-64 or mCherry (magenta) corresponding to the arrow in the adjacent merged image from (d). Overlapping peaks indicate colocalization between the two signals.

Four unique *HKT1;1* alleles from K51-40 and 140 Ruggeri display different functional properties

HKT1;1 coding sequences were isolated from the two parents of the mapping population, K51-40 and 140 Ruggeri, and given the prefix *Vis* for *Vitis interspecific*. Four unique *VisHKT1.1* alleles were identified, two from each parent (Figs 3a, S5). CAPS markers designed to the *VisHKT1;1* alleles were used to score hybrids for their allelic inheritance. Resulting marker scores were identical to that of SNPs mapped nearby (Fig. 1a); hence, we named the *VisHKT1.1* alleles as per the associated *NaE* locus (*VisHKT1;1-E^K* and *VisHKT1;1-e^K* from K51-40; *VisHKT1;1-E^R* and *VisHKT1;1-e^R* from 140 Ruggeri). Eighteen amino acid differences were observed between encoded proteins of the four alleles (Figs 3a, S5). Six polymorphic residues, at positions 106, 129, 163, 391, 534 and 537, were conserved between the two *VisHKT1;1-E* allelic variants and also between the two *VisHKT1;1-e* variants (Fig. 3a).

In order to assess whether allele-specific expression contributes to the variation in Na⁺ exclusion in the hybrid population, absolute transcript abundance of these four alleles in root fractions was quantified in the parents using allele-specific primers. Expression of *HKT1;1* alleles in root epidermal/cortical and stelar fractions, assayed by qPCR, showed *VisHKT1;1-E* alleles to be approximately two-fold more abundant than *VisHKT1;1-e* alleles (Fig. 3b). There were no differences in expression of *VisHKT1;1-E^K* and *VisHKT1;1-E^R* or between *VisHKT1;1-e^K* and *VisHKT1;1-e^R* alleles (Fig. 3a). The sum of *VisHKT1;1-E* and *VisHKT1;1-e* transcript copy number was equivalent to the total *VisHKT1;1* copy number using non-allele-specific *HKT1;1* primers in each sample, demonstrating that the PCR primers were highly allele-specific (Fig. 3b).

For functional analysis, the *VisHKT1;1* alleles were first expressed in yeast. On control plates containing glucose, which represses gene expression, all strains grew at the same rate demonstrating equal dilution (Fig. 3c). When *VisHKT1;1* allelic variants were expressed by substituting glucose with raffinose and galactose (which induces gene expression), all strains grew at a similar rate on low (0.5 mM) Na⁺ (Fig. 3c). Conversely, growth of yeast expressing *VisHKT1;1* allelic variants on induction medium was strongly inhibited by 50 mM Na⁺, whereas growth of yeast containing an empty vector was not inhibited (Fig. 3c). This suggests that each grapevine *VisHKT1;1* allelic variant transports Na⁺ in yeast. Na⁺-induced growth-inhibition was greater in yeast strains expressing *VisHKT1;1-E* variants compared to *VisHKT1;1-e* variants from both parents (Fig. 3c), implying that *VisHKT1;1-E* proteins have higher Na⁺ transport activity than *VisHKT1;1-e* proteins.

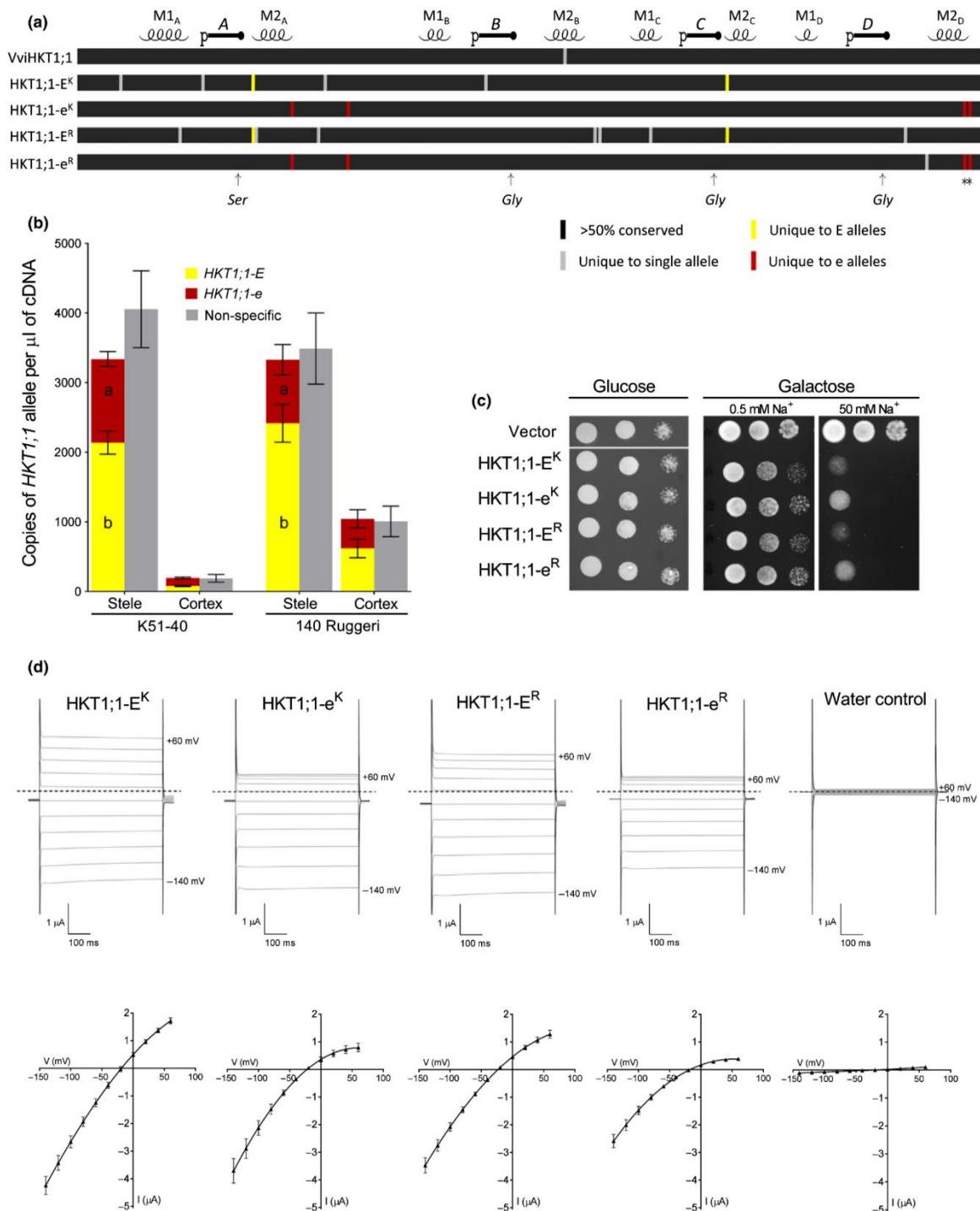
In order to confirm these differences, we performed TEVC of *X. laevis* oocytes injected with different *VisHKT1;1* allelic variants. When perfused with 30 mM external Na⁺ ([Na⁺]_{ext}), *VisHKT1;1-E* variants mediated Na⁺ transport in both directions across the oocyte membrane (Fig. 3d). Conversely, both *VisHKT1;1-e* variants displayed inward rectification – characterized by inward currents at negative voltages but restricted outward currents at positive voltages (Fig. 3d). We quantified

inward rectification as the ratio between inward (−140 mV) and outward (+60 mV) chord conductance (G_{Na^+}), where a ratio of 1 indicates equal G_{Na^+} in both directions. From both rootstocks, *VisHKT1;1-E* variants had lower (*c.* 50%) inward rectification ratios than *VisHKT1;1-e*, irrespective of [Na⁺]_{ext} (Fig. S6). Inward rectification is an intrinsic property of grapevine *VisHKT1;1-e* variants, and not due to differences in [Na⁺]_{int}, because increasing [Na⁺]_{ext} did not significantly alter the reversal potential (E_{rev}) between allelic variants, and E_{rev} followed a positive Nernstian shift (Fig. S7). In addition to differences in inward rectification, we also observed differences in the inward current at physiologically relevant negative membrane potentials in plants (−140 to −80 mV) between the *VisHKT1;1* variants (Fig. 3d). To examine this in detail, we thoroughly investigated the difference between *VisHKT1;1-E^K* and *VisHKT1;1-e^K*, finding that the *VisHKT1;1-E^K* variant displayed *c.* 25% larger currents at −140 mV in 30 mM Na⁺ solutions, and that this difference was consistent across different batches of oocytes (Fig. S8).

We examined monovalent cation selectivity of different *VisHKT1;1* allelic variants in oocytes. All variants were highly selective for Na⁺, mediating large inward currents in 10 mM NaCl, each with an E_{rev} close to the predicted Nernst potential for this cation (Fig. S9). When Na⁺ was substituted for lithium (Li⁺), potassium (K⁺), rubidium (Rb⁺) or caesium (Cs⁺), all *VisHKT1;1* allelic variants were unable to mediate inward currents (Fig. S9). This demonstrates that all *VisHKT1;1* allelic variants characterized here were selective only for Na⁺.

Two polymorphisms (Ser-534-Arg and Gly-537-Asp) are responsible for differences in Na⁺ conductance and rectification

Of six polymorphic residues conserved between *VisHKT1;1-E* and *VisHKT1;1-e* allelic variants, two residues occur in the predicted M2_D transmembrane region near the carboxy (C)-terminus, where charged residues are important for correct functioning of plant and bacterial Trk/Ktr/HKT proteins (Kato *et al.*, 2007). In *VisHKT1;1-E* variants, these residues are uncharged, Ser-534 and Gly-537, but differ in *VisHKT1;1-e* variants with oppositely charged Arg-534 (positive) and Asp-537 (negative) (Figs 3a, S5). To investigate whether these SNPs affected protein function, we performed mutagenesis of *VisHKT1;1-e^K* to generate two single mutant proteins, *VisHKT1;1-e^K_{D537G}*, *VisHKT1;1-e^K_{R534S}*, and a double mutant protein *VisHKT1;1-e^K_{R534S/D537G}*. Expression of mutant alleles in oocytes revealed that the D537G mutation alone had no effect on G_{Na^+} or rectification, as this protein behaved like the original *VisHKT1;1-e^K* (Figs 4a, S10). Conversely, a single R534S mutation resulted in larger outward currents, reducing the inward rectification observed in *VisHKT1;1-e^K*, and also resulted in significantly higher inward slope G_{Na^+} in oocytes compared to wild-type (WT) (Figs 4a, S10). When R534S mutation was combined with D537G mutation in *e^K_{R534S/D537G}*, to mimic residues present at the C-terminus of *VisHKT1;1-E* variants, rectification was abolished and the inward slope G_{Na^+} was further increased compared to the *e^K_{R534S}* single mutant (Fig. 4a), although this



increase was not statistically significant compared to the R534S single mutant (Fig. S10). These mutations had no effect on cation selectivity of the e^K protein (Fig. S11). Comparing the chord conductance ratio of each protein confirmed that Arg-534

is the rectification residue in VisHKT1;1, as e^K -WT and e^K_{D537G} variants had significantly higher ratios compared to e^K_{R534S} mutant and $e^K_{R534S/D537G}$ (Fig. 4b). When expressed in yeast, both single mutant proteins inhibited growth on 50 mM Na^+ to

Fig. 3 Grapevine rootstock *VisHKT1;1* allelic variants have different expression, and sodium (Na^+) transport properties. (a) Amino acid alignment of *Vitis vinifera* *HKT1;1* from Cabernet Sauvignon with protein sequences predicted from unique alleles of *VisHKT1;1* present in K51-40 (E^K and e^K) and 140 Ruggeri (E^R and e^R). Residues conserved in three or more sequences are shown in black with unique residues encoded by a single allele shown in grey. Encoded residues conserved between E alleles are highlighted in yellow and those conserved between e alleles are highlighted in red. Predicted transmembrane regions ($M1_{A-D}$ and $M2_{A-D}$), and P-loop domains (P_{A-D}) are shown above. Arrows indicate the position of residues in the selectivity filter. Asterisks indicate residues selected for mutagenesis. (b) Copy number of mRNAs encoding different *VisHKT1;1* alleles in root tissue enriched stelar or epidermal/cortical cells from grapevine rootstocks K51-40 (left) and 140 Ruggeri (right). Data are mean \pm SE of three biological replicates of pooled tissue from multiple plants. Significant differences are denoted by different letters ($P < 0.05$, one-way ANOVA with Tukey's post-hoc test). (c) *VisHKT1;1* allelic variants differentially inhibit yeast (*Saccharomyces cerevisiae*) growth on high Na^+ . Wild-type strain INVSc2 was transformed with pYES-DEST52 empty vector as a control, or the same vector containing allelic variants of *VisHKT1;1*. Diluted yeast strains were spotted (5 μl) onto plates containing D-glucose (spotting control), or D-raffinose and D-galactose (induction) \pm 50 mM NaCl. Plates were incubated at 30°C for 3 d. (d) Typical currents observed from oocytes injected with cRNA encoding *VisHKT1;1-E^K*, *VisHKT1;1-e^K*, *VisHKT1;1-E^R*, *VisHKT1;1-e^R*, and water, in solutions containing 30 mM Na^+ -gluconate. Dashed lines represent zero current levels. Data represent total oocyte currents without background subtraction. Data are mean \pm SE ($n \geq 5$ oocytes).

the same degree as e^K -WT (Fig. 4c). Only $e^K_{R534S/D537G}$ inhibited yeast growth on 50 mM Na^+ to the same degree as E^K -WT (Fig. 4c). This suggests that variable yeast growth inhibition mediated by the *VisHKT1;1* allelic variants is due to the larger inward Na^+ conductance of allele E variants and not due to differences in inward rectification. To further confirm the role of Arg-534 in rectification and reduced conductance of *VisHKT1.1-e* variants, we mutated the equivalent residue in wheat TaHKT1.5-D from serine to arginine. This mutation greatly reduced the inward Na^+ conductance, with TaHKT1.5-D_{S506R} showing currents half the magnitude of WT TaHKT1.5-D (Fig. 4d,e). Furthermore, TaHKT1.5-D showed almost no inward rectification, whereas TaHKT1.5-D_{S506R} was strongly inward rectifying (Fig. 4f).

Dominant *HKT1;1-E^K* and *HKT1;1-E^R* alleles associated with Na^+ exclusion are derived from *V. riparia* and *V. berlandieri*, respectively

In order to gain understanding of the origin of *VisHKT1;1* alleles, we sequenced *VisHKT1;1* from four *Vitis* species that make up this complex hybrid family (Fig. 5a). The dominant E^K and E^R alleles are likely to be derived from *V. riparia* and *V. berlandieri*, respectively. Both of these accessions were homozygous for E alleles and thus provide ideal material for breeding new grapevine rootstocks with strong Na^+ exclusion ability. Conversely, the recessive e^K allele was found to originate from *V. champinii*, which is heterozygous for the e^K allele and a unique E allele. The e^R allele of 140 Ruggeri was derived from *V. rupestris*, which is also heterozygous for the e^R allele and another unique E allele (Fig. S12).

The Na^+ exclusion ability of the four *Vitis* species was compared against the two parents and a selection of hybrids to determine if this trait behaved as predicted by their *HKT1;1* genotypes (Fig. 5b). Indeed, *V. riparia* and *V. berlandieri* both display strong Na^+ exclusion, with minimal Na^+ accumulation in leaves, which agrees with their homozygous *HKT1;1-E* allelic makeup. Furthermore, *V. champinii* and *V. rupestris*, which both carry a recessive *HKT1;1-e* allele, showed a moderate degree of Na^+ accumulation, which was lower than hybrids homozygous for *HKT1;1-e* alleles (HB55, HB25 and MI07-33) but greater than other heterozygous genotypes, K51-40 and 140 Ruggeri and hybrid HB76.

Ten *V. vinifera* wine grape cultivars commonly grown in Australia were assessed for their *HKT1;1* genetics by sequencing the SNPs underlying residues 534 and 537. All *V. vinifera* cultivars were homozygous for alleles encoding the Ser and Gly residues associated with dominant *VisHKT1;1-E* alleles. As predicted by their *HKT1;1* allelic makeup, these cultivars were strong Na^+ -excluders, except for Shiraz which was a moderate Na^+ -excluder (Fig. 5b). This result suggests that *HKT1;1* is the major gene contributing to Na^+ exclusion in grapevines, and other minor loci yet to be identified may also contribute.

Discussion

The *NaE* quantitative trait locus (QTL) for sodium (Na^+) exclusion in grapevine contained six tightly linked *HKT* genes, which is the entire complement of high-affinity potassium (K^+) transporter (*HKT*) genes in the grapevine reference genome. This contrasts with cereals, where single *HKT* genes have been found within QTLs for Na^+ exclusion (Ren *et al.*, 2005; Huang *et al.*, 2006; Byrt *et al.*, 2007), and tomato, where a QTL for Na^+ exclusion contained two closely linked *HKT* genes (Asins *et al.*, 2013). All six *HKT* genes within the *NaE* locus are predicted to encode class-1 HKT proteins containing Ser-Gly-Gly-Gly selectivity filters, suggesting that they may have evolved by gene duplication, and are likely to be Na^+ selective (Mäser *et al.*, 2002; Waters *et al.*, 2013). Genetic and functional analyses presented here strongly indicate that *VisHKT1;1* is the gene responsible for variation in Na^+ exclusion associated with the *NaE* locus. *VviHKT1;1* localized to the plasma membrane and was transcribed in cells associated with the root vasculature, suggesting that the Na^+ exclusion mechanism in *Vitis* species involves retrieval of Na^+ from root xylem vessels into surrounding cells, which is consistent with the role of HKT proteins in other plants (Munns & Tester, 2008; Horie *et al.*, 2009; Byrt *et al.*, 2014). *HKT1;3* was expressed in roots, but its function could not be determined here. The functions of grapevine *HKT1;2*, *HKT1;6*, *HKT1;7* and *HKT1;8* remain to be characterized; however, microarray data suggest they are not expressed in *V. vinifera* roots and are therefore unlikely to influence direct transfer of Na^+ into the root xylem. Whether they transport Na^+ and the tissues in which they function was beyond the scope of this study.

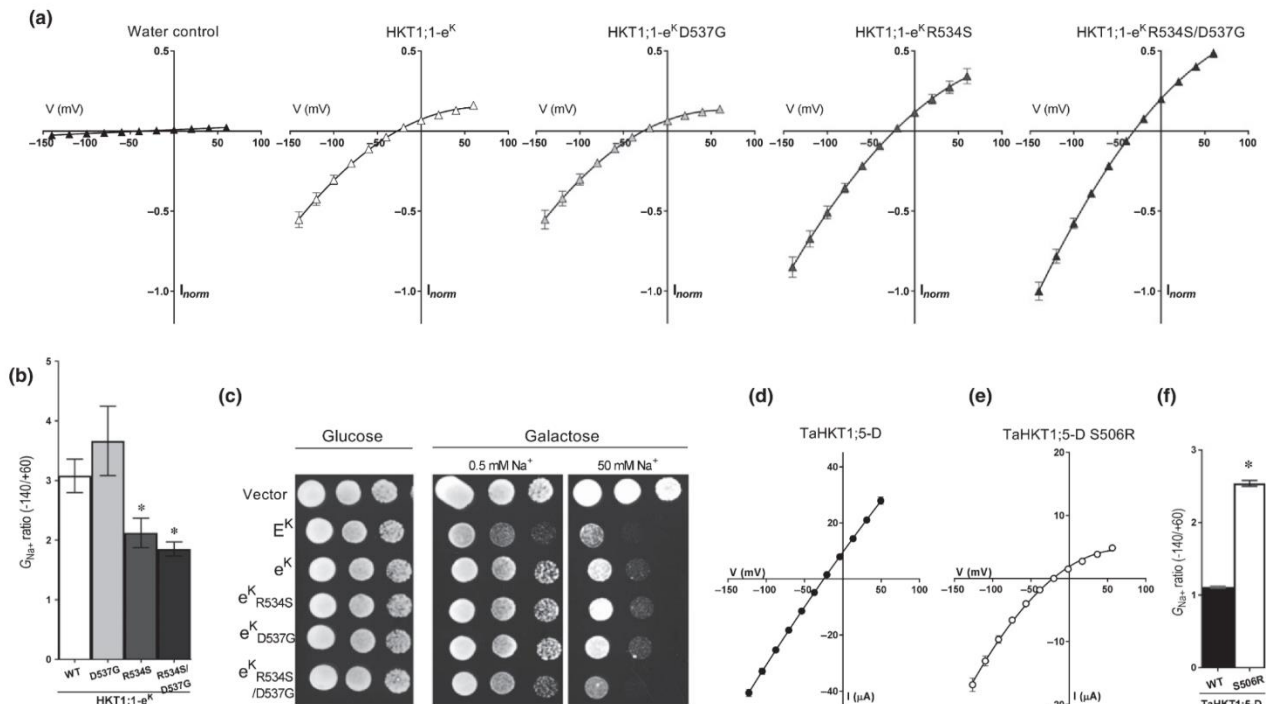


Fig. 4 Arg-534 and Asp-537 control the gating and sodium conductance of VisHKT1;1-e^K. (a) Normalized current–voltage relationships of oocytes injected with water or cRNA encoding VisHKT1;1-e^K, VisHKT1;1-e^K_{D537G}, VisHKT1;1-e^K_{R534S}, and VisHKT1;1-e^K_{R534S/D537G} in solutions with 30 mM Na⁺-gluconate. Data represent the HKT-mediated currents without background subtraction. Data are mean \pm SE ($n \geq 9$ oocytes from two batches). (b) The inward chord conductance (G_{Na^+}) ratio of *Xenopus laevis* oocytes expressing wild-type (WT) VisHKT1;1-e^K and mutated variants in solutions containing 30 mM Na⁺-gluconate. The rectification ratio was determined by dividing G_{Na^+} at -140 mV by G_{Na^+} at $+60$ mV. Chord conductances were calculated from current–voltage relationships using the equation $G_{Na^+} = I/(V_m - V_{rev})$. Data are mean \pm SE ($n \geq 5$ oocytes) and calculations were performed after subtraction of mean background currents from water-injected control oocytes. Asterisks denote significant difference from WT (*t*-test, $P < 0.05$). (c) Comparison of Na⁺-induced growth inhibition of yeast (*Saccharomyces cerevisiae*) strains expressing WT and mutant VisHKT1;1 alleles from K51–40. Yeast were spotted onto plates containing D-glucose (control), or D-raffinose and D-galactose (induction) \pm 50 mM NaCl. Plates were incubated at 30°C for 2 d (glucose) or 4 d (galactose). (d, e) Current–voltage relationships of oocytes injected with cRNA encoding (d) TaHKT1;5-D and (e) TaHKT1;5-D_{S506R} in solutions with 30 mM Na⁺-gluconate. Data represent the HKT-mediated currents after background subtraction. Data are mean \pm SE ($n \geq 9$ oocytes). (f) The inward chord conductance (G_{Na^+}) ratio of *Xenopus* oocytes expressing TaHKT1;5-D and TaHKT1;5-D_{S506R} in solutions containing 30 mM Na⁺-gluconate. Data are mean \pm SE ($n \geq 9$ oocytes). Asterisk denotes significant difference from WT (*t*-test, $P < 0.01$).

In other species, QTL mapping has identified allelic variants encoding HKT proteins that confer greater Na⁺ exclusion or greater K⁺ : Na⁺ ratios (Ren *et al.*, 2005; Asins *et al.*, 2013; Jaime-Pérez *et al.*, 2016). It has been suggested that single nucleotide polymorphisms (SNPs) within the coding region between tolerant and sensitive alleles of *OsHKT1;5* are responsible for the functional differences between HKT allelic variants (Cotsaftis *et al.*, 2011), but this has not been proven using mutagenesis and functional characterization of the encoded proteins. Thus, few specific amino acid residues have been identified within HKT proteins that are responsible for different Na⁺-exclusion abilities of tolerant and sensitive lines. Here, we identified amino acid residues 534 and 537 in VisHKT1;1 allelic variants that impart strong and weak shoot Na⁺ exclusion when uncharged (Ser-534, Gly-537) and charged (Arg-534, Asp-537), respectively.

Single point mutations in plant HKT proteins have been shown previously to have functional impacts. For example, a Ser or Gly residue in the first pore-loop domain (p-loop A)

determines Na⁺ or K⁺ permeability in HKTs from Arabidopsis, wheat, rice and Venus flytrap (*Dionaea muscipula*) (Mäser *et al.*, 2002; Böhm *et al.*, 2016). Mutation of an Asp to Asn in the second p-loop domain of *Thellungiella salsa* TsHKT1;2 and the Arabidopsis orthologue (to create TsHKT1;2_{D207N} and *AtHKT1;2_{N211D}*) altered their Na⁺/K⁺ selectivity, and expression of TsHKT1;2 or the mutant Arabidopsis protein conferred greater salt tolerance to Arabidopsis *hkt1-1* knockout plants due to increased K⁺ accumulation in shoots (Ali *et al.*, 2012). In the present study, the VisHKT1;1-e proteins had identical cation selectivity to VisHKT1;1-E variants, suggesting that the increased Na⁺ transport activity of VisHKT1;1-E variants confers the mechanism for improved Na⁺ exclusion in *NaE* progeny.

HKT proteins from rice that display strong (*OsHKT1;1*) and weak (*OsHKT1;3*) inward rectification have been observed (Jabnourne *et al.*, 2009). We identified a single amino acid residue (Arg-534) that caused greater inward rectification of VisHKT1;1-e variants compared to VisHKT1;1-E variants. We

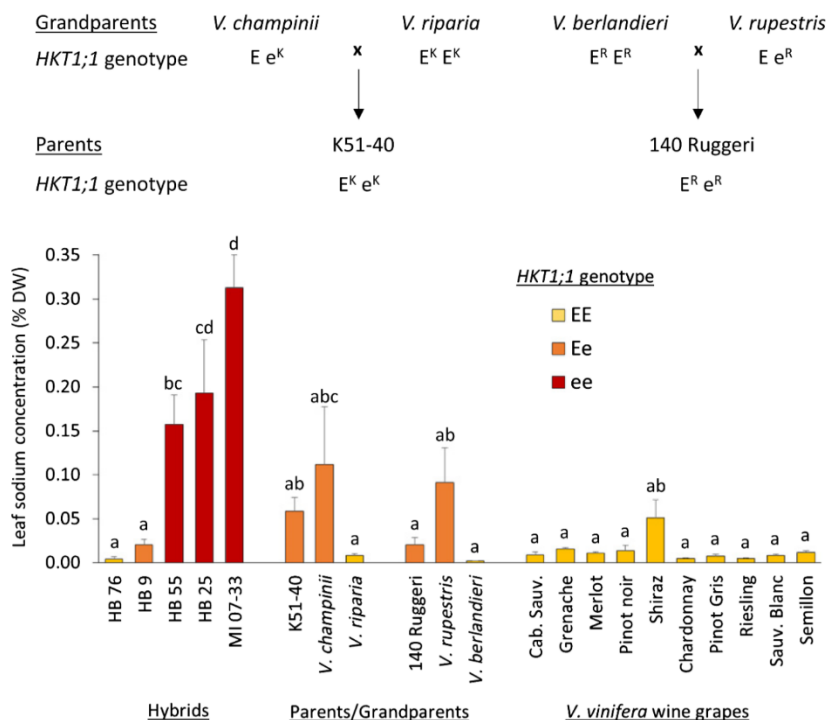


Fig. 5 Recessive alleles, *VisHKT1;1-e^K* and *VisHKT1;1-e^R*, are derived from *Vitis champinii* and *V. rupestris*, respectively. (a) Pedigree diagram of K51-40 and 140 Ruggeri illustrating the inheritance of *VisHKT1;1* alleles from four different grandparent *Vitis* species. *Vitis champinii* and *V. rupestris* are heterozygous carriers of the recessive *VisHKT1;1-e^K* and *VisHKT1;1-e^R* allele, respectively, whereas *V. riparia* and *V. berlandieri* appear to be homozygous for the dominant *VisHKT1;1-E^K* and *VisHKT1;1-E^R* alleles, respectively. (b) Sodium (Na^+) exclusion in selected progeny of K51-40 × 140 Ruggeri (from Fig. 1a), the parents and grandparents, and *V. vinifera* cultivars. Individuals are coloured according to their deduced amino acids at the key residues 534 and 537 of *VisHKT1;1* as determined by direct genomic DNA sequencing (Supporting Information Fig. S12). Yellow bars indicate genotypes homozygous for the dominant *HKT1;1-E* alleles (residues Ser-534 and Gly-537). Red bars indicate genotypes homozygous for the recessive *HKT1;1-e* alleles (residues Arg-534 and Asp-537), and orange bars indicate heterozygous genotypes that contain one dominant *HKT1;1-E* allele and one recessive *HKT1;1-e* allele. Bars are mean + SE of three biological replicates. Significant differences are denoted by different letters ($P < 0.05$, one-way ANOVA with Tukey's post-hoc test).

found that mutating the corresponding residue in wheat TaHKT1.5-D also caused inward rectification and reduced Na^+ conductance. Both rice OsHKT1;1 and 1;3 appear to rectify more strongly than *VisHKT1;1-e* and wheat TaHKT1.5-D_{S506R}, and neither contain a residue equivalent to Arg-534. TsHKT1;2 and AtHKT1_{N211D} showed inward rectification of Na^+ transport, but the reverse D207N mutation in TsHKT1;2 did not abrogate this (Ali *et al.*, 2016). These findings indicate that additional residues influence rectification in HKT proteins.

Ali *et al.* (2016) suggested that inward rectification of AtHKT1;1_{N211D} would impose a greater Na^+ retention in root cells, preventing Na^+ efflux to the xylem apoplast. However, they found no difference in shoot Na^+ accumulation between Arabidopsis plants expressing either the rectifying or nonrectifying AtHKT1 variants. By contrast, in our study, inheritance of the noninwardly rectifying *VisHKT1;1-E* alleles correlated with greater shoot Na^+ exclusion. Therefore, the greater Na^+ conductance observed through the HKT1 variants at physiologically relevant membrane potentials is likely to be the major contributing factor to shoot Na^+ exclusion. This aligns with the suggestion by Ren *et al.* (2005) that the rice *SKCI* allelic variant from salt-

tolerant variety Nona Bokra shows greater Na^+ conductance than the allele from salt-sensitive Koshihikari. It also agrees with thermodynamics of Na^+ transport in root xylem parenchyma cells, which is predicted to be inward (to the cytoplasm) through channel-like proteins such as HKT, and outward (towards to xylem apoplast) through secondary active Na^+/H^+ exchangers (Munns & Tester, 2008). The functional role of inward rectification of plant HKT proteins therefore remains unclear. However, it must be noted that a greater degree of rectification was correlated with a lower magnitude of Na^+ current at negative potentials in all the HKT variants and mutants studied here, so the two properties are likely to be linked.

In our study, the R534S mutation in *VisHKT1;1-e^K* reduced inward rectification and increased inward Na^+ conductance. Within physiological pH ranges, the side chain of Arg-534 in *VisHKT1;1-e^K* is expected to be positively charged. The importance of positively charged residues in the M2_D region of Trk/Ktr/HKT proteins has previously been demonstrated for AtHKT1 and TaHKT2;1 – mutation of Arg-519 in TaHKT2;1 and the equivalent Arg-487 in AtHKT1 to uncharged Gln reduced the transport activity of both proteins (Kato *et al.*,

2007). By contrast, we found that replacing the charged residues in the M2_D region with uncharged residues increased the activity of *VisHKT1;1-e^K*. The additive effect of a D537G substitution on transport activity in the *VisHKT1;1-e^K_{R534S/D537G}* double mutant protein in yeast, but no change in conductance of the *VisHKT1;1-e^K_{D537G}* single mutant, might be due to interactions between positive and negative side chains of the Arg-534 and Asp-537 residues in the original *VisHKT1;1-e^K*. Future structural investigations into plant HKT proteins through protein crystallization would help to explain these observations.

In the parental rootstocks, expression of recessive *VisHKT1;1-e* alleles was approximately two-fold less than the dominant *VisHKT1;1-E* alleles in the root stele. The F₁ progeny are likely to have similar expression levels of each allele. Arabidopsis double knockout mutants of two transcription factors *arr1/arr12* showed a six-fold increase in *AtHKT1* expression in roots, which correlated with a 50% reduction in shoot Na⁺ concentration (Mason *et al.*, 2010). A two-fold increase in transcript abundance of allele *E* variants over allele *e* is therefore probably not large enough to explain the large difference in leaf Na⁺ that we observed between the homozygous *NaE* and *Nae* hybrid progeny. Although expression differences may contribute to leaf Na⁺ exclusion, functional differences in Na⁺ transport are likely the major determining factor for the near-Mendelian inheritance of Na⁺ exclusion seen in our study.

Ten *V. vinifera* cultivars examined here, were all homozygous for *VvHKT1;1* alleles encoding Ser and Gly residues at 534 and 537 – typical of dominant *VisHKT1;1-E* alleles. The majority of these cultivars showed strong Na⁺ exclusion abilities consistent with their *HKT1;1* alleles. This finding highlights the importance of selecting for dominant *VisHKT1;1-E* alleles in new rootstock genotypes, as introducing recessive *VisHKT1;1-e* alleles could result in severely diminished Na⁺ exclusion capability compared with own-rooted *V. vinifera*.

In plants, both Na⁺ and Cl⁻ can be toxic in high enough concentrations (Tavakkoli *et al.*, 2011), and which ion is more damaging depends on both their relative accumulation and thresholds of toxicity (Munns & Tester, 2008). In grapevines, Cl⁻ has been attributed as the ion most associated with salinity related ion toxicity; however, early studies that established this link were limited to *V. vinifera* cultivars (Woodham, 1956; Ehlig, 1960; Downton, 1977b). In our study, all the *V. vinifera* cultivars were found to be relatively strong excluders of Na⁺. Considering that Na⁺ exclusion is much more variable in rootstock genotypes derived from other *Vitis* species and the prevalent use of rootstocks in viticulture, the impact of elevated Na⁺ accumulation on vine health warrants further investigation. The homozygous recessive *Nae* hybrids identified here provide the ideal rootstock material for quantifying the effect of high Na⁺ accumulation on vine health and yield in longer-term future studies.

In conclusion, we identified *VisHKT1;1* as a major gene controlling Na⁺ exclusion in grapevine rootstocks. Transgressive variation of Na⁺ exclusion in the progeny of a heterozygous rootstock cross is caused by the inheritance of *VisHKT1;1* alleles that encode proteins with differences in Na⁺ conductance, voltage

dependence, and have small differences in root expression levels. We propose that the mechanism for enhanced Na⁺ exclusion in *NaE* progeny is the enhanced Na⁺ conductance through *VisHKT1;1-E* variants, which also display limited rectification. These functional properties are conferred by a neutrally charged amino acid residue at the C-terminus of *VisHKT1;1*. Identification of dominant *VisHKT1;1-E* alleles provide a valuable genetic marker to select for strong Na⁺ exclusion in rootstock breeding programmes, which will assist with quality grape and wine production from saline soils.



Acknowledgements

We thank Diversity Array Technology (ACT) for GBS. Bettina Berger and Plant Accelerator staff (University of Adelaide), Annette Böttcher, Karin Sefton, Amy Rinaldo, Jim Speirs, Caroline Phillips, Alex Lawlor, Maria Mrinak, Inna Mazonka, Charlotte Jordans, Matthew Woodward and Simon Robinson (CSIRO) for assistance with Na⁺ screening. CSIRO Analytical Services Unit for ICP. Peter Clingeffer (CSIRO) for assistance with the grapevine cross and Arryn Clarke (CSIRO) for maintaining rootstock mothervines. Haijun Gong (Northwest A&F University, China), Lauren Hooper and Jacinta Watkins (CSIRO) for assistance with sequencing and cloning. Paul Boss (CSIRO) for assistance with QTL mapping. Wendy Sullivan (University of Adelaide) for technical assistance. Stefanie Wege (University of Adelaide) for microscopy assistance. Bo Xu (University of Adelaide) for TaHKT1;5-D in pGEMHE. Maria Hrmova (University of Adelaide) for discussions on experimental design. Steve Tyerman (University of Adelaide) for assistance with data analysis. This work was funded by Wine Australia grant CSP1302 (A.R.W., R.R.W., E.J.E., M.G.) and AGW_Ph1502 (Y.W.), with support from ARC grants FT130100709 and CE140100008 (both M.G.) and an Australian Department of Agriculture and Water Resources Science and Innovation Award (J.D.D.).

Author contributions

S.W.H. performed yeast assays, qRT-PCR, cloning, confocal microscopy, site-directed mutagenesis and electrophysiology of grapevine HKT variants; J.D.D. performed linkage mapping, QTL analysis, primer design, cloning of *HKT1;1* allelic variants, and sequencing of *HKT1;1* from *Vitis* species; Y.W. performed mutagenesis and electrophysiology of TaHKT1;5-D; A.R.W., E.J.E., R.R.W., D.H.B. and J.D.D., devised and performed grapevine Na⁺ screens and D.H.B. measured the leaf Na⁺ content; S.W.H. and J.D.D. analysed data; M.G., R.R.W. and A.R.W. supervised research; S.W.H. and J.D.D. wrote the manuscript; M.G., R.R.W. and A.R.W. revised the manuscript; and all authors commented on the manuscript.

ORCID

Sam W. Henderson  <http://orcid.org/0000-0003-3019-1891>
Matthew Gilliam  <http://orcid.org/0000-0003-0666-3078>

References

- Ali A, Raddatz N, Aman R, Kim S, Park HC, Jan M, Baek D, Khan IU, Oh D-H, Lee SY *et al.* 2016. A single amino-acid substitution in the sodium transporter HKT1 associated with plant salt tolerance. *Plant Physiology* 171: 2112–2126.
- Ali Z, Park HC, Ali A, Oh D-H, Aman R, Kropornicka A, Hong H, Choi W, Chung WS, Kim W-Y *et al.* 2012. TsHKT1;2, a HKT1 homolog from the extremophile *Arabidopsis* relative *Thellungiella salsuginea*, shows K⁺ specificity in the presence of NaCl. *Plant Physiology* 158: 1463–1474.
- Asins MJ, Villalta I, Aly MM, Olías R, Álvarez De Morales PAZ, Huertas R, Li JUN, Jaime-Pérez N, Haro R, Raga V *et al.* 2013. Two closely linked tomato HKT coding genes are positional candidates for the major tomato QTL involved in Na⁺/K⁺ homeostasis. *Plant, Cell & Environment* 36: 1171–1191.
- Baxter I, Brazelton JN, Yu D, Huang YS, Lahner B, Yakubova E, Li Y, Bergelson J, Borevitz JO, Nordborg M *et al.* 2010. A coastal cline in sodium accumulation in *Arabidopsis thaliana* is driven by natural variation of the sodium transporter AtHKT1;1. *PLoS Genetics* 6: e1001193.
- Benheim D, Rochfort S, Robertson E, Potter ID, Powell KS. 2012. Grape phylloxera (*Daktulosphaira vitifoliae*) – a review of potential detection and alternative management options. *Annals of Applied Biology* 161: 91–115.
- Böhm J, Scherzer S, Shabala S, Krol E, Neher E, Mueller TD, Hedrich R. 2016. Venus flytrap HKT1-type channel provides for prey sodium uptake into carnivorous plant without conflicting with electrical excitability. *Molecular Plant* 9: 428–436.
- Byrt CS, Platten JD, Spielmeier W, James RA, Lagudah ES, Dennis ES, Tester M, Munns R. 2007. HKT1;5-like cation transporters linked to Na⁺ exclusion loci in wheat, *Nax2* and *Kna1*. *Plant Physiology* 143: 1918–1928.
- Byrt CS, Xu B, Krishnan M, Lightfoot DJ, Athman A, Jacobs AK, Watson-Haigh NS, Plett D, Munns R, Tester M *et al.* 2014. The Na⁺ transporter, TaHKT1;5-D, limits shoot Na⁺ accumulation in bread wheat. *Plant Journal* 80: 516–526.
- Corratgé-Faillie C, Jabnoute M, Zimmermann S, Véry A-A, Fizames C, Sentenac H. 2010. Potassium and sodium transport in non-animal cells: the Trk/Ktr/HKT transporter family. *Cellular and Molecular Life Sciences* 67: 2511–2532.
- Cotsaftis O, Plett D, Johnson AAT, Walia H, Wilson C, Ismail AM, Close TJ, Tester M, Baumann U. 2011. Root-specific transcript profiling of contrasting rice genotypes in response to salinity stress. *Molecular Plant* 4: 25–41.
- Cotsaftis O, Plett D, Shirley N, Tester M, Hrmova M. 2012. A two-staged model of Na⁺ exclusion in rice explained by 3D modeling of HKT transporters and alternative splicing. *PLoS ONE* 7: e39865.
- Courtois B, Audebert A, Dardou A, Roques S, Ghneim-Herrera T, Droc G, Frouin J, Rouan L, Gozé E, Kilian A *et al.* 2013. Genome-wide association mapping of root traits in a japonica rice panel. *PLoS ONE* 8: e78037.
- Curtis MD, Grossniklaus U. 2003. A gateway cloning vector set for high-throughput functional analysis of genes in *planta*. *Plant Physiology* 133: 462–469.
- Davenport RJ, Munoz-Mayor A, Jha D, Essah PA, Rus ANA, Tester M. 2007. The Na⁺ transporter AtHKT1;1 controls retrieval of Na⁺ from the xylem in *Arabidopsis*. *Plant, Cell & Environment* 30: 497–507.
- Donkin R, Robinson S, Sumby K, Harris V, McBryde C, Jiranek V. 2010. Sodium chloride in Australian grape juice and its effect on alcoholic and malolactic fermentation. *American Journal of Enology and Viticulture* 61: 392–400.
- Downton WJS. 1977a. Chloride accumulation in different species of grapevine. *Scientia Horticulturae* 7: 249–253.
- Downton WJS. 1977b. Photosynthesis in salt-stressed grapevines. *Australian Journal of Plant Physiology* 4: 183–192.
- Ehlig CF. 1960. Effects of salinity on four varieties of table grapes grown in sand culture. *Proceedings of the American Society for Horticultural Science* 76: 323–331.
- Elliott J, Deryng D, Müller C, Frieler K, Konzmann M, Gerten D, Glotter M, Flörke M, Wada Y, Best N *et al.* 2014. Constraints and potentials of future irrigation water availability on agricultural production under climate change. *Proceedings of the National Academy of Sciences, USA* 111: 3239–3244.
- Fasoli M, Dal Santo S, Zenoni S, Tornielli GB, Farina L, Zamboni A, Porceddu A, Venturini L, Bicego M, Murino V *et al.* 2012. The grapevine expression atlas reveals a deep transcriptome shift driving the entire plant into a maturation program. *Plant Cell* 24: 3489–3505.
- Ferris H, Zheng L, Walker MA. 2012. Resistance of grape rootstocks to plant-parasitic nematodes. *Journal of Nematology* 44: 377–386.
- Fort KP, Heinritz CC, Walker MA. 2015. Chloride exclusion patterns in six grapevine populations. *Australian Journal of Grape and Wine Research* 21: 147–155.
- Gong H, Blackmore D, Clingeleffer P, Sykes S, Jha D, Tester M, Walker R. 2011. Contrast in chloride exclusion between two grapevine genotypes and its variation in their hybrid progeny. *Journal of Experimental Botany* 62: 989–999.
- Gong HJ, Blackmore DH, Clingeleffer PR, Sykes SR, Walker RR. 2014. Variation for potassium and sodium accumulation in a family from a cross between grapevine rootstocks K 51-40 and 140 Ruggeri. *Vitis* 53: 65–72.
- Grefen C, Donald N, Hashimoto K, Kudla J, Schumacher K, Blatt MR. 2010. A ubiquitin-10 promoter-based vector set for fluorescent protein tagging facilitates temporal stability and native protein distribution in transient and stable expression studies. *Plant Journal* 64: 355–365.
- Henderson SW, Baumann U, Blackmore DH, Walker AR, Walker RR, Gilliam M. 2014. Shoot chloride exclusion and salt tolerance in grapevine is associated with differential ion transporter expression in roots. *BMC Plant Biology* 14: 1–18.
- Henderson SW, Wege S, Qiu J, Blackmore DH, Walker AR, Tyerman SD, Walker RR, Gilliam M. 2015. Grapevine and *Arabidopsis* cation-chloride cotransporters localize to the Golgi and *trans*-Golgi network and indirectly influence long-distance ion transport and plant salt tolerance. *Plant Physiology* 169: 2215–2229.
- Horie T, Hauser F, Schroeder JI. 2009. HKT transporter-mediated salinity resistance mechanisms in *Arabidopsis* and monocot crop plants. *Trends in Plant Science* 14: 660–668.
- Huang S, Spielmeier W, Lagudah ES, James RA, Platten JD, Dennis ES, Munns R. 2006. A sodium transporter (HKT7) is a candidate for *Nax1*, a gene for salt tolerance in durum wheat. *Plant Physiology* 142: 1718–1727.
- Jabnoute M, Espeout S, Mieulet D, Fizames C, Verdeil J-L, Conéjéro G, Rodríguez-Navarro A, Sentenac H, Guiderdoni E, Abdely C *et al.* 2009. Diversity in expression patterns and functional properties in the rice HKT transporter family. *Plant Physiology* 150: 1955–1971.
- Jaillon O, Aury JM, Noel B, Policriti A, Clepet C, Casagrande A, Choise N, Aubourg S, Vitulo N, Jubin C *et al.* 2007. The grapevine genome sequence suggests ancestral hexaploidization in major angiosperm phyla. *Nature* 449: 463–467.
- Jaime-Pérez N, Pineda B, García-Sogo B, Atares A, Athman A, Byrt CS, Olías R, Asins MJ, Gilliam M, Moreno V *et al.* 2016. The Na⁺ transporter encoded by the HKT1;2 gene modulates Na⁺/K⁺ homeostasis in tomato shoots under salinity. *Plant, Cell & Environment* 40: 658–671.
- James RA, Blake C, Byrt CS, Munns R. 2011. Major genes for Na⁺ exclusion, *Nax1* and *Nax2* (wheat *HKT1;4* and *HKT1;5*), decrease Na⁺ accumulation in bread wheat leaves under saline and waterlogged conditions. *Journal of Experimental Botany* 62: 2939–2947.
- Kato N, Akai M, Zulkifli L, Matsuda N, Kato Y, Goshima S, Hazama A, Yamagami M, Guy RH, Uozumi N. 2007. Role of positively charged amino acids in the M2D transmembrane helix of Ktr/Trk/HKT type cation transporters. *Channels* 1: 161–171.
- Leske PA, Sas AN, Coulter AD, Stockley CS, Lee TH. 1997. The composition of Australian grape juice: chloride, sodium and sulfate ions. *Australian Journal of Grape and Wine Research* 3: 26–30.
- Li B, Tester M, Gilliam M. 2017. Chloride on the move. *Trends in Plant Science* 22: 236–248.
- Li X-L, Wang C-R, Li X-Y, Yao Y-X, Hao Y-J. 2013. Modifications of Kyoho grape berry quality under long-term NaCl treatment. *Food Chemistry* 139: 931–937.
- de Loryn LC, Petrie PR, Hasted AM, Johnson TE, Collins C, Bastian SEP. 2014. Evaluation of sensory thresholds and perception of sodium chloride in grape juice and wine. *American Journal of Enology and Viticulture* 65: 124–133.

- Maas EV, Hoffman GJ. 1977. Crop salt tolerance – current assessment. *Journal of the Irrigation and Drainage Division* 103: 115–134.
- Mäser P, Hosoo Y, Goshima S, Horie T, Eckelman B, Yamada K, Yoshida K, Bakker EP, Shinmyo A, Oiki S *et al.* 2002. Glycine residues in potassium channel-like selectivity filters determine potassium selectivity in four-loop-per-subunit HKT transporters from plants. *Proceedings of the National Academy of Sciences, USA* 99: 6428–6433.
- Mason MG, Jha D, Salt DE, Tester M, Hill K, Kieber JJ, Eric Schaller G. 2010. Type-B response regulators ARR1 and ARR12 regulate expression of AtHKT1;1 and accumulation of sodium in Arabidopsis shoots. *Plant Journal* 64: 753–763.
- Møller IS, Gilliham M, Jha D, Mayo GM, Roy SJ, Coates JC, Haseloff J, Tester M. 2009. Shoot Na⁺ exclusion and increased salinity tolerance engineered by cell type-specific alteration of Na⁺ transport in *Arabidopsis*. *Plant Cell* 21: 2163–2178.
- Munns R, Gilliham M. 2015. Salinity tolerance of crops – what is the cost? *New Phytologist* 208: 668–673.
- Munns R, James RA, Xu B, Athman A, Conn SJ, Jordans C, Byrt CS, Hare RA, Tyerman SD, Tester M *et al.* 2012. Wheat grain yield on saline soils is improved by an ancestral Na⁺ transporter gene. *Nature Biotechnology* 30: 360–364.
- Munns R, Tester M. 2008. Mechanisms of salinity tolerance. *Annual Review of Plant Biology* 59: 651–681.
- Nelson BK, Cai X, Nebenführ A. 2007. A multicolored set of *in vivo* organelle markers for co-localization studies in Arabidopsis and other plants. *Plant Journal* 51: 1126–1136.
- Ollat N, Bordenave L, Tandonnet JP, Boursiquot JM, Marguerit E. 2016. Grapevine rootstocks: origins and perspectives. In: Gaiotti F, Battista F, Tomasi D, eds. *1 International symposium on grapevine roots*, Rauscedo, Italy: International Society for Horticultural Science, ISHS Acta Horticulturae 1136, 11–22.
- Pannell DJ. 2001. Dryland salinity: economic, scientific, social and policy dimensions. *Australian Journal of Agricultural and Resource Economics* 45: 517–546.
- Prior LD, Grieve AM, Cullis BR. 1992. Sodium-chloride and soil texture interactions in irrigated field-grown sultana grapevines. I. Yield and fruit-quality. *Australian Journal of Agricultural Research* 43: 1051–1066.
- Ren Z-H, Gao J-P, Li L-G, Cai X-L, Huang W, Chao D-Y, Zhu M-Z, Wang Z-Y, Luan S, Lin H-X. 2005. A rice quantitative trait locus for salt tolerance encodes a sodium transporter. *Nature Genetics* 37: 1141–1146.
- Rus A, Baxter I, Muthukumar B, Gustin J, Lahner B, Yakubova E, Salt DE. 2006. Natural variants of AtHKT1 enhance Na⁺ accumulation in two wild populations of *Arabidopsis*. *PLoS Genetics* 2: e210.
- Sainsbury F, Thuenemann EC, Lomonosoff GP. 2009. pEAQ: versatile expression vectors for easy and quick transient expression of heterologous proteins in plants. *Plant Biotechnology Journal* 7: 682–693.
- Serra I, Strever A, Myburgh PA, Deloire A. 2014. Review: the interaction between rootstocks and cultivars (*Vitis vinifera* L.) to enhance drought tolerance in grapevine. *Australian Journal of Grape and Wine Research* 20: 1–14.
- Stevens RM, Harvey G, Partington DL. 2011. Irrigation of grapevines with saline water at different growth stages: effects on leaf, wood and juice composition. *Australian Journal of Grape and Wine Research* 17: 239–248.
- Stevenson I. 1980. The diffusion of disaster: the phylloxera outbreak in the département of the Hérault, 1862–1880. *Journal of Historical Geography* 6: 47–63.
- Stockley CS, Lloyd-Davies S. 2001. *Analytical specifications for the export of Australian wine: a list of analysis requirements and specifications for Australian wine export destinations*. Glen Osmond, SA, Australia: The Australian Wine Research Institute.
- Sunarpri, Horie T, Motoda J, Kubo M, Yang H, Yoda K, Horie R, Chan W-Y, Leung H-Y, Hattori K *et al.* 2005. Enhanced salt tolerance mediated by AtHKT1 transporter-induced Na⁺ unloading from xylem vessels to xylem parenchyma cells. *Plant Journal* 44: 928–938.
- Tavakkoli E, Fatehi F, Coventry S, Rengasamy P, McDonald GK. 2011. Additive effects of Na⁺ and Cl⁻ ions on barley growth under salinity stress. *Journal of Experimental Botany* 62: 2189–2203.
- Tounsi S, Ben Amar S, Masmoudi K, Sentenac H, Brini F, Véry A-A. 2016. Characterization of two HKT1;4 transporters from *Triticum monococcum* to elucidate the determinants of the wheat salt tolerance *Nax1* QTL. *Plant and Cell Physiology* 57: 2047–2057.
- Tregeagle JM, Tisdall JM, Tester M, Walker RR. 2010. Cl⁻ uptake, transport and accumulation in grapevine rootstocks of differing capacity for Cl⁻ exclusion. *Functional Plant Biology* 37: 665–673.
- Van Ooijen J. 2006. *JoinMap[®] 4, Software for the calculation of genetic linkage maps in experimental populations*. Wageningen, the Netherlands: Kyazma BV. 33: 10.1371.
- Van Ooijen J, Kyazma B. 2009. *MapQTL 6. Software for the mapping of quantitative trait loci in experimental populations of diploid species*. Wageningen, the Netherlands: Kyazma BV.
- Walker RR, Blackmore DH, Clingeleffer PR, Correll RL. 2002. Rootstock effects on salt tolerance of irrigated field-grown grapevines (*Vitis vinifera* L. cv. Sultana). 1. Yield and vigour inter-relationships. *Australian Journal of Grape and Wine Research* 8: 3–14.
- Walker RR, Blackmore DH, Clingeleffer PR, Correll RL. 2004. Rootstock effects on salt tolerance of irrigated field-grown grapevines (*Vitis vinifera* L. cv. Sultana). 2. Ion concentrations in leaves and juice. *Australian Journal of Grape and Wine Research* 10: 90–99.
- Walker RR, Blackmore DH, Clingeleffer PR, Godden P, Francis L, Valente P, Robinson E. 2003. Salinity effects on vines and wines. *Bulletin de l'Office International de la Vigne et du Vin* 76: 200–227.
- Waters S, Gilliham M, Hrmova M. 2013. Plant high-affinity potassium (HKT) transporters involved in salinity tolerance: structural insights to probe differences in ion selectivity. *International Journal of Molecular Sciences* 14: 7660.
- Woodham R. 1956. The chloride status of the irrigated sultana vine and its relation to vine health. *Australian Journal of Agricultural Research* 7: 414–427.

Supporting Information

Additional Supporting Information may be found online in the Supporting Information tab for this article:

Fig. S1 Correlation between juice and leaf Na⁺ concentration.

Fig. S2 Consensus genomic map of K51-40 × 140 Ruggeri progeny.

Fig. S3 Amino acid sequence alignment of six VviHKT1 proteins present in the grapevine reference genome.

Fig. S4 VviHKT1;3 does not function as a sodium transporter in yeast.

Fig. S5 Amino acid alignment of VviHKT1;1 from Cabernet Sauvignon *VisHKT1;1* alleles from K51-40 and 140 Ruggeri.

Fig. S6 Inward and outward sodium chord conductance allelic variants of *VisHKT1;1*.

Fig. S7 Effect of [Na⁺]_{ext} on the reversal potential of *VisHKT1;1* allelic variants.

Fig. S8 Functional differences in the transport properties between *VisHKT1;1-e^K* and *VisHKT1;1-E^K*.

Fig. S9 Allelic variants of *VisHKT1;1* are each highly sodium-selective.

Fig. S10 Comparing the inward sodium transport rate of *VisHKT1;1-eK* and mutant variants.

Fig. S11 C-terminal mutations of K51-40 *VisHKT1;1* alleles do not affect sodium selectivity.

Fig. S12 Tracing the origin of the *VisHKT1;1* alleles.

Table S1 List of primers used in this study

Table S2 *HKT1* gene accession numbers

Table S3 CAPS markers designed to score K51-40 × 140 Ruggeri hybrid progeny for their inheritance of *HKT1;1* alleles

Table S4 Genes located with the mapped *NaE* locus

Please note: Wiley Blackwell are not responsible for the content or functionality of any Supporting Information supplied by the authors. Any queries (other than missing material) should be directed to the *New Phytologist* Central Office.



About New Phytologist

- *New Phytologist* is an electronic (online-only) journal owned by the New Phytologist Trust, a **not-for-profit organization** dedicated to the promotion of plant science, facilitating projects from symposia to free access for our Tansley reviews and Tansley insights.
- Regular papers, Letters, Research reviews, Rapid reports and both Modelling/Theory and Methods papers are encouraged. We are committed to rapid processing, from online submission through to publication 'as ready' via *Early View* – our average time to decision is <26 days. There are **no page or colour charges** and a PDF version will be provided for each article.
- The journal is available online at Wiley Online Library. Visit **www.newphytologist.com** to search the articles and register for table of contents email alerts.
- If you have any questions, do get in touch with Central Office (np-centraloffice@lancaster.ac.uk) or, if it is more convenient, our USA Office (np-usaoffice@lancaster.ac.uk)
- For submission instructions, subscription and all the latest information visit **www.newphytologist.com**

Chapter 5: The *HKT1* gene family in grapevine (*Vitis vinifera* L.) encodes sodium-selective transporters with diverse features

Yue Wu¹, Sam W Henderson¹, Stefanie Wege¹, Fei Zheng¹, Rob R Walker², Matthew Gilliam^{1,*}

¹ ARC Centre of Excellence in Plant Energy Biology, School of Agriculture, Food and Wine, University of Adelaide, Glen Osmond, South Australia 5064, Australia

² CSIRO Agriculture and Food, Locked Bag 2, Glen Osmond, South Australia 5064, Australia

* Correspondence should be addressed to:

Professor Matthew Gilliam

Email: matthew.gilliam@adelaide.edu.au

Phone: +61 8 8313 8145

Email addresses:

YW: yue.wu@adelaide.edu.au

SWH: sam.henderson@adelaide.edu.au

SW: stefanie.wege@adelaide.edu.au

FZ: fei.zheng@student.adelaide.edu.au

RRW: rob.walker@csiro.au

MG: matthew.gilliam@adelaide.edu.au

Running title: Grapevine HKT1s are Na⁺ transporters with diverse features

Key words: sodium transporter, sodium homeostasis, grapevine, HKT

Statement of Authorship

Title of Paper	The <i>HKT1</i> gene family in grapevine (<i>Vitis vinifera</i> L.) encodes sodium-selective transporters with diverse features.
Publication Status	<input type="checkbox"/> Published <input type="checkbox"/> Accepted for Publication <input type="checkbox"/> Submitted for Publication <input checked="" type="checkbox"/> Unpublished and Unsubmitted work written in manuscript style
Publication Details	Wu, Y., Henderson, S.W., Wege, S., Zheng, F., Walker, R.R., Gilliam, M (2019) The <i>HKT1</i> gene family in grapevine (<i>Vitis vinifera</i> L.) encodes sodium-selective transporters with diverse features.

Principal Author

Name of Principal Author (Candidate)	Yue Wu		
Contribution to the Paper	Performed VviHKT1;6, 1;7 and 1;8 allele construction, electrophysiology and yeast growth assay, analysed the data and wrote the manuscript.		
Overall percentage (%)	55		
Certification:	This paper reports on original research I conducted during the period of my Higher Degree by Research candidature and is not subject to any obligations or contractual agreements with a third party that would constrain its inclusion in this thesis. I am the primary author of this paper.		
Signature		Date	02.07.2019

Co-Author Contributions

By signing the Statement of Authorship, each author certifies that:

- i. the candidate's stated contribution to the publication is accurate;
- ii. permission is granted for the candidate to include the publication in the thesis; and
- iii. the sum of all co-author contributions is equal to 100% less the candidate's stated contribution.

Name of Co-Author	Sam Henderson		
Contribution to the Paper	Conceived the project, performed VviHKT1;7 and 1;8 cloning, supervised the research and edited the manuscript.		
Signature		Date	03/07/2019

Name of Co-Author	Stefanie Wege		
-------------------	---------------	--	--

Contribution to the Paper	Performed subcellular localisation of VviHKT1;6, 1;7 and 1;8.		
Signature		Date	02.07.2019

Name of Co-Author	Fei Zheng		
Contribution to the Paper	Processed the grapevine <i>HKT1</i> RNA-seq data.		
Signature		Date	03.07.2019

Name of Co-Author	Rob Walker		
Contribution to the Paper	Supervised the research and assisted in editing the manuscript.		
Signature		Date	5/7/19

Name of Co-Author	Matthew Gilliam		
Contribution to the Paper	Contributed to project conception, supervised the research and assisted in editing the manuscript.		
Signature		Date	01.07.2019

Abstract

Grapevine is a valuable crop for human consumption and wine production, and is prone to salinity stress in arid regions or when irrigated with low quality water. A previous study identified a QTL (*NaE*) containing six *HKT* genes that was associated with shoot Na^+ exclusion in grapevine. While *VisHKT1;1* was predicted to be the most likely gene within this QTL to encode for this important salinity tolerance sub-trait, four other *HKTs* within the QTL remained uncharacterised. In this study, two allelic variants each of *VviHKT1;6*, *VviHKT1;7* and *VviHKT1;8* from the heterozygous grapevine variety Cabernet Sauvignon were functionally characterised. Using the *Xenopus laevis* oocyte heterologous expression system, as well as the tobacco leaf transient expression, we found that the *VviHKT1;6* and *VviHKT1;7* allelic variants encoded plasma membrane localised proteins that facilitated significant non-rectifying Na^+ transport. Conversely, proteins encoded by the *VviHKT1;8* alleles were inwardly-rectifying, weak Na^+ transporters that localised to endosomal compartments. Mining of previous RNA-seq gene expression data suggested that all these *HKTs* are weakly expressed in grapevine roots, flower buds, and seeds under normal conditions and different nutrient regimes. We propose that *VviHKT1;6* and *VviHKT1;7* may have minor roles in grapevine Na^+ homeostasis, and *VviHKT1;8* may be involved in intracellular cargo shipping which may affect vacuolar compartmentalisation of Na^+ .

Introduction

Grapevine (*Vitis vinifera* L.) is used to produce wines, dried grapes, and table grapes, and is one of the world's most valuable crops. However, grapevine is particularly sensitive to climate variation (Hannah *et al.* 2013, Wolkovich *et al.* 2018) and moderately sensitive to salinity (Maas and Hoffman 1977) – two environmental issues that are closely linked. Grapevines are challenged by dry land salinity, and sodium (Na^+) and chloride (Cl^-) accumulation from rain and irrigation practices (Maas and Hoffman 1977, Munns and Gilliam 2015, Walker *et al.* 2002a). High salt in the root-zone can stress the plants osmotically, which reduces plant water uptake and transpiration (Neumann 2011). Accumulation of excess Na^+ and Cl^- in plant tissues can induce ion toxicity symptoms such as reduced photosynthesis, leaf necrosis and uneven berry development (Walker and Clingeleffer 2009). Both osmotic and ionic stress cost plants energy which may result in yield reductions (Munns *et al.* 2019, Munns and Gilliam 2015). Grapes that are cultivated under salt stress may produce must and juice with higher concentrations of salts and a higher pH (Stevens *et al.* 2011, Walker *et al.* 2007). Elevated salt in grape juice can stress yeast during fermentation (Donkin *et al.* 2010) and introduce unpleasant salty and soapy flavours (de Loryn *et al.* 2014), while an increased pH can reduce the tartrate and microbial stability of the ferment (Berg and Keefer 1958) and requires expensive pH adjustment during vinification. Finally, there are legal concentration thresholds for Na^+ and Cl^- in finished wines (de Loryn *et al.* 2014, Leske *et al.* 1997).

One major practise to reduce the effect of salts on grapevines is to use salt excluding rootstocks, which are known to reduce the root-to-scion translocation of Na^+ and Cl^- . Recent studies have focussed on identifying genes that are likely to confer shoot Na^+ exclusion to scions. Using a small biparental mapping population of the contrasting rootstocks K51-40 and 140-Ruggeri, 70% of the variation in shoot Na^+ accumulation was associated with the *NaE* quantitative trait locus (QTL) containing the six high affinity potassium transporter (HKT) genes annotated within the *V. vinifera* genome (*HKT1;1-3*; *HKT1;6-8*) (Henderson *et al.* 2018a). Transgressive segregation for the Na^+ accumulation trait was near-Mendelian indicating that it was due to a single heritable unit within the population screened. The major candidate gene responsible for the trait was identified as *VisHKT1;1* based on its high expression in roots, and its variation in

functionality between the four alleles characterised. The gene, *VisHKT1;1*, was found to encode a Na⁺ transporter likely to function in retrieving Na⁺ from the root xylem apoplast and reducing shoot Na⁺ accumulation. However, all the *HKTs* within the grapevine genome are contained within the *NaE* locus, and belong to the HKT1 subgroup. Across the plant kingdom, the HKT1 subgroup encode transporters that are highly-selective for Na⁺ over other cations (Horie *et al.* 2009, Mäser *et al.* 2002b, Waters *et al.* 2013). Henderson *et al.* (2018a) functionally characterised grapevine HKT1;1 and showed that HKT1;3 was non-functional; however, the four remaining grapevine *HKT* genes remained uncharacterised.

The first HKT identified was a wheat HKT (now known as TaHKT2;1) which was originally considered a potassium (K⁺) transporter (Schachtman and Schroeder 1994), but soon found to be a K⁺/Na⁺ symporter and/or a Na⁺ uniporter depending on the extracellular Na⁺ concentration *in vitro* (Gassman *et al.* 1996, Rubio *et al.* 1995). Then, HKTs were studied intensively in rice (*Oryza sativa*) (Garcia-deblás *et al.* 2003, Horie *et al.* 2001, Ren *et al.* 2005a), wheat (*Triticum aestivum*) (Byrt *et al.* 2007) and Arabidopsis (*Arabidopsis thaliana*) (Mäser *et al.* 2002a, Uozumi *et al.* 2000), and more Na⁺ transporting HKTs were discovered. Later HKTs were classified into two subfamilies based on their function and phylogenetic relationships (Platten *et al.* 2006); the HKT1 group members are generally Na⁺ uniporters, while the HKT2 members are considered dual K⁺/Na⁺ transporters (Waters *et al.* 2013). The composition of *HKTs* in each plant species varies; monocots were observed to have both *HKT1* and *HKT2* members, but dicots tend to lack *HKT2* genes (Platten *et al.* 2006). Several group 1 HKTs were found to play important roles in plant salinity tolerance. AtHKT1;1, the only HKT in the model dicot *A. thaliana*, was found to reduce shoot Na⁺ accumulation by retrieving Na⁺ from the transpiration stream (Berthomieu *et al.* 2003, Gong *et al.* 2004, Plett *et al.* 2010a, Sunarpi *et al.* 2005). Orthologues such as OsHKT1;5 in rice (Kobayashi *et al.* 2017), TmHKT1;5-A and TaHKT1;5-D in wheat (Byrt *et al.* 2014, James *et al.* 2011, Munns *et al.* 2012) were found to retrieve Na⁺ from the root xylem apoplast, thus preventing shoot Na⁺ accumulation, and increasing plant salt tolerance and yield.

Here, we build on the study of Henderson *et al.* (2018a) by investigating and functionally characterising additional *HKT1* genes from within the grapevine *NaE* locus,

that we have termed *VviHKT1;6*, *VviHKT1;7* and *VviHKT1;8*. *In vitro* experiments using *Xenopus laevis* oocytes were able to identify *VviHKT1;6*, *HKT1;7* and *HKT1;8* as Na⁺ transporters. We conclude that *VviHKT1;6*, *HKT1;7* may play minor roles in Na⁺ homeostasis, and *VviHKT1;8* may affect intracellular cargo shipping and Na⁺ partitioning.

Materials and methods

Gene identification

The *VviHKT* gene sequences were obtained from the *V. vinifera* PN40024 genome database using the gene IDs listed in Henderson *et al.* (2018a). The sequences of the other plant, moss, yeast and bacterium HKTs were obtained using the gene IDs listed in Waters *et al.* (2013) and Garciadeblás *et al.* (2003). Protein alignments were generated using Clustal W (Larkin *et al.* 2007), and the phylogenetic tree was generated using Geneious version 8.1.7 with the default settings.

Molecular cloning

The sequences of *VviHKT1;6* (VIT_11s0103g00150), *VviHKT1;7* (VIT_11s0103g00140) and *VviHKT1;8* (VIT_11s0103g00130) alleles were obtained from the genomic DNA sequence of *V. vinifera* (cv. Cabernet Sauvignon) (Chin *et al.* 2016, Minio *et al.* 2017, Minio *et al.* 2018), and cloning primers were designed to amplify all full length alleles (Table S2). *VviHKT1;7* allele A and *VviHKT1;8* allele A coding sequences (CDS) were amplified from Cabernet Sauvignon root cDNA (Henderson *et al.* 2014a) with Phusion High-Fidelity DNA Polymerase (New England Biolabs). The PCR products were ligated into the entry vector pCR8 using pCR8/GW/TOPO TA Cloning Kit (Invitrogen) or the vector pENTR using pENTR/D-TOPO Cloning Kit (Invitrogen) as per manufacturer's instructions. One Shot TOP10 *Escherichia coli* (Invitrogen) were transformed with the entry vectors as per manufacturer's instructions. Plasmids were harvested using ISOLATE II Plasmid Mini Kit (Biolone), and successful cloning was confirmed by Sanger sequencing.

Further attempts to clone all the remaining HKT genes and alleles by RT-PCR with gene specific primers failed; therefore, *VviHKT1;6B*, *VviHKT1;7B* and *VviHKT1;8B* were constructed based on *VviHKT1;7A* and *VviHKT1;8A* that were already cloned and present in entry vectors. pCR8-*VviHKT1;6B* was constructed by In-Fusion ligation (In-Fusion HD cloning kit, Clontech) of 3 synthesized fragments and 2 PCR fragments cloned from the *VviHKT1;7A* entry vector. pCR8-*VviHKT1;7* mock allele B was constructed by site-directed mutagenesis of *VviHKT1;7A*, and pCR8-*VviHKT1;8* mock allele B was constructed by sited-directed mutagenesis of *VviHKT1;8A* using In-Fusion

ligation. The constructed *VviHKT1;7B* and *VviHKT1;8B* mock alleles fully mimic the original alleles as they translate into the same amino acid sequences in Cabernet Sauvignon.

Gene expression analyses

RMA-normalized signal intensities were extracted from the Corvina microarray gene expression study by Fasoli *et al.* (2012). Data were log₂ transformed, and the mean signal intensities of the 4 probes and 3 biological replicates were analysed.

The RNA-seq data of 1 month old grapevine root tips from a NO₃⁻ application experiment (Cochetel *et al.* 2017), flower buds 3 weeks before flowering (BioProject: PRJNA307079), seeds from pea sized berries (BioProject: PRJNA307074), whole berries at 2 different stages with or without nitrogen fertilisation (Helwi *et al.* 2016), 9-week-old leaves under drought treatments (Zhu *et al.* 2018), and woody stems with and without fungi inoculation (Massonnet *et al.* 2017) were obtained from the Sequence Read Archive (<https://www.ncbi.nlm.nih.gov/sra>). The *VviHKT* expression data were normalised and presented as counts per million, and plotted using GraphPad PRISM v.7.00 for Windows (GraphPad).

Electrophysiology

The *VviHKT1;6*, *VviHKT1;7* and *VviHKT1;8* full length alleles in entry vectors were recombined into the *X. laevis* oocyte expression vector pGEMHE-DEST (Shelden *et al.* 2009) using LR Clonase II (Life Technologies) to generate vectors encoding T7:*HKT*. The pGEMHE recombinant vectors were linearised with NheI (New England Biolabs). The capped RNA (cRNA) for oocyte expression was synthesized with the mMACHINE mMACHINE T7 Transcription Kit (Invitrogen) using the linearised vectors as templates.

Stage IV and V *X. laevis* oocytes were injected with 6 ng of *VviHKT* cRNA or water in 42 nL volumes. The oocytes were incubated in Ringer's solution (96 mM NaCl, 2 mM KCl, 5 mM MgCl₂, 5 mM HEPES, 0.6 mM CaCl₂, 5% w/v horse serum, 500 µg/mL tetracycline and 1 × penicillin-streptomycin (Sigma P4333)) for 2 days post injection.

For the Na⁺ and K⁺ permeability assays, the basal perfusion solution for oocyte current recording contained 6 mM MgCl₂, 1.8 mM CaCl₂ and 5 mM MES. Basal buffers were supplemented with 0.3 to 50 mM Na gluconate, or 30 mM K gluconate. The pH of each solution was adjusted to 5.5 using Tris base; the osmolality was adjusted to 250 mOsm/kg using D-mannitol. Oocyte whole cell currents were recorded using an Oocyte Clamp OC-725C amplifier (Warner Instruments), digitised using an Axon Digidata 1400A (Molecular Devices) and the software Clampex 10.2 (Molecular Devices). The voltage step protocol was set with a holding potential equal to the resting membrane potential for 350 ms either side of stepwise pulses from -140 mV to +60 mV in 20 mV increments for 550 ms. The data was analysed using Smart-IV (Wu *et al.* 2019c) and plotted using GraphPad PRISM v.7.00 for Windows (GraphPad).

Subcellular localisation in tobacco (*Nicotiana benthamiana*) leaf epidermal cells

The *VviHKT1;6*, *VviHKT1;7* and *VviHKT1;8* full length alleles without stop codons in entry vectors were recombined into pMDC83 using LR Clonase II (Life Technologies) to generate binary vectors encoding 2x35S:*HKT-GFP*. The vectors were used to transform *Agrobacterium tumefaciens* strain Agl-1 using the freeze thaw method, and successful transformation was confirmed by colony PCR.

The transformed *Agrobacterium* colonies were used to inoculate 1 mL of LB liquid starter cultures containing 50 µg/mL Kanamycin and 50 µg/mL Rifampicin. *Agrobacteria* harbouring pB7RWG2 *AtCBL1n* (*AtCBL1n-RFP*, plasma membrane marker) (Batistič *et al.* 2008, Karimi *et al.* 2002) were used for co-localisation. *Agrobacteria* harbouring pEAQ-HT-DEST, which contains the p19 suppressor of gene silencing (Sainsbury *et al.* 2009), was used to maximise expression. Starter cultures of *Agrobacterium* harbouring the markers and pEAQ-HT-DEST were prepared from glycerol stocks with appropriate antibiotics. All starter cultures were incubated at 28 °C at 150 rpm for 2 days. 4 mL of LB with antibiotics were inoculated with 150 µL of starter culture and incubated at 28 °C at 150 rpm overnight. Cultures were pelleted at 4000 × g and resuspended in AS medium (10 mM MgCl₂, 150 µM acetosyringone and 10 mM MES, pH 5.6). Final suspensions were prepared by combining different cultures together in AS medium to a final OD₆₀₀ indicated in brackets: *pMDC83* expression vectors (OD₆₀₀ = 0.25); pEAQ-HT-DEST (OD₆₀₀ = 0.1); co-localising marker (OD₆₀₀

= 0.25). The combined suspensions were infiltrated into the abaxial side of fully expanded leaves of 5-6 week old tobacco with a 1 mL syringe.

Two days after infiltration, leaf sections were imaged using a Nikon A1R confocal laser scanning microscope and NIS-Elements C software (Nikon Corporation). Excitation/emission conditions were GFP (488 nm/ 500 – 550 nm), RFP (561 nm/ 570 – 620 nm).

Results and discussion

***VviHKT1;6*, *VviHKT1;7* and *VviHKT1;8* are candidate genes for grapevine Na⁺ homeostasis**

The *NaE* locus for grapevine Na⁺ exclusion (identified previously) contains 6 *HKT* genes: *VviHKT1;1*, *VviHKT1;2*, *VviHKT1;3*, *VviHKT1;6*, *VviHKT1;7* and *VviHKT1;8* (Figure 1A). We previously investigated *HKT1;1* and *VviHKT1;3* which were both highly expressed in roots (Henderson *et al.* 2018a). Here, we investigated the remaining genes.

Two annotated genes within *NaE* did not belong to the HKT family (Figure 1A). One gene showed homology to AtLTL1 – a putative Gly-Asp-Ser-Leu (GDSL) esterase/lipase gene that was previously reported to increase the salt tolerance of Arabidopsis when overexpressed (Naranjo *et al.* 2006), so is another target that could be followed up at a later date. The other gene was a putative chloroplastic/mitochondrial phenylalanine-tRNA ligase (NCBI LOC100265994), which is considered not relevant to salinity tolerance at this stage.

The remaining *HKTs* within the QTL were lowly expressed in the roots (Figure S1). Therefore, they are unlikely to have a major role in reducing the root-to-shoot translocation of Na⁺ via xylem retrieval in the root stele (Henderson *et al.* 2018a). However, these HKT genes may participate in Na⁺ homeostasis in other tissue types. Multiple sequence alignment showed that the *VviHKT1;2* CDS contained a premature stop codon (Figure 1B). According to the HKT selectivity-filter and pore region model described by Hauser and Horie (2010), the stop codon of *VviHKT1;2* occurs upstream of the first pore-forming domain. Hence *VviHKT1;2* is most likely to encode a non-functional HKT protein, and was therefore excluded from functional analyses here.

The predicted *VviHKT1;6*, *VviHKT1;7* and *VviHKT1;8* proteins encoded within the PN40024 reference genome are full length and show a high sequence similarity (85-97% identity, Figure 1C). Phylogenetic analysis showed that they are most closely related to EcHKT1;1 and EcHKT1;2 from Eucalyptus (Figure 2), which are reported to be permeable to Na⁺ and K⁺ (Liu *et al.* 2001). We therefore considered them likely to be Na⁺ and/or K⁺ transporters, and performed an in-depth functional characterisation of

these genes from Cabernet Sauvignon – a commercially important grapevine variety that has been used for previous molecular studies (Henderson *et al.* 2014a, Henderson *et al.* 2015).

Cabernet Sauvignon is heterozygous for *VviHKT1;6*, *VviHKT1;7* and *VviHKT1;8*

V. vinifera grapevines, including Cabernet Sauvignon, are heterozygous. While cloning *VviHKT1;6*, *VviHKT1;7* and *VviHKT1;8* from Cabernet Sauvignon cDNA, we found some minor differences between our clones and the reference genome sequence derived from the highly inbred *V. vinifera* (cv. Pinot Noir) PN40024. Therefore, to confirm our CDS, Cabernet Sauvignon genomic DNA sequences were used as the reference instead (Chin *et al.* 2016, Minio *et al.* 2017, Minio *et al.* 2018). We found that *VviHKT1;6*, *VviHKT1;7* and *VviHKT1;8* of Cabernet Sauvignon each have two alleles, which were confirmed by Sanger sequencing of the *VviHKT* genomic DNA. In this study, the allele most similar to the PN40024 reference genome was designated as “allele A”, while the other was named “allele B”. *VviHKT1;6A* has a premature stop codon between the pore-forming domains A and B (Hauser and Horie 2010), hence it is predicted to be non-functional and was not interrogated further. Amino acid sequence alignment showed that the *VviHKT1;6B*, *VviHKT1;7A* and *VviHKT1;7B* are highly similar (Figure 1C and D). *VviHKT1;7A* and *VviHKT1;7B* differ by only 2 amino acid residues, while *VviHKT1;8A* and *VviHKT1;8B* differ by only 1 residue.

Polymorphisms in *VviHKT1;6*, *VviHKT1;7* and *VviHKT1;8* alleles reveal candidate residues for influencing Na⁺ conductance

All full length allelic variants of *VviHKT1;6*, *VviHKT1;7* and *VviHKT1;8* were expressed in *Xenopus laevis* oocytes and tested for Na⁺ and K⁺ conductance using two electrode voltage clamping (TEVC). According to the current-voltage (I-V) plots, *VviHKT1;6B*, *VviHKT1;7A* and *VviHKT1;7B* were strong Na⁺ transporters and impermeable to K⁺ (Figure 3A – C). Although *VviHKT1;6B* and *VviHKT1;7B* differed by seven amino acid residues, their I-V properties were indistinguishable (Figure 3A and C). Conversely, the presence of only two polymorphic residues Thr-420 and Arg-466 in *VviHKT1;7A* compared to *VviHKT1;7B* resulted in a slight increase in the current magnitudes (Figure 3B and C). *VviHKT1;8A* was a relatively weak Na⁺ transporter, and impermeable to K⁺ (Figure 3D). However, although *VviHKT1;8B*

differed from VviHKT1;8A by only 1 residue (Lys-394), its cation currents were significantly smaller than those of VviHKT1;8A (Figure 3E). Numerous studies using site-directed mutagenesis have demonstrated that polymorphisms can alter the function of plant HKT proteins (Diatloff *et al.* 1998, Mäser *et al.* 2002b, Xu *et al.* 2018). The residues identified here could therefore be used in future structure-function studies of HKT-mediated plant Na⁺ transport – especially Arg-466 (VviHKT1;7A) and Lys-394 (VviHKT1;8A) as they are positively charged and therefore more likely to impact upon protein structure and transport properties.

To test the Na⁺ transport activity in another heterologous system, VviHKT1;7A transformed yeast were supplied with 50 mM NaCl to examine whether it inhibited its growth. When the transgene expression was induced by galactose, 3 independent transformed yeast lines containing VviHKT1;7A all showed Na⁺ induced growth inhibition (Figure S2), which suggest that VviHKT1;7A functions as a Na⁺ transporter in the yeast system.

***HKT1;6*, *HKT1;7* and *HKT1;8* were very lowly expressed in grapevine root tips, flower buds and seeds**

Microarray expression data suggested that *VviHKT1;6* and *VviHKT1;8* transcripts were lowly abundant in flowers and berries under normal conditions (Figure S1). Due to the low expression levels, we aimed to confirm these findings using complementary methods. We attempted RT-qPCR using cDNA samples from a range of grapevine tissues (high or low [NO₃⁻] treated roots, salt treated roots, separated flowers, pea sized berries, berries post veraison, berry skins, seeds from berries at a range of ages, rachis and tendril), but our candidate genes could not be amplified from these samples. As RNA-seq count numbers are based on alignments rather than probes, we decided that RNA-seq data might better represent the expression levels of *HKT1;6*, *HKT1;7* and *HKT1;8* in grapevines. The benefits of RNA-seq compared to microarray hybridisation include superior detection of low abundance transcripts, ability to differentiate biologically critical isoforms, identification of genetic variants, and the avoidance of technical issues inherent to microarray probe performance such as cross-hybridization (Zhao *et al.* 2014).

RNA-seq data of different grapevine tissues from several projects were obtained from the Sequence Read Archive. As expected, *HKT1;2* had no counts in any of the datasets, and the patterns of counts of *HKT1;1* and *HKT1;3* were mostly consistent with the microarray gene expression data (Figure 4, Figure S1). In the NO₃⁻ application experiment, *HKT1;6*, *HKT1;7* and *HKT1;8* were very lowly expressed in the 1-month-old root tips of the rootstock Riparia Gloire de Montpellier (*V. riparia*), and they were not expressed in the rootstock 1103 Paulsen (*V. berlandieri* × *V. rupestris*) under any NO₃⁻ treatments (Cochetel *et al.* 2017) (Figure 4A). *HKT1;8* was also very lowly expressed in the flower buds of both clones of Prieto Picudo (*V. vinifera*) (BioProject: PRJNA307079) (Figure 4B), while *HKT1;6* and *HKT1;7* were lowly expressed in the seeds of pea sized berries of the Red Globe (*V. vinifera*) × Crimson Seedless (*V. vinifera*) F1 seeded progeny (BioProject: PRJNA307074) (Figure 4C). In Sauvignon Blanc (*V. vinifera*) whole berries in a nitrogen fertilisation study (Helwi *et al.* 2016), Pinot Noir (*V. vinifera*) leaves in a drought stress study (Zhu *et al.* 2018), and in Cabernet Sauvignon woody stem in a fungal infection study (Massonnet *et al.* 2017), *HKT1;6*, *HKT1;7* and *HKT1;8* were not expressed. As these genes encode Na⁺ transporters, it might be useful in future studies to measure the expression of *HKT1;6*, *HKT1;7* and *HKT1;8* in response to Na⁺ application using RNA-seq. However this was beyond the scope of this study.

VviHKT1;6, VviHKT1;7 and VviHKT1;8 are unlikely to have major roles in long-distance Na⁺ translocation

Transient expression of the HKT allelic variants with C-terminal GFP tags in tobacco epidermal cells was performed. The GFP fluorescence showed that VviHKT1;6B, VviHKT1;7A and VviHKT1;7B all co-localised with the plasma membrane (PM) RFP marker. As VviHKT1;6 and VviHKT1;7 alleles were found to induce large Na⁺ dependant currents in *Xenopus* oocytes (Figure 3), these data suggest that they could participate in Na⁺ uptake into cells where they are expressed.

Conversely, VviHKT1;8A and VviHKT1;8B were localised to the endosomal compartments (Figure 5). VviHKT1;8 alleles conducted relatively small Na⁺ currents in the oocytes. and they were likely to be on the Golgi in plant cells (Figure 5). This aligns with previous findings in rice, where OsHKT1;3 was a Golgi localised Na⁺ transporter that was able to interact with a rice cornichon OsCHIH1 in the ER, and it

was also an inward rectifying Na⁺ transporter in *Xenopus* oocytes (Rosas-Santiago *et al.* 2015). Interestingly as currents were evoked in oocytes following VviHKT1;8 expression it suggests that the protein is functional on the plasma membrane in oocytes despite it not being present on the PM in plants, this is similar to other proteins such as VviCCC (Henderson *et al.* 2015).

Two endosomal compartment localised Na⁺ transporters, AtNHX5 and AtNHX6, were found to affect the plasma membrane to vacuole trafficking (Bassil *et al.* 2011). The *Arabidopsis nhx5 nhx6* double knockout mutant had smaller plant size due to its smaller cell sizes and slower cell proliferation rate; the knock out mutants also displayed high sensitivity to salt stress (Bassil *et al.* 2011). It was observed that the labelling of vacuoles by FM4-64 was delayed in the knockout mutant cells, and a vacuolar destined cargo (carboxypeptidase) was missorted into the apoplast (Bassil *et al.* 2011). It was proposed that the knockout of *AtNHX5* and *AtNHX6* disrupted the vacuolar destined cargo shipping, and the inability of efficient vacuolar Na⁺ sequestration could have led to the Na⁺ sensitivity of the knockout mutants (Bassil *et al.* 2011). This information suggests that the VviHKT1;8 could potentially be important in intracellular cargo transport and Na⁺ partitioning.

Given that *HKT1;6*, *HKT1;7* and *HKT1;8* were very lowly expressed in grapevine root tips, flowers and seeds (Figure 4), it is unlikely that they could have comparable significant roles in whole-plant Na⁺ homeostasis as the *VisHKT1;1* characterised by Henderson *et al.* (2018a). We cannot eliminate the possibility that the grapevine *HKT1;6*, *HKT1;7* and *HKT1;8* proteins are relatively more abundant compared to their gene expression levels, that they are only expressed in certain cell types which are in low numbers, that their expression is only induced in certain growth stages which we have not tested, or are induced by certain stimuli. To determine the *in planta* function of these HKT proteins, *VviHKT* knockout or knockdown mutants could be tested for phenotypes. To test the expression pattern of *VviHKT1;6*, *VviHKT1;7* and *VviHKT1;8* *in planta*, *Arabidopsis* plants could be transformed with the *VviHKT promoter::GUS* or *VviHKT promoter::GFP* constructs to reveal the protein expression patterns, and environmental stimuli could be applied to these plants to test if the expression could be altered.

Acknowledgements

We thank Yu Long (University of Adelaide) for advice on TEVC; Wendy Sullivan (University of Adelaide) for harvesting oocytes and assistance with the grapevine hardwood cuttings; Mandy Walker (CSIRO) for supplying 60 mM NaCl treated Cabernet Sauvignon roots; Jake Dunlevy (CSIRO) and Paul Boss (CSIRO) for supplying grapevine berry skin, seed, tendril and rachis cDNA. Steve Tyerman (University of Adelaide) was the independent advisor. Y.W. was supported by the University of Adelaide (Adelaide Graduate Research Scholarship) and Wine Australia (AGWA Research Supplementary Scholarship (AGW Ph1502)). This research was funded by Australian grape growers and winemakers through their investment body Wine Australia with matching funds from the Australian government (AGW Ph1502).

References

- Bassil, E., Ohto, M.-a., Esumi, T., Tajima, H., Zhu, Z., Cagnac, O., Belmonte, M., Peleg, Z., Yamaguchi, T. and Blumwald, E. (2011) The *Arabidopsis* intracellular Na⁺/H⁺ antiporters NHX5 and NHX6 are endosome associated and necessary for plant growth and development. *The Plant cell*, **23**, 224-239.
- Batistič, O., Sorek, N., Schültke, S., Yalovsky, S. and Kudla, J. (2008) Dual fatty acyl modification determines the localization and plasma membrane targeting of CBL/CIPK Ca²⁺ signaling complexes in arabidopsis. *The Plant Cell*, **20**, 1346-1362.
- Berg, H.W. and Keefer, R.M. (1958) Analytical determination of tartrate stability in wine. I. Potassium bitartrate. *American Journal of Enology and Viticulture*, **9**, 180-193.
- Berthomieu, P., Conéjéro, G., Nublat, A., Brackenbury, W.J., Lambert, C., Savio, C., Uozumi, N., Oiki, S., Yamada, K., Cellier, F., Gosti, F., Simonneau, T., Essah, P.A., Tester, M., Véry, A.-A., Sentenac, H. and Casse, F. (2003) Functional analysis of AtHKT1 in *Arabidopsis* shows that Na⁺ recirculation by the phloem is crucial for salt tolerance. *The EMBO Journal*, **22**, 2004-2014.
- Byrt, C., Xu, B., Krishnan, M., Lightfoot, D., Athman, A., Jacobs, A., Watson-Haigh, N., Munns, R., Tester, M. and Gilliam, M. (2014) The Na⁺ transporter, TaHKT1;5-D, limits shoot Na⁺ accumulation in bread wheat. In *The Plant Journal*.
- Byrt, C.S., Platten, J.D., Spielmeyer, W., James, R.A., Lagudah, E.S., Dennis, E.S., Tester, M. and Munns, R. (2007) HKT1;5-like cation transporters linked to Na⁺ exclusion loci in wheat, *Nax2* and *Kna1*. *Plant Physiology*, **143**, 1918-1928.
- Chin, C.-S., Peluso, P., Sedlazeck, F.J., Nattestad, M., Concepcion, G.T., Clum, A., Dunn, C., O'Malley, R., Figueroa-Balderas, R., Morales-Cruz, A., Cramer, G.R., Delledonne, M., Luo, C., Ecker, J.R., Cantu, D., Rank, D.R. and Schatz, M.C. (2016) Phased diploid genome assembly with single-molecule real-time sequencing. *Nature Methods*, **13**, 1050.
- Cochetel, N., Escudie, F., Cookson, S.J., Dai, Z., Vivin, P., Bert, P.F., Munoz, M.S., Delrot, S., Klopp, C., Ollat, N. and Lauvergeat, V. (2017) Root transcriptomic responses of grafted grapevines to heterogeneous nitrogen availability depend on rootstock genotype. *Journal of Experimental Botany*, **68**, 4339-4355.
- de Loryn, L.C., Petrie, P.R., Hasted, A.M., Johnson, T.E., Collins, C. and Bastian, S.E.P. (2014) Evaluation of sensory thresholds and perception of sodium chloride in grape juice and wine. *American Journal of Enology and Viticulture*, **65**, 124-133.
- Diatloff, E., Kumar, R. and Schachtman, D.P. (1998) Site directed mutagenesis reduces the Na⁺ affinity of HKT1, an Na⁺ energized high affinity K⁺ transporter. *FEBS Letters*, **432**, 31-36.
- Donkin, R., Robinson, S., Sumby, K., Harris, V., McBryde, C. and Jiranek, V. (2010) Sodium chloride in Australian grape juice and its effect on alcoholic and malolactic fermentation. *American Journal of Enology and Viticulture*, **61**, 392-400.
- Fasoli, M., Dal Santo, S., Zenoni, S., Tornielli, G.B., Farina, L., Zamboni, A., Porceddu, A., Venturini, L., Bicego, M., Murino, V., Ferrarini, A., Delledonne, M. and Pezzotti, M. (2012) The grapevine expression atlas reveals a deep transcriptome shift driving the entire plant into a maturation program. *The Plant Cell*, **24**, 3489-3505.
- Garciadeblás, B., Senn, M.E., Bañuelos, M.A. and Rodríguez-Navarro, A. (2003) Sodium transport and HKT transporters: the rice model. *The Plant Journal*, **34**, 788-801.
- Gassman, W., Rubio, F. and Schroeder, J.I. (1996) Alkali cation selectivity of the wheat root high-affinity potassium transporter HKT1. *The Plant Journal*, **10**, 869-852.
- Gong, J.M., Waner, D.A., Horie, T., Li, S.L., Horie, R., Abid, K.B. and Schroeder, J.I. (2004) Microarray-based rapid cloning of an ion accumulation deletion mutant in *Arabidopsis thaliana*. *Proceedings of the National Academy of Sciences*, **101**, 15404-15409.

- Hannah, L., Roehrdanz, P.R., Ikegami, M., Shepard, A.V., Shaw, M.R., Tabor, G., Zhi, L., Marquet, P.A. and Hijmans, R.J. (2013) Climate change, wine, and conservation. *Proceedings of the National Academy of Sciences*, **110**, 6907-6912.
- Hauser, F. and Horie, T. (2010) A conserved primary salt tolerance mechanism mediated by HKT transporters: a mechanism for sodium exclusion and maintenance of high K⁺/Na⁺ ratio in leaves during salinity stress. *Plant, Cell & Environment*, **33**, 552-565.
- Helwi, P., Guillaumie, S., Thibon, C., Keime, C., Habran, A., Hilbert, G., Gomes, E., Darriet, P., Delrot, S. and van Leeuwen, C. (2016) Vine nitrogen status and volatile thiols and their precursors from plot to transcriptome level. *BMC Plant Biology*, **16**, 173.
- Henderson, S.W., Baumann, U., Blackmore, D.H., Walker, A.R., Walker, R.R. and Gilliham, M. (2014) Shoot chloride exclusion and salt tolerance in grapevine is associated with differential ion transporter expression in roots. *BMC Plant Biology*, **14**.
- Henderson, S.W., Dunlevy, J.D., Wu, Y., Blackmore, D.H., Walker, R.R., Edwards, E.J., Gilliham, M. and Walker, A.R. (2018) Functional differences in transport properties of natural HKT1;1 variants influence shoot Na⁺ exclusion in grapevine rootstocks. *New Phytologist*, **217**, 1113-1127.
- Henderson, S.W., Wege, S., Qiu, J., Blackmore, D.H., Walker, A.R., Tyerman, S., Walker, R.R. and Gilliham, M. (2015) Grapevine and Arabidopsis cation-chloride cotransporters localise to the Golgi and trans-Golgi network and indirectly influence long-distance ion homeostasis and plant salt tolerance. *Plant Physiology*.
- Horie, T., Hauser, F. and Schroeder, J.I. (2009) HKT transporter-mediated salinity resistance mechanisms in Arabidopsis and monocot crop plants. *Trends in Plant Science*, **14**, 660-668.
- Horie, T., Yoshida, K., Nakayama, H., Yamada, K., Oiki, S. and Shinmyo, A. (2001) Two types of HKT transporters with different properties of Na⁺ and K⁺ transport in *Oryza sativa*. *The Plant Journal*, **27**, 129-138.
- James, R.A., Blake, C., Byrt, C.S. and Munns, R. (2011) Major genes for Na⁺ exclusion, *Nax1* and *Nax2* (wheat *HKT1;4* and *HKT1;5*), decrease Na⁺ accumulation in bread wheat leaves under saline and waterlogged conditions. *Journal of Experimental Botany*, **62**, 2939-2947.
- Karimi, M., Inze, D. and Depicker, A. (2002) GATEWAY vectors for Agrobacterium-mediated plant transformation. *Trends in Plant Science*, **7**, 193-195.
- Kobayashi, N.I., Yamaji, N., Yamamoto, H., Okubo, K., Ueno, H., Costa, A., Tanoi, K., Matsumura, H., Fujii-Kashino, M., Horiuchi, T., Nayef, M.A., Shabala, S., An, G., Ma, J.F. and Horie, T. (2017) OsHKT1;5 mediates Na⁺ exclusion in the vasculature to protect leaf blades and reproductive tissues from salt toxicity in rice. *The Plant Journal*, **91**, 657-670.
- Larkin, M.A., Blackshields, G., Brown, N.P., Chenna, R., McGettigan, P.A., McWilliam, H., Valentin, F., Wallace, I.M., Wilm, A., Lopez, R., Thompson, J.D., Gibson, T.J. and Higgins, D.G. (2007) Clustal W and Clustal X version 2.0. *Bioinformatics*, **23**, 2947-2948.
- Leske, P.A., Sas, A.N., Coulter, A.D., Stockley, C.S. and Lee, T.H. (1997) The composition of Australian grape juice: chloride, sodium and sulfate ions. *Australian Journal of Grape and Wine Research*, **3**, 26-30.
- Liu, W., Fairbairn, D.J., Reid, R.J. and Schachtman, D.P. (2001) Characterization of two HKT1 homologues from *Eucalyptus camaldulensis* that display intrinsic osmosensing capability. *Plant Physiology*, **127**, 283-294.
- Maas, E.V. and Hoffman, G.J. (1977) Crop salt tolerance - current assessment. *Journal of the Irrigation and Drainage Division*, **103**, 115-134.
- Mäser, P., Eckelman, B., Vaidyanathan, R., Horie, T., Fairbairn, D.J., Kubo, M., Yamagami, M., Yamaguchi, K., Nishimura, M. and Uozumi, N. (2002a) Altered shoot/root Na⁺

- distribution and bifurcating salt sensitivity in Arabidopsis by genetic disruption of the Na⁺ transporter AtHKT1. *FEBS letters*, **531**, 157-161.
- Mäser, P., Hosoo, Y., Goshima, S., Horie, T., Eckelman, B., Yamada, K., Yoshida, K., Bakker, E.P., Shinmyo, A., Oiki, S., Schroeder, J.I. and Uozumi, N.** (2002b) Glycine residues in potassium channel-like selectivity filters determine potassium selectivity in four-loop-per-subunit HKT transporters from plants. *Proceedings of the National Academy of Sciences*, **99**, 6428-6433.
- Massonnet, M., Figueroa-Balderas, R., Galarneau, E.R.A., Miki, S., Lawrence, D.P., Sun, Q., Wallis, C.M., Baumgartner, K. and Cantu, D.** (2017) *Neofusicoccum parvum* colonization of the grapevine woody stem triggers asynchronous host responses at the site of infection and in the leaves. *Frontiers in Plant Science*, **8**.
- Minio, A., Lin, J., Gaut, B.S. and Cantu, D.** (2017) How single molecule real-time sequencing and haplotype phasing have enabled reference-grade diploid genome assembly of wine grapes. *Frontiers in Plant Science*, **8**.
- Minio, A., Massonnet, M., Vondras, A., Figueroa-Balderas, R., Blanco-Ulate, B. and Cantu, D.** (2018) Isoform-scale annotation and expression profiling of the Cabernet Sauvignon transcriptome using single-molecule sequencing of full-length cDNA. *bioRxiv*, 269530.
- Munns, R., Day, D.A., Fricke, W., Watt, M., Arsova, B., Barkla, B.J., Bose, J., Byrt, C.S., Chen, Z.-H., Foster, K.J., Gilliham, M., Henderson, S.W., Jenkins, C.L.D., Kronzucker, H.J., Miklavcic, S.J., Plett, D., Roy, S.J., Shabala, S., Shelden, M.C., Soole, K.L., Taylor, N.L., Tester, M., Wege, S., Wegner, L.H. and Tyerman, S.D.** (2019) Energy costs of salt tolerance in crop plants. *New Phytologist*.
- Munns, R. and Gilliham, M.** (2015) Salinity tolerance of crops – what is the cost? *New Phytologist*, **208**, 668-673.
- Munns, R., James, R.A., Xu, B., Athman, A., Conn, S.J., Jordans, C., Byrt, C.S., Hare, R.A., Tyerman, S.D., Tester, M., Plett, D. and Gilliham, M.** (2012) Wheat grain yield on saline soils is improved by an ancestral Na⁺ transporter gene. *Nature Biotechnology*, **30**, 360-364.
- Naranjo, M.A., Forment, J., Roldan, M., Serrano, R. and Vicente, O.** (2006) Overexpression of *Arabidopsis thaliana* LTL1, a salt-induced gene encoding a GDSL-motif lipase, increases salt tolerance in yeast and transgenic plants. *Plant Cell Environ*, **29**, 1890-1900.
- Neumann, P.M.** (2011) Chapter 2 - Recent advances in understanding the regulation of whole-plant growth inhibition by salinity, drought and colloid stress. In *Advances in Botanical Research* (Turkan, I. ed: Academic Press, pp. 33-48.
- Platten, J.D., Cotsaftis, O., Berthomieu, P., Bohnert, H., Davenport, R.J., Fairbairn, D.J., Horie, T., Leigh, R.A., Lin, H.-X. and Luan, S.** (2006) Nomenclature for HKT transporters, key determinants of plant salinity tolerance. *Trends in plant science*, **11**, 372-374.
- Plett, D., Safwat, G., Gilliham, M., Skrumsager Moller, I., Roy, S., Shirley, N., Jacobs, A., Johnson, A. and Tester, M.** (2010) Improved salinity tolerance of rice through cell type-specific expression of AtHKT1;1. *PLoS One*, **5**, e12571.
- Ren, Z.-H., Gao, J.-P., Li, L.-G., Cai, X.-L., Huang, W., Chao, D.-Y., Zhu, M.-Z., Wang, Z.-Y., Luan, S. and Lin, H.-X.** (2005) A rice quantitative trait locus for salt tolerance encodes a sodium transporter. *Nature Genetics*, **37**, 1141.
- Rosas-Santiago, P., Lagunas-Gómez, D., Barkla, B.J., Vera-Estrella, R., Lalonde, S., Jones, A., Frommer, W.B., Zimmermannova, O., Sychrová, H. and Pantoja, O.** (2015) Identification of rice cornichon as a possible cargo receptor for the Golgi-localized sodium transporter OsHKT1;3. *Journal of Experimental Botany*, **66**, 2733-2748.
- Rubio, F., Gassmann, W. and Schroeder, J.I.** (1995) Sodium-driven potassium uptake by the plant potassium transporter HKT1 and mutations conferring salt tolerance. *Science*, **270**, 1660-1663.

- Sainsbury, F., Thuenemann, E.C. and Lomonosoff, G.P.** (2009) pEAQ: versatile expression vectors for easy and quick transient expression of heterologous proteins in plants. *Plant Biotechnology Journal*, **7**, 682-693.
- Schachtman, D.P. and Schroeder, J.I.** (1994) Structure and transport mechanism of a high-affinity potassium uptake transporter from higher plants. *Nature*, **370**, 655-658.
- Shelden, M.C., Howitt, S.M., Kaiser, B.N. and Tyerman, S.D.** (2009) Identification and functional characterisation of aquaporins in the grapevine, *Vitis vinifera*. *Functional Plant Biology*, **36**, 1065-1078.
- Stevens, R.M., Harvey, G. and Partington, D.L.** (2011) Irrigation of grapevines with saline water at different growth stages: effects on leaf, wood and juice composition. *Australian Journal of Grape and Wine Research*, **17**, 239-248.
- Sunarpi, Horie, T., Motoda, J., Kubo, M., Yang, H., Yoda, K., Horie, R., Chan, W.Y., Leung, H.Y., Hattori, K., Konomi, M., Osumi, M., Yamagami, M., Schroeder, J.I. and Uozumi, N.** (2005) Enhanced salt tolerance mediated by AtHKT1 transporter-induced Na⁺ unloading from xylem vessels to xylem parenchyma cells. *The Plant Journal*, **44**.
- Uozumi, N., Kim, E.J., Rubio, F., Yamaguchi, T., Muto, S., Tsuboi, A., Bakker, E.P., Nakamura, T. and Schroeder, J.I.** (2000) The *Arabidopsis* HKT1 gene homolog mediates inward Na⁺ currents in *Xenopus laevis* oocytes and Na⁺ uptake in *Saccharomyces cerevisiae*. *Plant Physiology*, **122**, 1249-1260.
- Walker, R. and Clingeleffer, P.** (2009) Rootstock attributes and selection for Australian conditions. *Australian Viticulture*, **13**, 70-76.
- Walker, R.R., Blackmore, D., Clingeleffer, P. and Gibberd, M.** (2002) How vines deal with salt. In *Managing Water: Australian Society of Viticulture and Oenology*.
- Walker, R.R., Blackmore, D.H., Clingeleffer, P.R. and Tarr, C.R.** (2007) Rootstock effects on salt tolerance of irrigated field-grown grapevines (*Vitis vinifera* L. cv. Sultana). 3. Fresh fruit composition and dried grape quality. *Australian Journal of Grape and Wine Research*, **13**, 130-141.
- Waters, S., Gilliam, M. and Hrmova, M.** (2013) Plant High-Affinity Potassium (HKT) Transporters involved in salinity tolerance: structural insights to probe differences in ion selectivity. *International Journal of Molecular Sciences*, **14**, 7660-7680.
- Wolkovich, E.M., García de Cortázar-Atauri, I., Morales-Castilla, I., Nicholas, K.A. and Lacombe, T.** (2018) From Pinot to Xinomavro in the world's future wine-growing regions. *Nature Climate Change*, **8**, 29-37.
- Wu, Y., Li, J. and Gilliam, M.** (2019) An R-based web app Smart-IV for automated and integrated high throughput electrophysiology data processing.
- Xu, B., Waters, S., Byrt, C.S., Plett, D., Tyerman, S.D., Tester, M., Munns, R., Hrmova, M. and Gilliam, M.** (2018) Structural variations in wheat HKT1;5 underpin differences in Na⁺ transport capacity. *Cellular and Molecular Life Sciences*, **75**, 1133-1144.
- Zhao, S., Fung-Leung, W.P., Bittner, A., Ngo, K. and Liu, X.** (2014) Comparison of RNA-Seq and microarray in transcriptome profiling of activated T cells. *PLoS One*, **9**, e78644.
- Zhu, K., Wang, X., Liu, J., Tang, J., Cheng, Q., Chen, J.-G. and Cheng, Z.-M.M.** (2018) The grapevine kinome: annotation, classification and expression patterns in developmental processes and stress responses. *Horticulture Research*, **5**, 19-19.

Figures

Figure 1

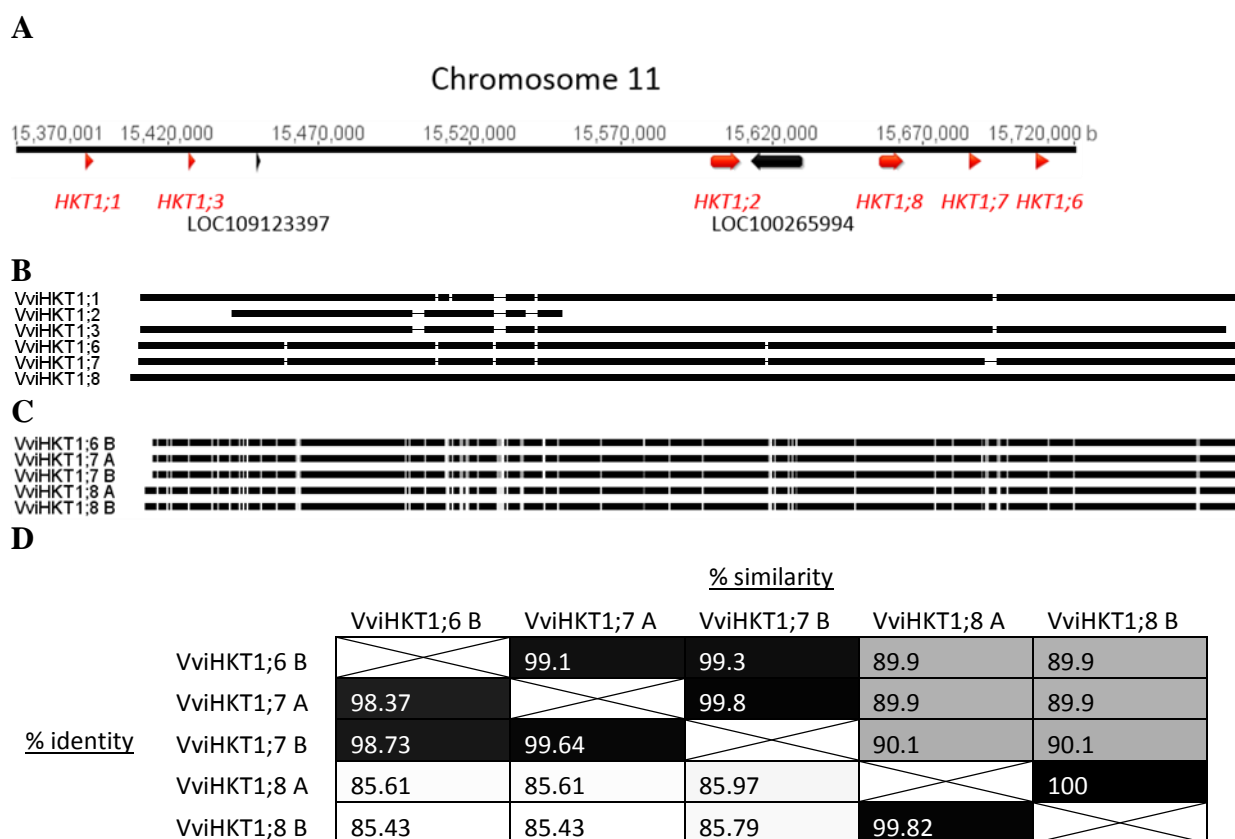


Figure 1. Sequence analysis of the VviHKT1 members. (A) Schematic of the grapevine *NaE* locus on chromosome 11 showing the cluster of six *VviHKT1* genes and two other annotated genes. (B) Schematic translational alignment of HKT proteins from the grapevine PN40024 reference genome. VviHKT1;1, HKT1;3, HKT1;6, HKT1;7 and HKT1;8 are full length HKT proteins while HKT1;2 is truncated. (C) A protein sequence alignment which demonstrates the amino acid sequence similarities of the Cabernet Sauvignon VviHKT1;6, VviHKT1;7 and VviHKT1;8 full length allelic variants. The colours represent 100% similarity (black), 80-100% similarity (dark grey), 60-80% similarity (light grey), <60% similarity (white). (D) The protein identity and similarity among the VviHKT1;6, VviHKT1;7 and VviHKT1;8 allelic variants. Protein alignments were generated using Clustal W (Larkin *et al.* 2007) in Geneious version 8.1.7 with default settings.

Figure 2

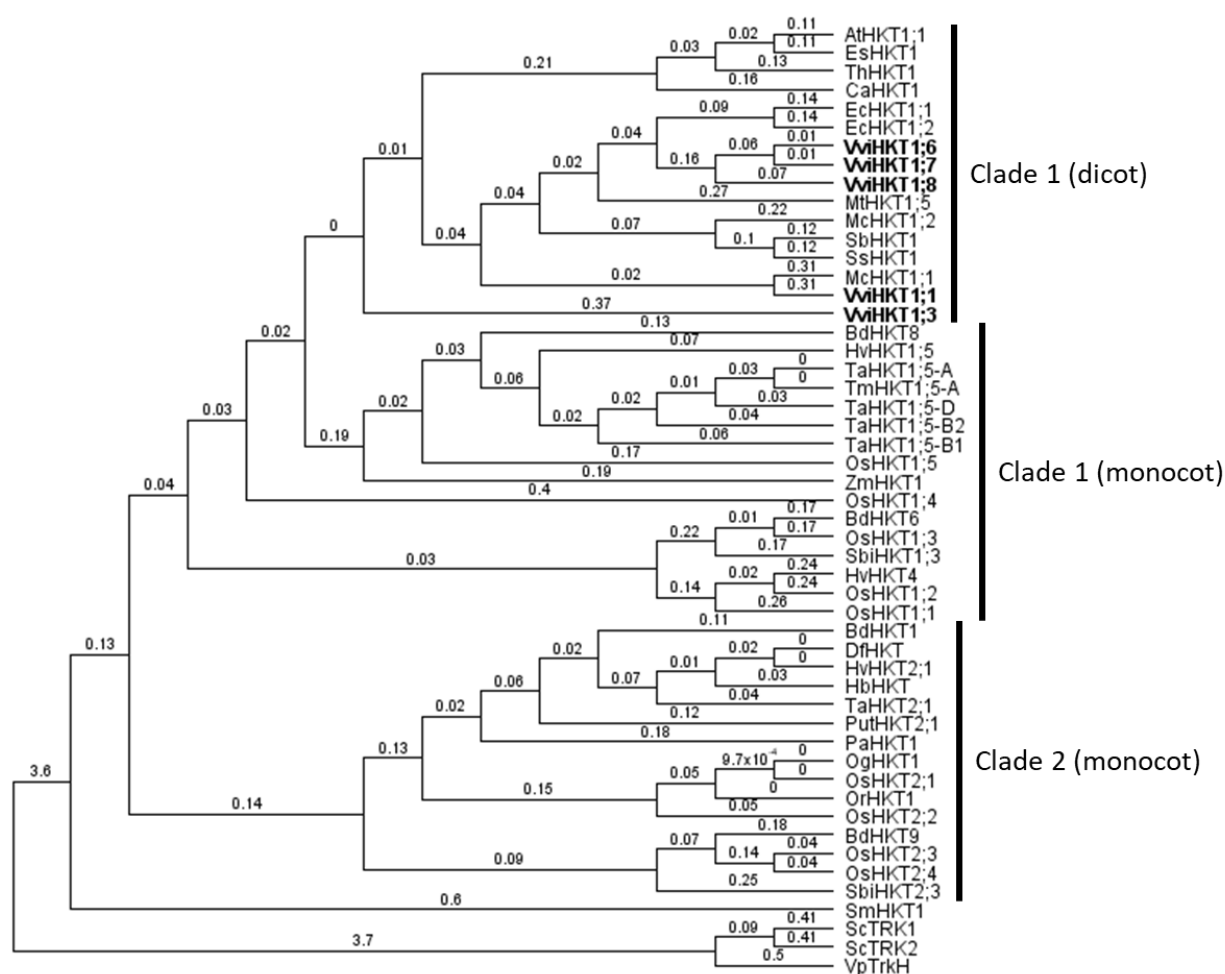


Figure 2: Phylogenetic analysis of full-length VviHKT and other plant HKT proteins, with the moss, yeast and bacteria K^+ and Na^+ transporters as outgroups. Protein alignments were generated using Clustal W (Larkin *et al.* 2007), and the phylogenetic tree was generated using Geneious version 8.1.7 with default settings. HKT1 and HKT2 proteins form two distinct clades as indicated. The VviHKT proteins belong to clade 1 (dicot), and are shown in boldface.

Figure 3

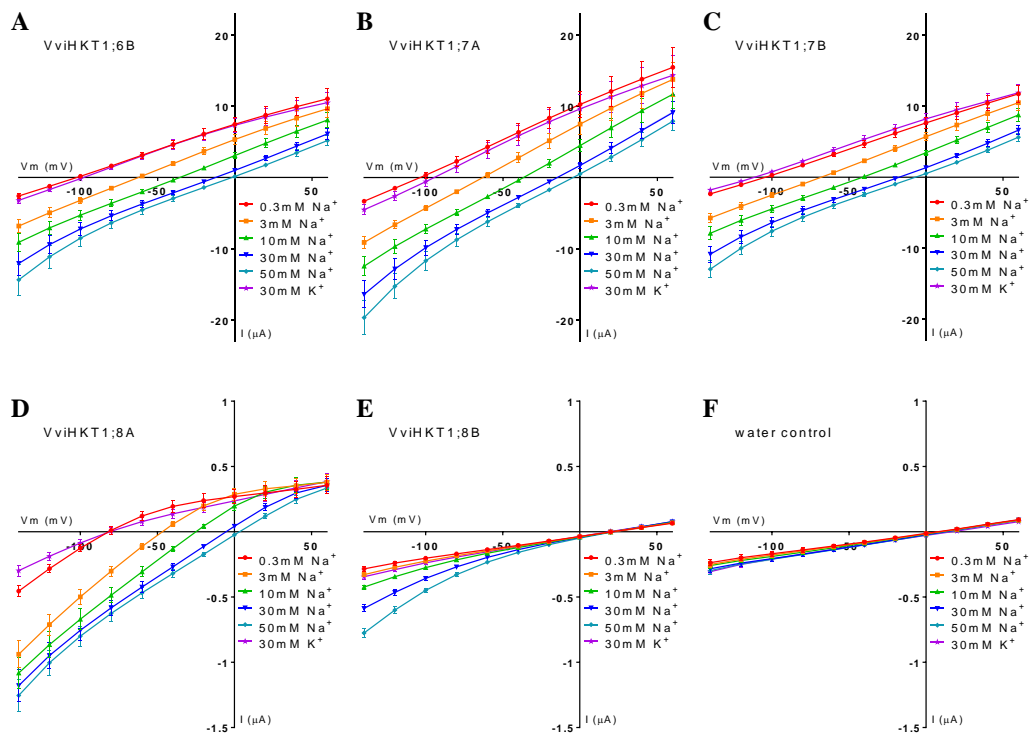


Figure 3: The electrophysiological properties of VviHKT1;6, VviHKT1;7 and VviHKT1;8 allelic variants as determined by two electrode voltage clamping in *Xenopus* oocytes. (A – D) Current-voltage curves of oocytes injected with (A) *VviHKT1;6B*, (B) *VviHKT1;7A*, (C) *VviHKT1;7B*, (D) *VviHKT1;8A*, (E) *VviHKT1;8B* cRNA and (F) water control in solutions containing 0.3 – 50 mM Na⁺ or 30 mM K⁺. Currents were measured two days post-injection of cRNA or water. Data are mean ± SEM (n = 5 – 8 oocytes).

Figure 4

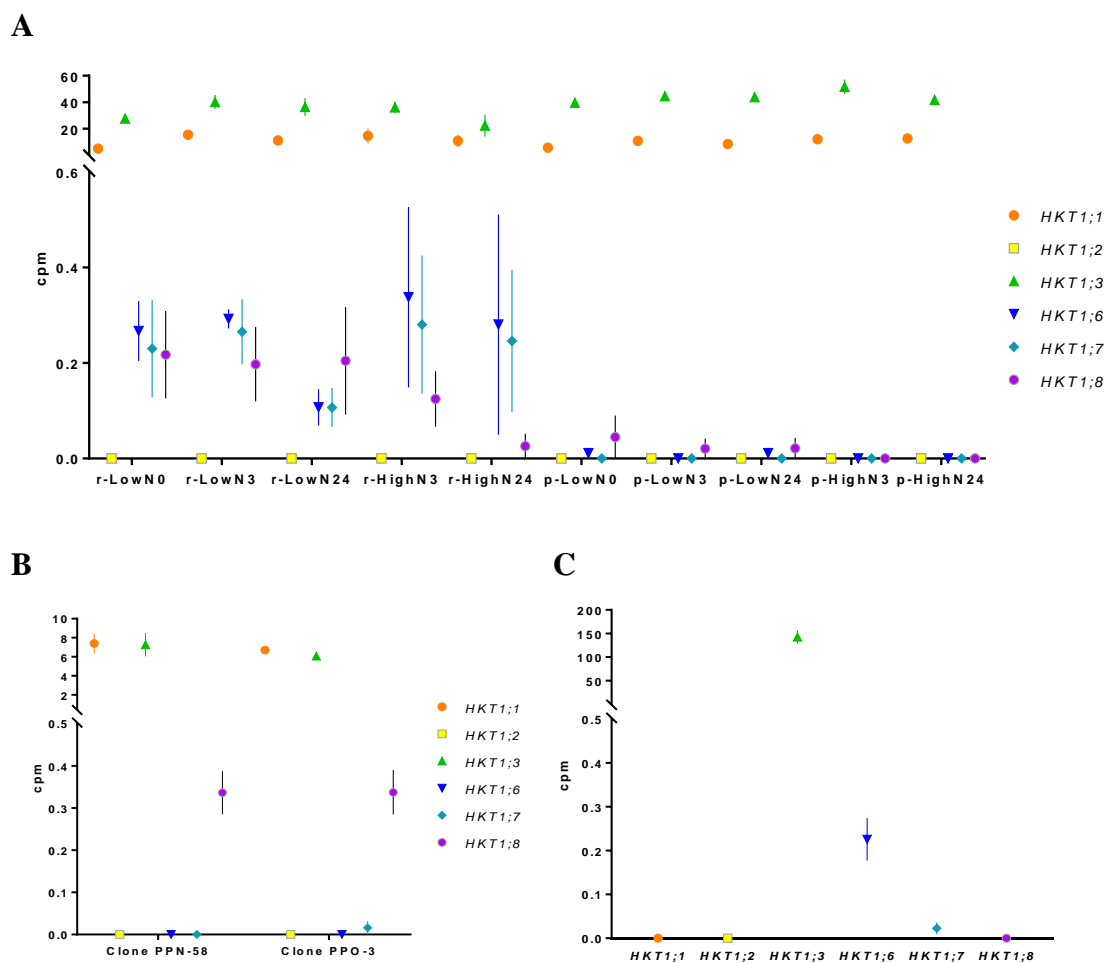


Figure 4: *HKT1;6*, *HKT1;7* and *HKT1;8* were lowly expressed in grapevine root tips, flower buds and seeds. The RNA-seq data of different grapevine tissue types from several projects were normalised and the expression levels of the *HKTs* are presented as counts per million (cpm). (A) The cpm of the *HKTs* in Riparia Gloire de Montpellier (r) and 1103 Paulsen (p) root tips under low (LowN) or high NO_3^- (HighN) treatments; the roots were harvested 0, 3 or 24 hours post NO_3^- treatments (Cochetel *et al.* 2017). (B) The cpm of the *HKTs* in flower buds of two clones of Prieto Picudo (BioProject: PRJNA307079). (C) The cpm of the *HKTs* in the seeds of the F1 seeded progeny of Red Globe \times Crimson Seedless (BioProject: PRJNA307074). Data are mean of multiple biological replicates \pm SEM.

Figure 5

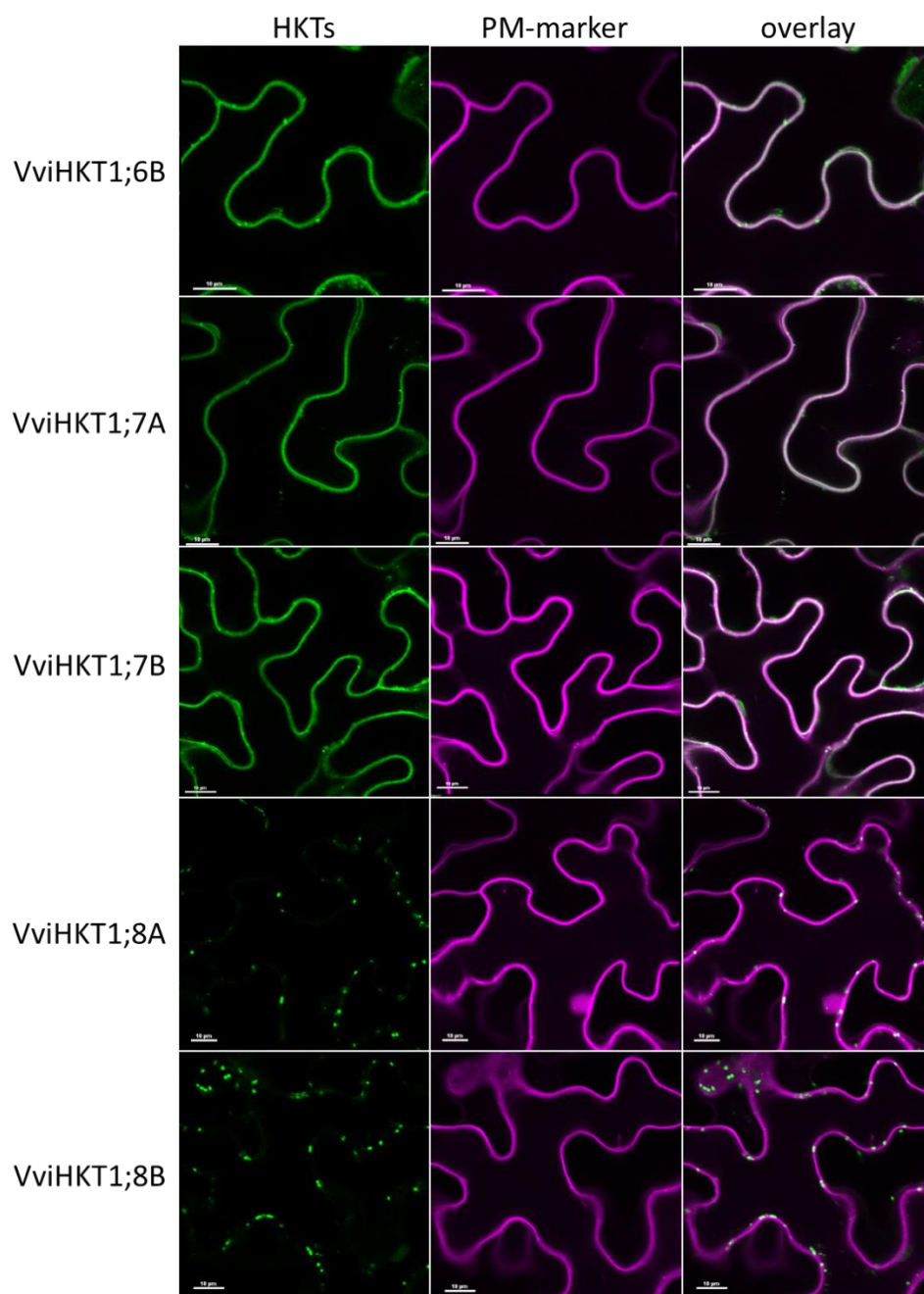


Figure 5: VviHKT1;6 and VviHKT1;7 allelic variants are localised to the plasma membrane, and VviHKT1;8 variants are localised to endosomal compartments. HKT proteins were transiently co-expressed with the PM marker in epidermal cells of *N. benthamiana*. Leaves were co-infiltrated with *A. tumefaciens* strains harbouring C-terminally tagged VviHKTs-GFP (green) and PM marker CBL1n-RFP (magenta). Leaf sections were imaged by confocal laser-scanning microscopy; co-localisation of green and magenta signals appears in white in the right panel. Scale bar = 10 µm.

Supporting information

Figure S1

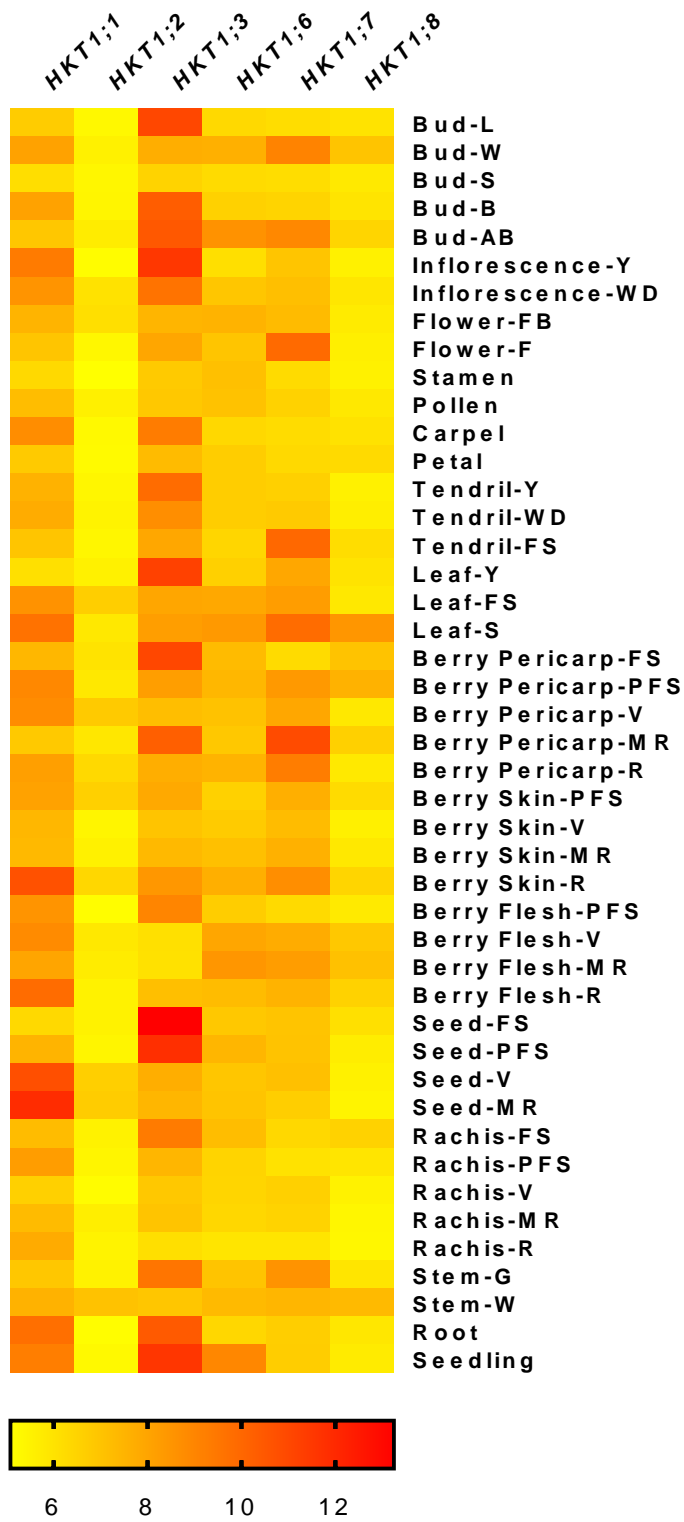


Figure S1: *VviHKT1;6* and *HKT1;7* are most highly expressed in berry pericarp and berry skin, while *VviHKT1;8* is generally lowly expressed in all tested tissue types. RMA-normalized signal intensities were obtained from the microarray gene expression study by Fasoli *et al.* (2012). Data presented in the heat map are the log₂ mean transformed signal intensities of the 4 probes and 3 biological predicates.

Figure S2

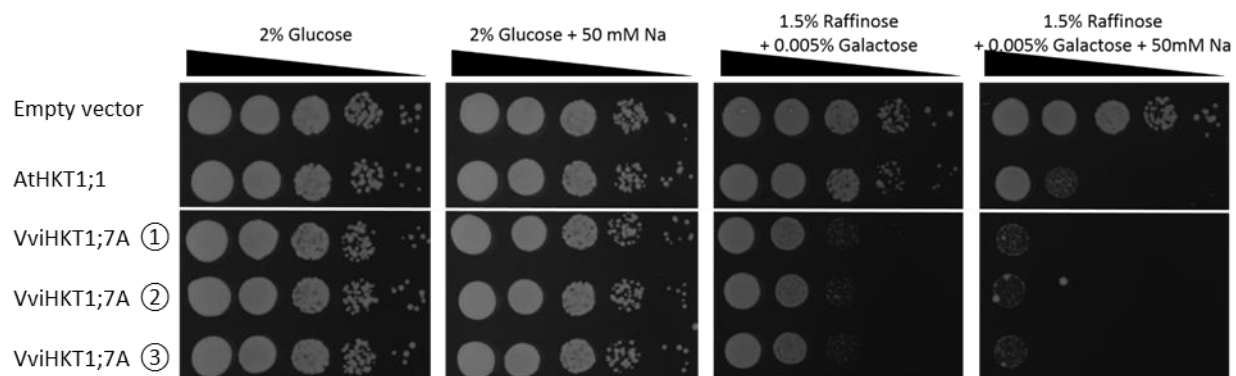


Figure S2: Growth of VviHKT1;7A expressing yeasts were inhibited by 50 mM Na⁺. INVSc2 yeasts (MATa, *his3Δ-1*, *ura3-52*) were transformed with pYES-DEST52 empty vector (negative control) or the same vector containing either *AtHKT1;1* (positive control) or *VviHKT1;7A*. SD (-Uracil) phytigel (0.3%) media plates containing either D-glucose (control) or D-galactose (induction) with or without 50 mM NaCl were used as growth media. Yeasts from overnight liquid cultures were diluted to OD₆₀₀ = 1, and then four 1 in 10 serial dilutions of each strain were made; 5 μL of each dilution were spotted onto each plate. Plates were incubated at 28 °C for 3 days. The ①②③ symbols represent different individual transformation events.

Table S1: Primers used in this study for molecular cloning and allele construction.

Gene	Direction	Sequence (5'-3')
<i>VviHKT1</i> ;6 and <i>VviHKT1</i> ;7	Forward	ATGATGAACTCTGCTAGTTTC
<i>VviHKT1</i> ;8	Forward	ATGAAATTAAGATGATGATCTCTGCTAGTTTCGT
<i>VviHKT1</i> ;6 B	Reverse (with stop codon)	TTATAAGAGCCTCCATGCTCT
	Reverse (no stop codon)	TAAGAGCCTCCATGCTCTAC
<i>VviHKT1</i> ;7 and <i>VviHKT1</i> ;8	Reverse (with stop codon)	TTACAAGAGCTTCCATGCTC
	Reverse (no stop codon)	CAAGAGCTTCCATGCTCTAC
<i>VviHKT1</i> ;6 B allele mutagenesis from <i>VviHKT1</i> ;7 A (In-Fusion fragment 1 cloning)	Forward	AATTCGACCCAGCTTTCTTGTA
	Reverse	CTAGAAAGCAGATTGATCGGC
<i>VviHKT1</i> ;6 B allele mutagenesis from <i>VviHKT1</i> ;7 A (In-Fusion fragment 2 cloning)	Forward	GATTGGATTTCTGCACTTGCTT
	Reverse	TGGGTAGGAAAGAAGTATAAGGAG
<i>VviHKT1</i> ;6 B allele mutagenesis from <i>VviHKT1</i> ;7 A (In-Fusion fragment 3 synthesized)	Forward	CAATCTGCTTTCTAGTCTCATCCTTTTATCGTTTCGT AATTCTCCGGTTCAACACTTTCTCGGTTACAGCTTTGT TATTTCCCTGTGCTTTTCATTTACAGGATTCTGGATCC TCAAGGCTTTGAAGCCGAGGACTCCTTTGAGGCCTA GAAACTTGGATTTGTTCTTACCTCTGTGTCCGGCAG CTACTGTTTCTAGCATGTCCACAGTGGAAATGGAGG TTTTTTCCAACAACCAGCTTCTGATTTTGACTCTTCT AATGTTTGTAGGCGGAGAGATTTTCACTTCGATGGT AGAACTCCAGTTGTGGAGGTCTAAACTTAAGAAACC ATTGATAGCAGAAAACCAAGTCAATTCGGTTAGTAA CAATAGCAGTGCTCCTCCGGATCCTAGAAATCCTTT TGGTCAATTTGAGTTGCGCGTGGTAACGGTTCTTAG TATGAGTAATTCAACACTAGAACTGATGAGGTTCA GACCCAAATTGAGGGCCGAACCTAAGTCG
<i>VviHKT1</i> ;6 B allele mutagenesis from <i>VviHKT1</i> ;7 A (In-Fusion fragment 4 synthesized)	Forward	GAGGGCCGAACCTAAGTCGTTGTCTAGTGAGTCTCTC AAATACCATTCCATCAAATTTTTAGGCTTTGTGGTG ATGGGGTACCTTGTAGTAGTTCATGTCCTTGGAGTC ACACTAGTGTCTGCTTACATAGCCCTTGTGTCAAGT GCGAGAGATGTAATAAGCAAAGGGCCTCAATCT CTTCACCTTTTCACTCTTACCACAGTATCAACTCTT GCAAGTTGCGGTTTTGTCCCGACAAATGAAAACATG ATAGTGTTGAGCAAGAAGTCAAGGCTGCTTCTTATC ATCATTCTCAGGTCCTTCTCGGGAACACCTTGTTC CCTCTTGCTGCGTTTTTCCATATGGACTCTGGGGAA GTTTAAGAAAGTGGAGTCCAATTACCTGTTGACCAA CACAAGGGTGATTGGATTTCTGCACTT
<i>VviHKT1</i> ;6 B allele mutagenesis from <i>VviHKT1</i> ;7 A (In-Fusion fragment 5 synthesized)	Forward	CTTCTTTTCTACCCATAAAAAGGTGATGAACAGTCTT CAGAAATATGCAATGGAGGAAGGAAGAGAAGAAG GGGAAAGATTGTGGAGAATTTAATATTCTCACAAC ATCGTACCTGGCCATCTTCATCATCCTTATCTGCATA ACGGAGAGGAAAAAGATGAAAGATGATCCTCTCAA CTTCACTGTGTTAAATATTGTGATAGAAGTAATCAG TGCCTATGGAATGTTGGGTTTACAGCAGGCTACAG TTGTGAACGGTTGTTGAAACCTGATAGTAGCTGCCA AAGTAAATGGTTTGGATTCTCGGGAAAATGGAGTG ATGAGGGGAAAATAATTCTCATTTTTGTTCATGTTTTT

		TGGAAGACTAAAGAAGTTTAATATGGATGGAGGTA GAGCATGGAGGCTCTTATAA
<i>VviHKT1;7 B allele</i> <i>mutagenesis</i> from <i>VviHKT1;7 A</i> (In-Fusion fragment 1 cloning)	Forward	CCTACCCATAAAAGGTGATGAACAGTCTTCAGA
	Reverse	CATCTTTTTCTCTCCGTTATGCAGATAAG
<i>VviHKT1;7 B allele</i> <i>mutagenesis</i> from <i>VviHKT1;7 A</i> (In-Fusion fragment 2 cloning)	Forward	GAGAGGAAAAAGATGAAAGATGATCCTCTCAAC
	Reverse	CCTTTTATGGGTAGGAAAGAAGTATAAGGAG
<i>VviHKT1;8 B allele</i> <i>mutagenesis</i> from <i>VviHKT1;8 A</i>	Forward	GAACTCAAAGCATACAGGCGAAACAATT
	Reverse	GTATGCTTTGAGTTCACGCTCTGGAAC

Chapter 6: An R-based web app Smart-IV for automated and integrated high throughput electrophysiology data processing

Yue Wu^{1, *}, Junda Li^{1, *†}, Matthew Gilliam^{1, †}

¹ ARC Centre of Excellence in Plant Energy Biology, School of Agriculture, Food and Wine, University of Adelaide, Glen Osmond, South Australia 5064, Australia

* These authors contributed equally

† Correspondence should be addressed to:

Mr Junda Li

Email: imlijunda@gmail.com

Phone: +61 4 4808 1973

Professor Matthew Gilliam

Email: matthew.gilliam@adelaide.edu.au

Phone: +61 8 8313 8145

Email addresses:

YW: yue.wu@adelaide.edu.au

JL: imlijunda@gmail.com

MG: matthew.gilliam@adelaide.edu.au

Running title: Smart-IV, a web app for automated electrophysiology data processing

Key words: electrophysiology, TEVC, IV, high-throughput data processing, R web app

Smart-IV, automatic I-V sampling, R package abftools, *Xenopus* oocyte

Statement of Authorship

Title of Paper	An R-based web app Smart-IV for automated and integrated high throughput electrophysiology data processing
Publication Status	<input type="checkbox"/> Published <input type="checkbox"/> Accepted for Publication <input type="checkbox"/> Submitted for Publication <input checked="" type="checkbox"/> Unpublished and Unsubmitted work written in manuscript style
Publication Details	Wu, Y., Li, J. and Gilliam, M. (2019) An R-based web app Smart-IV for automated and integrated high throughput electrophysiology data processing.

Principal Authors

Name of Principal Author (Candidate)	Yue Wu	
Contribution to the Paper	Conceived the project, designed the data processing work flow, tested the R package abftools and the R Shiny web app Smart-IV, compared the TEVC IV data extracted by Smart-IV and the Clampfit method, and wrote the manuscript.	
Overall percentage (%)	40	
Certification:	This paper reports on original research I conducted during the period of my Higher Degree by Research candidature and is not subject to any obligations or contractual agreements with a third party that would constrain its inclusion in this thesis. I am the primary author of this paper.	
Signature		Date 02.07.2019

By signing the Statement of Authorship, each author certifies that:

- i. the candidate's stated contribution to the publication is accurate;
- ii. permission is granted for the candidate to include the publication in the thesis; and
- iii. the sum of all co-author contributions is equal to 100% less the candidate's stated contribution.

Name of Principal Author	Junda Li	
Contribution to the Paper	Conceived the project, developed the R package abftools, developed the Smart-IV web app, and wrote the manuscript.	
Signature		Date 02.07.2019

Co-Author Contributions

Name of Co-Author	Matthew Gilliam
-------------------	-----------------

Contribution to the Paper	Supervised the research and assisted in editing the manuscript.		
Signature		Date	01.07.2019

Abstract

Data processing of electrophysiology data can be repetitive and time consuming. We have developed Smart-IV, a sophisticated R Shiny based application to streamline common electrophysiology current (I) versus voltage (V) data processing tasks including (i) exploratory data analysis, (ii) automatic IV relationship analysis and generation, (iii) one-click figure and data export and (iv) programmatic API for advanced users. Using Smart-IV, the default IV data analysis workflow of 100 files takes as few as 15 seconds, whereas comparable manual analysis would take many hours. Standard outputs include standard and baseline subtracted IV relations, conductance (G), membrane capacitance, GV relations, specific I or G normalised to membrane capacitance. We also demonstrate that Smart-IV produced graphs comparable to existing packages that require manual data input. At present this workflow is optimised for use with Molecular devices (Axon, *.ABF) data files, but future versions could also use Heka data files (*.DAT). Further future upgrades could include specific analysis tools for voltage ramp protocols and single channel analysis.

Background

Electrophysiological data analysis often requires repetitive and tedious steps in order to present averaged data for publications or reports. Voltage clamp methods including patch clamp and electrode voltage clamp (especially Two Electrode Voltage Clamp, TEVC) are commonly used for the functional characterisation of membrane ion channels. The information desired from analysis of the data is usually the substrate and/or the kinetics of the channel. Besides the non-gated channels, ion channels can be gated by the membrane voltage (V_m), by their binding ligands (ions, lipids, nucleic acids or other chemicals,), or both (reviewed in Guan *et al.* 2013). The TEVC technique was introduced by Hodgkin, Huxley and Katz (1952), which enabled the control of both V_m of the cell and the extracellular chemical composition, the patch clamp technique was introduced by Neher and Sakmann (Hamill *et al.* 1981, Sakmann and Neher 1984). Both of these teams have garnered the Nobel Prize for physics. When performing TEVC, two microelectrodes are inserted into a cell submerged in a buffer; one electrode injects current into a cell, while the other monitors the actual voltage. Both electrodes are connected to an amplifier which records the signals, evaluates the difference between the user defined command V_m and the actual voltage, and sends the feedback to the current electrode to achieve the command V_m . Patch clamp electrophysiology is a modification of this technique that allows current and voltage to be controlled by the one electrode across a patch of membrane or a whole cell adhered to a capillary. By recording and analysing the current readings, the electrical responses of the cell under different voltages and chemical treatments can be revealed.

The *Xenopus laevis* oocyte system is widely used for TEVC. The use of *Xenopus laevis* (African frog) oocytes for the heterologous expression genes was first published by Miledi *et al.* (1982). It became a popular single cell system for the electrophysiological studies, as it is large in size, short in endogenous channels, easy for injection and reliable in expressing the channel proteins on the plasma membrane (Papke and Smith-Maxwell 2009, Sakmann and Neher 1995). Originally, mRNA needed to be extracted from the tissue of interest for oocyte injection and gene expression (Miledi *et al.* 1982); later with the cloning technique, RNA can be synthesised from the cloned gene of interest for expression in the oocytes. Patch clamp electrophysiology can be applied to isolated cells with membranes exposed to the bathing media and patch pipette. Breaking

the membrane beneath the sealed pipette allows users to control the solutions either side of the membrane and therefore more accurately control the electrochemical gradients across them. Patch clamping can gain IV data equivalent to TEVC when in the whole cell mode but also study the activity of single proteins in isolated membrane patches.

Electrophysiological data is commonly digitised and acquired using proprietary computer software such as Clampex (Molecular Devices) or Patchmaster (HEKA Elektronik); free softwares also exist such as Strathclyde Electrophysiology Software (University of Strathclyde, Glasgow). The acquired data is usually a 3-d array of two channelled (one for voltage and one for current) multi-episodic time series data, and usually stored in a proprietary format. Each 3-d array is commonly viewed as a set of the current-time and voltage-time waveforms. Despite using the waveforms directly to present the data, the current (I), voltage (V) and time features of the data can be extracted and presented in different ways for demonstration of the electrophysiological characteristics of the samples. One commonly used protocol for studying the voltage dependant currents through the membrane of the sample is the multi-episodic fixed length voltage step protocol; the current-voltage (IV) plot is a standard type of its data presentation using the I and V data sampled from a certain time or time interval in the voltage step epoch using TEVC. This type of plot is used in many studies for the intuitive presentation of the voltage dependant current changes, and the shifts in reversal potential in different perfusion buffers (e.g. Cubero-Font *et al.* 2016, Munns *et al.* 2012, Preuss *et al.* 2010, Ramesh *et al.* 2015).

The conventional work flow for analysis of acquired IV data usually involves opening and displaying the data in another proprietary software package, manual positioning of data sampling cursors to the desired time points, exporting the cursor values to the results window, collecting results and formatting the data in yet another software for publication. Since this process allows one file to be processed at a time only, although not overly complicated, when dealing multiple data files, this process can be tediously repetitive and time consuming. A robust batch processing protocol become immediately critical in this situation.

Naïve batch processing approach of this type of data is available in some softwares, most commonly achieved by manually fixing the IV sampling cursors at the same time interval for the whole batch of files. One example, the Clampfit software in pClamp 11

(Molecular Devices), which processes the data acquired in Clampex in Axon Binary Files (ABF) format, reduces repetitiveness by allowing users to apply a same set of cursor positions and calculate measurements for multiple files. However, during IV acquisition, it is common that the same cursor positions may not be suitable for all data files, especially when actual V_m deviate from command V_m within the selected cursors or when current traces are not stable. As a result, it is likely that even using the macros users still need to inspect the voltage and current waveforms of each file to fine tune the cursors accordingly. Additionally, sorting and grouping multiple data files can only be performed manually or using the data file index (DFI) file created in Clampex. However, the file identifiers in DFI can only be numeric, which can be unintuitive at times, and grouping by one or multiple factors is not possible. Moreover, the Clampfit macro feature is only available in pClamp 11 which is blocked by an upgrade paywall from previous users.

Beside Clampfit, there are a few open-sourced software packages available to batch process ABF data, most notable the MATLAB library `abfload` by Forrest Collman, R package `readABF` by Stanislav Syekirin and `abf2` by Matthew Caldwell, and Python library `pyABF` by Scott W Harden. These software packages provide functionality to read ABF files to memory thus allowing further data process using specific programming languages.

If a technical middle-ground can be achieved, this should provide an interactive, integrated and high throughput experience for all users, while still maintaining a programmable interface for advanced users to implement specialised protocols for specific needs. Thus we developed an R (R Core Team 2019) based application, Smart-IV, which automates electrophysiological IV data analysis and visualisation that requires no coding experience, and the underlying R package `abftools` for programmers. Smart-IV is able to export IV data of 100 ABF files within 15 seconds in actual operations. To demonstrate that the automatic IV analysis can produce reliable IV data, the ABF data from the TaHKT1;5-D TEVC experiment (Henderson *et al.* 2018a) is processed again using Smart-IV and we are able to show that the Smart-IV exported IV data produced nearly identical plots when compared to data we extracted using Clampfit manually (Henderson *et al.* 2018a).

TEVC Experiments

We used the fixed length voltage step TEVC data from the grapevine VviNPF2.1 and VviNPF2.2 expressing *Xenopus laevis* oocytes (Wu *et al.* 2019a) to demonstrate the use of Smart-IV. Oocyte TEVC data were recorded using an Oocyte Clamp OC-725C amplifier (Warner Instruments), digitised using an Axon Digidata 1400A (Molecular Devices) and the software Clampex 10.2 (Molecular Devices). Gene expressing oocytes and the water injected negative control oocytes were perfused with a basal buffer for current recording, which contained 6 mM Mg gluconate, 1.8 mM Ca gluconate and 10 mM MES; Cl⁻ and NO₃⁻ buffers were made by supplementing the basal buffer with 50 mM NM-D-G Cl or NM-D-G NO₃. The pH of each solution was adjusted to 5.5 using tris base or MES, and the osmolality was adjusted to 230 mOsm/kg using d-mannitol. The voltage step protocol was set with a holding potential of -40 mV for 300 ms and 300 ms either side of stepwise pulses from +80 mV to -120 mV in 20 mV decrements for 550 ms. Data were in ABF2 format. This experiment aimed to find out the Cl⁻ and NO₃⁻ permeability of VviNPF2.1 and VviNPF2.2 when expressed in the oocytes.

The TEVC data from the TaHKT1;5-D experiment in the study of Henderson *et al.* (2018a) was used to compare the Smart-IV extracted data to the published conventionally extracted data. *Xenopus* oocytes were injected with cRNA encoding TaHKT1;5-D, TaHKT1;5-D S506R or water (negative control). Oocyte TEVC data was recorded as described for the VviNPF experiment. Oocytes were perfused with a 0 mM Na⁺ basal buffer for current recording, which contained 6 mM MgCl₂, 1.8 mM CaCl₂ and 10 mM MES; Na⁺ buffers were made by supplementing the basal buffer with 3 or 30 mM Na⁺-gluconate. The pH of each solution was adjusted to 5.5 using Tris-base, and the osmolality was adjusted to 230 mOsm/kg using D-mannitol. The voltage step protocol was set with a holding potential of -40 mV for 300 ms and 300 ms either side of stepwise pulses from +60 mV to -140 mV in 20 mV decrements for 500 ms. Data were saved in ABF files. When processing the data using abftools, TaHKT1;5-D was abbreviated as “WT”, TaHKT1;5-D S506R was abbreviated as “SR”, and the water control was abbreviated as “H2O” in the index; “0”, “3” and “30” represent 0 mM, 3 mM and 30 mM Na⁺ buffer respectively. The aim of this experiment was to compare the rectification characteristics of Na⁺ currents through TaHKT1;5-D and its mutant, and to determine whether R506 is the key amino acid residue which causes inward

rectification of Na⁺ transport. The findings improved the understanding of the key amino acid residues for the rectification property of the HKT proteins.

Smart-IV: overview

Data management. A working folder (Figure 1) is required by Smart-IV. A working folder for Smart-IV should contain (i) a Comma Separated Values (CSV) data index file `index.csv`, which can be constructed using software such as Microsoft Excel and Google Sheets, and (ii) an “abf” subfolder storing all related ABF files. The only requirement for `index.csv` is that ABF file names must be in the first column. All other columns are recognised as potential grouping factors (for example: sample numbers, genotypes, perfusion buffers, pre-treatments, resting V_m , etc.). A demonstrative `index.csv` is shown in Table 1.

Loading and grouping data. Users can load a working folder to Smart-IV in the “Index” section by clicking on the “Load Working Folder” button (Figure 2A). A table of loaded data is shown in main panel on the right and users can select grouping factors using the “Group by” selection box on the left panel (Figure 2B – C). As shown in Figure 2B, “Gene” and “Buffer” are the selected grouping factors among all possible factors. It is also possible to preview individual waveform by selecting an entry in the table (Figure 2D), and to filter out unneeded data using the filter feature (Figure 2E).

Automatic IV sampling interval. One of the major steps in TEVC IV analysis is selecting proper sampling time intervals in the recorded data for IV plot presentation. Smart-IV performs this step automatically yet provides flexible interval search criteria controls for users. Users can find relevant settings in the “Interval & Preview” section (Figure 3) and change these settings per group or globally by applying the “Apply Interval Settings Globally” switch. In addition to automatic interval search method, users are also given the freedom to apply a fixed interval by switching “Interval Selection Method” from “Auto” to “Fixed” (Figure 3A, D & E), or by turning on the “Preview Waveform” switch and dragging the desired interval on the specific waveform directly (Figure 3B).

Interactive IV preview. On the top right panel of the “Interval & Preview” section, there is an interactive IV traces area, which shows the IV trace of each entry of the selected group (Figure 3C). Users can zoom, pan, read/compare data points and even save the plot directly on the IV preview. Since the IV relationship is often the focus of electrophysiological data processing, and it is sensitive to data treatment methods; the

IV preview is made “reactive” and is able to reflect changes users have made in real time. This character is especially helpful in exploratory data analysis stage. As an example shown in Figure 3C, an abnormal data entry ID “19214002” can be identified immediately, allowing users to identify problems efficiently.

Realtime baseline subtraction. Another frequently used step in IV analysis is baseline subtraction. Smart-IV provides two ways to subtract baseline: (i) subtracting a baseline calculated by a shape-preserving baseline function of a selected episode (“Episode”) (Figure 3F) and (ii) subtracting a baseline calculated from a holding epoch of each episode (“Holding Epoch”) (Figure 3G). The results of baseline subtraction can vary a lot depending on the selected holding epoch/episode. Fortunately, IV preview also tracks changes made to baseline subtraction so user can also optimise these settings judging from the IV preview plot visually. The example shown in Figure 4 demonstrates the effects of the different baseline subtraction algorithms. Since the IV and waveform previews are updated in real time, users can adjust and optimise settings accordingly with visual hints. For time dependant waveform data, the “Holding Epoch” subtraction function can be used to normalise the data in the IV sampling interval to the values in a user selected time point.

Programmatic approach. The underlying package of Smart-IV, *abftools*, provides an even more flexible programmatic approach for exploratory data analysis. The highlighted functions are *abf_plot_td()* and *abf_plot_cd()*, which stand for plotting an ABF object in time domain (channel vs time) and channel domain (channel vs channel) respectively. These two functions transform the 3-d ABF data into a *ggplot* object when provided with a mapping or sampling function. For example, users can use *abf_plot_cd()* along with a mapping function *deriv()*, which calculates first derivatives (slope); and the output will become a conductance vs voltage plot, since the slope of current with regard to voltage is conductance, and this is exactly how conductance plot is implemented in Smart-IV. For another example, we assume that a user wishes to observe the maximum current of every 100 data points for every sweep of an “ABF” object. All the user has to do is calling *abf_plot_td()* with *sample_ratio=100* and *sample_func=“max”*, which tells *abf_plot_td()* to sample data every 100 points and use function *max()* on those sampled points then finally plot the results in time domain.

These two functions together provide a rapid solution to visualise ABF data since users can now focus on “what to plot” instead of worrying about “how to plot”.

Smart-IV: automatic IV analysis

Aggregated IV plotting. In usual cases, the default settings of Smart-IV are robust enough to generate reliable aggregated IV plots for selected grouping factors. After loading a working folder and selecting the grouping factors, users can directly jump to the “IV Plots” section to view and modify the aggregated IV graphs. IV traces of different groups can be arranged in the same graph by selecting the grouping factor in the “Plot by” list; variables are automatically grouped and combined accordingly, and no manual intervention is needed (Figure 5). The “Plot Type” can be switched in the left panel (Figure 5A). Currently IV (current vs voltage), GV (conductance vs voltage) and their specific versions (current/conductance density) are the available plotting types. The conductance is calculated by the first order derivatives from the piecewise cubic splines fitted to the original IV data points. Just like the IV preview in “Interval & Preview” section, the aggregated IV plots are also interactive and plotted in real time.

Specific current/conductance. The specific current/conductance (current/conductance density) is calculated by dividing current/conductance by the membrane capacitance. Membrane capacitance is commonly measured in patch clamping but less often in TEVC. However, membrane capacitance is useful for normalising current magnitude to membrane area as membrane area contributes to membrane capacitance (Liu 2016, Sakmann and Neher 1995). Smart-IV is able to automatically identify a membrane test pulse and calculate membrane conductance from the pulse. When such membrane test pulse is not found and specific current/conductance is still requested by the users, it exploits the Vcmd since the stepped voltage epochs can also be viewed as “membrane test pulses” and Smart-IV derives membrane capacitances from the charging current of those epochs.

Subtract control. Control subtracting (blanking) can be simply achieved by turning on the “Subtract Control” switch and selecting proper blanking variable in the “Subtract by” and “Control” lists (Figure 6). In Figure 6, the negative control “Gene” “H2O” was selected, then it was subtracted from all the corresponding data points, and the SEMs were re-evaluated.

Programmatic approach. When using the abftools programming interface for aggregated I-V analysis, the highlighted functions are *IGVSummary()*, which calculates

average current, conductance and voltage of multiple ABF objects, and *SpIGVSummary()*, which in addition to current, conductance and voltage, also reports their densities. Internally these functions are able to identify units correctly and select proper unit in the report. Moreover, abftools borrows the map-reduce paradigm to achieve consistent data processing logic across all protocols, which greatly simplifies data aggregation when dealing with multiple ABF data. Please see the details discussed in “Methods and Implementation” section.

Smart-IV: one-click data export

The extracted and analysed IV data can be exported into CSV files in the “Export Data” section (Figure 7) for further data processing using compatible softwares. Two types of data can be exported depending on the users’ preferences. When “IV Summaries” is selected, the aggregated current, conductance and voltage data of each group will be exported (Table 2A), as well as a “long” format file containing all aggregated IV data “long-iv.csv” that can be easily transformed to a pivot table for further data analysis. When “IV Individual” is selected, the extracted current, voltage, conductance values of every individual sample will be exported (Table 2B). Users are also able to determine whether to include current and conductance density using the “Include Specific Properties” switch. Depending on whether “Subtract Baseline” and “Subtract Control” are applied, the exported results may differ. Users can find the exported data in the “export” subfolder in the working folder.

Results and discussion

Smart-IV generates reliable IV output

When manually extracting IV data from waveforms acquired with Clampfit, it is expected that the values obtained from two extraction runs will not be identical, as it is unlikely that the IV sampling cursors can be placed at the exact same position in two different runs. Likewise, we do not expect that the I and V values acquired from ABF files using Smart-IV will be identical to the manually acquired values. Instead, we aimed to test if the automatically and manually acquired data similar enough to lead to the same conclusion.

To address this question, the I-V data of the TaHKT1;5-D expressing oocytes extracted by the auto interval search method in Smart-IV was compared to the data we manually extracted using Clampfit in the study of Henderson *et al.* (2018a). The IV plots were generated in GraphPad Prism (GraphPad Software, Inc.), and we are able to see a near perfect overlap of the two IV graphs (Figure 8). It is clear that the Smart-IV acquired IV data reveals the same features as the conventionally acquired data. ABF data from the VviNPF2.1 and VviNPF2.2 experiment was also run through Smart-IV and manual data extraction (Figure S1). Again, when comparing the results from the two methods, the same conclusion can be made that they are essentially identical. However, Smart-IV took a fraction of the time to implement (e.g. 5 to 15 min, compared to 1 to 3 hours for fully manual analysis).

Auto interval search and time-dependent waveform compatibility

When applying proper sampling intervals to derive IV data from ABF data, researchers tend to inspect each file to ensure the sampling intervals are valid and representative, and to eliminate possible inclusion of artefacts. We have developed a binary search algorithm to find suitable intervals following the manual logic: to find intervals that is as close to V_{cmd} as possible in the voltage channel and is stable enough in the current channel. The algorithm is very adaptive and an extreme example of the auto interval search is demonstrated in Figure 9. For users who prefer to apply the same sampling interval across the batch, we designed a solution “One Interval for ALL” (Figure 3E). Like the traditional manually fixed intervals, this approach tries to find a common

interval for all data files which matches the user defined auto interval selection criteria, thus is also suitable for IV sampling from the time-dependent waveform protocols.

Performance of Smart-IV

When the interval selection is automated, the whole process of reading and grouping 100 ABF files, IV data extraction and export by Smart-IV can take less than 15 seconds on a Windows 7 64 bits system with 4 core i5 CPU and 8GB RAM. The IV plots generated in Smart-IV can be saved and directly used in reports, presentations and meetings. As we have demonstrated the reliability of Smart-IV extracted data, we propose that reliable IV graphs can be exported within minutes, and since the interactive IV preview plots every IV curve immediately, there is no need to perform manual waveform inspection and interval fine tuning unless problems are spotted in the IV preview (Figure 3C).

Remarks on standard error means of IV data

We have demonstrated that IV values generated by Smart-IV are effectively identical to manual analysis results (Figure 8; S1). This is expected since the algorithm follows same logic as manual analysis. Selecting intervals that V is matched by V_{cmd} can be easily and accurately achieved by human inspection on the voltage waveforms. However, when judging whether the current waveforms are “stable” enough, very different perceptions can happen to different people or even the same person across different samples. On the other hand, “stability” is strictly defined as variance of data in Smart-IV and can be accurately measured, so more consistent interval search criteria are guaranteed, which leads to slightly smaller random error. In conclusion, we expect more consistent SEMs when compared to manual results. However, this difference won't necessarily lead to different conclusions since the majority of SEMs are contributed by variance of samples and the conditions of repeated experiments.

Smart-IV reports mean values and SEMs for all calculated measurements, namely current, voltage and conductance. It is worth noting that SEMs of conductance are reported because the mean conductance is calculated by averaging individual conductance instead of calculating the slope of mean IV curve. Though reported, users should not directly compare SEMs of conductance, because the errors of voltage are not accounted for; thus the values could be misleading especially when voltage SEMs

are relatively large. In this case, the only reliable way to compare conductance SEMs is to perform error and residual analysis on the fitted conductance model itself, but this is beyond the scope of the paper and won't be discussed further. We suggest users to emphasise that the SEMs of conductance are only indicative values reflecting the variance of original current data when plotting or interpreting conductance data.

Conclusion

We have demonstrated the performance and reliability of Smart-IV for batch processing TEVC I-V data. Compared to conventional workflow of exporting data then visualising data, Smart-IV emphasises the capability of displaying real time results before exporting. Performance wise, Smart-IV is able to batch process hundreds or even thousands (depending on available memory) files at a time. The underlying programming interface abftools also provides a full set of tools ranging from data analysis to data visualisation and its implementation logic helps programmers to focus on what to analyse instead of how to deal with data structures. We believe that Smart-IV is able to provide a full experience for users of every level to achieve streamlined and high-throughput ABF data processing protocols in the fraction of the time of current platforms that require greater manual intervention.

The software Smart-IV and the R package abftools are available for download from <https://github.com/Crystal-YWu>.

Future perspectives

As of the current version of abftools, ABF data and Heka data are the two data formats supported. We plan to implement more file readers so that abftools can be accessible for a broader userbase and be more flexible in scientific research projects. The most important requirement for supporting more file formats is to design efficient generic data structures and algorithms for multi-channel and multi-episode data. The 3-d array we proposed in the paper is generally sufficient to store any electrophysiology data. However, stimulus waveforms are stored in different ways by different softwares and data acquiring tools; for example, they can be stored by epochs of the predefined waveform (the waveform editor in Clampex) or stored by values in the time domain (ATF files). Currently, when loading files into R using abftools, the stimulus waveform is stored as additional information, whose structure could vary depending on the file formats. It will be convenient if a uniformed structure can be designed to store this stimulus waveform information across all file types, so that the users do not need to parse and develop different routines to analyse data from different file formats.

As for Smart-IV, since the R package abftools has already implemented the underlying programming facilities for electrophysiology data processing, analysing and plotting, Smart-IV can be flexibly expanded. In the current stage, Smart-IV focuses on IV data processing; however, we could expand Smart-IV to a full suite of applications that adapts to (i) more electrophysiological analysis, such as voltage ramps and single channel analysis, and (ii) more data formats, such as Heka data files into Smart-IV in the future.

Methods and implementation

Details of Smart-IV

Smart-IV is designed to be configuration free. However, there are cases that settings will need to be altered manually to produce high quality results. These settings are mostly for automatically finding proper IV sampling time intervals. In addition to these highlighted settings, we will also elaborate on some details of the algorithms used in Smart-IV.

Noisy Data Enhancement. It is possible that background noise of some episodes, especially when the currents are relatively small, becomes prominent. While the interval search algorithm is usually still competent to find proper intervals, it might fail in extreme cases. By turning on “Noisy Data Enhancement” (Figure 3E), a first order Butterworth low-pass filter (Butterworth 1930) is first applied to current channel before the search is committed. We have found that this technique with a 75Hz low-pass frequency is sufficient to handle extremely noisy data and provide reasonable results in most cases.

Use Full Epoch if No Interval Found. When no interval is found, the automatic interval search algorithm returns a NULL interval, i.e. the specific ABF data is discarded in the following calculation. If users intend to include the data, a manual interval can be selected on the waveform preview or by turning on “Use Full Epoch if No Interval Found” (Figure 3E), the whole IV epoch except heading and tailing 10% will be used. In usual situations, this option yields reasonable results and slightly larger SEMs.

Manual Voltage Delta. The default allowed deviation from V_{cmd} is $\pm 5\%$ of the maximum absolute value of the voltage step protocol settings. If this value is larger than the voltage increment/decrement per step, it is adjusted via an adaptive scheme, whose maximum deviation must be smaller than the medium value of those within the voltage increment/decrement range. In cases where the voltage deviates considerably from V_{cmd} , the automatic scheme will fail and users can manually define a larger absolute maximum voltage delta to guarantee an interval can be found (Figure 3E). However,

this can lead to large SEMs of voltage or even unreasonable voltages so users should be cautious when setting a very large manual voltage delta.

Automatic Interval Search. The process of automatically searching for IV sampling intervals has two major steps: (i) marking the voltage interval that falls within the allowed voltage delta; and, (ii) finding sub-intervals that have the most stable current within those voltage intervals. Step (i) is fairly straightforward and step (ii) can also be simply achieved by a moving window algorithm. The moving window is achieved by a greedy binary search, which halves window size and compares the stableness of the left window to the right window. The less stable one is discarded while the other is kept and halved then compared again until the most stable interval is found. This algorithm does not find a global optimal solution but it is capable to find stable intervals even in very extreme cases (Figure 9); the algorithm is stable which means it gives consistent local optimal result when given the same input and it has much better performance than a recursive linear moving window algorithm. We believe that the performance advantage outweighs the need to find a true global optimal especially when dealing with hundreds or even thousands of data entries.

Details of abftools

We designed abftools to provide an accessible R programming interface for researchers who prefer developing ABF data processing protocols programmatically, and also for driving Smart-IV tailored for IV analysis.

Concept of abftools. Abftools is a package for reading and analysing abf data in R. The tasks of abftools are split into three major parts: **data acquisition, data processing and plotting**. All of these features are built upon the R S3 class “abf”. However, unlike most available software libraries that support ABF data, “abf” objects are simply an extension of 3-d arrays with the dimensions of time, episode and channel regardless of the ABF operations mode be it episodic, gap-free or event driven variable length. This design guarantees consistent sub-setting across all “abf” objects and compatibility of R base functions and many 3rd party functions.

Data acquisition. ABF files can be loaded by calling *abf2_load()* and *abf2_loadlist()*, which loads a single ABF file and a list of ABF files respectively. A loaded “abf” object is 3-d array with attached attributes that stores extra information, mainly the clamping

protocol. An “abf” object also stores some useful information in addition to the protocol, amongst which the most important ones are title of the “abf” object, names, units and descriptive names of recorded channels and sampling frequency of recorded data.

Data processing. As ABF files are 3-d data structures, when processing or analysing “abf” objects, the final goals are usually to “flatten” the data to some 2-d form, be it plotting or presenting statistics than can be printed on paper. Abftools borrows the map-reduce paradigm and facilitates functional programming of R to achieve consistent data processing for variable protocols. The logic of this data processing is mapping a function along specific dimensions (time, episode or channel) by calling *map()* then collecting and reshaping the data properly by calling *reduce()*. For users convenience, wrapping functions *wrap()* and *wrap_along()* are created. These functions wrap a normal function and return a new function that work for an “abf” object. For example, *f <- wrap(mean)* wraps function *mean()*, which calculates numeric average, to a new function *f()* which calculates episodic average of channels of an “abf” object. Internally, what the generated *f()* does is mapping *mean()* along time dimension of an “abf” object then reducing the values by *as.data.frame()*.

Plotting. As mentioned before, *abf_plot_cd()* and *abf_plot_td()* provide very fundamental yet powerful plotting functionality. In addition to these two functions, a series of high-level functions built on top of them are available for an even more convenient plotting experience. The most notable ones are *PlotChannelAbf()*, *PlotXYAbf()* and *PlotIVSummary()*, which plots channel waveform of an “abf” object, channel vs channel of an “abf” object and aggregated IV plots of multiple “abf” objects respectively. A convenient function *QuickPlot()* is also available. It recognises most possible plotting situations and calls proper plotting functions accordingly to generate plots with default settings. So it is also suitable for rapid data visualisation.

Help for every feature of abftools is available in the user guide within the package.

Acknowledgements

We thank Yu Long (University of Adelaide) for advice on electrophysiology; Stephen Pederson (University of Adelaide, Bioinformatics Hub) for R related support, and Steve Tyerman (University of Adelaide) for discussion. We thank the University of Adelaide (Adelaide Graduate Research Scholarship) and Wine Australia (AGWA Research Supplementary Scholarship (AGW Ph1502)) for supporting Y.W. in this study, and the ARC Centre of Excellence funding CE1400008 for supporting M.G. and Y.W..

References

- Butterworth, S.** (1930) On the theory of filter amplifiers. *Experimental Wireless and the Wireless Engineer*, **7**, 536-541.
- Cubero-Font, P., Maierhofer, T., Jaslan, J., Rosales, M.A., Espartero, J., Diaz-Rueda, P., Muller, H.M., Hurter, A.L., Al-Rasheid, K.A., Marten, I., Hedrich, R., Colmenero-Flores, J.M. and Geiger, D.** (2016) Silent S-Type anion channel subunit SLAH1 gates SLAH3 open for chloride root-to-shoot translocation. *Current Biology*, **26**, 2213-2220.
- Guan, B., Chen, X. and Zhang, H.** (2013) Two-electrode voltage clamp. In *Ion Channels: Methods and Protocols* (Gamper, N. ed. Totowa, NJ: Humana Press, pp. 79-89.
- Hamill, O.P., Marty, A., Neher, E., Sakmann, B. and Sigworth, F.J.** (1981) Improved patch-clamp techniques for high-resolution current recording from cells and cell-free membrane patches. *Pflügers Archiv*, **391**, 85-100.
- Henderson, S.W., Dunlevy, J.D., Wu, Y., Blackmore, D.H., Walker, R.R., Edwards, E.J., Gilliam, M. and Walker, A.R.** (2018) Functional differences in transport properties of natural HKT1;1 variants influence shoot Na⁺ exclusion in grapevine rootstocks. *New Phytologist*, **217**, 1113-1127.
- Hodgkin, A.L., Huxley, A.F. and Katz, B.** (1952) Measurement of current-voltage relations in the membrane of the giant axon of *Loligo*. *The Journal of Physiology*, **116**, 424-448.
- Liu, Z.** (2016) *Practical Patch Clamp Techniques 2* edn. Beijing: Beijing Science and Technology Press.
- Miledi, R., Parker, I. and Sumikawa, K.** (1982) Properties of acetylcholine receptors translated by cat muscle mRNA in *Xenopus* oocytes. *The EMBO journal*, **1**, 1307-1312.
- Munns, R., James, R.A., Xu, B., Athman, A., Conn, S.J., Jordans, C., Byrt, C.S., Hare, R.A., Tyerman, S.D., Tester, M., Plett, D. and Gilliam, M.** (2012) Wheat grain yield on saline soils is improved by an ancestral Na⁺ transporter gene. *Nature Biotechnology*, **30**, 360-364.
- Papke, R.L. and Smith-Maxwell, C.** (2009) High throughput electrophysiology with *Xenopus* oocytes. *Combinatorial Chemistry & High Throughput Screening*, **12**, 38-50.
- Preuss, C.P., Huang, C.Y., Gilliam, M. and Tyerman, S.D.** (2010) Channel-Like characteristics of the low-affinity barley phosphate transporter PHT1;6 when expressed in *Xenopus* oocytes. *Plant Physiology*, **152**, 1431-1441.
- R Core Team** (2019) R: A language and environment for statistical computing. Vienna, Austria: R Foundation for Statistical Computing.
- Ramesh, S.A., Tyerman, S.D., Xu, B., Bose, J., Kaur, S., Conn, V., Domingos, P., Ullah, S., Wege, S., Shabala, S., Feijo, J.A., Ryan, P.R. and Gilliam, M.** (2015) GABA signalling modulates plant growth by directly regulating the activity of plant-specific anion transporters. *Nature Communications*, **6**.
- Sakmann, B. and Neher, E.** (1984) Patch clamp techniques for studying ionic channels in excitable membranes. *Annual Review of Physiology*, **46**, 455-472.
- Sakmann, B. and Neher, E.** (1995) *Single-channel recording 2* edn. New York: Plenum Press.
- Wu, Y., Henderson, S.W., Walker, R.R. and Gilliam, M.** (2019) Expression of the grapevine NPF2.2 in Arabidopsis roots reduces shoot Cl⁻ accumulation under salt stress.

Tables and figures

Table 1: A data index for Smart-IV can have flexible columns, but the first column must be the ABF file names. (A – B) Examples of a data index for Smart-IV.

A.

FileName	SampleNumber	Gene	Buffer	RestingVm	DataType	Exclude
17d07099	0	H2O	Basal		Gap free	
19214000	1	H2O	Basal	-80		yes
19214001	1	H2O	Cl	-40		yes
19214002	1	H2O	NO3	-20		yes
19214006	2	H2O	Basal	-85		
19214007	2	H2O	Cl	-39		
19214008	2	H2O	NO3	-18		
19214024	5	VviNPF2.1	Basal	-54		
19214025	5	VviNPF2.1	Cl	-13		
19214026	5	VviNPF2.1	NO3	-2		
19214030	6	VviNPF2.1	Basal	-60		

B.

ABF-ID	Genotype	Malate Injection
17201000	H2O	Y
17201001	H2O	Y
17201002	H2O	Y
17201003	H2O	
17201004	H2O	
17201005	H2O	
17201006	H2O	Y
17201007	H2O	Y
17201008	H2O	Y
17201009	WT	
17201010	WT	

Table 2: Two types of processed data can be exported from Smart-IV. (A) The IV statistics summary of each episode of the fixed-length voltage step protocol, which includes the voltage mean, voltage SEM (mV), current mean, current SEM (nA) and the number of samples for TaHKT1;5-D (WT) expressing oocytes in the 0 mM Na⁺ buffer. (B) The current data (nA) of each individual sample of the TaHKT1;5-D (WT) expressing oocytes in the 0 mM Na⁺ buffer.

A.

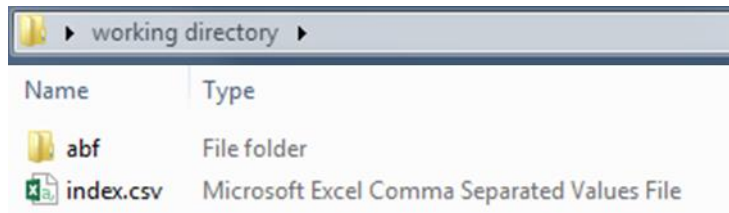
	Voltage	SEM Voltage	Current	SEM Current	Num Samples
epi1	46.02339019	0.287617307	33376.65937	1351.561515	9
epi2	27.41699763	0.299659919	27458.02056	1053.201373	9
epi3	8.926205257	0.283289984	21981.37833	792.4031897	9
epi4	-9.2534181	0.263840612	16860.2778	586.5801786	9
epi5	-27.2262345	0.247687676	12115.98443	433.31501	9
epi6	-44.97763904	0.226151856	7860.301778	327.6819814	9
epi7	-62.66530278	0.197299176	4194.862106	272.8650481	9
epi8	-80.55401602	0.165923587	1195.551016	260.0507619	9
epi9	-98.96466471	0.174541745	-1081.661373	256.2299889	9
epi10	-117.9096841	0.165308667	-2684.264715	257.709206	9
epi11	-137.2372491	0.184824944	-3926.980761	304.5427564	9

B.

	17201053.abf	17201056.abf	17201059.abf	17201062.abf	17201065.abf	17201068.abf	17201071.abf	17201074.abf	17201077.abf
epi1	30045.72	31753.59	42628.07	35335.77	33554.2	27248.46	30438.35	32704.16	36681.62
epi2	24521.21	26030.36	34312.29	29130.31	28041.77	22504.03	25097.05	27435.92	30049.23
epi3	19435.29	20757.93	26587.62	23432.82	22947.05	18043.6	20170.93	22478.77	23978.4
epi4	14695.39	15818.11	19594.04	18107.4	18099.46	13801.48	15570.07	17718.29	18338.26
epi5	10343.34	11238.37	13349.08	13148.75	13519.22	9832.851	11297.71	13199.58	13114.95
epi6	6476.782	7139.631	7914.219	8648.963	9319.027	6336.772	7422.939	9054.352	8430.031
epi7	3161.938	3628.84	3375.705	4734.017	5614.37	3395.654	4031.301	5411.547	4400.388
epi8	375.7896	761.2459	-167.882	1536.975	2506.622	1061.765	1202.215	2366.815	1116.414
epi9	-1778.22	-1402.41	-2658.97	-864.812	23.63789	-642.016	-986.303	-20.6348	-1405.22
epi10	-3370.78	-2871.03	-4307.73	-2463.07	-1833.35	-1861.45	-2520.11	-1713.81	-3217.05
epi11	-4441.15	-3974.54	-5954.46	-3466.71	-3422.45	-2761.36	-3587.47	-2908.98	-4825.71

Figure 1

A.



B.

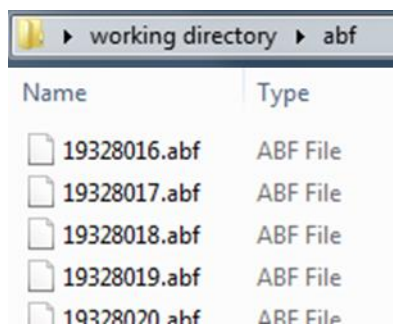


Figure 1: Working directory preparation and R package installation before running Smart-IV. (A – B) The structure of a working directory for Smart-IV. (A) A working directory should contain an index CSV file and a folder named “abf”. (B) The “abf” folder should contain all ABF data files listed in the index.

Figure 2

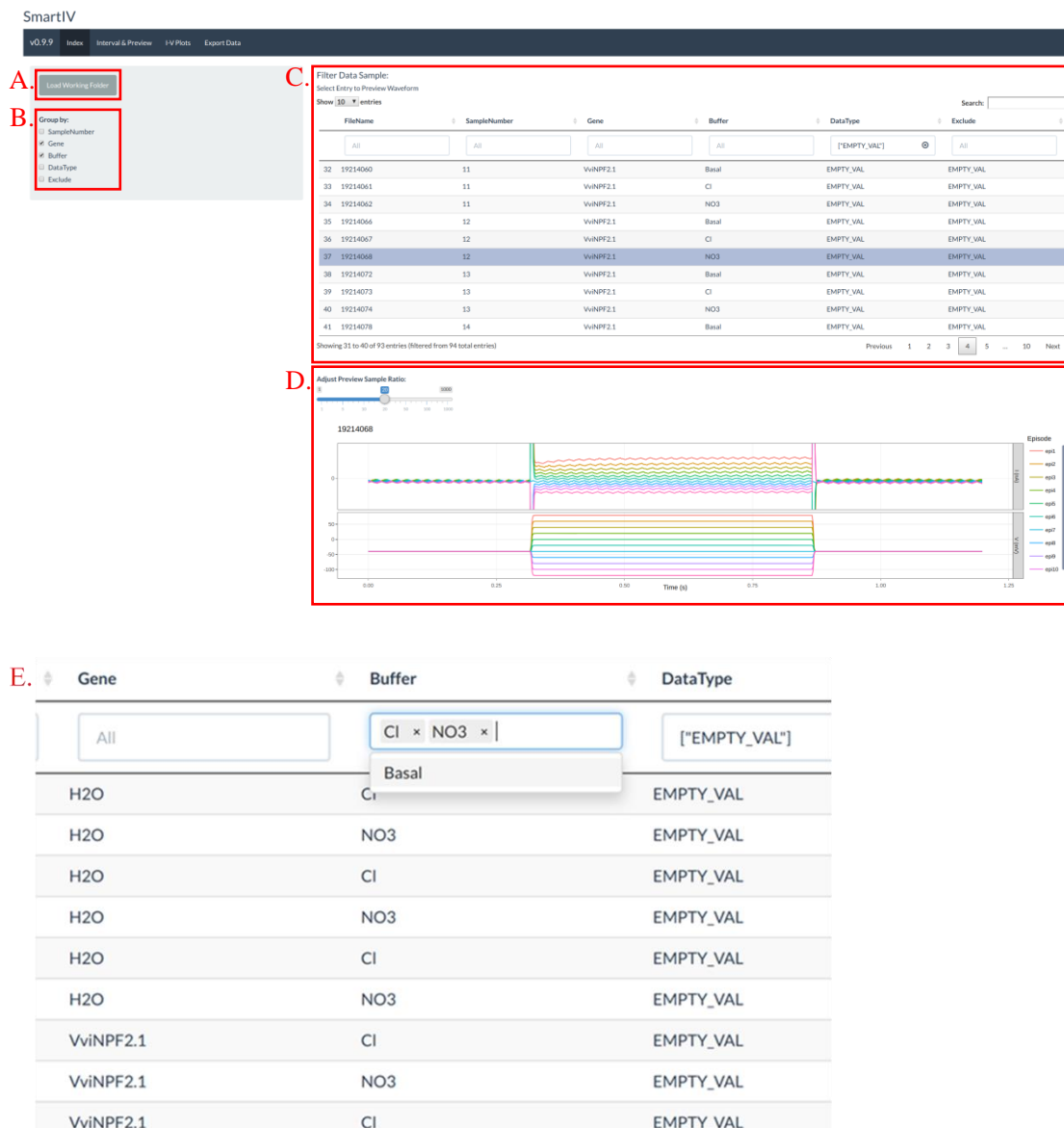


Figure 2: Smart-IV Index section. (A) Load a working folder. The starting point of Smart-IV workflow is loading a working folder which contains the ABF files and the data index to be processed. By clicking on “Load Working Folder” users can select the folder from the directory. (B) Select grouping factors. After loading a working folder, possible grouping factors will be automatically displayed for users to select. The column names in the index are recognised as grouping factors. (C) Data index shows a preview of all loaded files. Users can select an entry to preview and data entries can also be filtered. (D) Waveform preview. The waveform preview of the selected data entry is plotted. The sample ratio is set to 20 by default, so that 1 per 20 data points is shown in the preview. (E) Data index filtering. Data columns are categorised

automatically, with empty values replaced by the placeholder “EMPTY_VAL”. By clicking or typing on the filter box, users can select the desired catalogues and achieve efficient data filtering.

Figure 3

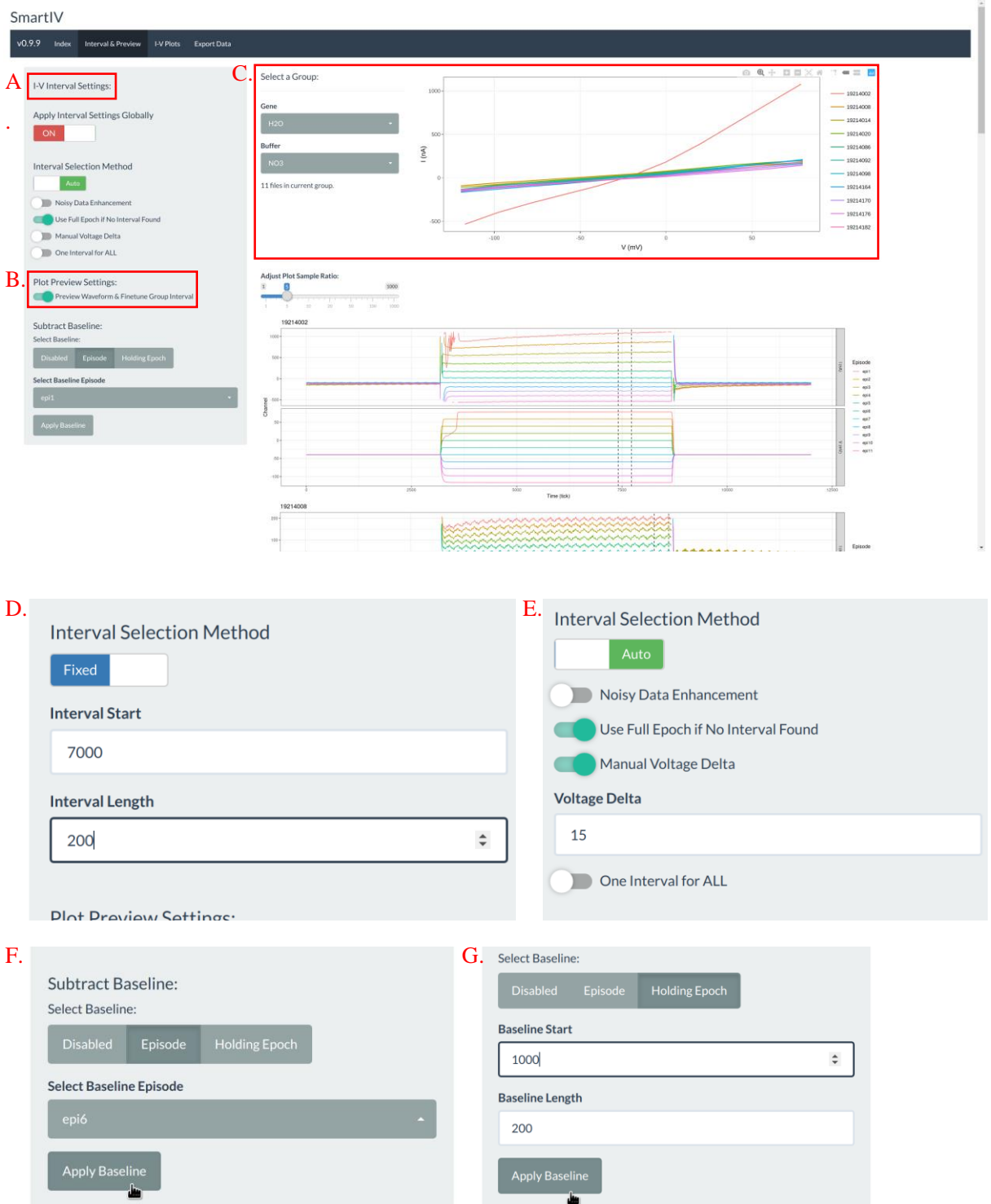
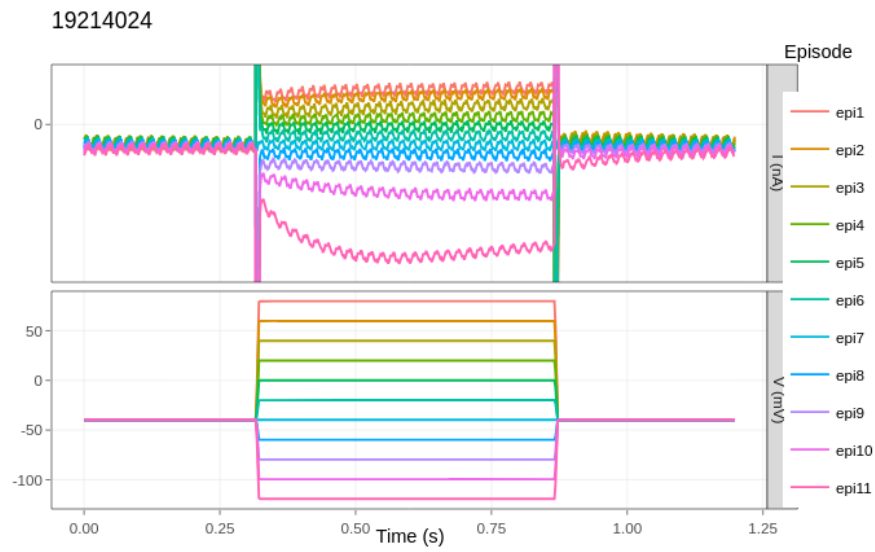


Figure 3. Smart-IV Interval & Preview section. (A) Apply various settings. Users can modify settings in the left panel for batch IV sampling time interval selection. The interval can be automatically selected according to the settings, or fixed at a user defined position for a batch of files. Baseline subtraction is also configured here. (B)

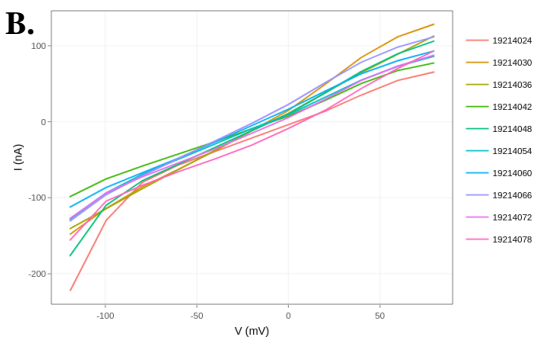
Waveform plot preview and manual interval selection. All waveform plots of the selected group are displayed on the same page by turning on the “Preview Waveform & Finetune Group Interval”. Interval borders are labelled by dashed lines; the interval for each data entry can be manually selected or updated by clicking and dragging a new interval on the waveform plot. (C) Interactive IV traces. Users are able to select a group and preview all IV traces of all data entries interactively. (D) Fixed interval. To apply a fixed interval for all data entries of the same group, users are required to input the interval start time and the interval length (unit = time ticks). (E) Auto interval. By turning on “Manual Voltage Delta”, the maximum allowed voltage delta between V_m and V_{cmd} can be changed to a user defined value (unit = mV). (F) Baseline subtraction by a static holding epoch of each episode. Users can select starting point of the holding epoch and the length of the epoch. The subtracting baselines are calculated accordingly. However, if “Apply Baseline” is not click, the changes won’t be applied. (G) Baseline subtraction by an episode. Users are asked to select an episode served as the baseline. A shape preserving baseline is calculated from the selected episode. Since the algorithm is shape preserving, the peaks of the original episode are preserved after the subtraction.

Figure 4

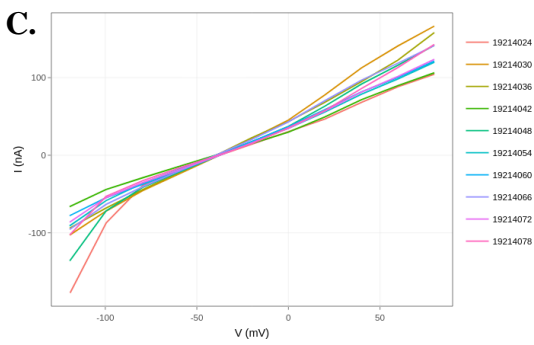
A.



B.



C.



D.

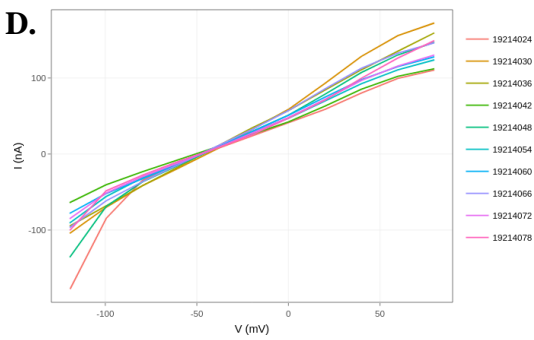
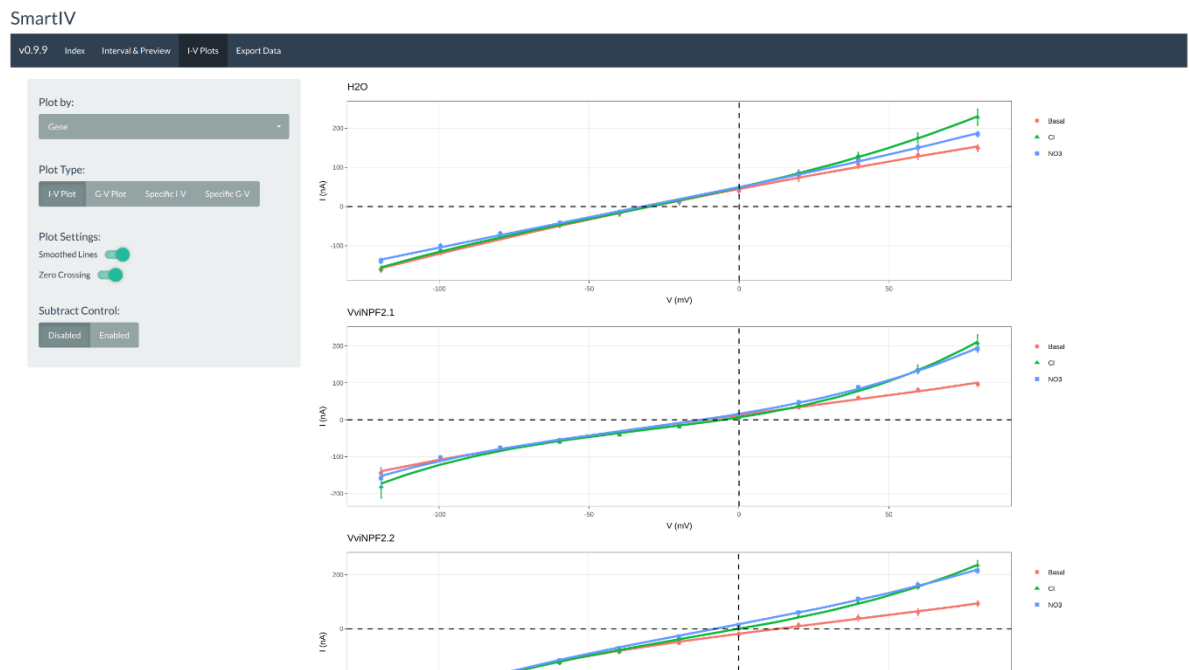


Figure 4: Interactive IV traces can reflect baseline subtraction changes in real time. (A) A set of the sample waveform plots from the group of data to be baseline subtracted. (B) No baseline subtraction. (C) Baseline subtracted by the first holding epoch (time: 0.2 – 0.25 s). (D) Baseline subtracted by episode 7.

Figure 5

A.



B.

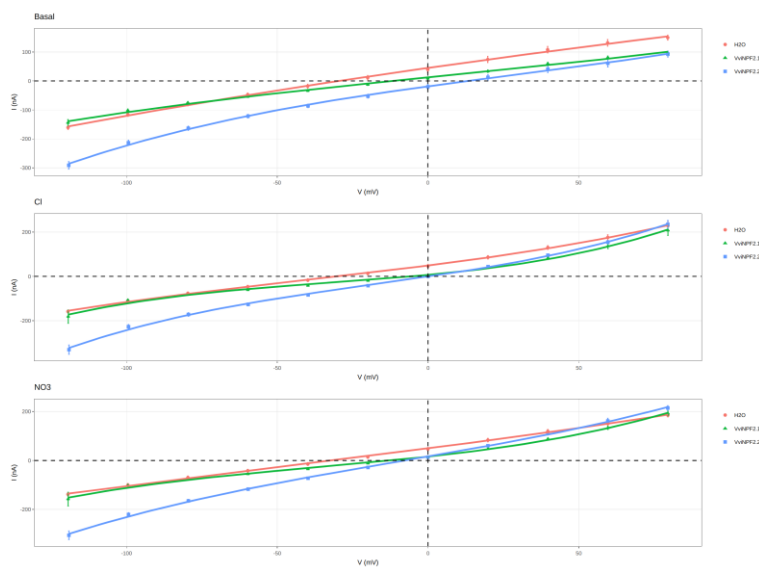


Figure 5: Smart-IV IV Plots section. IV traces with SEM can be grouped onto graphs by a grouping factor. IV, GV, specific IV and specific GV are the 4 types of plots to select from. Control subtraction is also configured here. (A) IV graphs grouped by “Gene”; (B) IV graphs grouped by “Buffer”. The plots are also interactive; variables of generated plots are updated in real time.

Figure 6

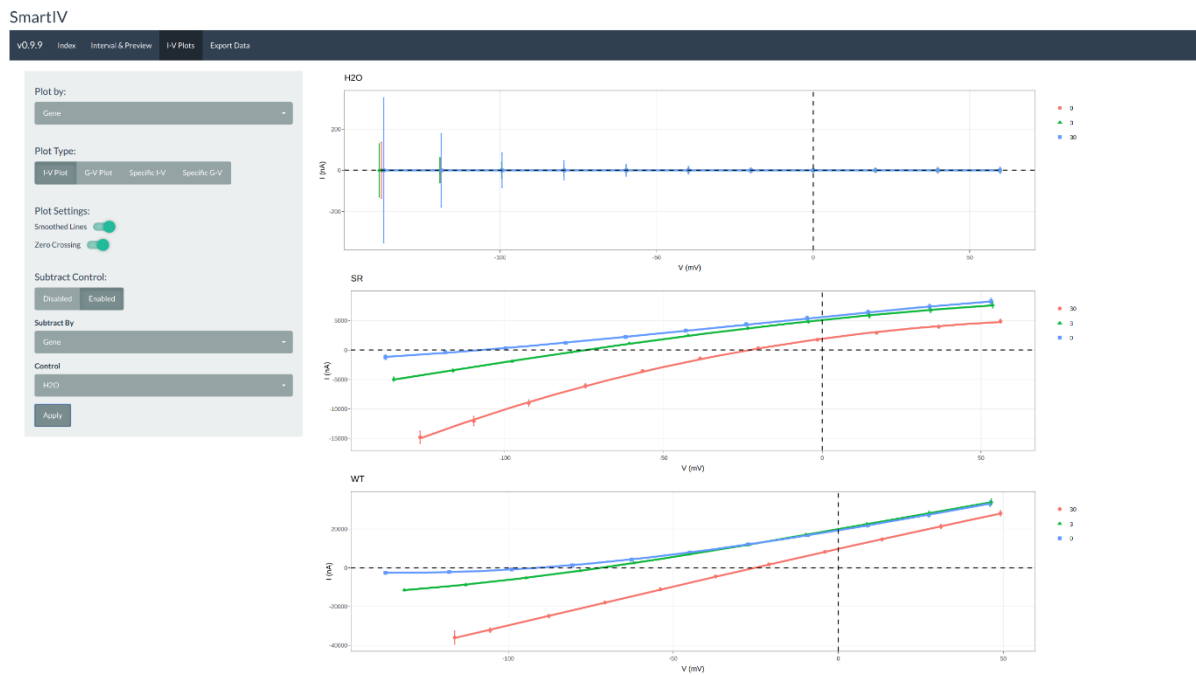


Figure 6: Control subtraction. If “Subtract Control” is enabled, users are asked to select what to subtract by. Variables and groups are automatically recognised and subtracted. When the “Gene” “H2O” is selected as control, it is subtracted from all data of the batch. As a result, the IV traces of the “H2O” group are all lying around the I (nA) = 0 line.

Figure 7

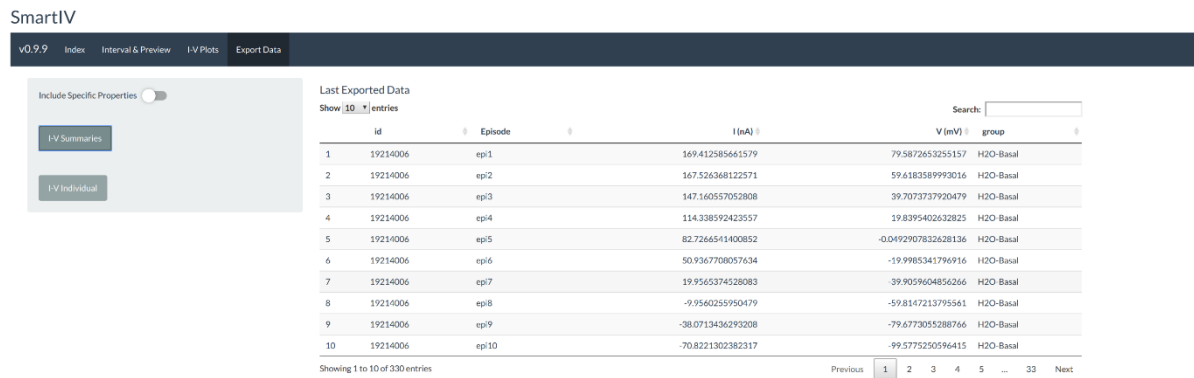


Figure 7: Smart-IV Export Data section. By exporting the “IV Summaries” or “IV Individual”, the grouped data output will be in the working folder in CSV format. Application of baseline subtraction, control subtraction, conductance plotting in the previous sections will change the export accordingly.

Figure 8

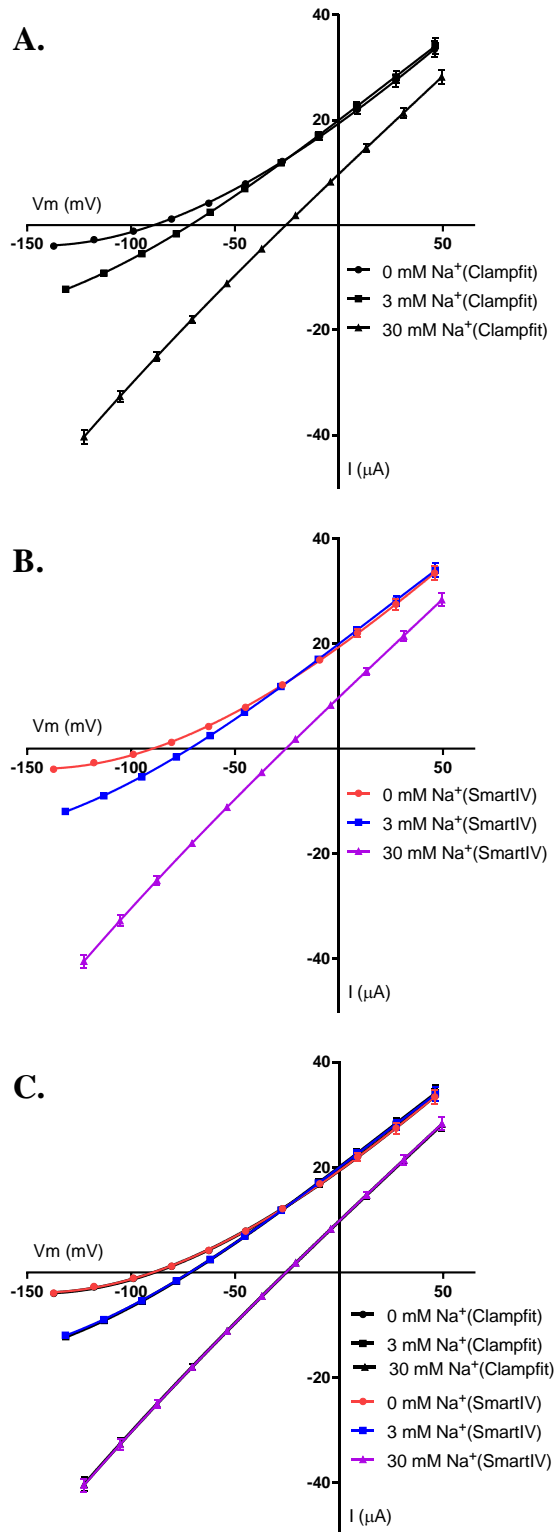


Figure 8: The IV data of the TaHKT1;5-D expressing oocytes extracted using Clampfit and using the auto IV sampling interval selection function of Smart-IV yielded the same

IV plot. (A) The IV plot using data we extracted with Clampfit (Henderson *et al.* 2018a). (B) The IV plot using data extracted by the Smart-IV app using the settings in Figure 7B. (C) The IV plot overlay of data extracted by both the Clampfit and the Smart-IV method. Data are mean \pm SEM (n = 9 samples).

Figure 9

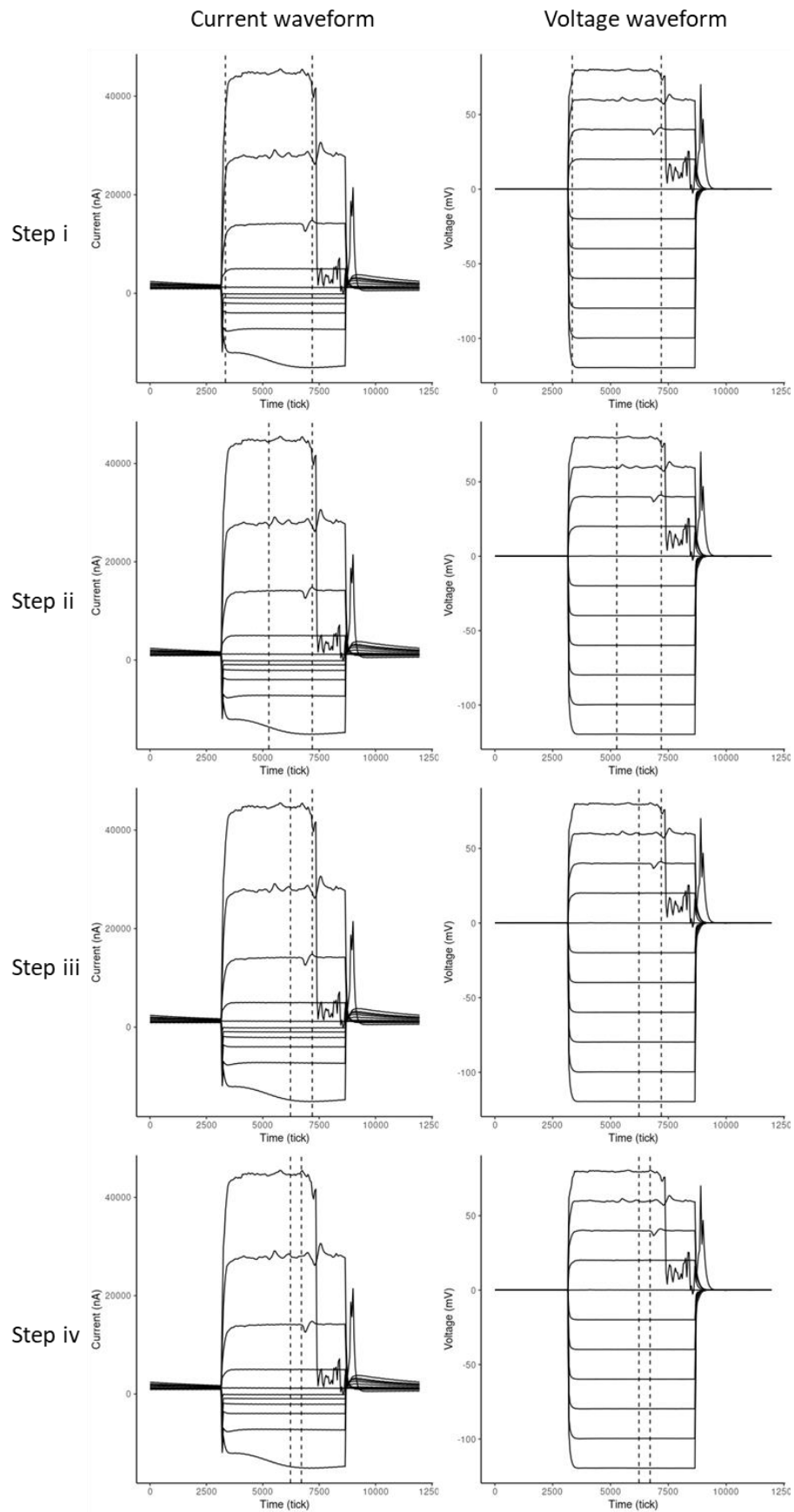
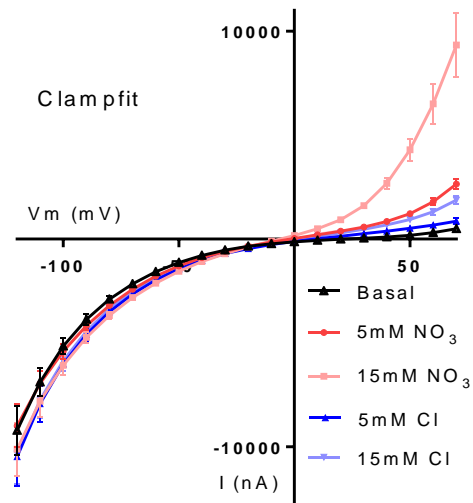


Figure 6: An example of the auto IV sampling time interval search process. The IV sampling time interval (the borders are shown by the black dash lines) is narrowed down from step i to step iv.

Supporting information

Figure S1

A.



B.

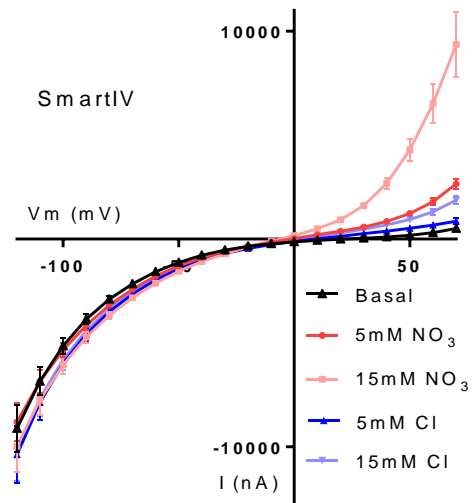


Figure S1: The IV data of the *VviALMT2* expressing oocytes extracted using Clampfit and using the auto IV sampling interval selection function of Smart-IV yielded the same IV plot. (A) The IV plot using data we extracted with Clampfit (unpublished data). (B) The IV plot using data extracted by the Smart-IV app using the auto interval search method with no manual interval finetuning. Data are mean \pm SEM (n = 7 samples).

Chapter 7: Conclusions and future directions

7.1 Background

The grapevine rootstock 140 Ruggeri is well known for its salt exclusion capacity, but the key genes which contribute to this character have not been previously identified. In recent years our knowledge in grapevine salt exclusion related genes has been expanded by a microarray gene expression study which highlighted a list of genes that are differentially expressed in between the roots of 140 Ruggeri and those of the poor Cl^- excluder K51-40 (Henderson *et al.* 2014a), and by the discovery of a quantitative trait locus (QTL) named *NaE* for shoot Na^+ exclusion (Henderson *et al.* 2018a) (Chapter 4). This thesis aimed to functionally characterise several putative anion and cation channels/transporters selected from the microarray and the QTL, to elucidate their roles in grapevine ion transport, and to evaluate whether they could be used as molecular markers for breeding salt tolerant rootstock germplasms.

7.2 Characterisation of the putative anion channels/transporters

Four putative anion channels/transporters were selected from the microarray gene expression results (Henderson *et al.* 2014a); all 4 candidates, *VviALMT2*, *VviALMT8*, *VviNPF2.1* and *VviNPF2.2* were significantly more highly expressed in the roots of 140 Ruggeri than in the roots of K51-40.

7.2.1 *VviALMT2* and *VviALMT8*

Recent studies have demonstrated that the ALMT family members are capable of transporting inorganic anions and have roles in plant salt tolerance (Baetz *et al.* 2016, De Angeli *et al.* 2013b), therefore we hypothesized that *VviALMT2* may function in Cl^- transport in roots, which contributes to reducing shoot Cl^- accumulation. In Chapter 2, *VviALMT2* was found to be plasma membrane localised and was most permeable to NO_3^- among the 7 anions tested, and it was also permeable to Cl^- . Since *VviALMT2* was more highly expressed in the root stelar enriched fraction than in the cortex enriched fraction, and its expression levels in grapevine roots were up-regulated by high NO_3^- re-supply post starvation, we proposed that *VviALMT2* may function in NO_3^-

loading from the root xylem parenchyma into the root xylem, which could improve the NO_3^- status in the shoots, and potentially reduce the shoot $\text{Cl}^-/\text{NO}_3^-$ ratio during Cl^- stress. To test *VviALMT2*'s effect on Arabidopsis, Arabidopsis root stelar specific *VviALMT2* expression lines were treated with high NaCl and harvested for shoot $[\text{Cl}^-]$ and $[\text{NO}_3^-]$. Interestingly, the expression of *VviALMT2* was correlated with shoot $[\text{Cl}^-]$ reduction, but not with shoot $[\text{NO}_3^-]$. The results suggest that *VviALMT2* could benefit the plants by reducing shoot $[\text{Cl}^-]$ and shoot $\text{Cl}^-/\text{NO}_3^-$ ratio under salt stress.

It was unexpected that the Arabidopsis root stelar specific *VviALMT2* over-expression did not statistically significantly modify the shoot $[\text{NO}_3^-]$. However, whether the shoot $[\text{NO}_3^-]$ is a good measurement of *VviALMT2*'s effect on root to shoot NO_3^- transport is in question. Unlike Cl^- , NO_3^- is metabolised by the plants (Wege *et al.* 2017), therefore the shoot $[\text{NO}_3^-]$ we measured is also affected by factors including the rate of shoot NO_3^- metabolism, which is a variable that we could not control. Compared to the shoot $[\text{NO}_3^-]$ measurements, xylem sap $[\text{NO}_3^-]$ measurements should better represent the effect of *VviALMT2* on root to shoot NO_3^- transport. As we suspected that *VviALMT2* could alter the ratio of $\text{Cl}^-/\text{NO}_3^-$ which entered the root xylem from the xylem parenchyma, it is likely that the xylem sap shoot $[\text{NO}_3^-]$ and $[\text{Cl}^-]$ measurements could give us the answer. Another method to trace the amount of NO_3^- translocated from root to shoot is to add $^{15}\text{NO}_3^-$ tracer into the Arabidopsis treatment nutrient solution. In this case even the total NO_3^- translocated from root to shoot after the treatment can be accurately measured even if the NO_3^- isotope was metabolised in shoots. The plants could also be grown for biomass measurements under different conditions including control, salt stress, NO_3^- starvation and NO_3^- abundance to evaluate the effect of root stelar *VviALMT2* expression on Arabidopsis performance. The function of *VviALMT2* could also be studied by generating and phenotyping the grapevine *VviALMT2* over-expression, knockout or knockdown mutants, or by expressing *VviALMT2* in a deficient (e.g. NO_3^- transport deficient) genotype to test if the phenotype could be complemented.

In our study, *VviALMT8* had similar electrophysiological characteristics as *VviALMT2*. However, we were not successful in confirming the subcellular localisation of *VviALMT8* in Arabidopsis. *VviALMT8* was not found differentially expressed between the stelar and cortex enriched root fraction, and its expression in

roots was not regulated by mild Cl^- stress or different NO_3^- treatments. In addition, the expression levels of *VviALMT8* were significantly lower than the expression levels of *VviALMT2*, *VviNPF2.1* and *VviNPF2.2* in the same cDNA samples (data not shown), which suggests that *VviALMT8* is less likely to play a major role in anion homeostasis compared to the other 3 candidates. Therefore it was put into lower priority in this study.

The RT-qPCR results suggest that *VviALMT8* was highly expressed in grapevine roots and flowers; the *promoter:GUS* experiment shows that the *proVviALMT8* driven GUS activities on mature *Arabidopsis* leaves were in the trichomes. There are glandular and non-glandular trichomes, and *Vitis vinifera* and *Arabidopsis thaliana* both have only non-glandular trichomes (reviewed in Ma *et al.* 2016, Schilmiller *et al.* 2008). Non-glandular trichomes generally function in protecting the leaves from herbivores, insects, harsh temperatures and photo damages (reviewed in Ma *et al.* 2016). *VviALMT8* were able to transport multiple diprotic organic acids and Cl^- . Interestingly, salt bladders are often modified trichomes (reviewed in Yuan *et al.* 2016); chick peas were found to secrete oxalic acid (a diprotic acid) into their trichomes for the *Helicoverpa armigera* insect larvae resistance (Yoshida *et al.* 1997). However, these are both glandular trichomes, therefore it is unclear if the information is relevant to the wine grapes that we study.

VviALMT2 is more closely related to several *Arabidopsis* ALMTs, but *VviALMT8* is most closely related to a single *Arabidopsis* ALMT, which is *AtALMT8*. *AtALMT8* has not been characterised yet, therefore characterising the *Arabidopsis* ALMT8 could reveal whether the *AtALMT8* have similar expression pattern and substrates as *VviALMT8*, and the phenotyping of an *Arabidopsis* *AtALMT8* knockout or knockdown mutant could potentially facilitate our understanding in *VviALMT8*.

7.2.2 *VviNPF2.1* and *VviNPF2.2*

One common substrate of the NPF family is NO_3^- , and the *AtNPF2.4* and *AtNPF2.5* were recently found to be Cl^- transporters which could affect shoot Cl^- accumulation (Li *et al.* 2016, Li *et al.* 2017a). Therefore, in Chapter 3, *VviNPF2.1* and *VviNPF2.2* were expressed in *Xenopus* oocytes to test their Cl^- and NO_3^- conductance; however, the experiments using the oocyte system yielded inconclusive results. As both *VviNPF2.1* and *VviNPF2.2* were more highly expressed in the grapevine roots when

NO_3^- starved than post high NO_3^- re-supply, we suspected that the function of their proteins could be NO_3^- transport. As the oocyte system may not be suitable for the substrate analysis of these proteins, we constructed Arabidopsis root epidermis and cortex specific *VviNPF* expression (OEX) lines for functional characterisation. Initially the over-expression lines were constructed for measuring the Cl^- and NO_3^- movements near the root surface using MIFE; however, when phenotyping the plants, we found that the *VviNPF2.2* OEX lines have lower shoot $[\text{Cl}^-]$ than the null segregants post the NaCl treatment. Therefore we propose that *VviNPF2.2* is beneficial for the plants to have as it could reduce the shoot $[\text{Cl}^-]$ under salt stress.

Unfortunately all the Arabidopsis *VviNPF2.1* transgenic T2 lines had no transgene expression. The expressions of the *GFP* and the transgene are activated by the same activator (GAL4) and the upstream activation sequence (UAS) in the Arabidopsis enhancer trap line J1551, but the *GFP* and the transgene are not directly linked together. In all Arabidopsis *VviNPF2.1* transgenic T2 lines, GFP activities were not seen, while the GFP signals in the roots of the non-transformed J1551 line were strong. This suggests the likeliness that in all the *VviNPF2.1* transgenic lines we screened, the expression activation system was not functioning. The *VviNPF2.2* transgenic lines other than the OEX line 3 and line 4 used in the study were not expressing the transgene and the *GFP* as well. Therefore, we had a low success rate in obtaining Arabidopsis J1551 *VviNPF* OEX lines; but this also suggests that it's likely that the *VviNPF2.1* OEX lines can be obtained if more *VviNPF2.1* transgenic lines are screened. If *VviNPF2.1* OEX lines can be obtained in the future, it would be pertinent to test if *VviNPF2.1* has similar effects on Arabidopsis as *VviNPF2.2*.

Regarding the shoot $[\text{NO}_3^-]$ measurements, the concern is the same for the Arabidopsis *VviNPF2.2* OEX lines as the *VviALMT2* OEX lines mentioned before. Although the expression of *VviNPF2.2* did not make a statistically significant difference in shoot $[\text{NO}_3^-]$, we cannot conclude that *VviNPF2.2* did not function in NO_3^- transport in Arabidopsis. To address this problem, xylem sap ion concentration measurements and plant growth could be measured under different Cl^- and NO_3^- environments. In a preliminary experiment, the Arabidopsis *VviNPF2.2* OEX line 3 plants (which had significantly higher *VviNPF2.2* expression levels than the OEX line 4) were observed to have larger plant sizes compared to the OEX line 4 and the non-transformed J1551

plants under NO_3^- starvation (Figure 7.1). It is possible that the expression of *VviNPF2.2* could facilitate plant growth under NO_3^- starvation conditions, but the experiment needs to be modified and repeated to support this prediction.

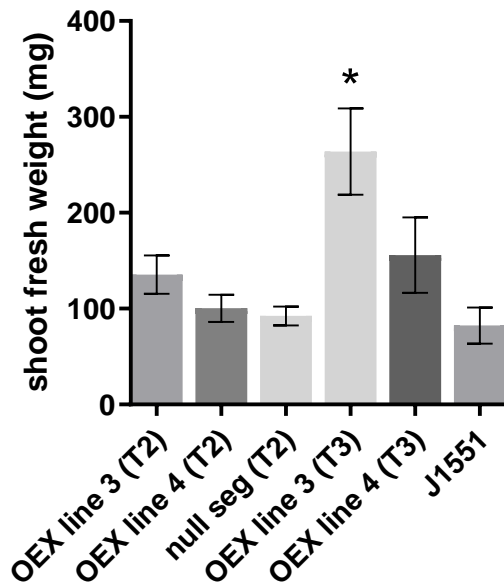


Figure 7.1: Shoot fresh weight of the 7-week-old *Arabidopsis* J1551 *VviNPF2.2* over-expression (OEX) lines, null segregants and non-transformed J1551 post 5 days of NO_3^- starvation. Both the T2 and T3 OEX lines were used; T2 OEX lines were compared to the null segregant T2 line, and T3 OEX lines were compared to the J1551 wild type line. The plants were grown in hydroponics under standard conditions for 6 weeks and starved with 0.8 mM total NO_3^- nutrient solution for 5 days before harvesting. Data are mean \pm SEM. Asterisks indicate statistically significant difference between the OEX lines and their corresponding null segregant or wild type lines ($P < 0.05$, Student's t-test).

As the *Xenopus* oocyte system was giving inconclusive results on the Cl^- and NO_3^- permeability, we did not have direct evidence to suggest the substrates of *VviNPF2.1* and *VviNPF2.2*. We found that *VviNPF2.1* and *VviNPF2.2* injected oocytes have altered membrane potentials compared to the negative control oocytes (Figure 7.2). However, the net shift in membrane potential of the *VviNPF* expressing oocytes appeared to be the same as the water injected controls while changing the anion buffers. It is possible that *VviNPF2.1* and *VviNPF2.2* transport other substrates than Cl^- and NO_3^- , or they require co-expression partners to function as anion transporters in oocytes.

Taochy *et al.* (2015) used proteoliposomes to characterise the NO_3^- transport activity of AtNPF2.3, which is an approach that could be attempted in the future for VviNPF2.1 and VviNPF2.2. The substrates of the NPF family proteins include NO_3^- , oligopeptides, auxin, Cl^- ; there is evidence for dual Cl^- and NO_3^- transporting activity of *Aspergillus nidulans* NRT2 (Zhou *et al.* 2000), and evidence for NO_3^- regulated auxin uptake by AtNPF6.3 (Krouk *et al.* 2010). When propagating the Arabidopsis VviNPF2.2 transgenic lines for seed harvesting, some individuals exhibited prolonged vegetative growth and delayed flowering phenotypes (data not shown). It could be also interestingly to test if VviNPF2.1 and VviNPF2.2 are permeable to auxin.

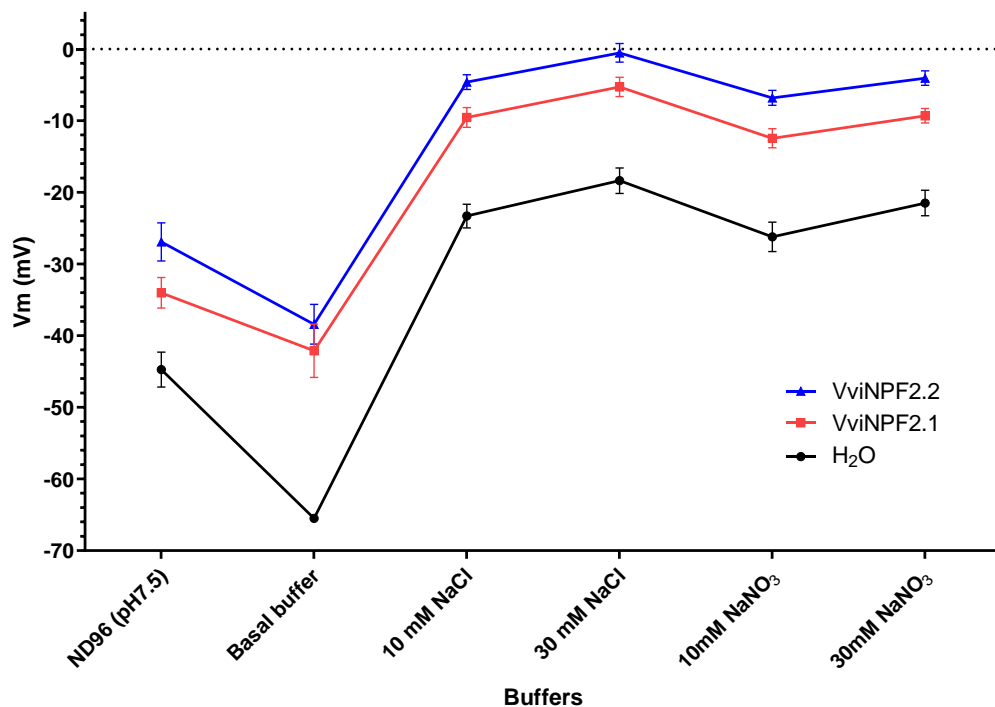


Figure 7.2: VviNPF2.1 and VviNPF2.2 injected oocytes have different membrane potentials compared to the water injected controls. *Xenopus* oocytes were injected with cRNA or water and incubated in the Ringer's solution for 2 days. The resting membrane potential (V_m) of the oocytes in each buffer were recorded using the TEVC rig. The pH of the buffers were adjusted to 5.5 except for the ND96 buffer. Data are mean \pm SEM ($n = 5 - 7$).

7.3 Characterisation of the *HKTs* in the QTL for grapevine Na⁺ exclusion

In the quantitative trait locus *NaE* for shoot Na⁺ exclusion, there are 6 *HKTs* and their locations are in close proximity. *VviHKT1;2* is not a full length *HKT*, therefore it was excluded from the downstream study. *VviHKT1;1* and *VviHKT1;3* are the only 2 *HKTs* in the QTL which were highly expressed in the roots, therefore they were considered the main candidates for shoot Na⁺ exclusion (Fasoli *et al.* 2012, Henderson *et al.* 2018a). The *VisHKT1;1* alleles were then found to be Na⁺ transporter genes, and the Na⁺ current magnitudes and the Na⁺ rectification properties were linked to the shoot [Na⁺] (Henderson *et al.* 2018a). In the same study, *VviHKT1;3* was expressed in *Xenopus* oocytes for two electrode voltage clamping (TEVC), but there were no Na⁺ or K⁺ associated currents observed.

7.3.1 The structure-function study of *VisHKT1;1*, *VviHKT1;3* and several plant *HKTs*

In Chapter 4, two key amino acid residue polymorphisms, S534R and G537D, which determined the Na⁺ conductance and the inward rectification property of the *VisHKT1;1*, were discovered based on the differences between the *VisHKT1;1* alleles. By mutating the S534 equivalent residue in *TaHKT1;5-D* (S506), *TaHKT1;5-D* could be turned into an inwardly rectifying Na⁺ transporter. Based on these findings, Dunlevy *et al.* (2018) proposed 3D models of the *VisHKT1;1* proteins based on the structural similarity between the *HKT* class of proteins and the *KtrB* K⁺ transporter from *Bacillus subtilis* (Vieira-Pires *et al.* 2013). The models displayed a pore restriction theory based on the possible interactions between the charged and uncharged key residues inside the pore of the *VisHKT1;1* protein, to explain the mechanism of the inward rectification.

In Appendix II, to validate the model, the proposed key residues of *OsHKT1;3* were mutated and expressed in the *Xenopus* oocyte system to test if the inward rectification could be released. However, none of the mutants displayed the predicted electrophysiological behaviour. We concluded that the 3D model proposed is a poor model for the plant *HKT* structure. The C-terminal tail of the *VviHKT1;3* is 9 amino acid residues shorter than that of *VviHKT1;1*. We suspected that the lack of cation transporting function of *VviHKT1;3* is due to this short truncation, therefore the 9-

residue-tail was added to the C-terminal of VviHKT1;3 by mutagenesis to create a chimera. The chimera was expressed in yeast to examine its effect on the Na⁺ dependant yeast growth inhibition, but no positive results were observed. We also attempted several other modification on the chimera based on its sequence alignment with VviHKT1;1 and the pore-forming region model proposed by Hauser and Horie (2010), but none of the mutants were successful in turning VviHKT1;3 a functional Na⁺ transporter in yeasts. The structural functional study of VviHKT1;3 was concluded unsuccessful.

At the early stage of the VisHKT1;1 characterisation, we attempted to examine the localisation of the protein transfecting Arabidopsis mesophyll protoplasts with N-terminal YFP tagged *VisHKT1;1* plasmids, but we were not able to find protoplasts with YFP signals in all attempts. Later, in order to correlate the amount of VisHKT1;1 proteins on the *Xenopus* oocyte plasma membrane with the TEVC current magnitudes, N-terminally tagged VisHKT1;1 was expressed in oocytes. The rectification properties of VisHKT1;1 were not altered by the N-terminal YFP tag, but no YFP signals could be detected on the oocytes under the confocal microscope. Therefore we considered N-terminal YFP tagging not appropriate for the localisation and expression study of the VisHKT1;1 (Appendix D).

7.3.2 VviHKT1;6, VviHKT1;7 and VviHKT1;8

The other 3 *HKTs* in the *NaE* QTL are *VviHKT1;6*, *VviHKT1;7* and *VviHKT1;8*. The microarray gene expression data (Fasoli *et al.* 2012) suggested that they were not highly expressed in the roots; however, it is possible that they could participate in Na⁺ homeostasis in other grapevine tissues, which could potentially affect Na⁺ partitioning. We characterised these *HKTs* in Chapter 5. Due to the heterozygosity of Cabernet Sauvignon and the sequence disagreements on the reference genome (Pinot Noir), we cloned and constructed all full-length alleles of *VviHKT1;6*, *VviHKT1;7* and *VviHKT1;8* from Cabernet Sauvignon. The TEVC data suggested that VviHKT1;6 and VviHKT1;7 alleles were strong Na⁺ transporters with no inward rectification, while the VviHKT1;8 alleles were inwardly rectifying weak Na⁺ transporters. The subcellular localisation results in tobacco leaf cells showed that the strong Na⁺ transporters were all localised to the plasma membrane, while the VviHKT1;8 alleles were both in the endosomal compartments. However, after the expression analyses using RT-qPCR and

using published RNA-seq data, we found that all of these *HKTs* were very poorly expressed in the tissue types tested. Given their low expression levels, we suggested that their role in grapevine Na^+ homeostasis are likely to be minor compared to *VviHKT1;1*; it's also possible that their expression was specific in certain cell types of low numbers, or their expression are triggered by certain stimuli which were not included in our study.

The *VviHKT1;8* allele A and B differ by only 1 amino acid residue, and the TEVC data showed that this difference resulted in significant changes in Na^+ conductance of the protein. It could be interesting to investigate whether this residue could be a key residue in the Na^+ conductance of the plant *HKTs*.

In the anion transporter study (Chapter 2), the RT-qPCR gene expression data showed that *VviALMT8* was lowly expressed in mature leaves; however, the *Arabidopsis promoter:GUS* results demonstrated that the low expression level may not be a result of the general low expression in leaf cells, but a result of its specific expression in the trichomes. Therefore, a *promoter:GUS* or *promoter:GFP* experiment in *Arabidopsis* could be an option for revealing the cell type specific, or stimuli triggered expression patterns of these *VviHKTs*.

7.4 Development of the R web app “Smart-IV” for automated ABF data IV processing

During the functional study of the anion and cation channels/transporters, two electrode voltage clamping was a technique which was intensively used. The conventional method for current (I) and voltage (V) data processing is a one-by-one data extraction process, which is overly time consuming and repetitive. In Chapter 5, we introduced the R web app “Smart-IV” and the R package “abftools” developed for reading and processing the electrophysiological data (mainly in the format of ABF2), for achieving automatic bulk processing of data. Smart-IV is specialised for multi-episodic fixed length voltage step TEVC data processing which requires no coding experience. It enables auto data grouping according to the index, automatic IV sampling time interval selection, waveform viewing, IV plotting and one-click data (voltage, current,

capacitance, conductance, specific current/conductance) export in a streamlined and user friendly manner. The TaHKT1;5-D TEVC IV data exported using the Smart-IV app was plotted with the same data extracted using the conventional method in Henderson *et al.* (2018a), and the IV curves demonstrated near perfect overlaps. Smart-IV can greatly accelerate the TEVC IV data extraction without compromising the flexibility of downstream data processing.

7.5 Summary

In summary, several new hypotheses can be formed out of this thesis at varying levels of maturity:

- 1) *VviALMT2* is a promising candidate that influences grapevine shoot Cl^- exclusion, mostly likely indirectly through increasing delivery of shoot NO_3^- .
- 2) *VviNPF2.1* and *VviNPF2.2*, resulting from a gene duplication event, also contribute towards shoot Cl^- exclusion.
- 3) Grapevine *HKT1;6*, *1;7* and *1;8* have minor roles in shoot Na^+ exclusion.

The key information pertinent to identifying genes associated with shoot salt exclusion in grapevine still needing to be gathered associated with this thesis are:

- A. Xylem NO_3^- levels from Arabidopsis overexpressing *VviALMT2* and *VviNPF2.1* and *VviNPF2.2*.
- B. Establishing a cell-based assay for *VviNPF2.1* and *VviNPF2.2* transport function.
- C. The conditions or cell types in which *VviHKT1;6* and *VviHKT1;7* are expressed.

References

- Baetz, U., Eisenach, C., Tohge, T., Martinoia, E. and De Angeli, A. (2016) Vacuolar chloride fluxes impact ion content and distribution during early salinity stress. *Plant Physiology*.
- De Angeli, A., Zhang, J., Meyer, S. and Martinoia, E. (2013) AtALMT9 is a malate-activated vacuolar chloride channel required for stomatal opening in *Arabidopsis*. *Nature Communications*, **4**, 1804.
- Dunlevy, J.D., Edwards, E.J., Walker, R.R., Blackmore, D.H., Walker, A.R., Henderson, S.W. and Gilliham, M. (2018) Genetic and mechanistic characterisation of rootstock traits conferring abiotic stress tolerance to grapevines. In *Final Report to Wine Australia*.
- Fasoli, M., Dal Santo, S., Zenoni, S., Tornielli, G.B., Farina, L., Zamboni, A., Porceddu, A., Venturini, L., Bicego, M., Murino, V., Ferrarini, A., Delledonne, M. and Pezzotti, M. (2012) The grapevine expression atlas reveals a deep transcriptome shift driving the entire plant into a maturation program. *The Plant Cell*, **24**, 3489-3505.
- Hauser, F. and Horie, T. (2010) A conserved primary salt tolerance mechanism mediated by HKT transporters: a mechanism for sodium exclusion and maintenance of high K^+/Na^+ ratio in leaves during salinity stress. *Plant, Cell & Environment*, **33**, 552-565.
- Henderson, S.W., Baumann, U., Blackmore, D.H., Walker, A.R., Walker, R.R. and Gilliham, M. (2014) Shoot chloride exclusion and salt tolerance in grapevine is associated with differential ion transporter expression in roots. *BMC Plant Biology*, **14**.
- Henderson, S.W., Dunlevy, J.D., Wu, Y., Blackmore, D.H., Walker, R.R., Edwards, E.J., Gilliham, M. and Walker, A.R. (2018) Functional differences in transport properties of natural HKT1;1 variants influence shoot Na^+ exclusion in grapevine rootstocks. *New Phytologist*, **217**, 1113-1127.
- Krouk, G., Lacombe, B., Bielach, A., Perrine-Walker, F., Malinska, K., Mounier, E., Hoyerova, K., Tillard, P., Leon, S., Ljung, K., Zazimalova, E., Benkova, E., Nacry, P. and Gojon, A. (2010) Nitrate-regulated auxin transport by NRT1.1 defines a mechanism for nutrient sensing in plants. *Developmental Cell*, **18**, 927-937.
- Li, B., Byrt, C., Qiu, J., Baumann, U., Hrmova, M., Evrard, A., Johnson, A.A., Birnbaum, K.D., Mayo, G.M., Jha, D., Henderson, S.W., Tester, M., Gilliham, M. and Roy, S.J. (2016) Identification of a stelar-localized transport protein that facilitates root-to-shoot transfer of chloride in *Arabidopsis*. *Plant Physiology*, **170**, 1014-1029.
- Li, B., Qiu, J., Jayakannan, M., Xu, B., Li, Y., Mayo, G.M., Tester, M., Gilliham, M. and Roy, S.J. (2017) AtNPF2.5 modulates chloride (Cl^-) efflux from roots of *Arabidopsis thaliana*. *Frontiers in Plant Science*, **7**, 2013.
- Ma, Z.-Y., Wen, J., Ickert-Bond, S.M., Chen, L.-Q. and Liu, X.-Q. (2016) Morphology, structure, and ontogeny of trichomes of the grape genus (*Vitis*, Vitaceae). *Frontiers in plant science*, **7**, 704-704.
- Schillmiller, A.L., Last, R.L. and Pichersky, E. (2008) Harnessing plant trichome biochemistry for the production of useful compounds. *The Plant Journal*, **54**, 702-711.
- Taochy, C., Gaillard, I., Ipotesi, E., Oomen, R., Leonhardt, N., Zimmermann, S., Peltier, J.B., Szponarski, W., Simonneau, T. and Sentenac, H. (2015) The *Arabidopsis* root stele transporter NPF2.3 contributes to nitrate translocation to shoots under salt stress. *The Plant Journal*, **83**, 466-479.
- Vieira-Pires, R.S., Szollosi, A. and Morais-Cabral, J.H. (2013) The structure of the KtrAB potassium transporter. *Nature*, **496**, 323-328.
- Wege, S., Gilliham, M. and Henderson, S.W. (2017) Chloride: not simply a 'cheap osmoticum', but a beneficial plant macronutrient. *Journal of Experimental Botany*, **68**, 3057-3069.
- Yoshida, M., Cowgill, S.E. and Wightman, J.A. (1997) Roles of oxalic and malic acids in chickpea trichome exudate in host-plant resistance to *Helicoverpa armigera*. *Journal of Chemical Ecology*, **23**, 1195-1210.

- Yuan, F., Leng, B. and Wang, B.** (2016) Progress in studying salt secretion from the salt glands in recretohalophytes: how do plants secrete salt? *Frontiers in Plant Science*, **7**, 977-977.
- Zhou, J., Trueman, L.J., Boorer, K.J., Theodoulou, F.L., Forde, B.G. and Miller, A.J.** (2000) A high affinity fungal nitrate carrier with two transport mechanisms. *Journal of Biological Chemistry*, **275**, 39894-39899.

Appendix I: The effects of N-terminal YFP tagging on the localisation and function of the grapevine HKT1;1

Materials and methods

Subcellular localisation of *VisHKT1;1* in *Arabidopsis thaliana* mesophyll protoplasts

VisHKT1;1 E^R , e^R , E^K and e^k CDS were recombined with pYFP-attR using LR Clonase II (Life Technologies) to generate vectors encoding *35S:YFP-VisHKT1;1*. The vectors were used to transform *E. coli* DH5alpha competent cells. Plasmids were harvested using Plasmid Midi Kits (Qiagen), and successful mutations were confirmed by Sanger sequencing.

Arabidopsis mesophyll protoplasts were harvested by the Tape-*Arabidopsis* Sandwich method (Wu *et al.* 2009). Protoplasts were transfected using a modified TEAMP method (Yoo *et al.* 2007). Approximately 15 µg of plasmid containing *35S:YFP-VisHKT1;1* were added to 0.2 mL of MMg solution containing approximately 5×10^4 protoplasts at room temperature. An equal volume of 30% (w/v) PEG (MW 4000) solution in 0.1 M CaCl₂ and 0.2 M mannitol was added to the mixture and incubated at room temperature for 5 min. W2 wash solution (1 M MES, 0.4 M mannitol, 15 mM KCl, 10 mM CaCl₂ and 5 mM MgCl₂) was slowly added to the mixture to a total volume of 2 mL after incubation. The mixture was gently mixed and the protoplasts were pelleted by centrifugation at $100 \times g$ for 1 min. The supernatant was discarded and the wash step was repeated twice using W2 solution. The protoplasts were resuspended with 1 mL of W2 solution, and transferred to 12-well plates coated with 1% BSA for incubation. The protoplasts were incubated under normal day light regime for 16 h at room temperature.

Transfected protoplasts were imaged after incubation using a Nikon A1R confocal laser scanning microscope and NIS-Elements C software (Nikon Corporation). FM4-64 was added to the protoplast mixture in a 1 in 1000 ratio as a plasma membrane marker, and the protoplasts were imaged after a 10 minute incubation at room temperature. Excitation/ emission conditions were YFP (488 nm/ 500 – 550 nm), FM4-64 (561 nm/ 570 – 620 nm), and chlorophyll (640 nm/650 – 720).

Adding a N-terminal YFP-tag to *VisHKT1;1*

VisHKT1;1 E^k and *e^k* were recombined with pGEMHE-DEST-YFP using LR Clonase II (Life Technologies) to generate vectors encoding *T7:YFP-VisHKT1;1*. The recombined vectors were linearised with NheI or SbfI (New England Biolabs). Capped RNA (cRNA) samples of the linearised vectors was synthesized using mMACHINE mMESSAGE mMACHINE T7 Transcription Kit.

Functional characterisation of the YFP tagged *VisHKT1;1* using TEVC

The cRNA concentrations of *YFP-VisHKT1;1 E^k* and *YFP-VisHKT1;1 e^k* were adjusted to the same. Stage IV and V *Xenopus laevis* oocytes were selected and injected with 42 nL (21 ng) of cRNA or water. The perfusion buffers for oocyte TEVC contained 6 mM MgCl₂, 1.8 mM CaCl₂ and 10 mM MES and was supplemented with 0 mM or 30 mM Na gluconate. pH of each buffer was adjusted to 5.5 using TRIS base and osmolality was adjusted to 230 mOsm/kg using D-mannitol.

The oocytes were incubated in Ringer's solution for 2 days post injection. Oocyte whole cell currents were recorded using an Oocyte Clamp OC-725C amplifier (Warner Instruments), digitised using an Axon Digidata 1400A (Molecular Devices) and the software Clampex 10.2 (Molecular Devices). TEVC were performed on the oocytes using the voltage step protocol with a holding potential of -40 mV for 300 ms and 350 ms either side of stepwise pulses from -140 mV to +60 mV in 20 mV increments for 550 ms.

The TEVC tested YFP-*VisHKT1;1* expressing oocytes were viewed under a confocal laser scanning microscope for imaging the YFP signals.

Results and discussion

***YFP-VisHKT1;1* transfected Arabidopsis mesophyll protoplasts did not show YFP signals**

To find out the subcellular localisation of *VisHKT1;1 E^R*, *e^R*, *E^K* and *e^k*, we first attempted transforming Arabidopsis mesophyll protoplasts with the N-terminal YFP tagged *VisHKT1;1*. When the transfected protoplasts were viewed under the confocal laser scanning microscope, the fluorescence signals were not observed or were too weak

to be differentiated from the background signals (data not shown). It is possible that the *Arabidopsis* mesophyll protoplast system is not suitable for the expression of VisHKT1;1, the fluorescence of the YFP could be compromised by the pH, or the protein structure was disrupted by linking the VisHKT1;1 with an N-terminal YFP. A C-terminal fluorescence protein tag or another transient gene expression system should be used for the subcellular localisation of the VisHKT1;1.

The inward rectification properties of the VisHKT1;1 in *Xenopus* oocytes were not changed by N-terminal YFP tagging

We aimed to correlate the current magnitude of the VisHKT1;1 E^R , e^R , E^K or e^K expressing oocytes and the VisHKT1;1 protein levels in the oocytes, to demonstrate that the current magnitude and the rectification differences among the VisHKT1;1 alleles were not the result of different protein levels in the oocyte plasma membrane. To achieve this, VisHKT1;1 E^K and e^K were tagged with N-terminal YFP and expressed in the *Xenopus* oocytes. The I-V results show that the rectification characteristics of VisHKT1;1 E^K and e^K were preserved when tagged with N-terminus YFP (Figure A1.1). However, when the TEVC tested oocytes were imaged for the YFP signal intensity, the signals could not be differentiated from the background fluorescence. This observation was similar to the observation in the *Arabidopsis* protoplast YFP-VisHKT1;1 localisation experiment, therefore we consider N-terminal YFP tag not appropriate for the localisation and expression study of the VisHKT1;1.

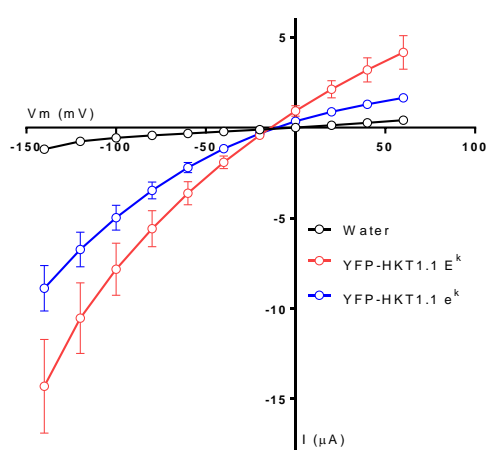


Figure A1.1: The I-V relationship of the N-terminal YFP tagged VisHKT1;1 expressing oocytes and the water controls in the basal buffer containing 30 mM Na⁺. Data are mean ± SEM (n= 7 – 11).

References

- Cao, H., Guo, S., Xu, Y., Jiang, K., Jones, A.M. and Chong, K.** (2011) Reduced expression of a gene encoding a Golgi localized monosaccharide transporter (OsGMST1) confers hypersensitivity to salt in rice (*Oryza sativa*). *Journal of Experimental Botany*, **62**, 4595-4604.
- Wu, F.H., Shen, S.C., Lee, L.Y., Lee, S.H., Chan, M.T. and Lin, C.S.** (2009) Tape-Arabidopsis sandwich - a simpler Arabidopsis protoplast isolation method. *Plant Methods*, **5**, 16.
- Yoo, S.D., Cho, Y.H. and Sheen, J.** (2007) Arabidopsis mesophyll protoplasts: a versatile cell system for transient gene expression analysis. *Nature Protocols*, **2**, 1565-1572.

Appendix II: Structure-function analyses of OsHKT1;3 and VviHKT1;3

Previously, Henderson *et al.* (2018a) found that the inward rectification property of VisHKT1;1 e^K can be released by the R534S mutation. To investigate the structural basis of the Na⁺ rectification activity of the grapevine HKTs, Dunlevy *et al.* (2018) collaborated with Professor Maria Hrmova (ACPF, University of Adelaide), and proposed 3D molecular models based on the structural similarity between the HKT proteins and chain I of the KtrB K⁺ transporter (accession number 4J7C:I) from *Bacillus subtilis* (Vieira-Pires *et al.* 2013) as performed for TaHKT1;5-D (Xu *et al.* 2018). In the VisHKT1;1 e^K model, it was proposed that the positively charged Arg-534 forms a salt link with Glu-193 with a separation of 3.1 Å, and a hydrogen bond to Tyr-445 (3.5 Å) (Figure A2.1A). These interactions could create a barrier to cations moving from the intracellular side of the protein through the pore, which result in the inward rectification property. To validate this model, several mutants of the inwardly rectifying Na⁺ transporter OsHKT1;3 were made to test whether the putative key residues could alter the rectification of OsHKT1;3.

In the study of Henderson *et al.* (2018a), VviHKT1;3 did not transport Na⁺ when expressed in *Xenopus laevis* oocytes and yeast. The fact that VviHKT1;3 is 9 residues shorter than VviHKT1;1 at the C-terminus was proposed to be the reason for the lack of Na⁺ transport activity through VviHKT1;3. However, the VviHKT1;3::1;1 chimera which adds the 9 residues of VviHKT1;1 to the C-terminal of VviHKT1;3 did not change the Na⁺ tolerance of the HKT expressing yeast. In this study, based on homology alignments of VviHKT1;1 and VviHKT1;3, we attempted several mutations on VviHKT1;3 and the VviHKT1;3::1;1 chimera, to test if VviHKT1;3 could be converted into a Na⁺ transporter.

Materials and methods

Site-directed mutagenesis

pGEMHE *OsHKT1;3*, pYES-DEST52 *VviHKT1;3* and pYES-DEST52 *VviHKT1;3::1;1 chimera* (obtained from Dunlevy *et al.* 2018) were used as templates to create 4 mutants of *OsHKT1;3* and 4 mutants of *VviHKT1;3* (Table A2.1). Primers

were designed as per manufacturer's instruction (In-Fusion HD Enzyme Premix, Clontech). The required gene fragments were amplified PCR reactions with Phusion High Fidelity DNA Polymerase (NEB). The PCR products were treated with cloning enhancer (Clontech) to remove the template, and treated with In-Fusion HD Enzyme Premix (Clontech) to recirculate as per manufacture's instruction. The In-Fusion reactions were used to transform 50 μ L *E.coli* Stellar competent cells (Clontech). Plasmids were harvested and successful mutations were confirmed by Sanger sequencing.

Electrophysiology with *Xenopus laevis* oocytes

pGEMHE-*OsHKT1;3* mutants were used as templates for cRNA synthesis (mMESSAGE mMACHINE T7 Transcription Kit, Invitrogen). Stage IV and V *X. laevis* oocytes were selected and were injected with the same amount of cRNA or 42 nL of water. The oocytes were incubated in Ca²⁺ Ringer's solution (96 mM NaCl, 2 mM KCl, 5 mM MgCl₂, 5 mM HEPES, 0.6 mM CaCl₂, 5% w/v horse serum, 500 μ g/mL tetracycline and 1 \times penicillin-streptomycin (Sigma P4333)) for 2 days post injection. TEVC were performed on the oocytes using the voltage step protocol with a holding potential of -40 mV for 300 ms and 350 ms either side of stepwise pulses from -140 mV to 60 mV in 20 mV increments for 550 ms.

Na⁺ inhibition of transgenic yeast growth

Mutants of pYES-DEST52 *VviHKT1;3* and pYES-DEST52 *VviHKT1;3::1;1 chimera* were used to transform *S. cerevisiae* strain INVSc2 (MATa, *his3 Δ -1*, *ura3-52*). Sterile yeast growth plates for Na⁺ growth inhibition tests were prepared using the SD-uracil liquid culture with 2% agar (Sigma) and supplemented with either 2% (w/v) D-glucose as control, or 2% (w/v) D-galactose for the induction of gene expression. Plates for the Na⁺ treatment were also supplemented with 50 mM NaCl. For the yeast spot test, yeast pre-cultures were made by incubating *HKT* transformed yeast and empty vector control yeast inoculated SD-uracil liquid cultures at 28 °C at 200 rpm overnight. Then overnight cultures were made by inoculating each 4.5 mL of SD-uracil liquid culture with 0.5 mL of the pre-culture. The overnight cultures were washed and diluted to an OD₆₀₀ of 1 with sterile water, and serially diluted (1 in 10). On each plate, 5 μ L of each

dilution were spotted on the surface and allowed to dry, then the plates were incubated at 28 °C for 2 days for glucose plates, and 3 days for galactose plates.

For the yeast streak plate Na⁺ growth inhibition test, a small amount of each selected yeast colony on plates was suspended in 40 µL of sterile water. Six regions with the same shape and area were marked on each plate; 4 µL of suspended yeasts were pipetted onto each region, streaked to spread and allowed to dry. Plates were incubated at 28 °C for 2 days for glucose plates, and 3 days for galactose plates.

Results and discussion

With the aim of confirming the proposed grapevine HKT Na⁺ rectification model, several VisHKT1;1 e^K mutants were made according to the proposed model (Figure A2.1), but none of the mutants showed the expected electrophysiological characteristics (Dunlevy *et al.* 2018). In this study, mutants of VisHKT1;1 and OsHKT1;3 were made in parallel to the structural functional study by Dunlevy *et al.* (2018) in order to test the model. A list of the mutants made, the expected outcomes and the actual outcomes is in Table A2.1.

The functional properties of the HKT mutants were tested using TEVC in the *Xenopus* oocyte system. It was proposed that the Na⁺ conductance of the HKTs could be normalised to the protein levels. We inserted a 9-amino-acid-long HA tag between residue 321 and 322 in VisHKT1;1 to enable TEVC measurements and Western-blotting on each oocyte, as it was predicted that this insertion would not affect the permeation of Na⁺ through the pore (Table A2.1). However, this insertion abolished the function of VisHKT1;1 e^K when expressed in oocytes (Figure A2.2).

To test if the model also applies to the HKTs in other plant species, we performed parallel mutations in rice OsHKT1;3 (Table A2.1) and tested their rectification properties in *Xenopus* oocytes using TEVC. The wild-type OsHKT1,3 displayed strong inward rectification (Figure A2.3A). The mutation of the VisHKT1;1 e^K R534 equivalent residue from asparagine to serine (N521S) did not release rectification as predicted (Figure A2.3B). The mutation of this asparagine residue into an arginine (N521R) did not increase rectification as predicted either (Figure A2.3C); however, it would be difficult to increase the already extreme inward rectification of this protein.

The model also predicted that the K518S mutation would release rectification (Table A2.1), but the rectification was not changed by this mutation (Figure A2.3D). In the report of Dunlevy *et al.* (2018), the VisHKT1;1 e^K loop region was deleted with the intention to increase the outward current, but the function of the protein was in fact abolished; the equivalent loop region in OshKT1;3 was also deleted and the Na⁺ transport activity was abolished as well (Figure A2.3E).

The construction of the VviHKT1;3::1;1 chimera aimed to turn VviHKT1;3 into a Na⁺ transporter by adding the last 9 residues of VviHKT1;1 to the tail of the wild type VviHKT1;3; however, growth of the chimera expressing yeast was not affected by the addition of Na⁺ (Dunlevy *et al.* 2018) (Figure A2.4A). We then aimed to identify potential key residues for the Na⁺ transporting property of VviHKT1;3 by homology alignments.

Several plant HKTs, including VviHKT1;1, which are known to transport Na⁺ have the conserved amino acid sequence GRLK[KT]F[SRN]M at the tail region, while VviHKT1;3 has the sequence GKLRKFGK (the residue differences between VviHKT1;1 and VviHKT1;3 are underlined). We prepared two mutant variants of the VviHKT1;3::1;1 chimera as proposed by Professor Maria Hrmova and tested them in yeast to see whether the modification of amino acids near the C-terminus could restore VviHKT1;3's ability in Na⁺ transport (Table A2.1). A VviHKT1;3::1;1 chimera G530S/K531M double mutant was made which aimed to convert the Gly-530 at the equivalent "rectification residue" (R534 in VisHKT1;1 e^K) to serine, and to change the Lys-531 to a methionine to make it the same as HKT1;1. The other mutant VviHKT1;3::1;1 chimera K525R/R527K was an attempt to make the tail region of VviHKT1;3 similar to the tail region of VviHKT1;1. On the HKT expression induction plates (galactose), growth of the yeast strains containing the VviHKT1;3::1;1 chimera and the empty vector negative control was not inhibited by 50 mM Na⁺, while the positive control AtHKT1;1 was strongly inhibited (Figure A2.4B), which is consistent with its role as a Na⁺ transporter. The mutant VviHKT1;3::1;1 chimera proteins, which were predicted to be functional, failed to confer Na⁺ dependant yeast growth inhibition from three independent transformants (Figure A2.4B). These results suggest the mutant proteins were non-functional as Na⁺ transporter, and these residues at the tail region are unlikely to be the key residues for the Na⁺ transport activity of VviHKT1;3.

To explore whether there could be other key residues which could make VviHKT1;3 a cation transporter, we compared the pore-forming region sequence of VviHKT1;3 to other HKTs in the homology model. In the plant HKT alignment in Hauser and Horie (2010), plant HKT1 subgroup members have highly conserved pore-forming region D sequences; however, the Gly-478 in the pore region D is substituted to alanine in VviHKT1;3, which was unique. The VviHKT1;3 A478G mutant was an attempt to convert the alanine back to a glycine, but this mutant failed to confer Na⁺ dependant yeast growth inhibition when the transgene was expressed (Figure A2.4C – D). Out of the 4 pore-forming regions, the pore region B of VviHKT1;3 is 5 residues different from the pore region B of VviHKT1;1. The VviHKT1;3 P_B domain swap mutant replaced the pore region B of HKT1;3 with the pore region B of VviHKT1;1, but the mutant did not confer a Na⁺ growth phenotype in yeast (Figure A2.4E – F). It's highly likely that residues in pore region B are not the key residues to turn VviHKT1;3 into a functional Na⁺ transporter.

Summary

In this study, mutations of the plant HKTs were performed as a functional test of the homology model (Dunlevy *et al.* 2018) (Figure A2.1) that we hoped could explain the structural basis of rectification and conductance in the grapevine HKTs. None of these mutations gave the result that was predicted by the homology model (Table A2.1). This suggests that this particular homology model is a poor indicator of grapevine HKT structure and might not be the optimum model for predicting the functional properties of this class of transporter in some plant species.

References

- Dunlevy, J.D., Edwards, E.J., Walker, R.R., Blackmore, D.H., Walker, A.R., Henderson, S.W. and Gilliam, M. (2018) Genetic and mechanistic characterisation of rootstock traits conferring abiotic stress tolerance to grapevines. In *Final Report to Wine Australia*.
- Hauser, F. and Horie, T. (2010) A conserved primary salt tolerance mechanism mediated by HKT transporters: a mechanism for sodium exclusion and maintenance of high K⁺/Na⁺ ratio in leaves during salinity stress. *Plant, Cell & Environment*, **33**, 552-565.
- Henderson, S.W., Dunlevy, J.D., Wu, Y., Blackmore, D.H., Walker, R.R., Edwards, E.J., Gilliam, M. and Walker, A.R. (2018) Functional differences in transport properties of natural HKT1;1 variants influence shoot Na⁺ exclusion in grapevine rootstocks. *New Phytologist*, **217**, 1113-1127.
- Vieira-Pires, R.S., Szollosi, A. and Morais-Cabral, J.H. (2013) The structure of the KtrAB potassium transporter. *Nature*, **496**, 323-328.

Xu, B., Waters, S., Byrt, C.S., Plett, D., Tyerman, S.D., Tester, M., Munns, R., Hrmova, M. and Gilliam, M. (2018) Structural variations in wheat HKT1;5 underpin differences in Na⁺ transport capacity. *Cellular and Molecular Life Sciences*, **75**, 1133-1144.

Figures and tables

Figure A2.1

VisHKT1;1 e^K

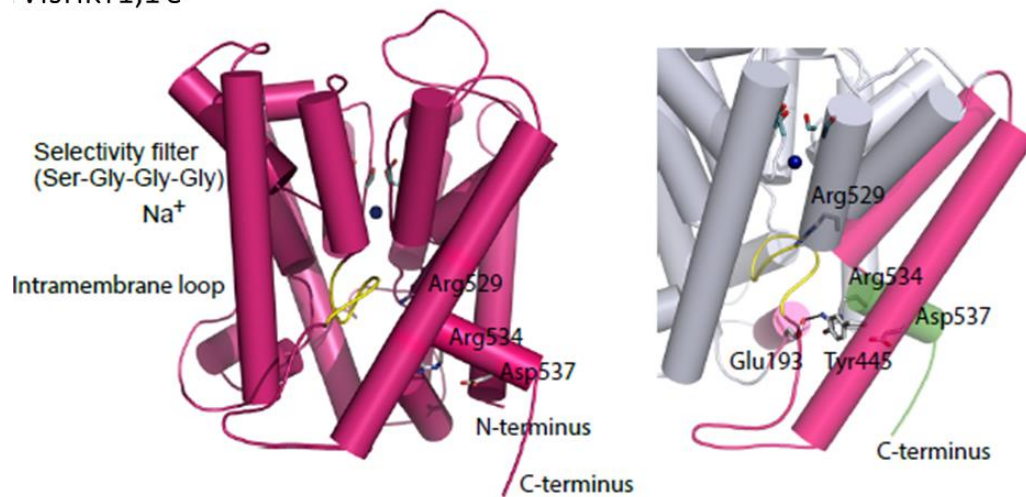


Figure A2.1: The three dimensional molecular model of VisHKT1;1 e^K (Dunlevy *et al.* 2018). The cartoon shows the overall fold of VisHKT1;1 e^K and its α -helices. Arg-534 on a C-terminal α -helix (green) forms a salt link with Glu-193 (3.1 Å) and a hydrogen bond with Tyr-445 (3.5 Å); the two latter residues are located on magenta α -helices.

Table A2.1: Summary of predicted and observed effects of mutating VisHKT1;1, OsHKT1;3 and VviHKT1;3 based on homology model proposed in the report of Dunlevy *et al.* (2018).

Protein	Allele	Mutation	Expression system	Predicted effect	Observed effect
VisHKT1;1	e ^K	Insert HA TAG (YPYDVPDYA) between I321 and S322	<i>Xenopus</i> oocyte	No change to wildtype	Function abolished
OsHKT1;3	N/A	N521S	<i>Xenopus</i> oocyte	Release rectification	No change to wildtype
		N521R	<i>Xenopus</i> oocyte	Increase rectification	No change to wildtype
		K518S	<i>Xenopus</i> oocyte	Release rectification	No change to wildtype
		Deletion of "loop" residues 396-407 (loop deleted)	<i>Xenopus</i> oocyte	Increased outward current	Function abolished
VviHKT1;3:1;1 chimera	Cabernet Sauvignon	K525R/R527K (inversion to "RLK")	Yeast	Transporter becomes functional	No change to wildtype
		G530S/K531M ("SM")	Yeast	Transporter becomes functional	No change to wildtype
VviHKT1;3	Cabernet Sauvignon	A478G	Yeast	Transporter becomes functional	No change to wildtype
		Replace residue 239-257 with residue 243-261 of VviHKT1;1 (P _B domain swap with VviHKT1;1)	Yeast	Transporter becomes functional	No change to wildtype

Figure A2.2

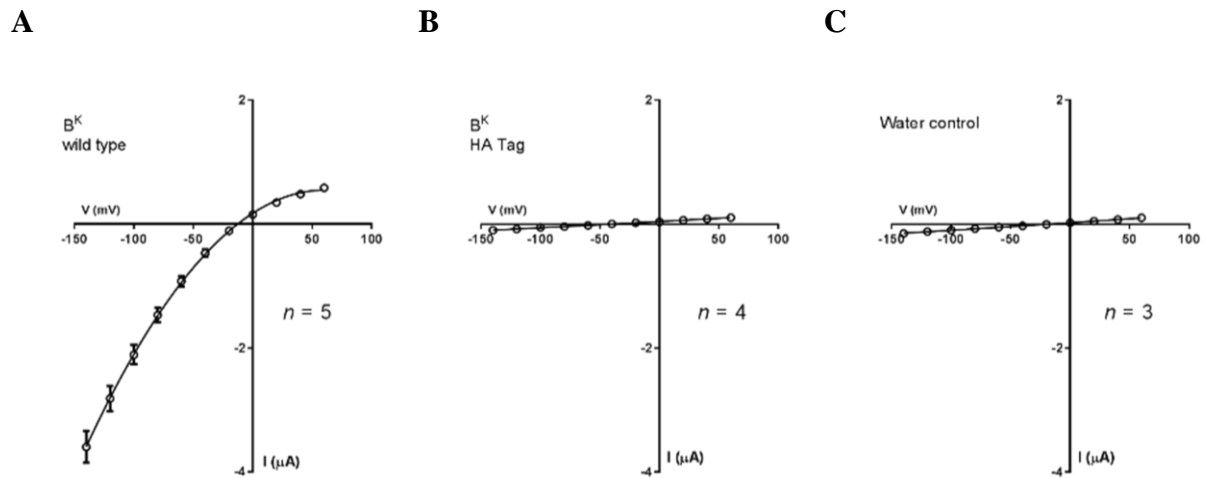


Figure A2.2: Comparison of the VisHKT1;1 e^K HA tag mutation to the wild type. (A – C) Current-voltage relationships of oocytes expressing (A) VisHKT1;1 e^K wild type (B) VisHKT1;1 e^K HA tag (C) water injected controls. The perfusion buffer contained 30 mM sodium gluconate. Oocytes were clamped 1-day post injection. Data are mean ± SEM (n shown inset).

Figure A2.3

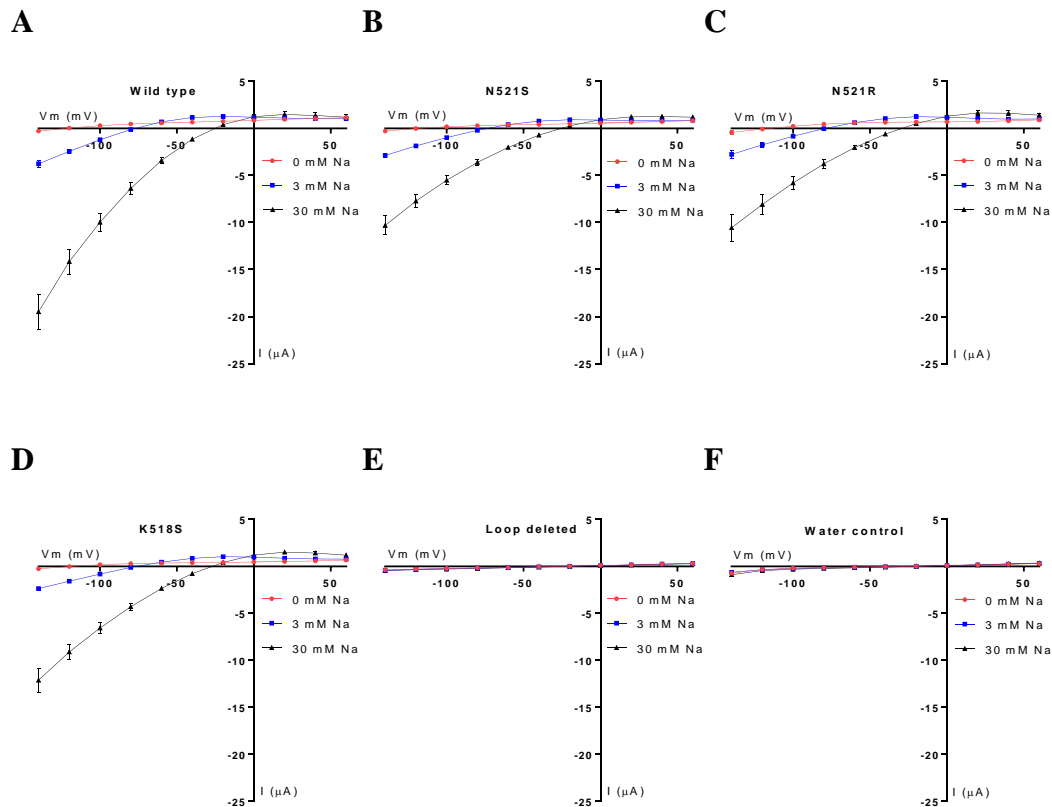


Figure A2.3: Electrophysiological properties of rice OsHKT1;3 mutants in *Xenopus* oocytes. (A – F) Voltage dependant currents of oocytes expressing (A) OsHKT1;3 wild type, (B) OsHKT1;3 N521S, (C) OsHKT1;3 N521R, (D) OsHKT1;3 K518S, (E) OsHKT1;3 loop deleted and (F) water injected controls, in perfusion buffers containing 0 mM Na⁺ (red line), 3 mM Na⁺ (blue line) or 30 mM Na⁺ (black line). Oocytes were TEVC tested 2-days post injection. Data are mean \pm SEM ($n = 4 - 10$ oocytes).

Figure A2.4

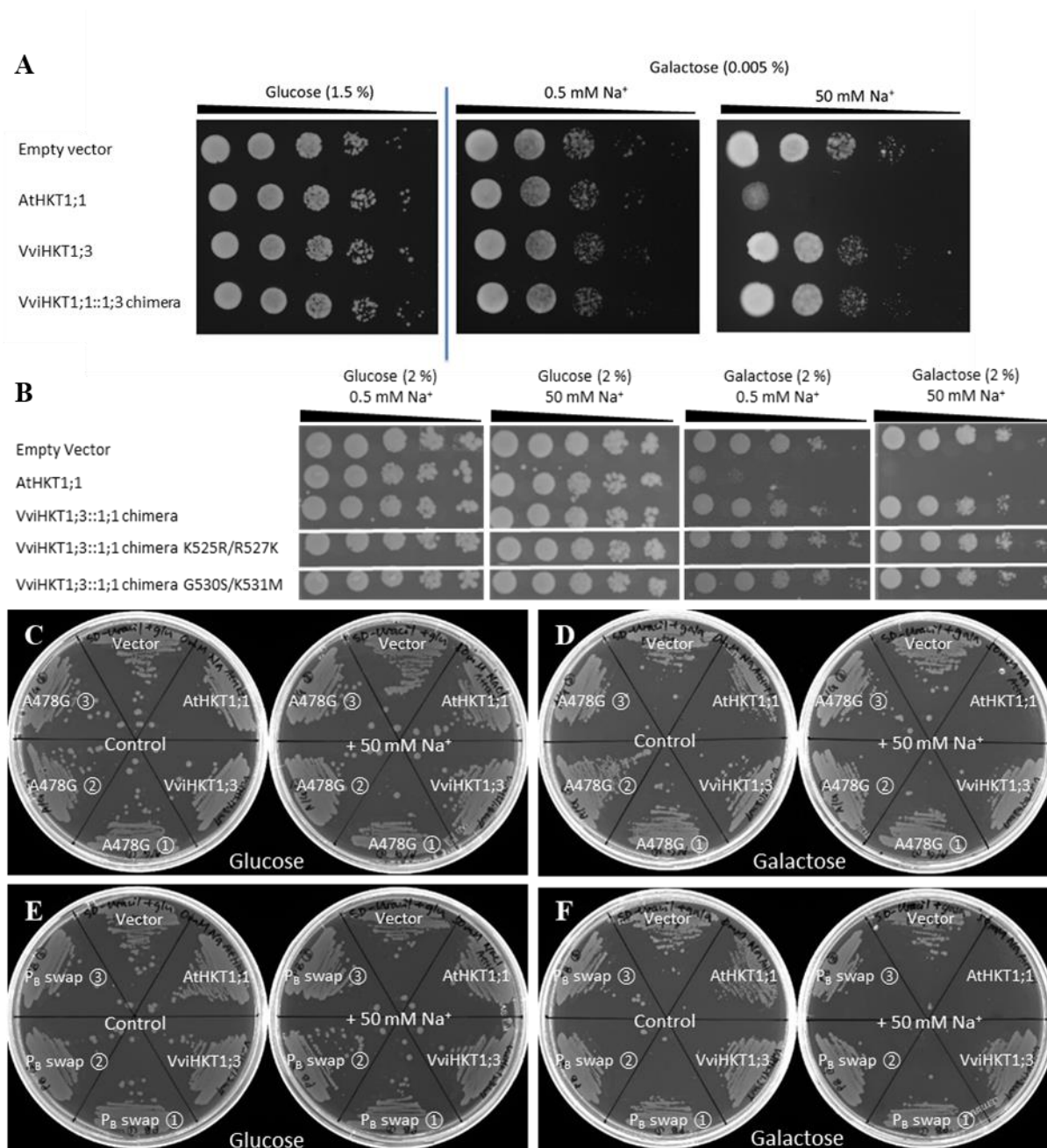


Figure A2.4: Growth of the VviHKT1;3 mutant expressing yeasts were not influenced by 50 mM Na⁺. INVSc2 yeasts (MATa, *his3Δ-1*, *ura3-52*) were transformed with pYES-DEST52 empty vector (negative control) or the same vector containing either *AtHKT1;1* (positive control), *VviHKT1;3*, *VviHKT1;3::1;1 chimera* or the *VviHKT1;3* mutants. Three individual transformation events of each mutant (*VviHKT1;3::1;1 chimera K525R R527K*, *VviHKT1;3::1;1 chimera G530S K531M*, *VviHKT1;3 A478G*, *VviHKT1;3 P_B domain swap with HKT1;1*) were tested. SD (–Uracil) agar plates

containing either D-glucose (control) or D-galactose (induction) with or without 50 mM NaCl were used as growth media. (A – B) Yeasts from overnight liquid cultures were diluted to $OD_{600} = 1$, and then four 1 in 10 serial dilutions of each strain were made; 5 μ L of each dilution were spotted onto each plate. Plates were incubated at 30 °C for 3 days. (C – F) A small amount of yeasts from each 3-day-old yeast stock plate were diluted in 40 μ L of water, and 4 μ L of the diluted yeasts were streaked onto each designated area on each plate. Plates were incubated at 30 °C for 3 days. The ①②③ symbols represent different individual transformation events. Figure A2.4A was obtained from Henderson, S.W. and presented with permission.

Bibliography

- Abbaspour, N.** (2008a) A comparative study of Cl⁻ transport across the roots of two grapevine rootstocks, K 51-40 and Paulsen, differing in salt tolerance. In *Discipline of Wine and Horticulture*. Adelaide: University of Adelaide.
- Abbaspour, N.** (2008b) A comparative study of Cl transport across the roots of two grapevine rootstocks, K 51-40 and Paulsen, differing in salt tolerance. In *Discipline of Wine and Horticulture*. Adelaide: University of Adelaide.
- Abbaspour, N., Kaiser, B. and Tyerman, S.** (2013) Chloride transport and compartmentation within main and lateral roots of two grapevine rootstocks differing in salt tolerance. *Trees*, **27**, 1317-1325.
- Abbaspour, N., Kaiser, B. and Tyerman, S.** (2014) Root apoplastic transport and water relations cannot account for differences in Cl⁻ transport and Cl⁻/NO₃⁻ interactions of two grapevine rootstocks differing in salt tolerance. *Acta Physiologiae Plantarum*, **36**, 687-698.
- Abdolzadeh, A., Shima, K., Lambers, H. and Chiba, K.** (2008) Change in uptake, transport and accumulation of ions in *Nerium oleander* (Rosebay) as affected by different nitrogen sources and salinity. *Annals of Botany*, **102**, 735-746.
- ABS** (2002) Salinity on Australian Farms, 2002: Australian Bureau of Statistics.
- Accardi, A. and Miller, C.** (2004) Secondary active transport mediated by a prokaryotic homologue of ClC Cl⁻ channels. *Nature*, **427**, 803-807.
- Allakhverdiev, S.I., Nishiyama, Y., Suzuki, I., Tasaka, Y. and Murata, N.** (1999) Genetic engineering of the unsaturation of fatty acids in membrane lipids alters the tolerance of *Synechocystis* to salt stress. *Proceedings of the National Academy of Sciences*, **96**, 5862-5867.
- Allakhverdiev, S.I., Sakamoto, A., Nishiyama, Y., Inaba, M. and Murata, N.** (2000a) Ionic and osmotic effects of NaCl-induced inactivation of photosystems I and II in *Synechococcus* sp. *Plant Physiology*, **123**, 1047-1056.
- Allakhverdiev, S.I., Sakamoto, A., Nishiyama, Y. and Murata, N.** (2000b) Inactivation of photosystems I and II in response to osmotic stress in *Synechococcus*. contribution of water channels. *Plant Physiology*, **122**, 1201-1208.
- Antcliff, A.J., Newman, H.P. and Barrett, H.C.** (1983) Variation in chloride accumulation in some American species of grapevine. *Vitis*, **22**, 357-362.
- Apse, M.P., Aharon, G.S., Snedden, W.A. and Blumwald, E.** (1999) Salt tolerance conferred by overexpression of a vacuolar Na⁺/H⁺ antiport in *Arabidopsis*. *Science*, **285**, 1256-1258.
- Arpat, A.B., Magliano, P., Wege, S., Rouached, H., Stefanovic, A. and Poirier, Y.** (2012) Functional expression of PHO1 to the Golgi and trans-Golgi network and its role in export of inorganic phosphate. *The Plant Journal*, **71**, 479-491.
- AWRI** (2015) Analytical requirements for the export of Australian wine: Sodium standards: The Australian Wine Research Institute.
- Baby, T., Collins, C., Tyerman, S.D. and Gilliam, M.** (2016) Salinity negatively affects pollen tube growth and fruit set in grapevines and is not mitigated by silicon. *American Journal of Enology and Viticulture*, **67**, 218-228.
- Baby, T., Hocking, B., Tyerman, S.D., Gilliam, M. and Collins, C.** (2014) Modified method for producing grapevine plants in controlled environments. *American Journal of Enology and Viticulture*.
- Baetz, U., Eisenach, C., Tohge, T., Martinoia, E. and De Angeli, A.** (2016) Vacuolar chloride fluxes impact ion content and distribution during early salinity stress. *Plant Physiology*.

- Bañuls, J., Legaz, F. and Primo-Millo, E.** (1990) Effect of salinity on uptake and distribution of chloride and sodium in some citrus scion-rootstock combinations. *Journal of Horticultural Science*, **65**, 715-724.
- Barragán, V., Leidi, E.O., Andrés, Z., Rubio, L., De Luca, A., Fernández, J.A., Cubero, B. and Pardo, J.M.** (2012) Ion exchangers NHX1 and NHX2 mediate active potassium uptake into vacuoles to regulate cell turgor and stomatal function in *Arabidopsis*. *The Plant Cell*, **24**, 1127-1142.
- Bassil, E., Ohto, M.-a., Esumi, T., Tajima, H., Zhu, Z., Cagnac, O., Belmonte, M., Peleg, Z., Yamaguchi, T. and Blumwald, E.** (2011) The *Arabidopsis* intracellular Na⁺/H⁺ antiporters NHX5 and NHX6 are endosome associated and necessary for plant growth and development. *The Plant cell*, **23**, 224-239.
- Batistič, O., Sorek, N., Schültke, S., Yalovsky, S. and Kudla, J.** (2008) Dual fatty acyl modification determines the localization and plasma membrane targeting of CBL/CIPK Ca²⁺ signaling complexes in arabidopsis. *The Plant Cell*, **20**, 1346-1362.
- Berg, H.W. and Keefer, R.M.** (1958) Analytical determination of tartrate stability in wine. I. Potassium bitartrate. *American Journal of Enology and Viticulture*, **9**, 180-193.
- Bergsdorf, E.-Y., Zdebik, A.A. and Jentsch, T.J.** (2009a) Residues important for nitrate/proton coupling in plant and mammalian CLC transporters. *Journal of Biological Chemistry*, **284**, 11184-11193.
- Bergsdorf, E.-Y., Zdebik, A.A. and Jentsch, T.J.** (2009b) Residues important for nitrate/proton coupling in plant and mammalian CLC transporters. *The Journal of Biological Chemistry*, **284**, 11184-11193.
- Bernstein, L., Ehlig, C.F. and Clark, R.A.** (1969) Effect of grape rootstocks on chloride accumulation in leaves. *Journal of the American Society for Horticultural Science*, **94**, 584-590.
- Berthomieu, P., Conéjéro, G., Nublat, A., Brackenbury, W.J., Lambert, C., Savio, C., Uozumi, N., Oiki, S., Yamada, K., Cellier, F., Gosti, F., Simonneau, T., Essah, P.A., Tester, M., Véry, A.-A., Sentenac, H. and Casse, F.** (2003) Functional analysis of AtHKT1 in *Arabidopsis* shows that Na⁺ recirculation by the phloem is crucial for salt tolerance. *The EMBO Journal*, **22**, 2004-2014.
- Biswas, T., Bourne, J., McCarthy, M. and Rengasamy, P.** (2008) Sustainable salinity management in your vineyard: South Australian Research and Development Institute.
- Black, R.** (1956) Effect of NaCl in Water Culture on the Ion Uptake and growth of *Atriplex Hastata* L. *Australian Journal of Biological Sciences*, **9**, 67-80.
- Bolaños, L., Martín, M., El-Hamdaoui, A., Rivilla, R. and Bonilla, I.** (2006) Nitrogenase inhibition in nodules from pea plants grown under salt stress occurs at the physiological level and can be alleviated by B and Ca. *Plant and Soil*, **280**, 135-142.
- Brumos, J., Colmenero-Flores, J.M., Conesa, A., Izquierdo, P., Sanchez, G., Iglesias, D.J., Lopez-Climent, M.F., Gomez-Cadenas, A. and Talon, M.** (2009) Membrane transporters and carbon metabolism implicated in chloride homeostasis differentiate salt stress responses in tolerant and sensitive *Citrus* rootstocks. *Funct Integr Genomics*, **9**, 293-309.
- Butterworth, S.** (1930) On the theory of filter amplifiers. *Experimental Wireless and the Wireless Engineer*, **7**, 536-541.
- Byrt, C., Xu, B., Krishnan, M., Lightfoot, D., Athman, A., Jacobs, A., Watson-Haigh, N., Munns, R., Tester, M. and Gilliam, M.** (2014) The Na⁺ transporter, TaHKT1;5-D, limits shoot Na⁺ accumulation in bread wheat. In *The Plant Journal*.
- Byrt, C.S., Platten, J.D., Spielmeyer, W., James, R.A., Lagudah, E.S., Dennis, E.S., Tester, M. and Munns, R.** (2007) HKT1;5-like cation transporters linked to Na⁺ exclusion loci in wheat, *Nax2* and *Kna1*. *Plant Physiology*, **143**, 1918-1928.

- Cataldo, D.A., Maroon, M., Schrader, L.E. and Youngs, V.L.** (1975) Rapid colorimetric determination of nitrate in plant tissue by nitration of salicylic acid. *Communications in Soil Science and Plant Analysis*, **6**, 71-80.
- Chen, C.-Z., Lv, X.-F., Li, J.-Y., Yi, H.-Y. and Gong, J.-M.** (2012) Arabidopsis NRT1.5 is another essential component in the regulation of nitrate reallocation and stress tolerance. *Plant Physiology*, **159**, 1582-1590.
- Chen, Z.C., Yamaji, N., Fujii-Kashino, M. and Ma, J.F.** (2016) A cation-chloride cotransporter gene is required for cell elongation and osmoregulation in rice. *Plant Physiology*, **171**, 494-507.
- Chin, C.-S., Peluso, P., Sedlazeck, F.J., Nattestad, M., Concepcion, G.T., Clum, A., Dunn, C., O'Malley, R., Figueroa-Balderas, R., Morales-Cruz, A., Cramer, G.R., Delledonne, M., Luo, C., Ecker, J.R., Cantu, D., Rank, D.R. and Schatz, M.C.** (2016) Phased diploid genome assembly with single-molecule real-time sequencing. *Nature Methods*, **13**, 1050.
- Clough, S.J. and Bent, A.F.** (1998) Floral dip: a simplified method for *Agrobacterium*-mediated transformation of *Arabidopsis thaliana*. *The Plant Journal*, **16**, 735-743.
- Cochetel, N., Escudie, F., Cookson, S.J., Dai, Z., Vivin, P., Bert, P.F., Munoz, M.S., Delrot, S., Klopp, C., Ollat, N. and Lauvergeat, V.** (2017) Root transcriptomic responses of grafted grapevines to heterogeneous nitrogen availability depend on rootstock genotype. *Journal of Experimental Botany*, **68**, 4339-4355.
- Colmenero-Flores, J.M., Martinez, G., Gamba, G., Vazquez, N., Iglesias, D.J., Brumos, J. and Talon, M.** (2007) Identification and functional characterization of cation-chloride cotransporters in plants. *The Plant Journal*, **50**, 278-292.
- Commonwealth of Australia** (2014) Wine production requirements (Australia only): Commonwealth of Australia.
- Conn, S., Hocking, B., Dayod, M., Xu, B., Athman, A., Henderson, S., Aukett, L., Conn, V., Shearer, M., Fuentes, S., Tyerman, S. and Gilliham, M.** (2013) Protocol: optimising hydroponic growth systems for nutritional and physiological analysis of *Arabidopsis thaliana* and other plants. *Plant Methods*, **9**, 4.
- Corratge-Faillie, C. and Lacombe, B.** (2017) Substrate (un)specificity of Arabidopsis NRT1/PTR FAMILY (NPF) proteins. *Journal of Experimental Botany*.
- Cubero-Font, P., Maierhofer, T., Jaslan, J., Rosales, M.A., Espartero, J., Diaz-Rueda, P., Muller, H.M., Hurter, A.L., Al-Rasheid, K.A., Marten, I., Hedrich, R., Colmenero-Flores, J.M. and Geiger, D.** (2016) Silent S-Type anion channel subunit SLAH1 gates SLAH3 open for chloride root-to-shoot translocation. *Current Biology*, **26**, 2213-2220.
- De Angeli, A., Baetz, U., Francisco, R., Zhang, J., Chaves, M. and Regalado, A.** (2013a) The vacuolar channel VvALMT9 mediates malate and tartrate accumulation in berries of *Vitis vinifera*. *Planta*, **238**, 283-291.
- De Angeli, A., Monachello, D., Ephritikhine, G., Frachisse, J.M., Thomine, S., Gambale, F. and Barbier-Brygoo, H.** (2006) The nitrate/proton antiporter AtCLCa mediates nitrate accumulation in plant vacuoles. *Nature*, **442**, 939-942.
- De Angeli, A., Monachello, D., Ephritikhine, G., Frachisse, J.M., Thomine, S., Gambale, F. and Barbier-Brygoo, H.** (2009) CLC-mediated anion transport in plant cells. *Philosophical Transactions of the Royal Society B-Biological Sciences*, **364**, 195-201.
- De Angeli, A., Zhang, J., Meyer, S. and Martinoia, E.** (2013b) AtALMT9 is a malate-activated vacuolar chloride channel required for stomatal opening in *Arabidopsis*. *Nature Communications*, **4**, 1804.
- de Loryn, L.C., Petrie, P.R., Hasted, A.M., Johnson, T.E., Collins, C. and Bastian, S.E.P.** (2014) Evaluation of sensory thresholds and perception of sodium chloride in grape juice and wine. *American Journal of Enology and Viticulture*, **65**, 124-133.

- Diatloff, E., Kumar, R. and Schachtman, D.P.** (1998) Site directed mutagenesis reduces the Na⁺ affinity of HKT1, an Na⁺ energized high affinity K⁺ transporter. *FEBS Letters*, **432**, 31-36.
- Diédhiou, C.J. and Gollmack, D.** (2006) Salt-dependent regulation of chloride channel transcripts in rice. *Plant Science*, **170**, 793-800.
- Donkin, R., Robinson, S., Sumby, K., Harris, V., McBryde, C. and Jiranek, V.** (2010) Sodium chloride in Australian grape juice and its effect on alcoholic and malolactic fermentation. *American Journal of Enology and Viticulture*, **61**, 392-400.
- Downton, W.J.S.** (1977a) Chloride accumulation in different species of grapevine. *Scientia Horticulturae*, **7**, 249-253.
- Downton, W.J.S.** (1977b) Photosynthesis in salt-stressed grapevines. *Functional Plant Biology*, **4**, 183-192.
- Downton, W.J.S. and Loveys, B.R.** (1981) Abscisic acid content and osmotic relations of salt-stressed grapevine leaves. *Functional Plant Biology*, **8**, 443-452.
- Downton, W.J.S., Loveys, B.R. and Grant, W.J.R.** (1990) Salinity effects on the stomatal behaviour of grapevine. *New Phytologist*, **116**, 499-503.
- Dunlevy, J.D., Edwards, E.J., Walker, R.R., Blackmore, D.H., Walker, A.R., Henderson, S.W. and Gilliham, M.** (2018) Genetic and mechanistic characterisation of rootstock traits conferring abiotic stress tolerance to grapevines. In *Final Report to Wine Australia*.
- Ehlig, C.F.** (1960) Effects of salinity on four varieties of table grapes grown in sand culture. In *Proceedings of the American Society for Horticultural Science*, pp. 323-331.
- FAO** (2005) Global network on integrated soil management for sustainable use of salt-affected soils: FAO Land and Plant Nutrition Management Services Rome.
- FAO** (2008) FAO Land and Plant Nutrition Management Service.
- Fasoli, M., Dal Santo, S., Zenoni, S., Tornielli, G.B., Farina, L., Zamboni, A., Porceddu, A., Venturini, L., Bicego, M., Murino, V., Ferrarini, A., Delledonne, M. and Pezzotti, M.** (2012) The grapevine expression atlas reveals a deep transcriptome shift driving the entire plant into a maturation program. *The Plant Cell*, **24**, 3489-3505.
- Felle, H.H.** (1994) The H⁺/Cl⁻ symporter in root-hair cells of *sinapis alba* (an electrophysiological study using ion-selective microelectrodes). *Plant Physiology*, **106**, 1131-1136.
- Fisarakis, I., Chartzoulakis, K. and Stavrakas, D.** (2001) Response of Sultana vines (*V. vinifera* L.) on six rootstocks to NaCl salinity exposure and recovery. *Agricultural Water Management*, **51**, 13-27.
- Fisarakis, I., Nikolaou, N., Tsikalas, P., Therios, I. and Stavrakas, D.** (2005) Effect of salinity and rootstock on concentration of potassium, calcium, magnesium, phosphorus, and nitrate–nitrogen in Thompson Seedless grapevine. *Journal of Plant Nutrition*, **27**, 2117-2134.
- Fort, K.P., Heinitz, C.C. and Walker, M.A.** (2015) Chloride exclusion patterns in six grapevine populations. *Australian Journal of Grape and Wine Research*, **21**, 147-155.
- Garcia-deblás, B., Senn, M.E., Bañuelos, M.A. and Rodríguez-Navarro, A.** (2003) Sodium transport and HKT transporters: the rice model. *The Plant Journal*, **34**, 788-801.
- Gassman, W., Rubio, F. and Schroeder, J.I.** (1996) Alkali cation selectivity of the wheat root high-affinity potassium transporter HKT1. *The Plant Journal*, **10**, 869-852.
- Gaxiola, R.A., Rao, R., Sherman, A., Grisafi, P., Alper, S.L. and Fink, G.R.** (1999) The *Arabidopsis thaliana* proton transporters, AtNhx1 and Avp1, can function in cation detoxification in yeast. *Proceedings of the National Academy of Sciences*, **96**, 1480-1485.
- Geelen, D., Lurin, C., Bouchez, D., Frachisse, J.-M., Lelièvre, F., Courtial, B., Barbier-Brygoo, H. and Maurel, C.** (2000a) Disruption of putative anion channel gene AtCLC-a in *Arabidopsis* suggests a role in the regulation of nitrate content. *The Plant Journal*, **21**, 259-267.

- Geelen, D., Lurin, C., Bouchez, D., Frachisse, J.M., Lelievre, F., Courtial, B., Barbier-Brygoo, H. and Maurel, C.** (2000b) Disruption of putative anion channel gene *AtCLC-a* in Arabidopsis suggests a role in the regulation of nitrate content. *The Plant Journal*, **21**, 259-267.
- Geiger, D., Maierhofer, T., AL-Rasheid, K.A.S., Scherzer, S., Mumm, P., Liese, A., Ache, P., Wellmann, C., Marten, I., Grill, E., Romeis, T. and Hedrich, R.** (2011) Stomatal closure by fast abscisic acid signaling is mediated by the guard cell anion channel SLAH3 and the receptor RCAR1. *Science Signaling*, **4**, ra32-ra32.
- Geiger, D., Scherzer, S., Mumm, P., Stange, A., Marten, I., Bauer, H., Ache, P., Matschi, S., Liese, A. and Al-Rasheid, K.A.** (2009) Activity of guard cell anion channel SLAC1 is controlled by drought-stress signaling kinase-phosphatase pair. *Proceedings of the National Academy of Sciences*, **106**, 21425-21430.
- George, R., McFarlane, D. and Nulsen, B.** (1997) Salinity threatens the viability of agriculture and ecosystems in Western Australia. *Hydrogeology Journal*, **5**, 6-21.
- Gilliham, M. and Tester, M.** (2005) The regulation of anion loading to the maize root xylem. *Plant Physiology*, **137**, 819-828.
- Gilliham, M. and Tyerman, S.D.** (2016) Linking metabolism to membrane signaling: the GABA-malate connection. *Trends in Plant Science*, **21**, 295-301.
- Gimeno, V., Syvertsen, J.P., Nieves, M., Simón, I., Martínez, V. and García-Sánchez, F.** (2009) Additional nitrogen fertilization affects salt tolerance of lemon trees on different rootstocks. *Scientia Horticulturae*, **121**, 298-305.
- Glass, A.D.M. and Siddiqi, M.Y.** (1985) Nitrate inhibition of chloride influx in barley: Implications for a proposed chloride homeostat. *Journal of Experimental Botany*, **36**, 556-566.
- Gong, H., Blackmore, D., Clingeleffer, P., Sykes, S., Jha, D., Tester, M. and Walker, R.** (2011) Contrast in chloride exclusion between two grapevine genotypes and its variation in their hybrid progeny. *Journal of Experimental Botany*, **62**, 989-999.
- Gong, J.M., Waner, D.A., Horie, T., Li, S.L., Horie, R., Abid, K.B. and Schroeder, J.I.** (2004) Microarray-based rapid cloning of an ion accumulation deletion mutant in *Arabidopsis thaliana*. *Proceedings of the National Academy of Sciences*, **101**, 15404-15409.
- Granett, J., Walker, M.A., Kocsis, L. and Omer, A.D.** (2001) Biology and management of grape phylloxera. *Annual Review of Entomology*, **46**, 387.
- Greenway, H. and Osmond, C.B.** (1972) Salt responses of enzymes from species differing in salt tolerance. *Plant Physiology*, **49**, 256-259.
- Greenway, H. and Rogers, A.** (1963) Growth and ion uptake of *Agropyron elongatum* on saline substrates, as compared with a salt-tolerant variety of *hordeum vulgare*. *Plant and Soil*, **18**, 21-30.
- Gruber, B.D., Ryan, P.R., Richardson, A.E., Tyerman, S.D., Ramesh, S., Hebb, D.M., Howitt, S.M. and Delhaize, E.** (2010) HvALMT1 from barley is involved in the transport of organic anions. *Journal of Experimental Botany*, **61**, 1455-1467.
- Guan, B., Chen, X. and Zhang, H.** (2013) Two-electrode voltage clamp. In *Ion Channels: Methods and Protocols* (Gamper, N. ed. Totowa, NJ: Humana Press, pp. 79-89.
- Guo, J., Zhou, Q., Li, X., Yu, B. and Luo, Q.** (2017) Enhancing NO₃⁻ supply confers NaCl tolerance by adjusting Cl⁻ uptake and transport in *G. max* & *G. soja*. *Journal of Soil Science and Plant Nutrition*, **17**, 194-202.
- Haas, M.** (1994) The Na-K-Cl cotransporters. *American Journal of Physiology-Cell Physiology*, **267**, C869-C885.
- Halfter, U., Ishitani, M. and Zhu, J.-K.** (2000) The Arabidopsis SOS2 protein kinase physically interacts with and is activated by the calcium-binding protein SOS3. *Proceedings of the National Academy of Sciences*, **97**, 3735-3740.

- Hamill, O.P., Marty, A., Neher, E., Sakmann, B. and Sigworth, F.J.** (1981) Improved patch-clamp techniques for high-resolution current recording from cells and cell-free membrane patches. *Pflügers Archiv*, **391**, 85-100.
- Hannah, L., Roehrdanz, P.R., Ikegami, M., Shepard, A.V., Shaw, M.R., Tabor, G., Zhi, L., Marquet, P.A. and Hijmans, R.J.** (2013) Climate change, wine, and conservation. *Proceedings of the National Academy of Sciences*, **110**, 6907-6912.
- Hanson, B. and May, D.** (2011) *Drip irrigation salinity management for row crops*: UCANR Publications.
- Harada, H., Kuromori, T., Hirayama, T., Shinozaki, K. and Leigh, R.A.** (2004) Quantitative trait loci analysis of nitrate storage in Arabidopsis leading to an investigation of the contribution of the anion channel gene, AtCLC-c, to variation in nitrate levels. *Journal of Experimental Botany*, **55**, 2005-2014.
- Hauser, F. and Horie, T.** (2010) A conserved primary salt tolerance mechanism mediated by HKT transporters: a mechanism for sodium exclusion and maintenance of high K⁺/Na⁺ ratio in leaves during salinity stress. *Plant, Cell & Environment*, **33**, 552-565.
- Hechenberger, M., Schwappach, B., Fischer, W.N., Frommer, W.B., Jentsch, T.J. and Steinmeyer, K.** (1996) A family of putative chloride channels from Arabidopsis and functional complementation of a yeast strain with a CLC gene disruption. *Journal of Biological Chemistry*, **271**, 33632-33638.
- Helwi, P., Guillaumie, S., Thibon, C., Keime, C., Habran, A., Hilbert, G., Gomes, E., Darriet, P., Delrot, S. and van Leeuwen, C.** (2016) Vine nitrogen status and volatile thiols and their precursors from plot to transcriptome level. *BMC Plant Biology*, **16**, 173.
- Henderson, S.W., Baumann, U., Blackmore, D.H., Walker, A.R., Walker, R.R. and Gilliham, M.** (2014a) Shoot chloride exclusion and salt tolerance in grapevine is associated with differential ion transporter expression in roots. *BMC Plant Biology*, **14**.
- Henderson, S.W., Dunlevy, J.D., Wu, Y., Blackmore, D.H., Walker, R.R., Edwards, E.J., Gilliham, M. and Walker, A.R.** (2018a) Functional differences in transport properties of natural HKT1;1 variants influence shoot Na⁺ exclusion in grapevine rootstocks. *New Phytologist*, **217**, 1113-1127.
- Henderson, S.W., Gilliham, M., Tyerman, S.D. and Walker, R.** (2014b) Investigating genes encoding membrane proteins in grapevine (*Vitis vinifera* L.) and *Vitis spp.* rootstocks to determine their role in chloride exclusion.
- Henderson, S.W., Wege, S. and Gilliham, M.** (2018b) Plant cation-chloride cotransporters (CCC): evolutionary origins and functional insights. *International Journal of Molecular Sciences*, **19**, 492.
- Henderson, S.W., Wege, S., Qiu, J., Blackmore, D.H., Walker, A.R., Tyerman, S., Walker, R.R. and Gilliham, M.** (2015) Grapevine and Arabidopsis cation-chloride cotransporters localise to the Golgi and trans-Golgi network and indirectly influence long-distance ion homeostasis and plant salt tolerance. *Plant Physiology*, **169**, 2215-2229.
- Hodgkin, A.L., Huxley, A.F. and Katz, B.** (1952) Measurement of current-voltage relations in the membrane of the giant axon of Loligo. *The Journal of Physiology*, **116**, 424-448.
- Hoekenga, O.A., Maron, L.G., Pineros, M.A., Cancado, G.M., Shaff, J., Kobayashi, Y., Ryan, P.R., Dong, B., Delhaize, E., Sasaki, T., Matsumoto, H., Yamamoto, Y., Koyama, H. and Kochian, L.V.** (2006) AtALMT1, which encodes a malate transporter, is identified as one of several genes critical for aluminum tolerance in Arabidopsis. *Proceedings of the National Academy of Sciences*, **103**, 9738-9743.
- Horie, T., Hauser, F. and Schroeder, J.I.** (2009) HKT transporter-mediated salinity resistance mechanisms in Arabidopsis and monocot crop plants. *Trends in Plant Science*, **14**, 660-668.
- Horie, T. and Schroeder, J.I.** (2004) Sodium transporters in plants. Diverse genes and physiological functions. *Plant Physiology*, **136**, 2457-2462.

- Horie, T., Yoshida, K., Nakayama, H., Yamada, K., Oiki, S. and Shinmyo, A. (2001) Two types of HKT transporters with different properties of Na⁺ and K⁺ transport in *Oryza sativa*. *The Plant Journal*, **27**, 129-138.
- Iland, P., Dry, P., Proffitt, T. and Tyerman, S. (2011) *The grapevine: from the science to the practice of growing vines for wine*: Patrick Iland Wine Promotions.
- Jabnounge, M., Espeout, S., Mieulet, D., Fizames, C., Verdeil, J.-L., Conéjéro, G., Rodríguez-Navarro, A., Sentenac, H., Guiderdoni, E., Abdelly, C. and Véry, A.-A. (2009) Diversity in expression patterns and functional properties in the rice HKT transporter family. *Plant Physiology*, **150**, 1955-1971.
- James, R.A., Blake, C., Byrt, C.S. and Munns, R. (2011) Major genes for Na⁺ exclusion, *Nax1* and *Nax2* (wheat *HKT1;4* and *HKT1;5*), decrease Na⁺ accumulation in bread wheat leaves under saline and waterlogged conditions. *Journal of Experimental Botany*, **62**, 2939-2947.
- Jha, D., Shirley, N., Tester, M. and Roy, S.J. (2010) Variation in salinity tolerance and shoot sodium accumulation in *Arabidopsis* ecotypes linked to differences in the natural expression levels of transporters involved in sodium transport. *Plant, Cell & Environment*, **33**, 793-804.
- Ji, H., Pardo, J.M., Batelli, G., Van Oosten, M.J., Bressan, R.A. and Li, X. (2013) The Salt Overly Sensitive (SOS) pathway: Established and emerging roles. *Molecular Plant*, **6**, 275-286.
- Jossier, M., Kroniewicz, L., Dalmas, F., Le Thiec, D., Ephritikhine, G., Thomine, S., Barbier-Brygoo, H., Vavasseur, A., Filleur, S. and Leonhardt, N. (2010) The *Arabidopsis* vacuolar anion transporter, AtCLC_c, is involved in the regulation of stomatal movements and contributes to salt tolerance. *The Plant Journal*, **64**, 563-576.
- Karimi, M., Inze, D. and Depicker, A. (2002) GATEWAY vectors for *Agrobacterium*-mediated plant transformation. *Trends in Plant Science*, **7**, 193-195.
- Kobayashi, N.I., Yamaji, N., Yamamoto, H., Okubo, K., Ueno, H., Costa, A., Tanoi, K., Matsumura, H., Fujii-Kashino, M., Horiuchi, T., Nayef, M.A., Shabala, S., An, G., Ma, J.F. and Horie, T. (2017) OsHKT1;5 mediates Na⁺ exclusion in the vasculature to protect leaf blades and reproductive tissues from salt toxicity in rice. *The Plant Journal*, **91**, 657-670.
- Köhler, B. and Raschke, K. (2000) The delivery of salts to the xylem. Three types of anion conductance in the plasmalemma of the xylem parenchyma of roots of barley. *Plant Physiology*, **122**, 243-254.
- Köhler, B., Wegner, L.H., Osipov, V. and Raschke, K. (2002) Loading of nitrate into the xylem: apoplastic nitrate controls the voltage dependence of X-QUAC, the main anion conductance in xylem-parenchyma cells of barley roots. *The Plant Journal*, **30**, 133-142.
- Kollist, H., Nuhkat, M. and Roelfsema, M.R.G. (2014) Closing gaps: linking elements that control stomatal movement. *New Phytologist*, **203**, 44-62.
- Krake, L.R., Scott, N.S., Rezaian, M.A. and Taylor, R.H. (1999) *Graft-transmitted diseases of grapevines* Collingwood, Australia: CSIRO Publishing.
- Kriedemann, P.E., Loveys, B.R. and Downton, W.J.S. (1975) Internal control of stomatal physiology and photosynthesis. II. Photosynthetic responses to phaseic acid. *Functional Plant Biology*, **2**, 553-567.
- Krouk, G., Lacombe, B., Bielach, A., Perrine-Walker, F., Malinska, K., Mounier, E., Hoyerova, K., Tillard, P., Leon, S., Ljung, K., Zazimalova, E., Benkova, E., Nacry, P. and Gojon, A. (2010) Nitrate-regulated auxin transport by NRT1.1 defines a mechanism for nutrient sensing in plants. *Developmental Cell*, **18**, 927-937.
- Lanyon, D. (2011) *Salinity management interpretation guide* Waite Campus, Adelaide: Arris Pty Ltd.

- Larkin, M.A., Blackshields, G., Brown, N.P., Chenna, R., McGettigan, P.A., McWilliam, H., Valentin, F., Wallace, I.M., Wilm, A., Lopez, R., Thompson, J.D., Gibson, T.J. and Higgins, D.G. (2007) Clustal W and Clustal X version 2.0. *Bioinformatics*, **23**, 2947-2948.
- Läuchli, A., James, R.A., Huang, C.X., McCully, M. and Munns, R. (2008) Cell-specific localization of Na⁺ in roots of durum wheat and possible control points for salt exclusion. *Plant, Cell & Environment*, **31**, 1565-1574.
- Lee, S.C., Lan, W., Buchanan, B.B. and Luan, S. (2009) A protein kinase-phosphatase pair interacts with an ion channel to regulate ABA signaling in plant guard cells. *Proceedings of the National Academy of Sciences*, **106**, 21419-21424.
- Leran, S., Garg, B., Boursiac, Y., Corratge-Faillie, C., Brachet, C., Tillard, P., Gojon, A. and Lacombe, B. (2015) AtNPF5.5, a nitrate transporter affecting nitrogen accumulation in Arabidopsis embryo. *Scientific Reports*, **5**, 7962.
- Léran, S., Varala, K., Boyer, J.-C., Chiurazzi, M., Crawford, N., Daniel-Vedele, F., David, L., Dickstein, R., Fernandez, E., Forde, B., Gassmann, W., Geiger, D., Gojon, A., Gong, J.-M., Halkier, B.A., Harris, J.M., Hedrich, R., Limami, A.M., Rentsch, D., Seo, M., Tsay, Y.-F., Zhang, M., Coruzzi, G. and Lacombe, B. (2014) A unified nomenclature of NITRATE TRANSPORTER 1/PEPTIDE TRANSPORTER family members in plants. *Trends in Plant Science*, **19**, 5-9.
- Leske, P.A., Sas, A.N., Coulter, A.D., Stockley, C.S. and Lee, T.H. (1997) The composition of Australian grape juice: chloride, sodium and sulfate ions. *Australian Journal of Grape and Wine Research*, **3**, 26-30.
- Li, B., Byrt, C., Qiu, J., Baumann, U., Hrmova, M., Evrard, A., Johnson, A.A., Birnbaum, K.D., Mayo, G.M., Jha, D., Henderson, S.W., Tester, M., Gilliham, M. and Roy, S.J. (2016) Identification of a stelar-localized transport protein that facilitates root-to-shoot transfer of chloride in Arabidopsis. *Plant Physiology*, **170**, 1014-1029.
- Li, B., Qiu, J., Jayakannan, M., Xu, B., Li, Y., Mayo, G.M., Tester, M., Gilliham, M. and Roy, S.J. (2017a) AtNPF2.5 modulates chloride (Cl⁻) efflux from roots of *Arabidopsis thaliana*. *Frontiers in Plant Science*, **7**, 2013.
- Li, B., Tester, M. and Gilliham, M. (2017b) Chloride on the move. *Trends in Plant Science*, **22**, 236-248.
- Li, X.L., Wang, C.R., Li, X.Y., Yao, Y.X. and Hao, Y.J. (2013) Modifications of Kyoho grape berry quality under long-term NaCl treatment. *Food chemistry*, **139**, 931-937.
- Ligaba, A., Katsuhara, M., Ryan, P.R., Shibasaka, M. and Matsumoto, H. (2006) The *BnALMT1* and *BnALMT2* genes from rape encode aluminum-activated malate transporters that enhance the aluminum resistance of plant cells. *Plant Physiology*, **142**, 1294-1303.
- Ligaba, A., Maron, L., Shaff, J., Kochian, L. and Pineros, M. (2012) Maize ZmALMT2 is a root anion transporter that mediates constitutive root malate efflux. *Plant, Cell & Environment*, **35**, 1185-1200.
- Liu, J., Ishitani, M., Halfter, U., Kim, C.-S. and Zhu, J.-K. (2000) The *Arabidopsis thaliana* SOS2 gene encodes a protein kinase that is required for salt tolerance. *Proceedings of the National Academy of Sciences*, **97**, 3730-3734.
- Liu, W., Fairbairn, D.J., Reid, R.J. and Schachtman, D.P. (2001) Characterization of two HKT1 homologues from *Eucalyptus camaldulensis* that display intrinsic osmosensing capability. *Plant Physiology*, **127**, 283-294.
- Liu, Z. (2016) *Practical Patch Clamp Techniques 2* edn. Beijing: Beijing Science and Technology Press.
- Lorenzen, I., Aberle, T. and Plieth, C. (2004) Salt stress-induced chloride flux: a study using transgenic Arabidopsis expressing a fluorescent anion probe. *The Plant Journal*, **38**, 539-544.

- Loveys, B.R. and Kriedemann, P.E.** (1974) Internal control of stomatal physiology and photosynthesis. I. Stomatal regulation and associated changes in endogenous levels of abscisic and phaseic acids. *Functional Plant Biology*, **1**, 407-415.
- Lunin, J. and Gallatin, M.H.** (1965) Salinity-fertility interactions in relation to the growth and composition of beans. I. Effect of N, P, and K. *Agronomy Journal*, **57**, 339-342.
- Lv, Q.-d., Tang, R.-j., Liu, H., Gao, X.-s., Li, Y.-z., Zheng, H.-q. and Zhang, H.-x.** (2009) Cloning and molecular analyses of the *Arabidopsis thaliana* chloride channel gene family. *Plant Science*, **176**, 650-661.
- Ma, Z.-Y., Wen, J., Ickert-Bond, S.M., Chen, L.-Q. and Liu, X.-Q.** (2016) Morphology, structure, and ontogeny of trichomes of the grape genus (*Vitis*, Vitaceae). *Frontiers in plant science*, **7**, 704-704.
- Maas, E.V. and Hoffman, G.J.** (1977) Crop salt tolerance - current assessment. *Journal of the Irrigation and Drainage Division*, **103**, 115-134.
- Maathuis, F.J., Verlin, D., Smith, F.A., Sanders, D., Fernandez, J.A. and Walker, N.A.** (1996) The physiological relevance of Na⁺-coupled K⁺-transport. *Plant Physiology*, **112**, 1609-1616.
- Mäser, P., Eckelman, B., Vaidyanathan, R., Horie, T., Fairbairn, D.J., Kubo, M., Yamagami, M., Yamaguchi, K., Nishimura, M. and Uozumi, N.** (2002a) Altered shoot/root Na⁺ distribution and bifurcating salt sensitivity in *Arabidopsis* by genetic disruption of the Na⁺ transporter AtHKT1. *FEBS letters*, **531**, 157-161.
- Mäser, P., Hosoo, Y., Goshima, S., Horie, T., Eckelman, B., Yamada, K., Yoshida, K., Bakker, E.P., Shinmyo, A., Oiki, S., Schroeder, J.I. and Uozumi, N.** (2002b) Glycine residues in potassium channel-like selectivity filters determine potassium selectivity in four-loop-per-subunit HKT transporters from plants. *Proceedings of the National Academy of Sciences*, **99**, 6428-6433.
- Massonnet, M., Figueroa-Balderas, R., Galarneau, E.R.A., Miki, S., Lawrence, D.P., Sun, Q., Wallis, C.M., Baumgartner, K. and Cantu, D.** (2017) *Neofusicoccum parvum* colonization of the grapevine woody stem triggers asynchronous host responses at the site of infection and in the leaves. *Frontiers in Plant Science*, **8**.
- McElrone, A.J., Choat, B., Gambetta, G.A. and Brodersen, C.R.** (2013) Water uptake and transport in vascular plants. *Nature Education Knowledge*, **4**.
- McFarlane, D.J. and Williamson, D.R.** (2002) An overview of water logging and salinity in southwestern Australia as related to the 'Ucarro' experimental catchment. *Agricultural Water Management*, **53**, 5-29.
- Meyer, S., Mumm, P., Imes, D., Endler, A., Weder, B., Al-Rasheid, K.A.S., Geiger, D., Marten, I., Martinoia, E. and Hedrich, R.** (2010) AtALMT12 represents an R-type anion channel required for stomatal movement in *Arabidopsis* guard cells. *The Plant Journal*, **63**, 1054-1062.
- Miledi, R., Parker, I. and Sumikawa, K.** (1982) Properties of acetylcholine receptors translated by cat muscle mRNA in *Xenopus* oocytes. *The EMBO journal*, **1**, 1307-1312.
- Miller, A.J., Fan, X., Orsel, M., Smith, S.J. and Wells, D.M.** (2007) Nitrate transport and signalling. *Journal of Experimental Botany*, **58**, 2297-2306.
- Minio, A., Lin, J., Gaut, B.S. and Cantu, D.** (2017) How single molecule real-time sequencing and haplotype phasing have enabled reference-grade diploid genome assembly of wine grapes. *Frontiers in Plant Science*, **8**.
- Minio, A., Massonnet, M., Vondras, A., Figueroa-Balderas, R., Blanco-Ulate, B. and Cantu, D.** (2018) Isoform-scale annotation and expression profiling of the Cabernet Sauvignon transcriptome using single-molecule sequencing of full-length cDNA. *bioRxiv*, 269530.
- Møller, I.S., Gilliam, M., Jha, D., Mayo, G.M., Roy, S.J., Coates, J.C., Haseloff, J. and Tester, M.** (2009) Shoot Na⁺ exclusion and increased salinity tolerance engineered by cell type-specific alteration of Na⁺ transport in *Arabidopsis*. *The Plant Cell*, **21**, 2163-2178.

- Mullins, M.G. and Rajasekaran, K.** (1981) Fruiting cuttings: Revised method for producing test plants of grapevine cultivars. *American Journal of Enology and Viticulture*, **32**, 35-40.
- Munns, R.** (2005) Genes and salt tolerance: bringing them together. *New Phytologist*, **167**, 645–663.
- Munns, R.** (2011) Plant adaptations to salt and water stress: differences and commonalities. *Advances in Botanical Research*, **57**, 1-32.
- Munns, R., Day, D.A., Fricke, W., Watt, M., Arsova, B., Barkla, B.J., Bose, J., Byrt, C.S., Chen, Z.-H., Foster, K.J., Gilliam, M., Henderson, S.W., Jenkins, C.L.D., Kronzucker, H.J., Miklavcic, S.J., Plett, D., Roy, S.J., Shabala, S., Shelden, M.C., Soole, K.L., Taylor, N.L., Tester, M., Wege, S., Wegner, L.H. and Tyerman, S.D.** (2019) Energy costs of salt tolerance in crop plants. *New Phytologist*.
- Munns, R. and Gilliam, M.** (2015) Salinity tolerance of crops – what is the cost? *New Phytologist*, **208**, 668-673.
- Munns, R. and James, R.A.** (2003) Screening methods for salinity tolerance: a case study with tetraploid wheat. *Plant and Soil*, **253**, 201-218.
- Munns, R., James, R.A. and Läuchli, A.** (2006) Approaches to increasing the salt tolerance of wheat and other cereals. *Journal of Experimental Botany*, **57**, 1025-1043.
- Munns, R., James, R.A., Xu, B., Athman, A., Conn, S.J., Jordans, C., Byrt, C.S., Hare, R.A., Tyerman, S.D., Tester, M., Plett, D. and Gilliam, M.** (2012) Wheat grain yield on saline soils is improved by an ancestral Na⁺ transporter gene. *Nature Biotechnology*, **30**, 360-364.
- Munns, R. and Sharp, R.E.** (1993) Involvement of abscisic acid in controlling plant growth in soil of low water potential. *Australian Journal of Plant Physiology*, **20**, 425-437.
- Munns, R. and Tester, M.** (2008) Mechanisms of salinity tolerance. In *Annual Review of Plant Biology*, pp. 651-681.
- Mustilli, A.-C., Merlot, S., Vavasseur, A., Fenzi, F. and Giraudat, J.** (2002) Arabidopsis OST1 protein kinase mediates the regulation of stomatal aperture by abscisic acid and acts upstream of reactive oxygen species production. *The Plant Cell*, **14**, 3089-3099.
- Naranjo, M.A., Forment, J., Roldan, M., Serrano, R. and Vicente, O.** (2006) Overexpression of *Arabidopsis thaliana* *LTL1*, a salt-induced gene encoding a GDSL-motif lipase, increases salt tolerance in yeast and transgenic plants. *Plant Cell and Environment*, **29**, 1890-1900.
- Negi, J., Matsuda, O., Nagasawa, T., Oba, Y., Takahashi, H., Kawai-Yamada, M., Uchimiya, H., Hashimoto, M. and Iba, K.** (2008) CO₂ regulator SLAC1 and its homologues are essential for anion homeostasis in plant cells. *Nature*, **452**, 483-U413.
- Nelson, B.K., Cai, X. and Nebenführ, A.** (2007) A multicolored set of *in vivo* organelle markers for co-localization studies in Arabidopsis and other plants. *The Plant Journal*, **51**, 1126-1136.
- Neumann, P.M.** (2011) Chapter 2 - Recent advances in understanding the regulation of whole-plant growth inhibition by salinity, drought and colloid stress. In *Advances in Botanical Research* (Turkan, I. ed: Academic Press, pp. 33-48.
- Neumann, P.M., Volkenburgh, E.V. and Cleland, R.E.** (1988) Salinity stress inhibits bean leaf expansion by reducing turgor, not wall extensibility. *Plant Physiology*, **88**, 233-237.
- Newman, H.P. and Antcliff, A.J.** (1984) Chloride accumulation in some hybrids and backcrosses of *Vitis berlandieri* and *Vitis vinifera*. *Vitis*, **23**, 106–112.
- Nguyen, C.T., Agorio, A., Jossier, M., Depré, S., Thomine, S. and Filleur, S.** (2016) Characterization of the chloride channel-like, AtCLCg, involved in chloride tolerance in *Arabidopsis thaliana*. *Plant and Cell Physiology*, **57**, 764-775.
- Noguero, M. and Lacombe, B.** (2016) Transporters involved in root nitrate uptake and sensing by *Arabidopsis*. *Frontiers in plant science*, **7**, 1391-1391.
- Ordish, G.** (1972) *The great wine blight*.

- Pannell, D.J. and Ewing, M.A.** (2006) Managing secondary dryland salinity: Options and challenges. *Agricultural Water Management*, **80**, 41-56.
- Papageorgiou, G.C., Alygizaki-Zorba, A., Ladas, N. and Murata, N.** (1998) A method to probe the cytoplasmic osmolality and osmotic water and solute fluxes across the cell membrane of cyanobacteria with chlorophyll a fluorescence: Experiments with *Synechococcus sp.* PCC7942. *Physiologia Plantarum*, **103**, 215-224.
- Papke, R.L. and Smith-Maxwell, C.** (2009) High throughput electrophysiology with *Xenopus* oocytes. *Combinatorial Chemistry & High Throughput Screening*, **12**, 38-50.
- Parker, J.L. and Newstead, S.** (2014) Molecular basis of nitrate uptake by the plant nitrate transporter NRT1.1. *Nature*, **507**, 68.
- Piccolo, A. and Pusch, M.** (2005) Chloride/proton antiporter activity of mammalian CLC proteins ClC-4 and ClC-5. *Nature*, **436**, 420-423.
- Pike, S., Gao, F., Kim, M.J., Kim, S.H., Schachtman, D.P. and Gassmann, W.** (2013) Members of the NPF3 transporter subfamily encode pathogen-inducible nitrate/nitrite transporters in grapevine and arabidopsis. *Plant and Cell Physiology*, **55**, 162-170.
- Piñeros, M.A., Cançado, G.M.A., Maron, L.G., Lyi, S.M., Menossi, M. and Kochian, L.V.** (2008) Not all ALMT1-type transporters mediate aluminum-activated organic acid responses: the case of ZmALMT1 – an anion-selective transporter. *The Plant Journal*, **53**, 352-367.
- Platten, J.D., Cotsaftis, O., Berthomieu, P., Bohnert, H., Davenport, R.J., Fairbairn, D.J., Horie, T., Leigh, R.A., Lin, H.-X. and Luan, S.** (2006) Nomenclature for HKT transporters, key determinants of plant salinity tolerance. *Trends in Plant Science*, **11**, 372-374.
- Plett, D., Safwat, G., Gilliam, M., Skrumsager Møller, I., Roy, S., Shirley, N., Jacobs, A., Johnson, A. and Tester, M.** (2010a) Improved salinity tolerance of rice through cell type-specific expression of *AtHKT1;1*. *PLoS One*, **5**, e12571.
- Plett, D., Safwat, G., Gilliam, M., Skrumsager Møller, I., Roy, S., Shirley, N., Jacobs, A., Johnson, A. and Tester, M.** (2010b) Improved salinity tolerance of rice through cell type-specific expression of *AtHKT1;1*. *PLoS ONE*, **5**, e12571.
- Plett, D.C.** (2008) Spatial and temporal alterations of gene expression in rice.
- Preuss, C.P., Huang, C.Y., Gilliam, M. and Tyerman, S.D.** (2010) Channel-Like characteristics of the low-affinity barley phosphate transporter PHT1;6 when expressed in *Xenopus* oocytes. *Plant Physiology*, **152**, 1431-1441.
- Prior, L.D., Grieve, A.M. and Cullis, B.R.** (1992a) Sodium chloride and soil texture interactions in irrigated field grown sultana grapevines. I. Yield and fruit quality. *Australian Journal of Agricultural Research*, **43**, 1051-1066.
- Prior, L.D., Grieve, A.M. and Cullis, B.R.** (1992b) Sodium chloride and soil texture interactions in irrigated field grown sultana grapevines. II. Plant mineral content, growth and physiology. *Australian Journal of Agricultural Research*, **43**, 1067-1083.
- Qiu, J., Henderson, S.W., Tester, M., Roy, S.J. and Gilliam, M.** (2016) SLAH1, a homologue of the slow type anion channel SLAC1, modulates shoot Cl⁻ accumulation and salt tolerance in *Arabidopsis thaliana*. *Journal of Experimental Botany*, **67**, 4495-4505.
- Qiu, Q.-S., Guo, Y., Quintero, F.J., Pardo, J.M., Schumaker, K.S. and Zhu, J.-K.** (2004) Regulation of vacuolar Na⁺/H⁺ exchange in *Arabidopsis thaliana* by the salt-overly-sensitive (SOS) pathway. *Journal of Biological Chemistry*, **279**, 207-215.
- Quesada, A., Galvan, A. and Fernandez, E.** (1994) Identification of nitrate transporter genes in *Chlamydomonas reinhardtii*. *The Plant Journal*, **5**, 407-419.
- Quintero, F.J., Ohta, M., Shi, H., Zhu, J.-K. and Pardo, J.M.** (2002) Reconstitution in yeast of the *Arabidopsis* SOS signaling pathway for Na⁺ homeostasis. *Proceedings of the National Academy of Sciences*, **99**, 9061-9066.
- R Core Team** (2019) R: A language and environment for statistical computing. Vienna, Austria: R Foundation for Statistical Computing.

- Ramesh, S.A., Tyerman, S.D., Gilliam, M. and Xu, B. (2017) γ -Aminobutyric acid (GABA) signalling in plants. *Cellular and Molecular Life Sciences*, **74**, 1577-1603.
- Ramesh, S.A., Tyerman, S.D., Xu, B., Bose, J., Kaur, S., Conn, V., Domingos, P., Ullah, S., Wege, S., Shabala, S., Feijo, J.A., Ryan, P.R. and Gilliam, M. (2015) GABA signalling modulates plant growth by directly regulating the activity of plant-specific anion transporters. *Nature Communications*, **6**.
- Ren, Z.-H., Gao, J.-P., Li, L.-G., Cai, X.-L., Huang, W., Chao, D.-Y., Zhu, M.-Z., Wang, Z.-Y., Luan, S. and Lin, H.-X. (2005a) A rice quantitative trait locus for salt tolerance encodes a sodium transporter. *Nature Genetics*, **37**, 1141.
- Ren, Z.H., Gao, J.P., Li, L.G., Cai, X.L., Huang, W., Chao, D.Y., Zhu, M.Z., Wang, Z.Y., Luan, S. and Lin, H.X. (2005b) A rice quantitative trait locus for salt tolerance encodes a sodium transporter. *Nature Genetics*, **37**.
- Roberts, S.K. (2006) Plasma membrane anion channels in higher plants and their putative functions in roots. *New Phytologist*, **169**, 647-666.
- Robinson, J. (2006) *The Oxford companion to wine* 3rd edn. Oxford, New York: Oxford University Press.
- Rosas-Santiago, P., Lagunas-Gómez, D., Barkla, B.J., Vera-Estrella, R., Lalonde, S., Jones, A., Frommer, W.B., Zimmermann, O., Sychrová, H. and Pantoja, O. (2015) Identification of rice cornichon as a possible cargo receptor for the Golgi-localized sodium transporter OsHKT1;3. *Journal of Experimental Botany*, **66**, 2733-2748.
- Roy, S.J., Gilliam, M., Berger, B., Essah, P.A., Cheffings, C., Miller, A.J., Davenport, R.J., Liu, L.-H., Skynner, M.J., Davies, J.M., Richardson, P., Leigh, R.A. and Tester, M. (2008) Investigating glutamate receptor-like gene co-expression in *Arabidopsis thaliana*. *Plant, Cell & Environment*, **31**, 861-871.
- Rubio, F., Gassmann, W. and Schroeder, J.I. (1995) Sodium-driven potassium uptake by the plant potassium transporter HKT1 and mutations conferring salt tolerance. *Science*, **270**, 1660-1663.
- Sainsbury, F., Thuenemann, E.C. and Lomonosoff, G.P. (2009) pEAQ: versatile expression vectors for easy and quick transient expression of heterologous proteins in plants. *Plant Biotechnology Journal*, **7**, 682-693.
- Sakmann, B. and Neher, E. (1984) Patch clamp techniques for studying ionic channels in excitable membranes. *Annual Review of Physiology*, **46**, 455-472.
- Sakmann, B. and Neher, E. (1995) *Single-channel recording* 2 edn. New York: Plenum Press.
- Sanders, D. (1980) The mechanism of Cl⁻ transport at the plasma membrane of *Chara corallina* L. Cotransport with H⁺. *J. Membranes Biol.*, **53**, 129-141.
- Sasaki, T., Mori, I.C., Furuichi, T., Munemasa, S., Toyooka, K., Matsuoka, K., Murata, Y. and Yamamoto, Y. (2010) Closing plant stomata requires a homolog of an aluminum-activated malate transporter. *Plant and Cell Physiology*, **51**, 354-365.
- Sasaki, T., Yamamoto, Y., Ezaki, B., Katsuhara, M., Ahn, S.J., Ryan, P.R., Delhaize, E. and Matsumoto, H. (2004) A wheat gene encoding an aluminum-activated malate transporter. *The Plant Journal*, **37**, 645-653.
- Sauer, M.R. (1968) Effects of vine rootstocks on chloride concentration in Sultana scions. *Vitis*, **7**, 223-226.
- Schachtman, D.P. and Schroeder, J.I. (1994) Structure and transport mechanism of a high-affinity potassium uptake transporter from higher plants. *Nature*, **370**, 655-658.
- Schillmiller, A.L., Last, R.L. and Pichersky, E. (2008) Harnessing plant trichome biochemistry for the production of useful compounds. *The Plant Journal*, **54**, 702-711.
- Segonzac, C., Boyer, J.C., Ipotesi, E., Szponarski, W., Tillard, P., Touraine, B., Sommerer, N., Rossignol, M. and Gibrat, R. (2007) Nitrate efflux at the root plasma membrane: identification of an *Arabidopsis* excretion transporter. *The Plant Cell*, **19**, 3760-3777.

- Shabala, L., Ross, T., McMeekin, T. and Shabala, S.** (2006) Non-invasive microelectrode ion flux measurements to study adaptive responses of microorganisms to the environment. *FEMS Microbiology Reviews*, **30**, 472-486.
- Sharma, T., Dreyer, I., Kochian, L. and Piñeros, M.A.** (2016) The ALMT Family of organic acid transporters in plants and their involvement in detoxification and nutrient security. *Frontiers in Plant Science*, **7**, 1488.
- Shavrukov, Y., Gupta, N., Miyazaki, J., Baho, M., Chalmers, K., Tester, M., Langridge, P. and Collins, N.** (2010) HvNax3—a locus controlling shoot sodium exclusion derived from wild barley (*Hordeum vulgare* ssp. *spontaneum*). *Funct Integr Genomics*, **10**, 277-291.
- Shelden, M.C., Howitt, S.M., Kaiser, B.N. and Tyerman, S.D.** (2009) Identification and functional characterisation of aquaporins in the grapevine, *Vitis vinifera*. *Functional Plant Biology*, **36**, 1065-1078.
- Shi, H., Ishitani, M., Kim, C. and Zhu, J.-K.** (2000) The Arabidopsis thaliana salt tolerance gene SOS1 encodes a putative Na⁺/H⁺ antiporter. *Proceedings of the National Academy of Sciences*, **97**, 6896-6901.
- Shi, H., Quintero, F.J., Pardo, J.M. and Zhu, J.-K.** (2002) The putative plasma membrane Na⁺/H⁺ antiporter SOS1 controls long-distance Na⁺ transport in plants. *The Plant cell*, **14**, 465-477.
- Skerrett, M. and Tyerman, S.D.** (1994) A channel that allows inwardly directed fluxes of anions in protoplasts derived from wheat roots. *Planta*, **192**, 295-305.
- Southey, J.M. and Jooste, J.H.** (1991) The effect of grapevine rootstock on the performance of *Vitis vinifera* L.(cv. Colombard) on a relatively saline soil. *South African Society for Enology & Viticulture*, **12**, 32-40.
- Stevens, R.M., Harvey, G. and Partington, D.L.** (2011) Irrigation of grapevines with saline water at different growth stages: effects on leaf, wood and juice composition. *Australian Journal of Grape and Wine Research*, **17**, 239-248.
- Storey, R., Schachtman, D.P. and Thomas, M.R.** (2003) Root structure and cellular chloride, sodium and potassium distribution in salinized grapevines. *Plant Cell and Environment*, **26**, 789-800.
- Storey, R. and Walker, R.R.** (1998) Citrus and salinity. *Scientia Horticulturae*, **78**, 39-81.
- Suhayda, C.G., Giannini, J.L., Briskin, D.P. and Shannon, M.C.** (1990) Electrostatic changes in *Lycopersicon esculentum* root plasma membrane resulting from salt stress. *Plant Physiology*, **93**, 471-478.
- Sun, J., Bankston, J.R., Payandeh, J., Hinds, T.R., Zagotta, W.N. and Zheng, N.** (2014) Crystal structure of the plant dual-affinity nitrate transporter NRT1.1. *Nature*, **507**, 73.
- Sun, J., Chen, S., Dai, S., Wang, R., Li, N., Shen, X., Zhou, X., Lu, C., Zheng, X. and Hu, Z.** (2009) NaCl-induced alternations of cellular and tissue ion fluxes in roots of salt-resistant and salt-sensitive poplar species. *Plant Physiology*, **149**, 1141-1153.
- Sunarpi, Horie, T., Motoda, J., Kubo, M., Yang, H., Yoda, K., Horie, R., Chan, W.Y., Leung, H.Y., Hattori, K., Konomi, M., Osumi, M., Yamagami, M., Schroeder, J.I. and Uozumi, N.** (2005) Enhanced salt tolerance mediated by AtHKT1 transporter-induced Na⁺ unloading from xylem vessels to xylem parenchyma cells. *The Plant Journal*, **44**.
- Sykes, S.** (1992) The inheritance of salt exclusion in woody perennial fruit species. *Plant and Soil*, **146**, 123-129.
- Sykes, S.R.** (1985) Variation in chloride accumulation by hybrid vines from crosses involving the cultivars Ramsey, Villard Blanc, and Sultana. *American Journal of Enology and Viticulture*, **36**, 30-37.
- Sykes, S.R.** (1987) Variation in chloride accumulation in hybrids and backcrosses of *Vitis berlandieri* and *Vitis vinifera* under glasshouse conditions. *American Journal of Enology and Viticulture*, **38**, 313-320.
- Szabolcs, I.** (1989) *Salt-affected soils* Boca Raton, Florida: CRC Press, Inc.

- Taiz, L., Zeiger, E., Møller, I.M. and Murphy, A.S.** (2015) *Plant physiology and development* Sixth edn.: Sinauer Associates, Inc.
- Taochy, C., Gaillard, I., Ipotesi, E., Oomen, R., Leonhardt, N., Zimmermann, S., Peltier, J.B., Szponarski, W., Simonneau, T. and Sentenac, H.** (2015) The Arabidopsis root stele transporter NPF2.3 contributes to nitrate translocation to shoots under salt stress. *The Plant Journal*, **83**, 466-479.
- Taylor, J.S. and Raes, J.** (2004) Duplication and divergence: The evolution of new genes and old ideas. *Annual Review of Genetics*, **38**, 615-643.
- Teakle, N., Flowers, T., Real, D. and Colmer, T.** (2007) *Lotus tenuis* tolerates the interactive effects of salinity and waterlogging by 'excluding' Na⁺ and Cl⁻ from the xylem. *Journal of Experimental Botany*, **58**, 2169-2180.
- Teakle, N.L. and Tyerman, S.D.** (2010) Mechanisms of Cl⁻ transport contributing to salt tolerance. *Plant, Cell & Environment*, **33**, 566-589.
- The International Organisation of Vine and Wine** (2011) Compendium of international methods of analysis-OIV: Maximum acceptable limits of various substances contained in wine: International Organisation of Vine and Wine.
- The International Organisation of Vine and Wine** (2015) International code of oenological practices: maximum acceptable limits International Organisation of Vine and Wine.
- Tregeagle, J.M., Tisdall, J.M., Blackmore, D.H. and Walker, R.R.** (2006) A diminished capacity for chloride exclusion by grapevine rootstocks following long-term saline irrigation in an inland versus a coastal region of Australia. *Australian Journal of Grape and Wine Research*, **12**, 178-191.
- Tregeagle, J.M., Tisdall, J.M., Tester, M. and Walker, R.R.** (2010) Cl⁻ uptake, transport and accumulation in grapevine rootstocks of differing capacity for Cl⁻-exclusion. *Functional Plant Biology*, **37**, 665-673.
- Tsay, Y.-F., Schroeder, J.I., Feldmann, K.A. and Crawford, N.M.** (1993) The herbicide sensitivity gene CHL1 of Arabidopsis encodes a nitrate-inducible nitrate transporter. *Cell*, **72**, 705-713.
- Tsay, Y.F., Chiu, C.C., Tsai, C.B., Ho, C.H. and Hsu, P.K.** (2007) Nitrate transporters and peptide transporters. *FEBS Letters*, **581**, 2290-2300.
- Tyerman, S.D. and Skerrett, I.M.** (1999) Root ion channels and salinity. *Scientia Horticulturae*, **78**, 175-235.
- Tzounopoulos, T., Maylie, J. and Adelman, J.P.** (1995) Induction of endogenous channels by high levels of heterologous membrane proteins in *Xenopus* oocytes. *Biophysical Journal*, **69**, 904-908.
- Uozumi, N., Kim, E.J., Rubio, F., Yamaguchi, T., Muto, S., Tsuboi, A., Bakker, E.P., Nakamura, T. and Schroeder, J.I.** (2000) The Arabidopsis *HKT1* gene homolog mediates inward Na⁺ currents in *Xenopus laevis* oocytes and Na⁺ uptake in *Saccharomyces cerevisiae*. *Plant Physiology*, **122**, 1249-1260.
- Vahisalu, T., Kollist, H., Wang, Y.F., Nishimura, N., Chan, W.Y., Valerio, G., Lamminmaki, A., Brosche, M., Moldau, H., Desikan, R., Schroeder, J.I. and Kangasjarvi, J.** (2008) SLAC1 is required for plant guard cell S-type anion channel function in stomatal signalling. *Nature*, **452**, 487-491.
- Vandesompele, J., De Preter, K., Pattyn, F., Poppe, B., Van Roy, N., De Paepe, A. and Speleman, F.** (2002) Accurate normalization of real-time quantitative RT-PCR data by geometric averaging of multiple internal control genes. *Genome Biology*, **3**, research0034.0031-research0034.0011.
- Vieira-Pires, R.S., Szollosi, A. and Morais-Cabral, J.H.** (2013) The structure of the KtrAB potassium transporter. *Nature*, **496**, 323-328.

- Von der Fecht-Bartenbach, J., Bogner, M., Dynowski, M. and Ludewig, U.** (2010) CLC-b-mediated NO_3^-/H^+ exchange across the tonoplast of *Arabidopsis* vacuoles. *Plant and Cell Physiology*, **51**, 960-968.
- Walker, G.R., Gilfedder, M. and Williams, J.** (1999) *Effectiveness of current farming systems in the control of dryland salinity*: CSIRO Land and Water.
- Walker, R. and Clingeleffer, P.** (2009) Rootstock attributes and selection for Australian conditions. *Australian Viticulture*, **13**, 70-76.
- Walker, R.R., Blackmore, D., Clingeleffer, P. and Gibberd, M.** (2002a) How vines deal with salt. In *Managing Water*: Australian Society of Viticulture and Oenology.
- Walker, R.R., Blackmore, D.H. and Clingeleffer, P.R.** (2010) Impact of rootstock on yield and ion concentrations in petioles, juice and wine of Shiraz and Chardonnay in different viticultural environments with different irrigation water salinity. *Australian Journal of Grape and Wine Research*, **16**, 243-257.
- Walker, R.R., Blackmore, D.H., Clingeleffer, P.R. and Correll, R.L.** (2002b) Rootstock effects on salt tolerance of irrigated field-grown grapevines (*Vitis vinifera* L. cv. Sultana): 1. Yield and vigour inter-relationships. *Australian Journal of Grape and Wine Research*, **8**, 3-14.
- Walker, R.R., Blackmore, D.H., Clingeleffer, P.R. and Correll, R.L.** (2004) Rootstock effects on salt tolerance of irrigated field-grown grapevines (*Vitis vinifera* L. cv. Sultana) 2. Ion concentrations in leaves and juice. *Australian Journal of Grape and Wine Research*, **10**, 90-99.
- Walker, R.R., Blackmore, D.H., Clingeleffer, P.R. and Emanuelli, D.** (2014) Rootstock type determines tolerance of Chardonnay and Shiraz to long-term saline irrigation. *Australian Journal of Grape and Wine Research*, **20**, 496-506.
- Walker, R.R., Blackmore, D.H., Clingeleffer, P.R., Godden, P., Francis, L., Valente, P. and Robinson, E.** (2003) Salinity effects on vines and wines. *Bulletin de l'Office International de la Vigne et du Vin*, **76**, 200-227.
- Walker, R.R., Blackmore, D.H., Clingeleffer, P.R. and Iacono, F.** (1997) Effect of salinity and Ramsey rootstock on ion concentrations and carbon dioxide assimilation in leaves of drip-irrigated, field-grown grapevines (*Vitis vinifera* L. cv. Sultana). *Australian Journal of Grape and Wine Research*, **3**, 66-74.
- Walker, R.R., Blackmore, D.H., Clingeleffer, P.R. and Tarr, C.R.** (2007) Rootstock effects on salt tolerance of irrigated field - grown grapevines (*Vitis vinifera* L. cv. Sultana). 3. Fresh fruit composition and dried grape quality. *Australian Journal of Grape and Wine Research*, **13**, 130-141.
- Walker, R.R., Blackmore, D.H., Gong, H., Henderson, S.W., Gilliham, M. and Walker, A.R.** (2018) Analysis of the salt exclusion phenotype in rooted leaves of grapevine (*Vitis* spp.). *Australian Journal of Grape and Wine Research*, **24**, 317-326.
- Walker, R.R., Torokfalvy, E., Scott, N.S. and Kriedemann, P.E.** (1981) An analysis of photosynthetic response to salt treatment in *Vitis vinifera*. *Functional Plant Biology*, **8**, 359-374.
- Waters, S., Gilliham, M. and Hrmova, M.** (2013) Plant High-Affinity Potassium (HKT) Transporters involved in salinity tolerance: structural insights to probe differences in ion selectivity. *International Journal of Molecular Sciences*, **14**, 7660-7680.
- Wege, S., De Angeli, A., Droillard, M.-J., Kroniewicz, L., Merlot, S., Cornu, D., Gambale, F., Martinoia, E., Barbier-Brygoo, H., Thomine, S., Leonhardt, N. and Filleur, S.** (2014) Phosphorylation of the vacuolar anion exchanger AtCLCa is required for the stomatal response to abscisic acid.
- Wege, S., Gilliham, M. and Henderson, S.W.** (2017) Chloride: not simply a 'cheap osmoticum', but a beneficial plant macronutrient. *Journal of Experimental Botany*, **68**, 3057-3069.

- Wege, S., Jossier, M., Filleur, S., Thomine, S., Barbier-Brygoo, H., Gambale, F. and De Angeli, A.** (2010) The proline 160 in the selectivity filter of the *Arabidopsis* NO₃⁻/H⁺ exchanger AtCLCa is essential for nitrate accumulation in planta. *The Plant Journal*, **63**, 861-869.
- Wen, Z., Tyerman, S.D., Dechorgnat, J., Ovchinnikova, E., Dhugga, K.S. and Kaiser, B.N.** (2017) Maize NPF6 proteins are homologs of Arabidopsis CHL1 that are selective for both nitrate and chloride. *The Plant Cell*, **29**, 2581-2596.
- White, P. and Broadley, M.** (2001) Chloride in soils and its uptake and movement within the plant: a review. *Annals of Botany*, **88**, 967-988.
- Wine Australia** (2018) National Vintage Report 2018: Wine Australia.
- Wolkovich, E.M., García de Cortázar-Atauri, I., Morales-Castilla, I., Nicholas, K.A. and Lacombe, T.** (2018) From Pinot to Xinomavro in the world's future wine-growing regions. *Nature Climate Change*, **8**, 29-37.
- Woodham, R.C.** (1956) The chloride status of the irrigated sultana vine and its relation to vine health. *Australian Journal of Agricultural Economics*, **7**, 414-427.
- Wu, F.H., Shen, S.C., Lee, L.Y., Lee, S.H., Chan, M.T. and Lin, C.S.** (2009) Tape-Arabidopsis sandwich - a simpler Arabidopsis protoplast isolation method. *Plant Methods*, **5**, 16.
- Wu, S.-J., Ding, L. and Zhu, J.-K.** (1996) SOS1, a genetic locus essential for salt tolerance and potassium acquisition. *The Plant Cell*, **8**, 617-627.
- Wu, Y., Henderson, S.W., Walker, R.R. and Gilliham, M.** (2019a) Expression of the grapevine *NPF2.2* in Arabidopsis roots reduces shoot Cl⁻ accumulation under salt stress.
- Wu, Y., Henderson, S.W., Walker, R.R. and Gilliham, M.** (2019b) Expression of the grapevine stelar localised anion transporter ALMT2 in Arabidopsis roots reduced shoot Cl⁻ accumulation under salt stress.
- Wu, Y., Li, J. and Gilliham, M.** (2019c) An R-based web app Smart-IV for automated and integrated high throughput electrophysiology data processing.
- Xu, B., Waters, S., Byrt, C.S., Plett, D., Tyerman, S.D., Tester, M., Munns, R., Hrmova, M. and Gilliham, M.** (2018) Structural variations in wheat HKT1;5 underpin differences in Na⁺ transport capacity. *Cellular and Molecular Life Sciences*, **75**, 1133-1144.
- Yeo, A.R.** (2007) Salinity. In *Plant Solute Transport*. Oxford: Blackwell publishing, pp. 340-370.
- Yoo, S.D., Cho, Y.H. and Sheen, J.** (2007) Arabidopsis mesophyll protoplasts: a versatile cell system for transient gene expression analysis. *Nat. Protoc.*, **2**, 1565-1572.
- Yoshida, M., Cowgill, S.E. and Wightman, J.A.** (1997) Roles of oxalic and malic acids in chickpea trichome exudate in host-plant resistance to *Helicoverpa armigera*. *Journal of Chemical Ecology*, **23**, 1195-1210.
- Yu, L., Nie, J., Cao, C., Jin, Y., Yan, M., Wang, F., Liu, J., Xiao, Y., Liang, Y. and Zhang, W.** (2010) Phosphatidic acid mediates salt stress response by regulation of MPK6 in *Arabidopsis thaliana*. *New Phytologist*, **188**, 762-773.
- Yuan, F., Leng, B. and Wang, B.** (2016) Progress in studying salt secretion from the salt glands in recretohalophytes: how do plants secrete salt? *Frontiers in Plant Science*, **7**, 977-977.
- Zhang, W.-H., Ryan, P.R. and Tyerman, S.D.** (2004) Citrate-Permeable Channels in the Plasma Membrane of Cluster Roots from White Lupin. *Plant Physiology*, **136**, 3771-3783.
- Zhang, X.K., Walker, R.R., Stevens, R.M. and Prior, L.D.** (2002) Yield-salinity relationships of different grapevine (*Vitis vinifera* L.) scion-rootstock combinations. *Australian Journal of Grape and Wine Research*, **8**, 150-156.
- Zhao, S., Fung-Leung, W.P., Bittner, A., Ngo, K. and Liu, X.** (2014) Comparison of RNA-Seq and microarray in transcriptome profiling of activated T cells. *PLoS One*, **9**, e78644.
- Zhou, J., Trueman, L.J., Boorer, K.J., Theodoulou, F.L., Forde, B.G. and Miller, A.J.** (2000) A high affinity fungal nitrate carrier with two transport mechanisms. *Journal of Biological Chemistry*, **275**, 39894-39899.

- Zhu, K., Wang, X., Liu, J., Tang, J., Cheng, Q., Chen, J.-G. and Cheng, Z.-M.M.** (2018) The grapevine kinome: annotation, classification and expression patterns in developmental processes and stress responses. *Horticulture Research*, **5**, 19-19.
- Ziska, L.H., Seemann, J.R. and DeJong, T.M.** (1990) Salinity induced limitations on photosynthesis in *Prunus salicina*, a deciduous tree species. *Plant Physiology*, **93**, 864-870.